

LENGTH-EFFECTS IN RELIABILITY ANALYSIS OF INTERNAL EROSION IN EARTHEN DIKES

BY

J.J. CASPERS

MASTER THESIS
CIVIL ENGINEERING

< Splitting of the Rhine and IJssel near Arnhem during the high water event of 2018 – edited photo of O. Kroezen (2018)

DELFT UNIVERSITY OF TECHNOLOGY

MASTER THESIS
CIVIL ENGINEERING

**LENGTH-EFFECTS IN RELIABILITY ANALYSIS
OF INTERNAL EROSION IN EARTHEN DIKES**

TO OBTAIN THE DEGREE OF
MASTER OF SCIENCE
IN HYDRAULIC ENGINEERING
AT THE DELFT UNIVERSITY OF TECHNOLOGY
TO BE DEFENDED PUBLICLY ON JUNE 3, 2020

Graduate Student:

J. Caspers, Delft University of Technology
HKV - Lijn in Water

[4390202]

Graduation Committee:

Prof. Dr. Ir. M. Kok, Delft University of Technology
Dr. Ir. R. Lanzafame, Delft University of Technology
Dr. Ir. B. van den Eijnden, Delft University of Technology
Ir. G. Pleijter, HKV - Lijn in Water

May 27, 2020



*“Among cords of equal thickness
the longest is the least strong”
- Leonardo Da Vinci*

Preface

This master thesis has been conducted in order to achieve the Master of Science degree in Hydraulic Engineering at the faculty of Civil Engineering and Geosciences of the Delft University of Technology. The research was carried out at HKV - Lijn in Water by means of an internship.

First of all, I would like to thank my thesis committee for their support expertise and guidance during this graduation project. A lot of gratitude to my daily supervisors Dr. Ir. Robert Lanzafame from the TU Delft and Ir. Gerbert Pleijter, for their time to answer my questions or brainstorm about ideas during all the (online) meetings we had. I would like to thank Dr. Ir. Bram van den Eijnden for his support and sharing knowledge. Thanks to Prof. Dr. Ir. Matthijs Kok for his positivity and guidance in the committee meetings as chairman of the thesis committee.

Special thanks to the waterboard Rijn & IJssel for making the data available to carry out this research. Especially to Ir. Gert de Jonge en Christien Veenstra-Huisman for providing support and feedback for the case study. Furthermore, I would like to thank Dr. Ir. Wim Kanning, Dr. Ir. Ruben Jongejan and Ir. Han Knoeff for their time to meet and expertise to give direction to this research.

Also I would like to thank HKV - Lijn in Water for the opportunity to perform this research in combination with an internship and provide me expertise and guidance. A big thanks to all colleagues for their interest in this master thesis and enjoyable conversations.

Finally, I would like to thank everyone who supported me during this graduation period. My family and friends made me enjoy my study time very much.

Delft, May 27, 2020

J.J. Caspers

Abstract

In this master thesis the current Dutch method of combining failure probabilities at different spatial scales is researched. This method is used in the Dutch flood risk analysis of earthen dikes to assess the probability of flooding. Currently, probabilities of flooding for geotechnical failure mechanisms are obtained which are not considered to be realistic. To obtain more realistic results the following steps are researched; the assessment of cross-sections, scaling to dike sections and combining sections to a dike trajectory. The increase of failure probability over increasing length, known as the length-effect, is of importance in the current Dutch method of combining failure probabilities. This method is known as the assembly procedure.

This research is based on a case study of dike trajectory 48-1 along the Dutch Rhine for the geotechnical failure mechanism internal erosion (or piping). If during high water events the flow of ground water underneath the earthen dike entrains sand, the dike can fail due to internal erosion. With a flood risk analysis of this geotechnical failure mechanisms the assembly procedure is researched. The objective is to answer the main research question:

Can the current Dutch assembly procedure of combining failure probabilities of geotechnical failure mechanisms be improved, and if so, how?

The assessment of cross-sectional failure probabilities is based on the provided tools by the Legal Assessment Instrument (WBI). It is shown that this a conservative approach because (i) unrealistic combinations of parameters are made, (ii) correlations between parameters are neglected and (iii) characteristic values for load and resistance are assumed.

This conservatism is shown with a (semi) probabilistic approach based on distribution parameters derived from field data at small spatial intervals using interpolation techniques. The resulting failure probabilities are lower than initially derived according to the WBI.

The scaling to sectional failure probabilities using the length-effect within sections is based on a Continuous Model of the Outcrossing Method. This method results in conservative scaling factors because (i) the nationwide calibrated length-effect parameters (a and b) are a conservative choice, (ii) the method is in most cases not applied to intervals much larger than the independent equivalent length, (iii) the method is not applied to intervals with statistically constant reliability and (iv) the method is based on the upper bound of the outcrossing method which is only a good approximation for small failure probabilities and outcrossing rates.

The field calibrated length-effect parameters reduce the length-effect significantly compared to the current length-effect parameters according to the WBI. Moreover, since the field calibrated length-effect parameters still include conservatism resulting from the mismatch between the theoretical assumptions and practical reality, the length-effect within sections approaches one. This indicates no length-effect within dike sections if the assessment is based on the normative cross-section (or 'weakest link') within dike sections of lengths not much larger than the equivalent independent length.

The combination of sections to a trajectory failure probability using the length-effect between sections is currently based on the fundamental independent boundary. In other words, the independent summation of the sectional failure probabilities. This is a conservative method because (i) the correlation between dike sections, mainly introduced by the load (or water level), is not negligible and (ii) knowledge about fluvial deposits is not taken into account.

Taking the correlation of consecutive dike sections into account reduces the trajectory failure probability. Therefore, the fundamental independent boundary is not a good approximation for dike trajectories. An efficient method to include the correlation between dike sections is the Equivalent Planes Method based on a probabilistic assessment.

Finally, in comparison to the dike safety assessment of trajectory 48-1 by the waterboard Rijn & IJssel, the trajectory failure probability of $1/6.3$ [1/y] is reduced over a factor 10 to $1/93$ [1/y]. This indicates the conservatism of the original assessment according to the WBI but is in line with the reported trajectory failure probability by the waterboard of '>1/100' [1/y]. The waterboard made a conscious decision not to report such high failure probability since it is not in line with the expectations. A reference is made to the disclaimer on page 7.

Contents

Preface	vii
Abstract	ix
Contents	xi
1 Introduction	1
I Method	3
2 Problem Statement	5
3 Research Objective	9
4 Research Method	11
4.1 Calculate	12
4.2 Scale	13
4.3 Combine	14
5 Case Study	17
II Data Analysis	21
6 Data Analysis	23
6.1 Water level	23
6.2 Seepage length	24
6.3 Ground level	25
6.4 Polder level	26
6.5 Cover layer	27
6.6 Aquifer layer	29
6.7 Grain size	30
6.8 Permeability	32
6.9 Volumetric weight	34
6.10 Reduction factor	34
III Reliability Analysis	35
7 Reliability Analysis	37
7.1 Semi-Probabilistic Method	38
7.2 Probabilistic Method	40
8 Conclusions of Sub Question 1	51
IV Length-Effect within Sections	55
9 Length-Effect within Sections	57
9.1 Outcrossing Method	58
9.2 Continuous Model of the Outcrossing Method	66
10 Conclusions of Sub Question 2	73

V Length-Effect between Sections	79
11 Length-Effect between Sections	81
11.1 Fundamental Boundaries	82
11.2 Ditlevsen Boundaries	82
11.3 Equivalent Planes Method	83
12 Conclusions of Sub Question 3	89
13 Discussion	91
14 Conclusion	95
15 Recommendation	97
References	98
List of Figures	100
List of Tables	103
Appendices	107
A Assembly Procedure WBI 2017	109
B Geotechnical Failure Mechanisms	111
C Data Analysis Details	115
D Kriging Interpolation	117
E Reliability Modelling	123
F Autocorrelation Function	127
G Derivation of Length-Effects	129
H Length-Effect of Serial Systems	135
I Generic Approach of Length-Effects	139

Chapter 1

Introduction

Earthen dikes serve as revetments to protect the polders during high water events. A dike trajectory typically consists of different geometries, orientations and subsoils. In order to compute the probability of flooding it is divided into sections. These sections are considered to be statistically homogeneous. The division will facilitate the computation of the failure probability of dike cross-sections that are representative for the dike sections it represent. For every representative cross-section different failure mechanisms have to be considered because a dike can fail due to different failure mechanisms like slope instability, overtopping, internal erosion (or piping), etc.

If failure occurs at one of the cross-sections for one of the failure mechanisms, the entire trajectory fails since it is considered as a series system. This is visualised in the fault tree in figure 1.1 below.

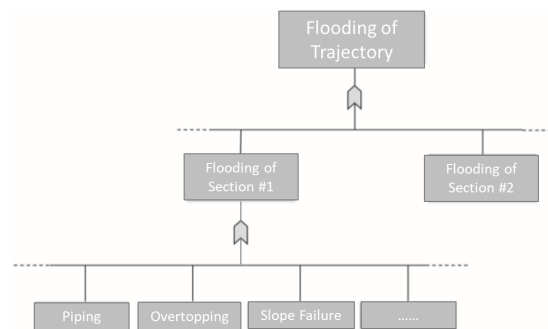


Figure 1.1: Fault tree of a dike trajectory (Jonkman et al., 2018)

Note that the greater the length of a dike trajectory, the more likely there will be a weak spot. This phenomenon is known as the length-effect and takes the increase of failure probability with increasing length into account (VNK2, 2011). Out of the context of earthen dikes, this phenomenon was already discussed by Leonardo Da Vinci in the 16th century, who observed that "Among cords of equal thickness the longest is the least strong" (Bazant, 2001).

This graduation project focuses on earthen dikes that are subjected to the geotechnical failure mechanism internal erosion, as explained in figure 1.3. More specific, on improving the length-effect between cross-sections and sections and between sections and trajectory.

Spatial Scales

It is of importance to distinguish the different spatial scales used in this report. Three different spatial scales are distinguished; cross-sections ('doorsnedes'), sections ('vakken') and trajectory ('traject').

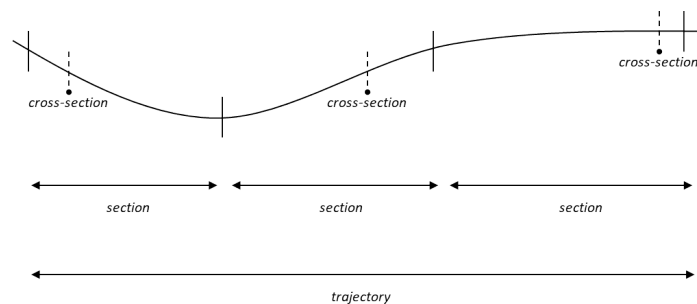


Figure 1.2: Schematic representation of the spatial scales

Structure of the Thesis

Part I - Method

In Chapter 2 the problem statement is given based on the use of the length-effects in the current assembly procedure. In Chapter 3 the problem statement is translated into research objectives including the main research question and related sub-questions. Chapter 4 describes the method proposed to achieve these research objectives based on a case study which is discussed in Chapter 5.

Part II - Data Analysis

Chapter 6 states the data required to execute the method proposed. This data is obtained for all required parameters to assess the failure mechanism internal erosion (or piping).

Part III - Reliability Analysis

In Chapter 7 the calculation of the cross-sectional failure probabilities of the piping failure mechanism will be discussed based on a semi-probabilistic (Level I) and probabilistic (Level II) approach. The importance factors and sensitivities of the limit state function parameters are derived and discussed. Chapter 8 contains the conclusions of the reliability analysis which are used to answer the first sub-research question.

Part IV - Length-Effect within Sections

In Chapter 9 the calibration of the length-effect within sections is discussed according to the VNK software and the WBI 2017 calibration study. These methods are compared to the calibration of the length-effect within sections for the case study specific. Chapter 10 contains the conclusions of the calibration of the sectional length-effect which are used to answer the second sub-research question.

Part V - Length-Effect between Sections

Chapter 11 approximates the length effect between sections with the use of the Equivalent Planes method in comparison to the current independent approximation in the WBI 2017. Additional comparisons are made to the known lithology of the case study. In Chapter 12 the conclusions of the length-effect between sections are discussed which are used to answer the third sub-research question.

Finally, Chapter 13 holds the discussion of the results, in Chapter 14 the conclusions of this master thesis will be given including the answer to the main research question and Chapter 15 contains recommendations based on the findings and conclusions.



Figure 1.3: Internal erosion (TAW, 1995)

IJsseldijk at Westervoort (DP215) - 1995

During the high water of January - February 1995 internal erosion (or piping) occurred along the IJsseldijk. The increasing water pressure of the river against the earthen dike induces the flow of groundwater through sand layers underneath the dike. This flow of groundwater will seepage into the polder at places with small resistance, like thin clay layers, causing the entrainment of sand. The continuous entrainment of sand results in a sand boil and could lead to subsidence and failure of the dike. With the use of sand bags and geotextiles sand boils can be controlled (see figure 1.3).

Part I
Method

Chapter 2

Problem Statement

With the use of the Legal Assessment Instrument 2017 (Wettelijk Beoordelings Instrumentarium 2017) engineers will assess the hydraulic structures, mostly earthen dikes, to the water safety requirements from the Waterlaw (Waterwet). Several (semi) probabilistic assessments of dike failure mechanisms are included in the WBI 2017 to determine the failure probability of a dike cross-section, representing a dike section in which strength, load and geometry can be supposed to be 'statistically homogeneous' within the dike trajectory. These assessments result in the failure probability of a dike cross-section and failure mechanism specific.

The addressed problem is with the combination of failure probabilities of cross-sections to a trajectory failure probability for geotechnical failure mechanisms. To give an indication of the nature of the problem the current assembling of cross-sectional failure probabilities to a trajectory failure probability will be discussed together with the disassembling of the trajectory safety requirement to sectional safety requirements according to the WBI 2017. An overview of both procedures is given in figure 2.1.

Assembly

The assessment results for failure mechanisms specific on cross-section level ($Pf_{cross-section}$) should be scaled to sectional level ($Pf_{i,j}$) and combined to trajectory level (Pf_j). Finally, all failure mechanisms are combined ($Pf_{trajectory}$) in order to be compared to the safety requirement. The assembling procedure of failure mechanisms specific depends on the length-effect from cross-section to section (N^*), shown in equation 2.1, and the length-effect from section to trajectory (N) combined with a serial system reliability approach based on independence as shown in equation 2.2. Furthermore, all failure mechanisms are independently combined as shown in equation 2.3 (Diermanse et al., 2017).

$$Pf_{i,j} = N^* \cdot Pf_{cross-section} \quad (2.1)$$

$$Pf_j = \min\left(1 - \prod_{i=1}^n (1 - Pf_{i,j}); N \cdot \max(Pf_{i,j})\right) \quad (2.2)$$

$$Pf_{trajectory} = 1 - \prod_{i=1}^n (1 - Pf_j) \quad (2.3)$$

The length-effect within sections (N^*) assures that higher failure probabilities for failure mechanisms result on sectional level compared to cross-sectional level. The length-effect between sections ($\perp(N)$ or $\perp\perp$) assures that higher failure probabilities for failure mechanisms result on trajectory level compared to sectional level. For failure mechanisms where the sections show high dependencies (overflow/overtopping) i.e. small length-effect, the failure probability of the trajectory is approximated with mutual dependence (\perp) using the length-effect on trajectory scale (N). Vice versa for failure mechanisms where the sections show low dependencies (internal erosion/macro-stability) i.e. large length-effect, the failure probability is approximated with mutual independence ($\perp\perp$) (Jonkman et al., 2018).

For geotechnical failure mechanisms this leads to a high trajectory failure probability since cross-sectional failure probabilities are increased to sectional failure probabilities which subsequently are numerated independently. This can be designated as the main problem of the assembly procedure.

Disassembly

The assessment results of failure mechanisms for dike sections ($P_{f_{i,j}}$) should be compared to the safety requirements for dike sections ($P_{i,j}$). This depends on the safety standard ($P_{trajectory}$), the maximum failure probability contribution of the failure mechanism under consideration (ω) and the length-effect on trajectory scale (N). This is shown in equation 2.4 (Rijkswaterstaat, 2016a).

$$P_{i,j} = \frac{P_{trajectory} \cdot \omega}{N} \quad (2.4)$$

The safety standards are stated in the Waterlaw for all dike trajectories. The failure probability contribution of the failure mechanisms are stated in the WBI based on the results of VNK and expert judgements (Jongejan, 2013). The length-effects of failure mechanisms are stated in the WBI 2017 and take the spatial correlation within and between sections into account (Rijkswaterstaat, 2016a).

The failure probability contributions of failure mechanisms specific (ω) and the length-effect on trajectory scale (N) ensure that higher safety requirements are set at sectional level compared to trajectory level. For failure mechanisms where the length-effect is small (overflow/overtopping) i.e. high spatial correlation, the safety requirement for each section will not differ much from the safety requirement of the trajectory. Vice versa for failure mechanisms where the length-effect is large (internal erosion/macro-stability) i.e. low spatial correlation, the safety requirement for each section will differ in a high extent from the safety requirement of the trajectory. This will lead to high safety requirements for geotechnical failure mechanisms on sectional level.

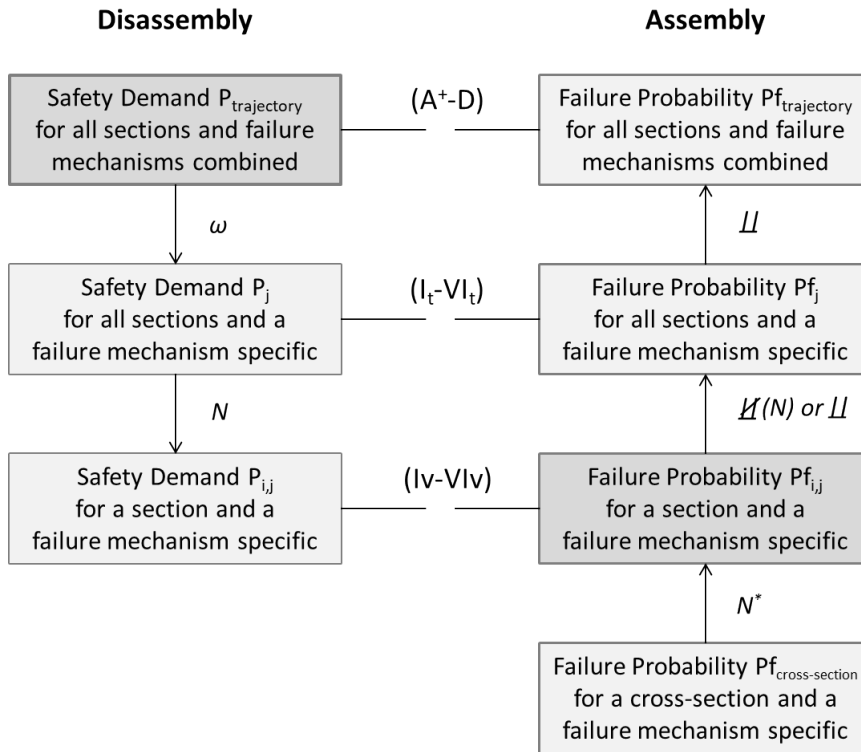


Figure 2.1: Disassembly and Assembly procedure of the WBI 2017

Practice

In practice both ways, disassembly and assembly, results in large length-effect factors. Based on an assessment performed by the Waterboard Rijn & IJssel (WRIJ) there are doubts in relation to these large length-effect factors. By comparing the assessment of piping for the 1995 high water event to the disassembled safety requirement of dike sections it is indicated that most sections will not fulfill the requirement, which in practice is experienced differently (WRIJ, 2018).

Furthermore, it is indicated that the assembly of the failure probabilities of individual sections for the failure mechanism piping leads to an unrealistic result. This is based on the assessment of dike trajectory 48-1 in which the combination of failure probabilities of all sections leads to a trajectory failure probability of $1/6.3$ [1/y] for piping specific. In practice this is experienced differently despite it is known to be a piping sensitive trajectory. Therefore, the waterboard made a conscious decision not to report such high failure probability. Instead a trajectory failure probability of $>1/100$ is reported to the Human Environment and Transport Inspectorate (ILT) (WRIJ, 2018). A reference is made to the disclaimer below.

This is in line with the memo 'Analyse hoge overstromingskansen WBI-2017' (ILT, 2019) where it is established by the ILT that in a lot of practical cases assessments results in failure probabilities larger than $1/100$. "high failure probabilities, as in several assessment reports from waterboards, are not in line with the expectations of the waterboards. Failure probabilities higher than once in ten years, while there have not been any known problems the question arises where the high failure probability originates" (ILT, 2019).

Disclaimer Safety Assessment Dike Trajectory 48-1

The waterboard Rijn & IJssel performed a flood risk analysis of dike trajectory 48-1. In the background report of the geotechnical failure mechanism piping the assessed failure probabilities of the dike sections are reported in table 8.1 (WRIJ, 2018). The independent summation of these sectional failure probabilities leads to a trajectory probability of failure due to piping of $1/6.3$ [1/y].

However, the waterboard made a conscious choice not to report this high failure probability since such probabilities of failure on trajectory scale are not in line with the expectations and knowledge of the waterboard. In 1995 the dike trajectory survived a high water event with an average occurrence of once in 80 to 100 years. At various locations along the trajectory emergency measures were taken to resist these hydraulic loads. After 1995 the dike trajectory is reinforced along several critical intervals.

Therefore, the waterboard explicitly renounce a trajectory failure probability of $1/6.3$ [1/y] and a probability of failure larger than $1/100$ [1/y] is reported. But the disapproval of the trajectory in comparison to the safety requirements of the failure mechanism piping is supported by the waterboard. During high water events with an occurrence of once in ten years sand boils are observed. Indicating the limitations of the trajectory with respect to piping. A reference is made to section 4 in the main report of the flood risk analysis (WRIJ, 2019) for more information about the interpretation of the safety judgement.

Chapter 3

Research Objective

As discussed in the Problem Statement, the current assembly and disassembly procedure within the WBI 2017 leads to large length-effect factors, especially for geotechnical failure mechanisms. This has already been experienced in practice by several waterboards, with waterboard Rijn & IJssel as one of many examples. So, the objective of this graduation project is:

Improve the length-effects in the assembly procedure of geotechnical failure mechanisms by making the scaling of cross-sections to sections and the combination of sections to trajectory field specific

In order to improve the current assembly procedure for geotechnical failure mechanisms the focus will be on the following steps within this assembly procedure which are highlighted in figure 3.1:

1. Calculate the cross-sectional failure probabilities representing a homogeneous section.
2. Scale the cross-sectional failure probabilities to sectional failure probabilities.
3. Combine the sectional failure probabilities to a trajectory failure probability.

Note that all three steps are executed in a case study for one geotechnical failure mechanism specific, namely internal erosion (or piping). The process of combining all failure mechanisms together is out of the scope of this graduation project.

The disassembly procedure is not directly in the scope of this research. However, improvements on the assembly procedure can be implemented in the disassembly procedure in deriving safety requirements on sectional scale. The safety requirements at different spatial scales are necessary to give safety judgements for dike sections ($I_v - VI_v$) and dike trajectories ($I_t - VI_t$) for failure mechanisms specific. A total safety judgement for the dike trajectory of all failure mechanisms combined ($A^+ - D$) indicated if the dike trajectory meets the safety requirements.

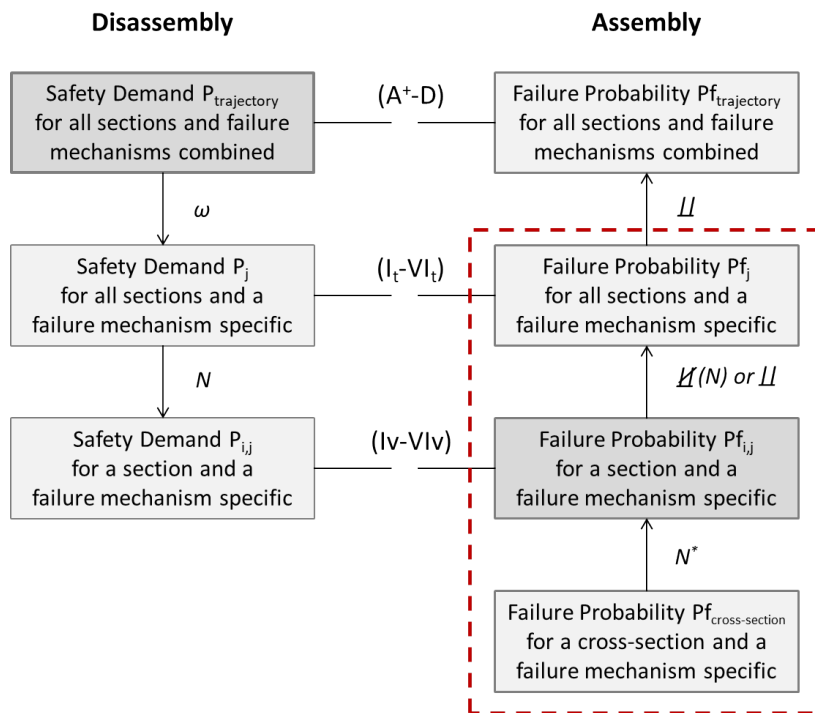


Figure 3.1: Disassembly and Assembly procedure of the WBI 2017

This research objective can be translated into a research question (RQ) with according sub-research questions (SQ), each contributing to answer the main research question.

RQ *Can the current Dutch assembly procedure of combining failure probabilities of geotechnical failure mechanisms be improved, and if so, how?*

This graduation project focuses on improving the current assembly procedure of failure probabilities for geotechnical failure mechanisms. This is done by making cross-sectional failure probabilities (i), the length-effect within sections (ii) and the length-effect between sections (iii) more accurate. This study focuses on the failure mechanism piping specific since the length-effect is most significant for the geotechnical cases and at such geotechnical sensitive trajectories all sectional failure probabilities are numerated independently in practice. The true numeration is between both elementary boundaries of fully dependent and independent numeration. This knowledge gap is a focus of this graduation project by taking the mutual dependence between consecutive sections into account.

SQ1 *In what amount is the calculated cross-sectional failure probability representative for the statistically homogeneous section it represent?*

This gives an indication in the amount of overestimation of the failure probability of an individual section by designating a conservative cross-section to represent the section based on certain reliability methods. Semi-probabilistic and probabilistic approaches will be compared.

SQ2 *How to use the length-effect within sections correctly to scale the cross-sectional failure probability to a sectional failure probability?*

This gives insight in the derivation of the current length-effect within sections and is compared to a field specific approach. Field related length-effect parameters will be derived for the case study specific.

SQ3 *How to use the length-effect between sections correctly by taking dependency into account for combining sectional failure probabilities to a trajectory failure probability?*

This gives an indication in the amount of overestimation of the current serial system approach by neglecting the possible mutual dependence between consecutive sections. A measure for dependence between consecutive sections will be derived and taken into account based on the correlation between local ground parameters that have most influence in the resistance against the geotechnical failure mechanisms.

Figure 3.2 shows a schematic representation of a dike trajectory as a 'chain' of dike sections which includes the three sub-research questions. Starting from the cross-sections (1) the length-effect within sections is represented by (2) and the length-effect between sections is represented by (3). Increasing length of the 'chains' or increasing the number of 'chains' will increase the probability of failure.

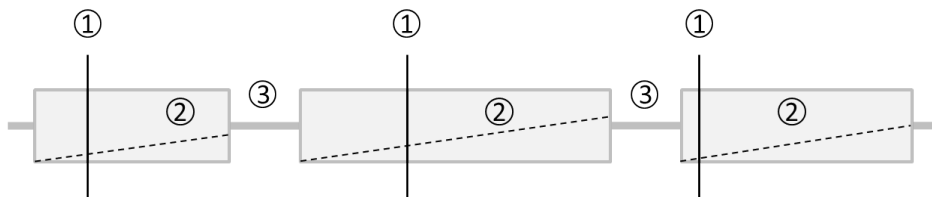


Figure 3.2: Research Objective - an improved assembly approach

Chapter 4

Research Method

The objective of this graduation project is to improve the length-effects in the current assembly procedure of cross-sectional reliabilities to a trajectory reliability for geotechnical failure mechanisms. Three spatial scales and two assembly steps can be distinguished in this assembly procedure. First, cross-sectional failure probabilities will be scaled to sectional failure probabilities using the length-effect within sections. Second, sectional failure probabilities will be combined to a trajectory failure probability using the length-effect between sections. The two assembly-steps are given in figure 4.1 below. The three different spatial scales distinguished are cross-sections, sections and trajectory.

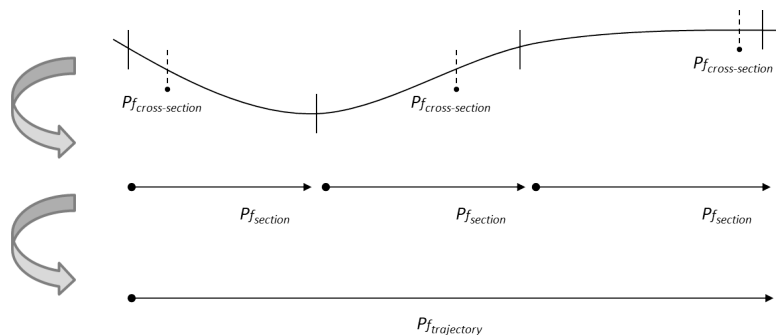


Figure 4.1: Schematic representation of the assembly procedure

RQ *Can the current Dutch assembly procedure of combining failure probabilities of geotechnical failure mechanisms be improved, and if so, how?*

In order to make the cross-sectional failure probabilities more accurate a study is performed on the choice of conservative cross-sections and ground parameters within dike sections. Since it is common to choose a normative cross-section with according normative ground-parameters for an assessment, there is a potential overestimation of the cross-sectional failure probability. Furthermore, the consequences of the choice of reliability methods are incorporated within this study.

To make the sectional failure probabilities more accurate the length-effect within sections should be taken into account in order to increase the failure probability with increasing length of the dike section. However, the use of field related uncertainties and small spatial intervals should reduce the uncertainty related to the length-effect within sections. This effect is researched in detail.

In order to make the trajectory failure probability more accurate, dependence between consecutive sections is taken into account based on the correlation between local ground parameters. If the number of sections increases (and the length of sections decreases) the independence between consecutive sections should not remain unchanged. So, there is a potential overestimation of the failure probability if consecutive sections have a certain correlation and are considered to be independent.

The method applied in this graduation project will be discussed in the sections Calculate, Scale and Combine which are based on the essence of the Dutch approach to system reliability analysis (Jongejan, 2017b). Three steps can be distinguished for this improved assembly approach.

1. Calculate the cross-sectional failure probabilities representing statistically homogeneous sections using reliability methods
2. Scale the cross-sectional failure probabilities to sectional failure probabilities using the length-effect within sections
3. Combine the sectional failure probabilities to a trajectory failure probability using the length-effect between sections

4.1 Calculate

The calculation of the cross-sectional failure probabilities using the legal assessment for the geotechnical failure mechanisms is currently based on Level I methods (semi-probabilistic design). The stochastic parameters are included as characteristic values. In level II methods (probabilistic design) stochastic parameters are included with their mean and standard deviation, and with the correlation between the stochastic variables. The choice of reliability method, normative cross-section and stochastic parameters results in different cross-sectional failure probabilities.

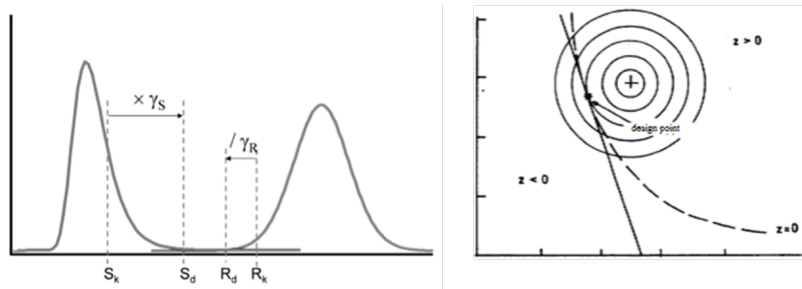


Figure 4.2: Level I and Level II (FORM) reliability methods

$$Z = R - S \quad (4.1)$$

SQ1 *In what amount is the calculated cross-sectional failure probability representative for the statistically homogeneous section it represent?*

Since it is common to choose a 'critical' cross-section to represent the homogeneous section there will be a certain conservatism. The amount of overestimation within a certain section division can be determined by analysing the results of multiple cross-sectional assessments within one homogeneous section in comparison to the original single cross-sectional assessment representing the homogeneous section. This is illustrated in figure 4.3 below where black indicates the original 'critical' cross-sectional result and gray indicates multiple cross-sectional results within the same section. The amount of overestimation is indicated with marked area.

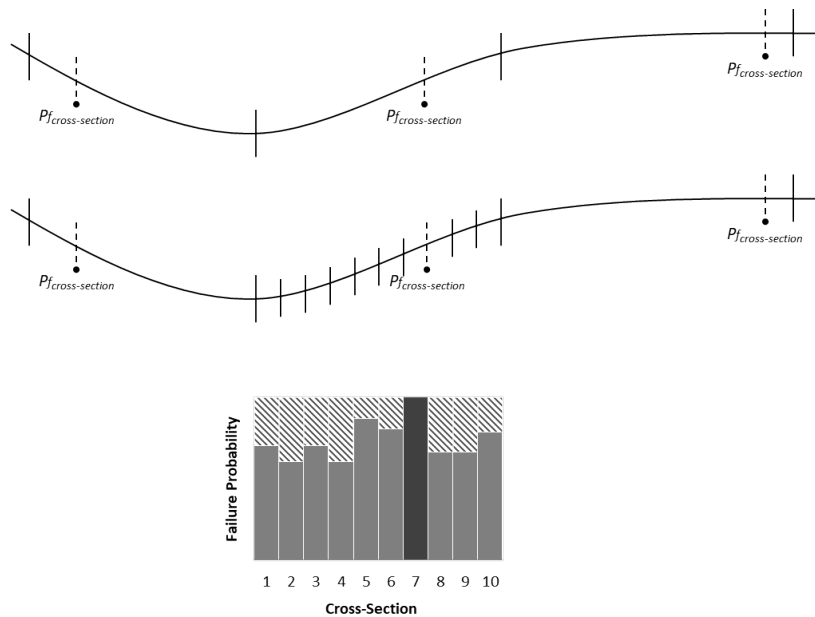


Figure 4.3: Overestimation within the assessment of dike sections

4.2 Scale

The scaling of cross-sectional failure probabilities to sectional failure probabilities will take the length-effect within statistically homogeneous sections into account. This scaling is currently based on the parameters a and b which indicates the failure mechanism sensitive interval and the intensity of the length-effect for the failure mechanism specific. In other words, over every equivalent independent length b within a section the sectional failure probability will increase with the cross-sectional failure probability. This increase is adjusted by a for the failure mechanism sensitive interval only. The length-effect within sections is given in equation 4.2 and visualised in figure 4.4.

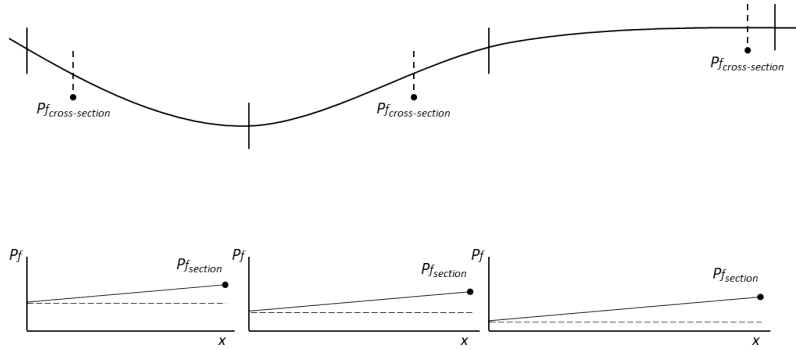
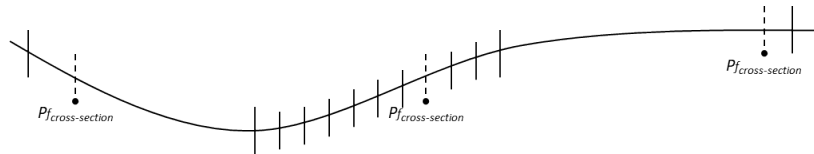


Figure 4.4: Length-effect within sections (1)

$$P_{f_{section}} = \left(1 + \frac{a \cdot L_{section}}{b} \right) \cdot P_{f_{cross-section}} \quad (4.2)$$

SQ2 *How to use the length-effect within sections correctly to scale the cross-sectional failure probability to a sectional failure probability?*

In practice, the failure mechanism sensitive interval (a) is not adjusted for each of the sections and remains constant. Furthermore, these length-effect parameters a and b are derived from a calibration study and applied to all trajectories. This results in a certain conservatism. The amount of overestimation within a section can be determined by analysing the ratio of the summation of multiple cross-sectional assessments to the maximum of the cross-sectional assessments within one homogeneous section in comparison to the original length-effect parameter applied to the homogeneous section. This is illustrated in figure 4.5 below where the left equation indicates the original length-effect parameter and the right equation indicates ratio of $\sum(P_{f_i})$ with respect to $\max(P_{f_i})$ within the same section.



$$N^* = 1 + \frac{a \cdot L_{section}}{b} \quad N^* = \frac{\sum P_{f_{cross-sections}}}{\max(P_{f_{cross-sections}})}$$

Figure 4.5: Length-effect within sections (2)

4.3 Combine

The combination of sectional failure probabilities to a trajectory failure probability will take the length-effect between dike sections into account. This combination is currently performed on the fundamental boundaries of complete independent and dependent sections. For geotechnical failure mechanisms specific the upper bound of independent summation of sectional failure probabilities is applied according to equation 4.3

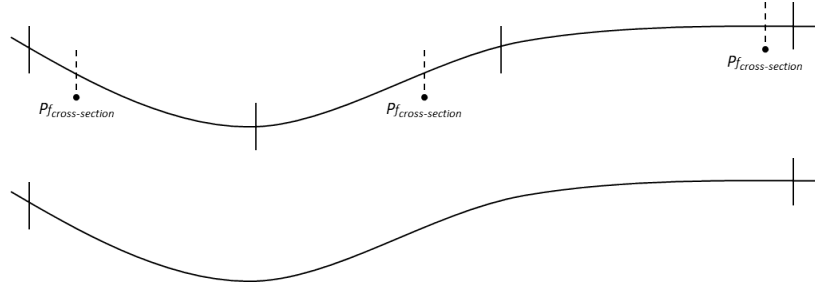
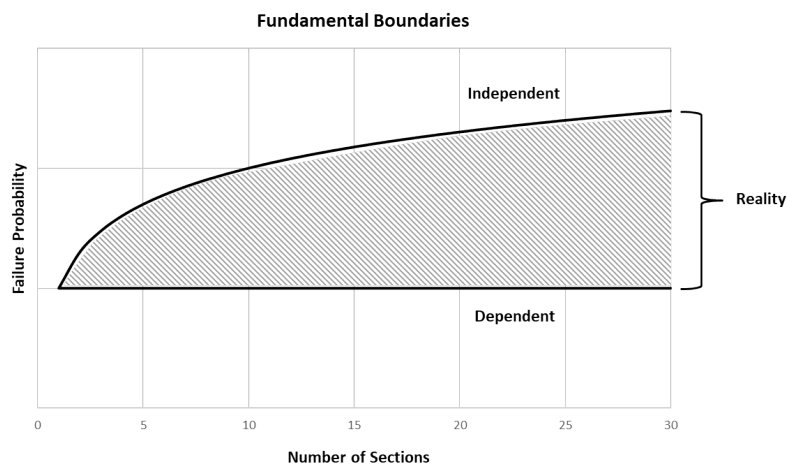


Figure 4.6: Length-effect between sections (1)

$$P_{f_{trajectory}} = 1 - \prod_{i=1}^n (1 - P_{f_{section,i}}) \tag{4.3}$$

SQ3 *How to use the length-effect between sections correctly by taking dependency into account for combining sectional failure probabilities to a trajectory failure probability?*

In reality, the most realistic combination of sections based on the real mutual dependence lies in between the fundamental boundaries which will be the aim of this improved assembly method and is stated in the equation below and visualised in figure 4.6. In order to approximate the mutual dependence between dike sections for geotechnical failure mechanisms a study will be performed on the local (ground) parameters of these sections that have most influence in the resistance against the geotechnical failure mechanisms. Based on this mutual correlation the assembly of sections to a trajectory can be a function of the mutual dependencies.



$$P_{f_{trajectory}} = f(P_{f_{section,i}}, \rho_{i,i+1})$$

Figure 4.7: Length-effect between sections (2)

Calculate - Scale - Combine

This three-step approach as discussed in the previous sections is visualised in figure 4.8 below. Note that the focus will be on attaining the conservatism with selecting normative cross-sectional failure probabilities, the use of the current length-effect within sections and the use of the length-effect between sections by neglecting the mutual dependence between succeeding dike sections. Finally, each step can be compared to indicate which has the largest positive impact on improving the current Dutch assembly approach.

RQ *Can the current Dutch assembly procedure of combining failure probabilities of geotechnical failure mechanisms be improved, and if so, how?*

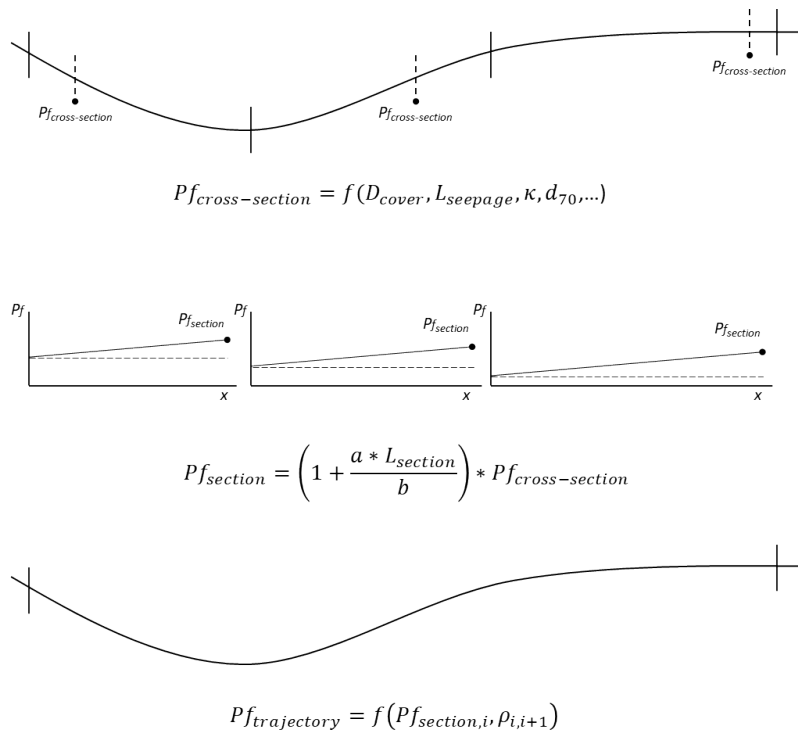


Figure 4.8: Overview of the assembly procedure - Calculate Scale Combine

For piping the most sensitive parameters to influence the assessment are the water level (river), the seepage length (entry to exit point), the permeability of the sandy aquifer, the grain size of the top of the sandy aquifer and the thickness of the cover layer (Forster et al., 2012).

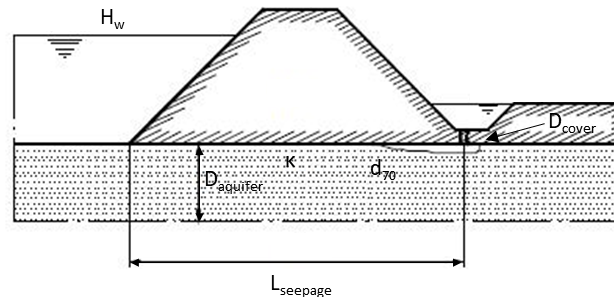


Figure 4.9: Sensitive parameters of the revised Sellmeijer Model

Chapter 5

Case Study

The data available for this research is provided by the waterboard Rijn & IJssel (WRIJ) which is used for the first assessment of the primary water defences of dike trajectory 48-1 (WRIJ, 2019). In this main report the safety judgement is described for dike trajectory 48-1 using the Legal Assessment Instrument 2017 (WBI 2017).

Dike trajectory 48-1 is located at the northern boundary of the Rhine, Pannerdens Channel and the IJssel, and is easterly adjacent to the German border. The trajectory spans from dike marker 0 + 000 to 274 + 095 with a length of approximate 27 kilometers. Trajectory 48-1 is shown in figure 5.1 where the dike markers are indicated with black dots, the hydraulic structures are indicated with red dots and special elements are indicated with purple lines (WRIJ, 2019).

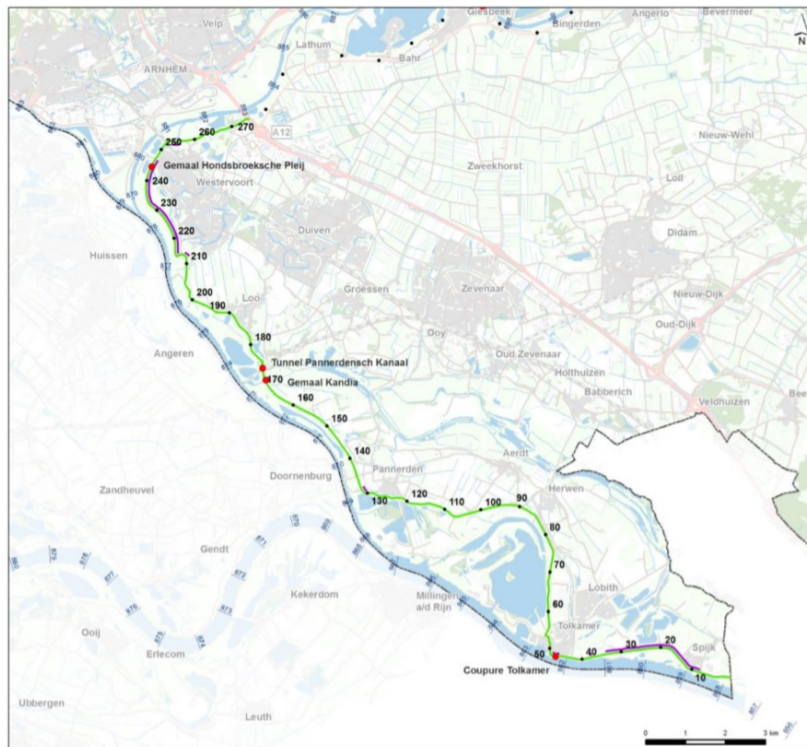


Figure 5.1: Dike trajectory 48-1 (WRIJ, 2019)

History

The last severe flooding of dike ring 48 was during the high water of 1926. The Deukerdijk, currently a regional water defence, was breached as a result of the high water at the Old Rhine. The most recent high water of 1995 resulted in multiple sandboils along trajectory 48-1 which indicate that internal erosion (or piping) is an important failure mechanism for this trajectory. However, no dike breach occurred but emergency measures were taken by creating 'box-structures' around the sandboils. An example is given in figure 1.3.

Since 1995 multiple dike reinforcements have been realised among which the dike sections between dike marker 132 + 60 - 135 (Pannerden-Loo), 165 - 213 (Kandia-Loo-Schans), 215 - 247 + 30 (Hondbroeksche Pleij) and 200 + 15 - 202 + 50 (Pannerden-Loo)

Safety Judgement

With the use of the WBI 2017, waterboard Rijn & IJssel has assessed the hydraulic structures, mostly earthen dikes, of trajectory 48-1 to the water safety requirements from the Waterlaw (Waterwet). This resulted in a safety judgement D, meaning that the calculated trajectory failure probability ($> 1 \cdot 10^{-2}$ per year) does not fulfill the lower boundary safety requirement for the trajectory specific ($1 \cdot 10^{-4}$ per year) as stated in the Waterlaw.

The safety judgements for each of the failure mechanisms specific on trajectory scale indicates which failure mechanisms have the most influence in the negative overall safety judgement. For failure mechanism group 1 and 2 (RWS, 2017b) a summarise is given below. As expected for this trajectory the failure mechanism piping ($V I_t$) and macro-stability of the inner slope (V_t) have a high importance in the overall safety judgement (D).

- Macro-stability inner slope (STBI) - $2.3 \cdot 10^{-3}$ per year
- Piping (STPH) - $> 1.0 \cdot 10^{-2}$ per year
- Grass-cover erosion inner slope (GEKB) - $3.0 \cdot 10^{-5}$ per year
- Height of hydraulic structure (HTKW) - $3.3 \cdot 10^{-6}$ per year
- Reliability closing hydraulic structure (BSKW) - $4.0 \cdot 10^{-7}$ per year
- Strength and stability hydraulic structures (STKWp) - $1.8 \cdot 10^{-7}$ per year

Piping

Since piping has the highest failure probability of all failure mechanisms and can be considered as most critical, the assessment of trajectory 48-1 for piping will be discussed using the background report Piping (STPH) (WRIJ, 2018). It is concluded that multiple dike sections along the dike trajectory add to the high trajectory failure probability. This is visualised in figure 5.2 below.



Figure 5.2: Assessment of the failure mechanism piping (STPH) of trajectory 48-1 (WRIJ, 2019)

Piping is calculated following the 'Schematiseringshandleiding Piping 2017' (RWS, 2017c) using the revised Sellmeijer model. Failure of a dike due to internal erosion only occurs if multiple sub-failure mechanisms (uplift, heave and piping) take place. This results in an unstable dike such it loses the water retaining function. This can be schematized as a parallel system where a water pressure difference between the outer- and inner dike water level makes the cohesive cover layer lift and eventually heave such that the water flow underneath the dike driven by the same water pressure difference transports sand grains to the surface. This 'pipe' will continue to grow until the dike settles and a breach occurs. Additional information about this failure mechanism is given in appendix B

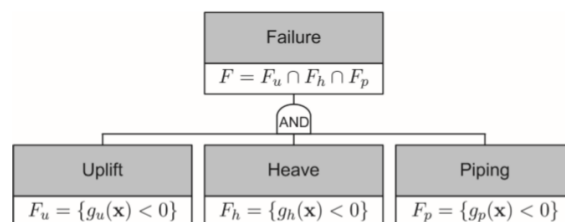


Figure 5.3: Fault tree of the failure mechanism internal erosion (Jonkman et al., 2018)

Parameters

The following spatial parameters are used in the limit state function of the failure mechanism internal erosion (or piping) for the assessment of trajectory 48-1 (WRIJ, 2019).

- Hydraulic Loads (Hydra-NL)
- Subsoil Schematisations (SOS-segments, boreholes and cone penetration tests)
 - Subsoil Parameters (soil investigations, sieve analysis and pumping tests)
- Dike Geometry (AHN-2 and laseraltimetry data)
 - Seepage Length (geophysical research)

Based on the initial assessment of piping in Riskeer using default values for the parameters necessary, an average sectional failure probability larger than 1/300 per year is the result. A sensitivity analysis was performed by varying the seepage length ($L_{seepage}$), permeability of the aquifer (k) and the grain size at the top of the aquifer (d_{70}) (WRIJ, 2019) to increase the accuracy of the assessment.

- Geophysical research at 50 meters from the outer toe of the dike is performed to increase the accuracy of the entry point of the seepage path. This increase in accuracy results in a reduction of the coefficient of variation of the seepage length. However, since the software Riskeer does not allow to make changes to predefined uncertainties the characteristic value of the seepage length is increased by moving the entry points 10 meters outward for all dike profiles.
- Pumping tests have been carried out to increase the accuracy of the bulk permeability of the aquifer underneath the cover layer of the dike. This resulted in a permeability of 75 m/day instead of 100 m/day for several dike sections.
- The grain size of the top of the aquifer is based on sieve analysis of the subsoil. In the final assessment the parameter values for the grain size remained the same according to the initial assessment of piping.

The final flood risk assessment of the failure mechanism piping using more realistic values for the sensitive parameters resulted in failure probabilities that are more representative compared to the case study performed for the 1995 high water situation (WRIJ, 2019). The results are summarized and discussed in chapter 8.

Research Parameters

To carry out the research proposed, all parameters necessary for the assessment of piping are required in a sufficient spatial interval over the length of the trajectory. The result of the initial data analysis is given in table 5.1 (RWS, 2017c) (WRIJ, 2018). The parameters of importance are (Pleijter and Knops, 2019);

- Water level (water level at safety requirement)
- Polder level (minimum of ditch water level and polder surface level)
- Seepage length (difference between entry and exit point)
- Grain size (d_{70} of the top of the aquifer)
- Permeability aquifer
- Thickness aquifer
- Volumetric weight cover layer
- Thickness cover layer

In order to give an indication of the overestimation of the cross-sectional failure probability (sub-research question 1), several piping assessments will be carried out within the identified dike sections compared to the the performed assessments of the dike sections. The available results of the performed assessments are provided in Riskeer by the waterboard (WRIJ, 2019).

The spatial intervals of the research parameters are given in table 5.1. Higher density of data will result in more accurate variograms and autocorrelation functions to determine the length-effect within sections (sub-research question 2).

Furthermore, in order to approximate the mutual dependence between dike sections for the geotechnical failure mechanism piping (sub-research question 3) a study will be performed on the spatial variation of local ground parameters that have most influence in the resistance against piping. For piping the most sensitive parameters to influence the assessment are (Forster et al., 2012);

- Water level
- Seepage length
- Permeability of the sandy aquifer
- Grain size of the sandy aquifer
- Thickness of the cover layer

Parameter	Uplift	Heave	Piping	Model	Source of WRIJ	Spatial Interval
Seepage length ($L_{seepage}$)			X	Stochastic	Geophysical Research	continuous
Entry point (x_{entry})			X	Deterministic	Geophysical Research	continuous
Exit point (x_{exit})			X	Deterministic	AHN-2	continuous
Thickness cover layer (D_{cover})	X	X	X	Stochastic	Site Investigation	$\approx 200m$
Top cover layer ($z_{cover,top}$)	X	X	X	Deterministic	Site Investigation	-
Bottom cover layer ($z_{cover,bottom}$)	X	X	X	Deterministic	Site Investigation	-
Thickness aquifer ($D_{aquifer}$)			X	Stochastic	Site Investigation	$\approx 200m$
Bottom aquifer ($z_{aquifer,bottom}$)			X	Deterministic	Site Investigation	-
Grain size (d_{70})			X	Stochastic	Sieve Analysis	$\approx 400m$
Grain size reference ($d_{70,m}$)			X	Deterministic	Default Risker	-
Volumetric weight cover ($\gamma_{sat,cover}$)	X			Stochastic	Soil Investigation	-
Volumetric weight grains ($\gamma_{sat,grains}$)			X	Deterministic	Default Risker	-
Permeability aquifer (k)			X	Stochastic	Pumping Tests	$\approx 10km$
Polder level (h_{exit})	X	X	X	Stochastic	AHN-2	continuous
Water level (h)	X	X	X	Stochastic	Hydra-NL	$\approx 120m$
Water level gradient ($h(t)$)	X	X	X	Deterministic	Helpdesk Water	-
Volumetric weight water (γ_{water})	X		X	Deterministic	Default Risker	-
Water pressures aquifer (ϕ_x)	X	X		Deterministic	Helpdesk Water	-
Leakage length (λ)	X	X		Stochastic	Pumping Tests	-
Damping factor (r_{exit})	X	X		Stochastic	Default Risker	-
Reduction factor (r_c)			X	Deterministic	Default Risker	-
Model factors (m_u, m_p)	X		X	Stochastic	Default Risker	-
Critical heave gradient ($i_{c,h}$)		X		Stochastic	Default Risker	-
Coefficient of White (η)			X	Deterministic	Default Risker	-
Internal friction angle (θ)			X	Deterministic	Default Risker	-

Table 5.1: Data analysis of the failure mechanism internal erosion (or piping)

Geophysical research is performed continuously along the length of the trajectory to identify the entry points and making the seepage length more accurate. Next to the existing site investigation data, additional site investigation is performed (90 cone penetration tests and 49 boreholes) to make the geotechnical length profile more accurate and making the thickness of the cover layer and aquifer more accurate. Based on several of these boreholes, sieve analysis is performed on samples of the top of the aquifer to identify the grain size (d_{70}) to make the standard grain size more specific. Three pumping tests are performed within the trajectory to identify the bulk permeability of the aquifer and so make the standard permeability more specific.

Dike Sections

The division of dike sections of trajectory 48-1 is based on clear changes in dike geometries (ground level at exit points of seepage water), seepage lengths (entry and exit lines of seepage water), SOS segments (stochastic subsurface classification) and grain sizes (underneath the cover layer). This led to the identification of 43 dike sections. Of the 43 dike sections 33 are taken into account for the assessment of the probability of failure since the other dike sections contains specific structures which prevent the occurrence of the failure mechanism internal erosion.

Part II

Data Analysis

Chapter 6

Data Analysis

To answer the research questions, spatial data of the parameters required for the piping assessment is obtained in order to compute the failure probability along the trajectory for small spatial intervals. A detailed example is given for section 139+090 - 155+000 of trajectory 48-1. Note that the lay-out of all figures in this chapter is from upstream (left) to downstream (right).

6.1 Water level

The hydraulic loads, or water levels, are available in the hydraulic load data base (Hydra-NL) from the government. At 257 points along the trajectory the water levels at multiple return periods ($>1/10$) are available. Water levels with a return period of 30.000 years (safety level) are given in figure 6.1. Using linear interpolation between the Hydra-NL points the water levels at every 10 meters are obtained. The water levels for each dike section is chosen as the nearest hydraulic load data base point to the chosen normative cross-section of the section. Comparing the sectional data in red with the interpolated data in black in figure 6.1 it is concluded that a linear interpolation between the hydraulic load data base points is a good approximation.

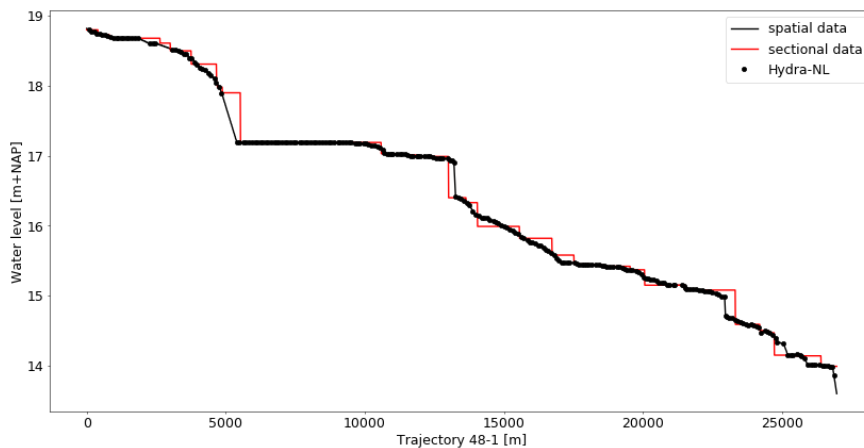


Figure 6.1: Water level trajectory 48-1 (*WBI2017-Bovenrijn- 48-1-v03*)

Detail: 15 hydraulic load data base points are located along section 139+090 - 155+000 as indicated in figure 6.2. Using linear interpolation values are obtained every 10 meters.

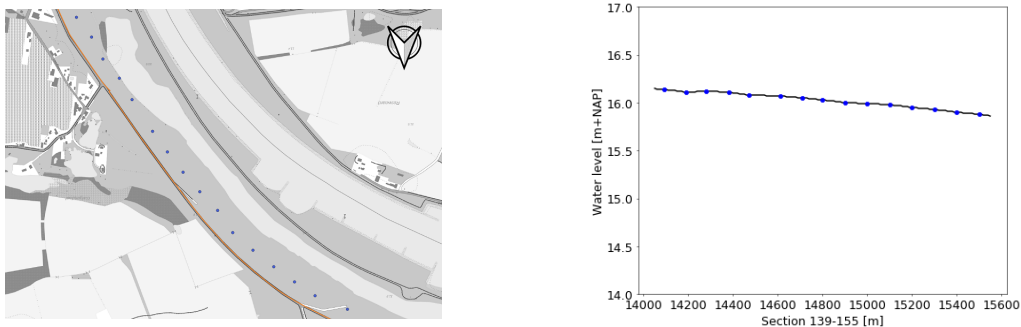


Figure 6.2: Water level detail section 139+090 - 155+000

6.2 Seepage length

The seepage length along the trajectory is determined using the predicted entry and exit lines (of seepage water) provided by the waterboard. The entry line is based on geophysical research over 50 meters from the outer toe of the dike along the stretch of the dike trajectory. The entry line is placed as far as possible to the river side fulfilling the requirement of 1.5m thick clay coverage over a distance of 100m parallel to the dike. The outer toe of the dike is chosen if there is less clay coverage outside the dike area. The exit line is chosen at the inner toe of the dike and adjusted for locations with for example approaching berms or seepage ditches. Using station lines perpendicular to the crest of the dike with a spacing of 10 meters the seepage length is determined as the distance between the intersections with the entry and exit line. At four sharp turns in the dike trajectory the perpendicular approximation is not correct and is adjusted to a shortest distance approximation.

The waterboard derived the seepage length for each section by taking the seepage length at the normative cross-section within the section. Note that the normative cross-section is chosen based on the median seepage length within the section and if necessary changed for a more critical combination of seepage length and ground level at the exit point of seepage water.

Comparing the sectional data in red with the computed data in black in figure 6.3 it is concluded that at most sections the initial seepage length (median value of section) is adjusted for a more critical combination with a smaller seepage length.

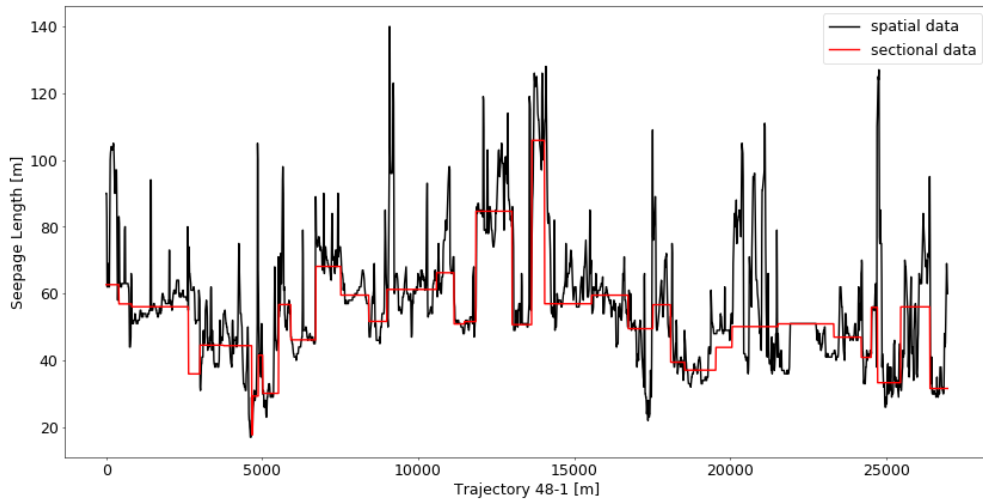


Figure 6.3: Seepage length trajectory 48-1

Detail: at every 10 meters along section 139+090 - 155+000 the entry, exit and crest line are known as indicated in figure 6.4. Using station lines the seepage lengths are obtained at a spatial interval of 10 meters.

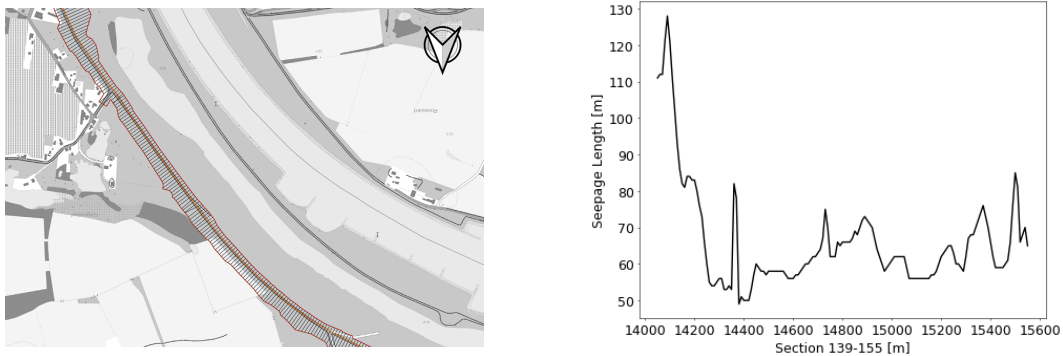


Figure 6.4: Seepage length detail section 139+090 - 155+000

6.3 Ground level

The ground level at the exit point (of seepage water) along the trajectory is determined using the intersections of the station lines with the exit line every 10 meters. Using point sampling with the AHN3 raster layer (dtm) the height at every exit point can be obtained. The dtm data base is used to filter out trees present around the inner toe of the dike.

Note that the exit line is validated by comparing the ground level at the exit point with the minimum ground level value along the according station line from crest to exit point. The waterboard derived the ground level for each section by taking the ground level at the exit point of the normative cross-section within the section. Note that the normative cross-section is chosen based on the median seepage length within the section and if necessary changed for a more critical combination of seepage length and ground level at the exit point.

Comparing the sectional data in red with the computed data in black in figure 6.5 it is concluded that at most locations the ground level is close to the smallest ground level within the section. This is a result of choosing a normative cross-section for a critical combination of seepage length and ground level.

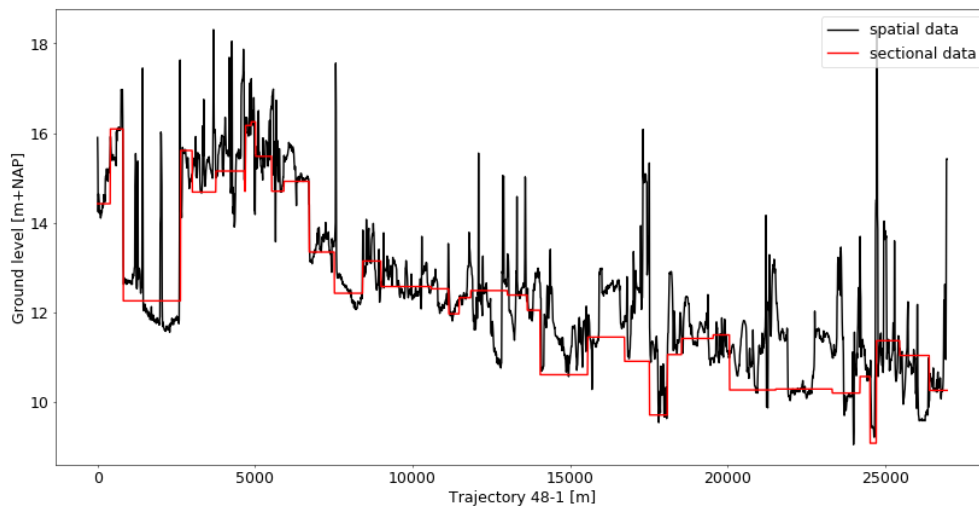


Figure 6.5: Ground level trajectory 48-1

Detail: at every 10 meters along section 139+090 - 155+000 the ground level from crest to exit point is known as indicated in figure 6.6. Using the minimum ground level along the station lines and the ground level at the exit point the ground level is obtained at a spatial interval of 10 meters

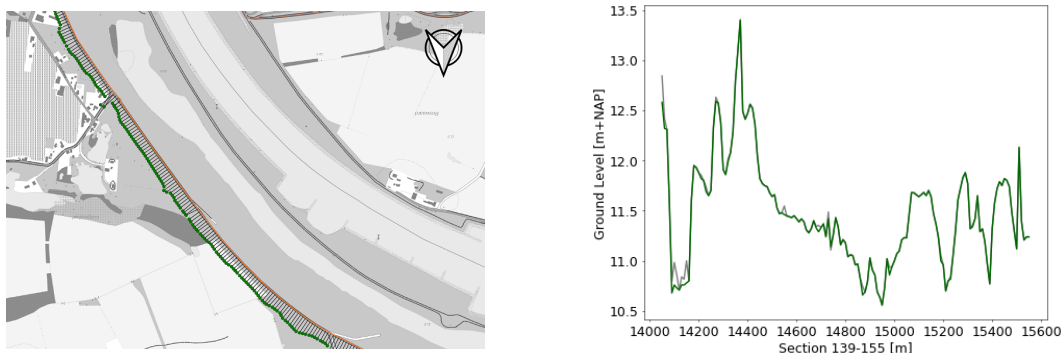


Figure 6.6: Ground level detail section 139+090 - 155+000

6.4 Polder level

The polder level, or ground water level, along the trajectory is determined using the ground level at the exit points along the trajectory. The polder level is determined as the minimum ground level over a distance of 50 meters parallel to the dike assuming a saturated polder due to rainfall and seepage during high water. Note that taking the minimum ground level over 50 meters gives a first approximation of the ground water level by filtering major ground surface elevations. Furthermore, this first approximation is corrected using a simple 'elevation' model which compares the ground levels at the intersections of the station lines with the exit line and a parallel line to the exit line at a distance of 25 meters outward. Comparing both lines indicates locations with approaching berms or seepage ditches such polder levels are decreased or increased to fulfill the assumption of a saturated polder. These adjustments are clearly visible at intervals with relative constant polder levels.

The waterboard derived the polder level for each section by taking the ground level at the exit point of the normative cross-section within the section under the assumption of a fully saturated polder due to rainfall and seepage. This assumption is supported by comparing the rainfall to the water levels during high water events in appendix C.

Comparing the sectional data in red with the spatial data in black in figure 6.7 it is concluded that at most locations the polder level is close to the lowest ground level of the section. This results from choosing a normative cross-section for a critical combination of seepage length and ground level.

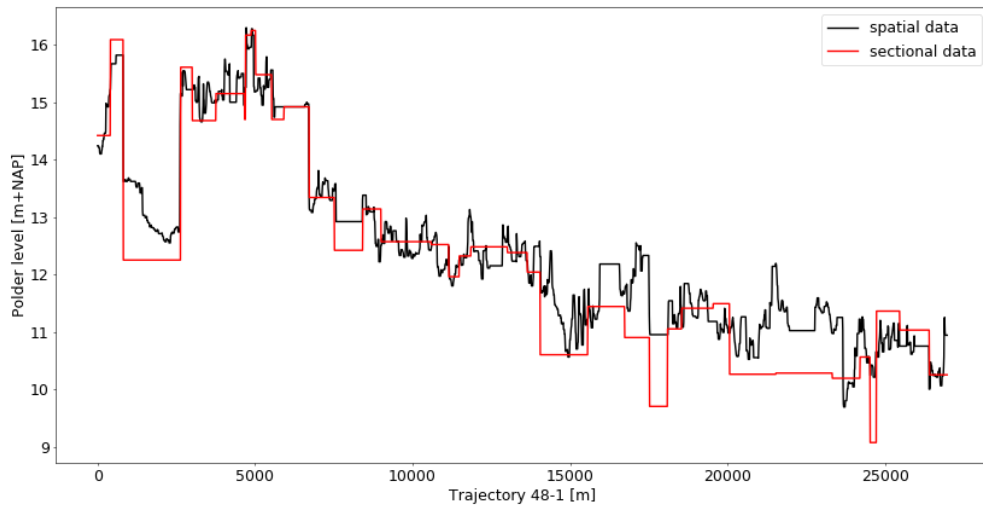


Figure 6.7: Polder level trajectory 48-1

Detail: at every 10 meters along section 139+090 - 155+000 the ground water level is obtained at a spatial interval of 10 meters by comparing the ground level at the exit line and 25 meters parallel to the exit line. For this section specific the polder level is increased for a seepage ditch at 14.1km as indicated in figure 6.8

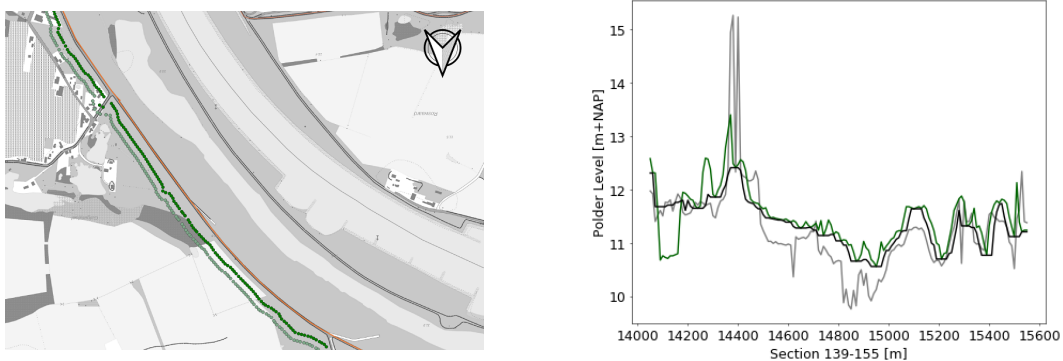


Figure 6.8: Polder level detail section 139+090 - 155+000

6.5 Cover layer

The cover layer thickness is calculated as the difference between the ground level and the bottom level of the clay layer at every 10 meters. In order to find the most likely bottom levels of the clay layer all available CPT data is used in a kriging interpolation (Baecher and Christian, 2019) to derive the bottom level of the clay layer along the trajectory. The theory behind this kriging interpolation technique is given in appendix D.

The waterboard derived the bottom of the clay layer from CPT data from the inner toe and hinterland along the trajectory in relation to the SOS segments. One, two or three scenarios with according probability of occurrence are chosen for each section. The thickness of the cover layer for each of these scenarios are computed as the difference with the ground level of the according section.

Comparing the sectional data in red (minimum and maximum scenario) with the computed data in black in figure 6.9 it is concluded that a kriging interpolation between the CPT data points is a good approximation for the bottom of the clay layer. However a clear difference is visible over an interval 4-8 kilometers. Based on only the CPT data at the inner toe no significant change is observed to change this interpolation.

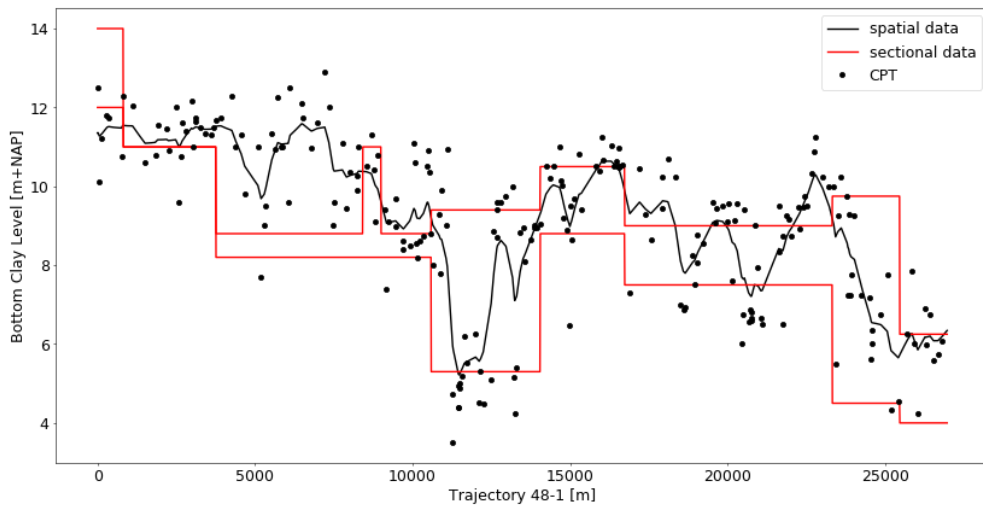


Figure 6.9: Bottom level clay layer trajectory 48-1

Detail: 14 data base points from the Dino Loket are located along section 139+090 - 155+000 as indicated in figure 6.10. From the kriging interpolation values are obtained at a spatial interval of 10 meters. Subsequently the cover layer thickness is obtained as the difference with the ground level at the exit point

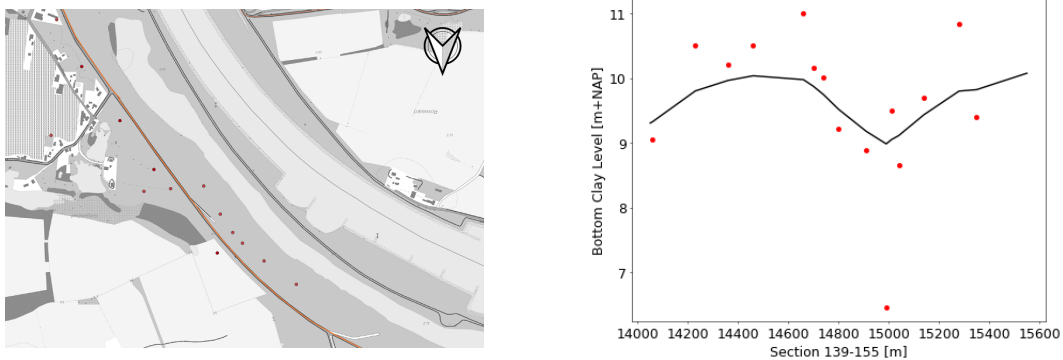


Figure 6.10: Bottom level clay layer detail section 139+090 - 155+000

An additional result of the kriging interpolation, next to the most likely spatial values, is the local standard deviation in relation to the overall standard deviation of the dataset. Note that the 95% confidence interval of figure 6.11 is a confidence interval related to the local mean and standard deviation of the point estimate and not related to the total dataset. In comparison to the default standard deviation of 0.5 obtained by expert judgements the local standard deviation along the trajectory is between 0.5 and 0.8 meters. This is visualised in figure 6.12.

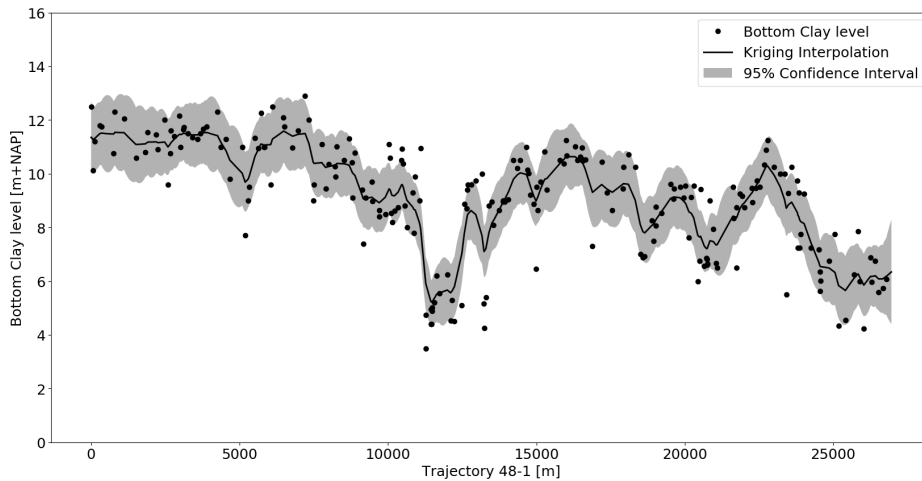


Figure 6.11: Kriging interpolation of the bottom clay level trajectory 48-1

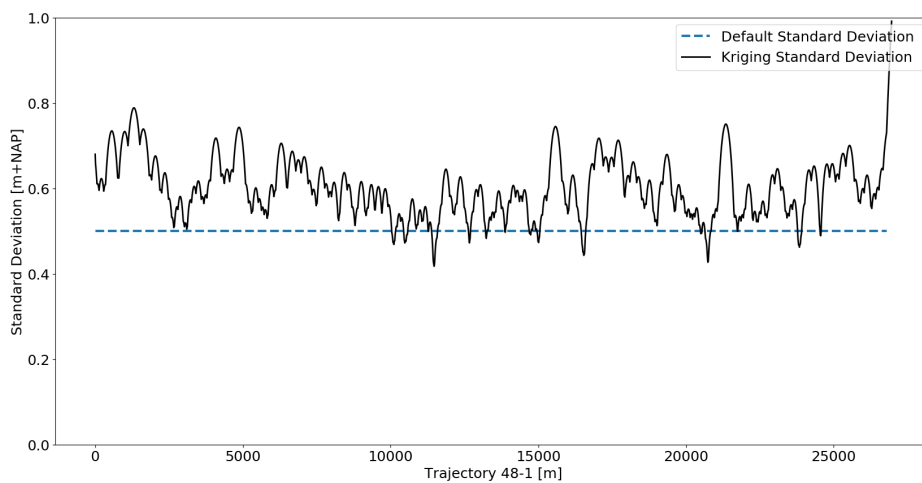


Figure 6.12: Standard deviation of the bottom clay level trajectory 48-1

6.6 Aquifer layer

The aquifer layer thickness is calculated as the difference between the bottom level of the clay layer and the bottom level of the sand layer. In order to find the most likely bottom level of the aquifer layer all available data from the REGIS II model is used to obtain the bottom level of the aquifer layer every 10 meters. The results from the REGIS II model are given in appendix C.

The waterboard derived the bottom of the sand layer from the SOS segments. One, two or three scenarios with according probability of occurrence are chosen for each of the sections. The thickness of the aquifer layer for each of these scenarios are computed as the difference with the bottom clay level of the according scenario and section.

Comparing the sectional data in red (minimum/maximum scenario) with the computed data in black in figure 6.13 it is concluded that the REGIS II data is a good approximation for the bottom of the sand layer.

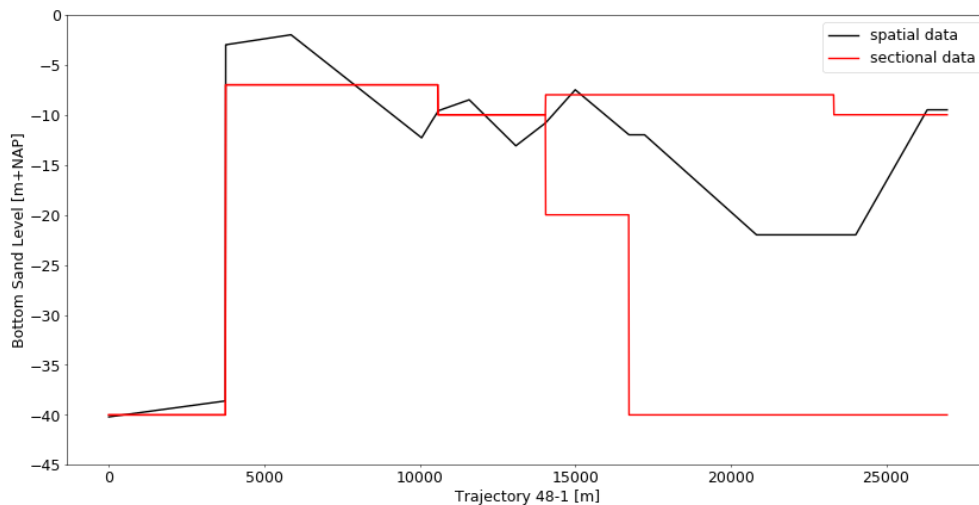


Figure 6.13: Bottom level aquifer layer trajectory 48-1

Detail: no specific data points from the Dino Loket are located along section 139+090 - 155+000 as indicated in figure 6.14. Using the REGIS II interpolation values are obtained at a spatial interval of 10 meters

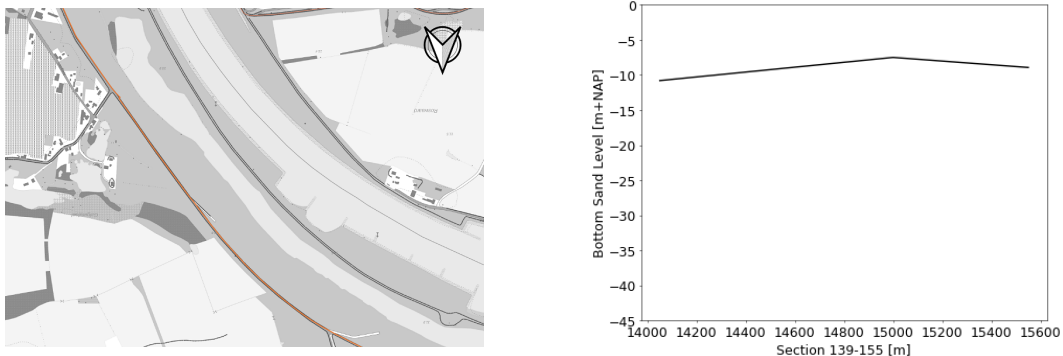


Figure 6.14: Bottom level aquifer layer detail section 139+090 - 155+000

6.7 Grain size

The grain size (d_{70}) is determined from sieve analyses performed on behalf of the waterboard. The grain size is determined at several depths from the ground level and only the grain sizes in an interval of approximate 4 meters underneath the derived bottom level of the clay layer are taken into account. The parameter of interest (d_{70}) is the 70%-quantile (mass) of the grain size distribution. In order to find the most likely grain size along the trajectory the representative grain size data is used in a kriging interpolation (Baecher and Christian, 2019) to derive the most likely d_{70} at every 10 meters. The theory behind this kriging interpolation technique is given in appendix D.

The waterboard derived the grain size from sieve analyses of samples by taking the average grain size over the defined segments the representative grain size for each section is determined.

Comparing the sectional data in red with the computed data in black in figure 6.15 it is concluded that a kriging interpolation between the sieve analysis data points is a good approximation for the representative grain size.

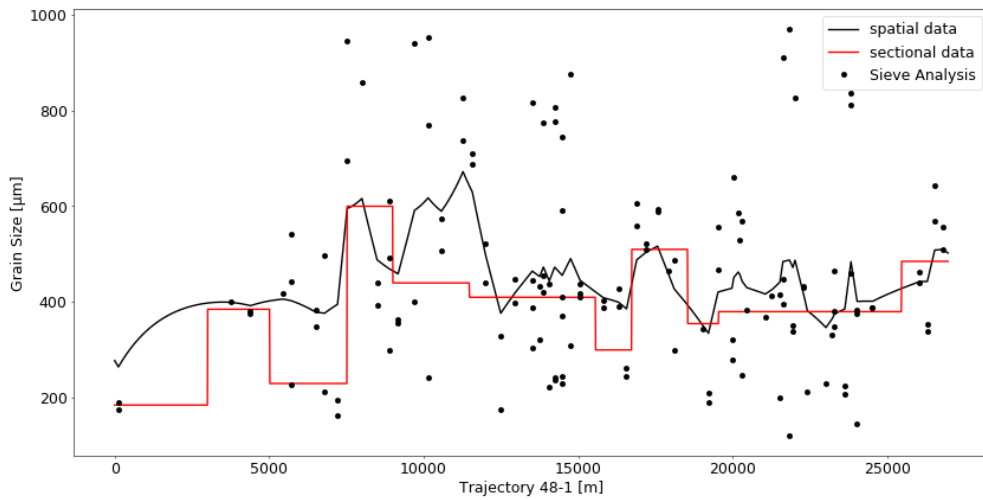


Figure 6.15: Grain size trajectory 48-1

Detail: 16 data points from the sieve analyses are located along section 139+090 - 155+000 as indicated in figure 6.16. From the kriging interpolation values are obtained at a spatial interval of 10 meters

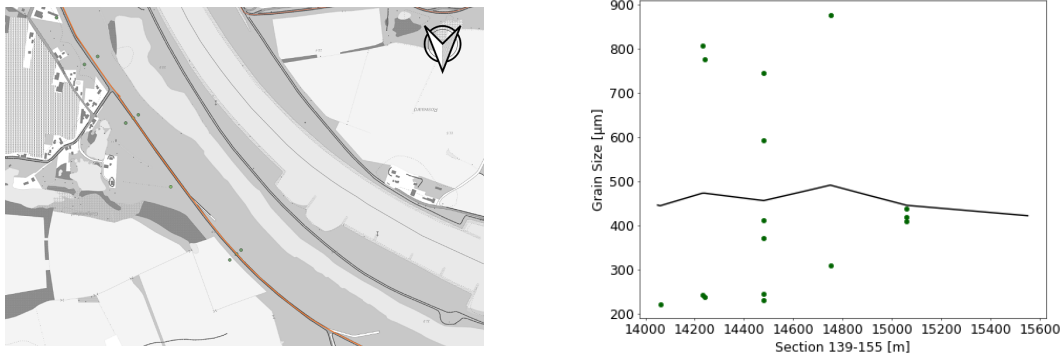


Figure 6.16: Grain size detail section 139+090 - 155+000

An additional result of the kriging interpolation, next to the most likely local values, is the local coefficient of variation in relation to the overall coefficient of variation of the dataset. Note that the 95% confidence interval of figure 6.17 is a confidence interval related to the local mean and standard deviation of the point estimate and not related to the total dataset. In comparison to the default coefficient of variation of 0.12 derived from expert judgements the local coefficient of variation along the trajectory is between 0.1 and 0.3. This is visualised in figure 6.18.

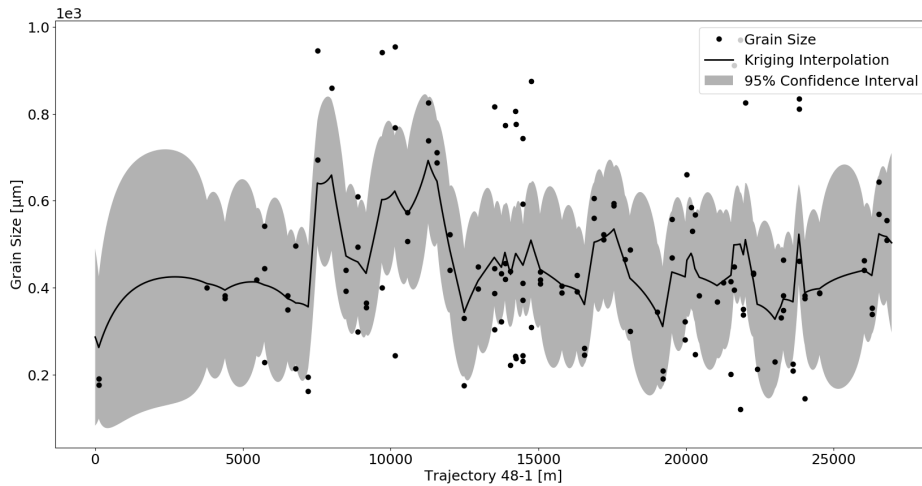


Figure 6.17: Kriging interpolation of the grain size trajectory 48-1

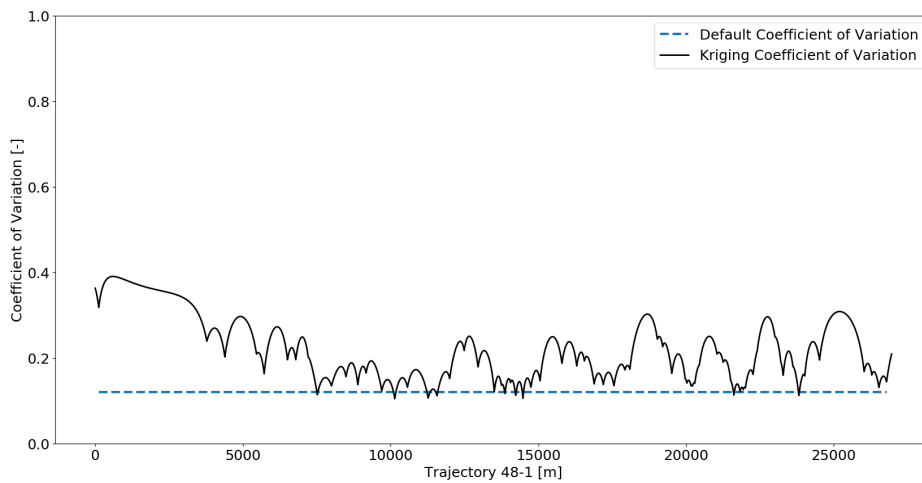


Figure 6.18: Coefficient of variation of the grain size trajectory 48-1

6.8 Permeability

The permeability is determined from sieve analyses performed on behalf of the waterboard. Using the representative grain size data (d_{70}) and the available coefficient of uniformity (C_u) the permeability is approximated using the Den Rooijen equation (Forster et al., 2012).

$$d_{10} = 0.9 \cdot \frac{d_{70}}{C_u} \quad (6.1)$$

$$k = (1.5 \cdot 10^{-4} - 1.83 \cdot 10^3 \cdot \ln(C_u)) \cdot d_{10}^2 \quad (6.2)$$

In order to find the most likely permeability the representative grain size data with a known coefficient of uniformity is used in a kriging interpolation (Baecher and Christian, 2019) to derive the permeability every 10 meters. The theory behind this kriging interpolation technique is given in appendix D. Note that at locations with unknown coefficient of uniformity no permeability could be approximated. This approximation is compared to the results of the three pumping tests performed.

The waterboard derived the permeability of the aquifer along the trajectory from the SOS segments and adjusted these initial default values using the results of three pumping tests. Pumping tests give a good indication of the bulk permeability of the aquifer layer in comparison to the spatial specific permeabilities resulting from the Den Rooijen equation given in 6.2.

Comparing the sectional data in red with the computed data in black and the pumping tests in blue in figure 6.19 it is concluded that a kriging interpolation between the computed permeability points is a good approximation for the representative permeability.

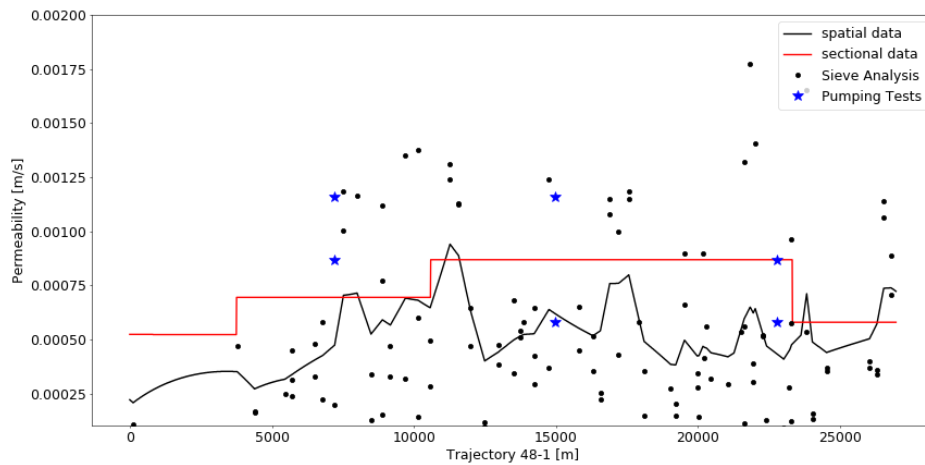


Figure 6.19: Permeability trajectory 48-1

Detail: 5 data points from the sieve analyses with a coefficient of uniformity are located along section 139+090 - 155+000 as indicated in figure 6.20. From the kriging interpolation values are obtained at a spatial interval of 10 meters. The results are compared to the boundaries of a pumping test performed within this dike section which are indicated in blue.

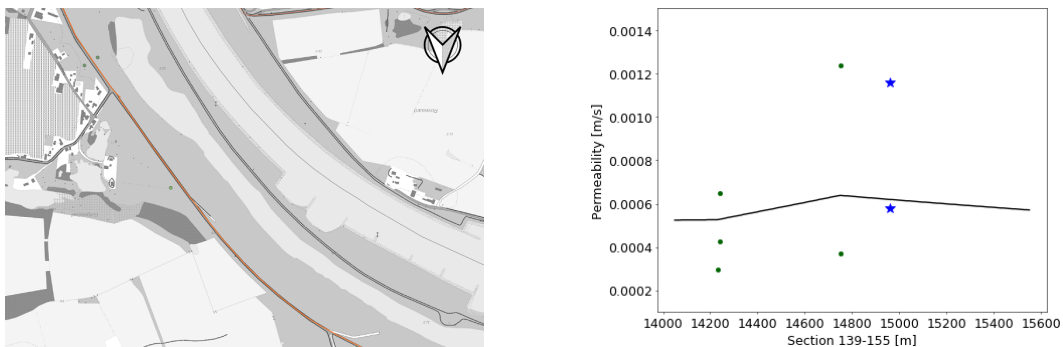


Figure 6.20: Permeability detail section 139+090 - 155+000

An additional result of the kriging interpolation, next to the most likely local values, is the local coefficient of variation in relation to the coefficient of variation of the dataset. Note that the 95% confidence interval of figure 6.11 is a confidence interval related to the local mean and standard deviation of the point estimate and not related to the total dataset. In comparison to the default coefficient of variation of 0.5 derived from expert judgements the local coefficient of variation along the trajectory is between 0.2 and 0.6. This is visualised in figure 6.22.

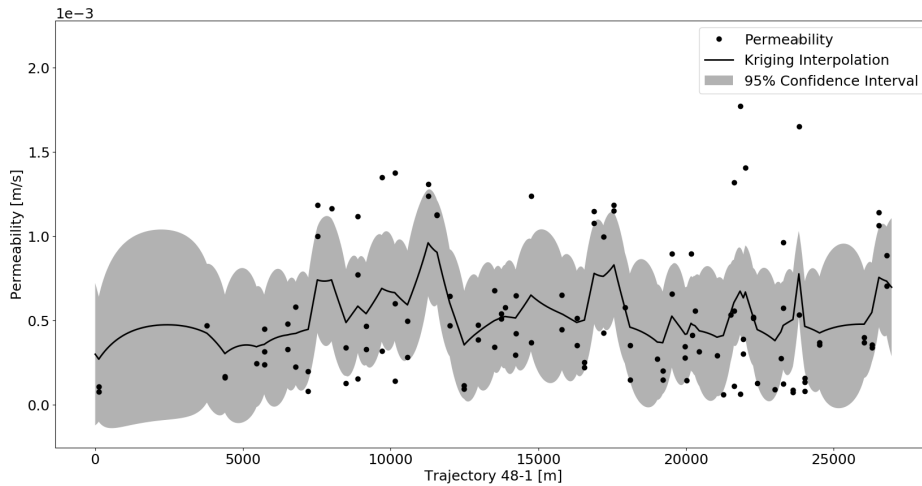


Figure 6.21: Kriging interpolation of the permeability trajectory 48-1

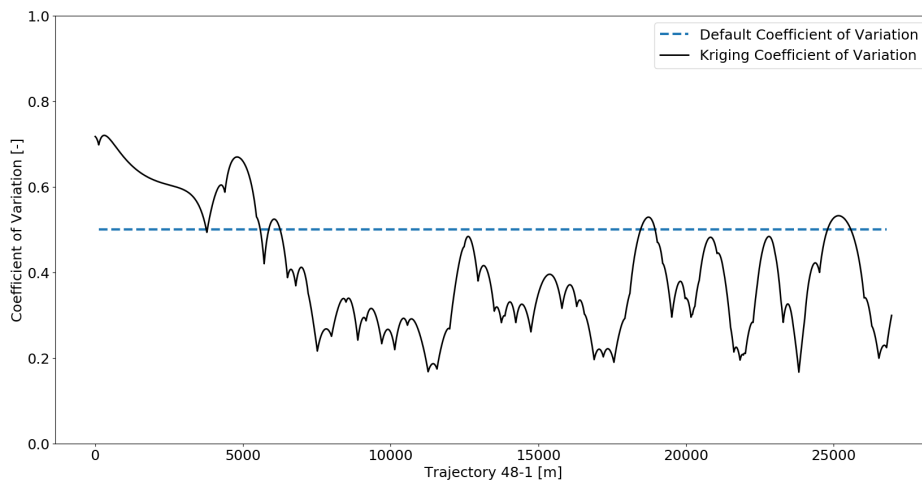


Figure 6.22: Coefficient of variation of the permeability trajectory 48-1

6.9 Volumetric weight

The volumetric weight along the trajectory is not obtained in a smaller spatial interval than provided by the waterboard since the resolution of the data is too low. The data used is based on laboratory research and default parameters. The minimum value along the trajectory is chosen to be representative.

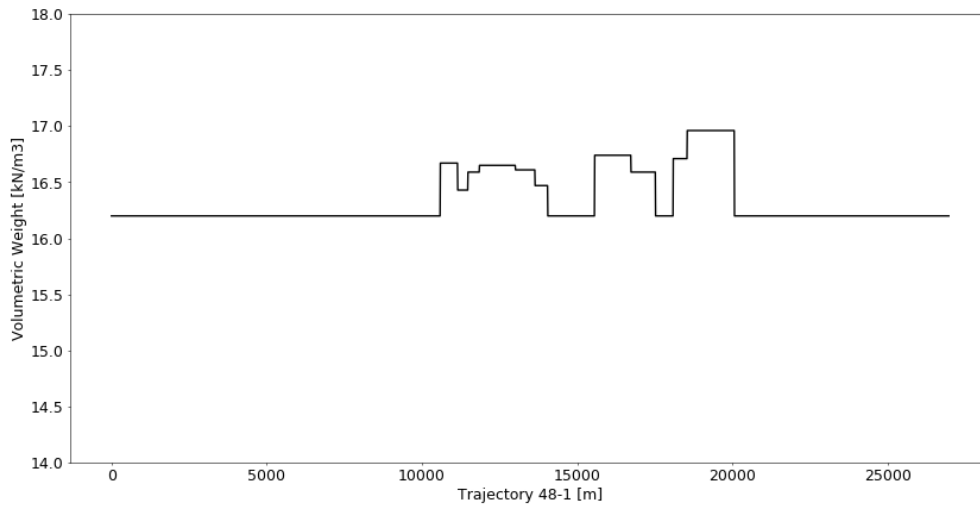


Figure 6.23: Volumetric weight trajectory 48-1

6.10 Reduction factor

The reduction factor along the trajectory is not adjusted from the data provided by the waterboard. The reduction factor is assumed to be equal to the default value.

Part III

Reliability Analysis

Chapter 7

Reliability Analysis

The failure probability of the failure mechanism piping is calculated following the 'Schematisering-shandleiding Piping 2017' (RWS, 2017c) using the revised Sellmeijer model. Failure of a dike due to internal erosion can only occur if multiple sub-failure mechanisms take place. These sub-failure mechanisms Uplift, Heave and Piping should all occur in order to make the dike unstable such it loses the water retaining function. This can be schematized as a parallel system where a water pressure difference between the outer- and inner dike water levels makes the cohesive cover layer lift and eventually heave such that the resulting water flow underneath the dike driven by the same water pressure difference transports sand grains to the surface. This 'pipe' will continue to grow backward until the dike settles and a breach occurs due to overflow. The limit state functions of Uplift, Heave and Piping are given in appendix B.

The calculation of the cross-sectional failure probabilities using the legal assessment for the geotechnical failure mechanisms is currently based on a Level I method (semi-probabilistic). The stochastic parameters are included as characteristic values. In a level II method (probabilistic) stochastic parameters are included with their mean and standard deviation, and with the correlation between the stochastic variables. The theory behind the First Order Reliability Method (FORM) is given in appendix E. Note that the choice of reliability method, normative cross-section and stochastic parameters results in different cross-sectional failure probabilities.

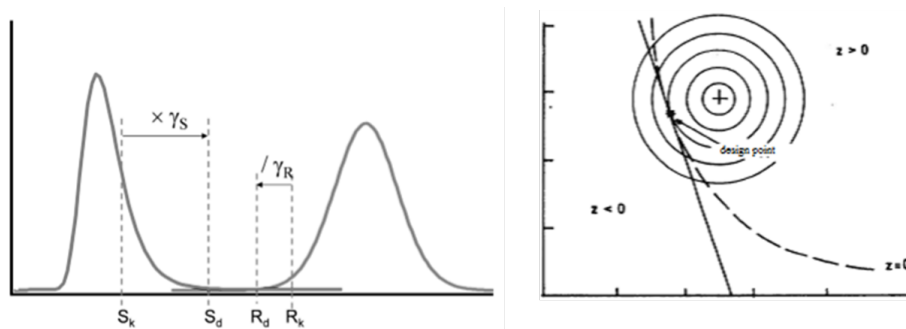


Figure 7.1: Level I and Level II (FORM) reliability methods

In section 7.1 a semi-probabilistic assessment will be performed based on the spatial parameters and standard deviations from the data analysis. This will be compared to a semi-probabilistic assessment using default standard deviations according to the WBI 2017. Furthermore, in section 7.2 a probabilistic assessment will be performed based on the spatial parameters and standard deviations from the data analysis. This will be compared to a probabilistic assessment using default standard deviations according to the WBI 2017. Finally, in Chapter 8 a comparison will be made with the sectional failure probabilities reported by the waterboard (WRIJ, 2018).

7.1 Semi-Probabilistic Method

In a semi-probabilistic approach, characteristic values should be used in the limit state functions for the stochastic variables. The derived spatial parameters along the trajectory are used as mean values in a predefined distribution with standard deviation (SD) or coefficient of variation (CV) conform Table 2.2 of the 'Schematiseringshandleiding Piping 2017' (RWS, 2017c). For load parameters an upper limit (95%) and for resistance parameters a lower limit (5%) is derived from these distributions (level I). Deterministic values applied in the limit state function are adopted from Appendix C of the 'Schematiseringshandleiding Piping 2017' (RWS, 2017c).

Semi-probabilistic calculations are performed at a spatial interval of 10 meters along trajectory 48-1. In order to make a reliable comparison with the sectional failure probabilities of the waterboard the same predefined distributions are applied for the stochastic variables. Besides, the same values are used for the deterministic variables. Note that the entry line of seepage water is determined accurately by geophysical research and gives a realistic approximation. Based on this research the waterboard concluded that the predefined standard deviation on the seepage length can be reduced. *Since the software Riskeer, used by the waterboard, does not allow this computation the waterboard increased the sectional seepage length with 10 meters in order to increase the characteristic value following from the lower limit.* This same approach has been applied to obtain the spatial failure probability every 10 meters. In comparison, reducing the predefined standard deviation of the seepage length from 0.1 to 0.01 has almost the same effect.

- Seepage length (CV) = 0.1 (*shift of 10*)
- Polder level (SD) = 0.1
- Grain size aquifer (CV) = 0.12
- Cover thickness (SD) = 0.5
- Aquifer thickness (SD) = 0.5
- Permeability aquifer (CV) = 0.5
- Volumetric weight cover (SD) = 0.9 (*shift of 10*)
- Reduction factor (SD) = 0.1

Next to the predefined standard deviations and coefficients of variation as listed above, uncertainty parameters are derived from the data analysis. The spatial uncertainties of the cover layer, grain size and permeability are already discussed and visualised in figures 6.12, 6.18 and 6.22. The coefficient of variation of the seepage length is already reduced based on geophysical research by the waterboard and will only be reduced by a factor 2 based on the reduced spatial interval. The standard deviation of the polder level is reduced by the same factor 2 based on the reduced spatial interval. The aquifer thickness from REGISS II includes certain uncertainty because the bottom level of the aquifer is quite uncertain. Since an upper level is chosen with the interpolation the standard deviation is reduced to 0.3. Since no additional information is available on the volumetric weight and reduction factor, the standard deviations remain unchanged.

- Seepage length (CV) = 0.05 (*shift of 10*)
- Polder level (SD) = 0.05
- Grain size aquifer (CV) - figure 6.18
- Cover thickness (SD) - figure 6.12
- Aquifer thickness (SD) = 0.3
- Permeability aquifer (CV) - figure 6.22
- Volumetric weight cover (SD) = 0.9 (*shift of 10*)
- Reduction factor (SD) = 0.1

Finally, the spatial semi-probabilistic failure probability based on default and field related standard deviations can be compared to the sectional failure probability reported by the waterboard Rijn & IJssel (WRIJ, 2018) in figures 7.2 and 7.3. *Note that for two dike sections the reported sectional failure probability of the waterboard is adjusted due to an error in the Riskeer software for cover layers with a value of zero resulting in infinitely small failure probabilities in the specific scenarios.*

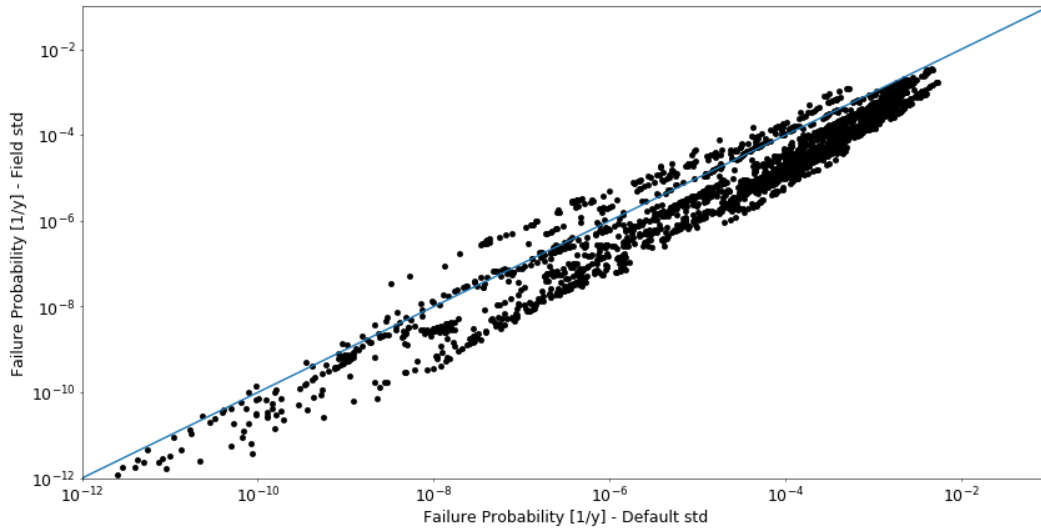


Figure 7.2: Semi-Probabilistic assessment trajectory 48-1 (σ_{field} versus $\sigma_{default}$)

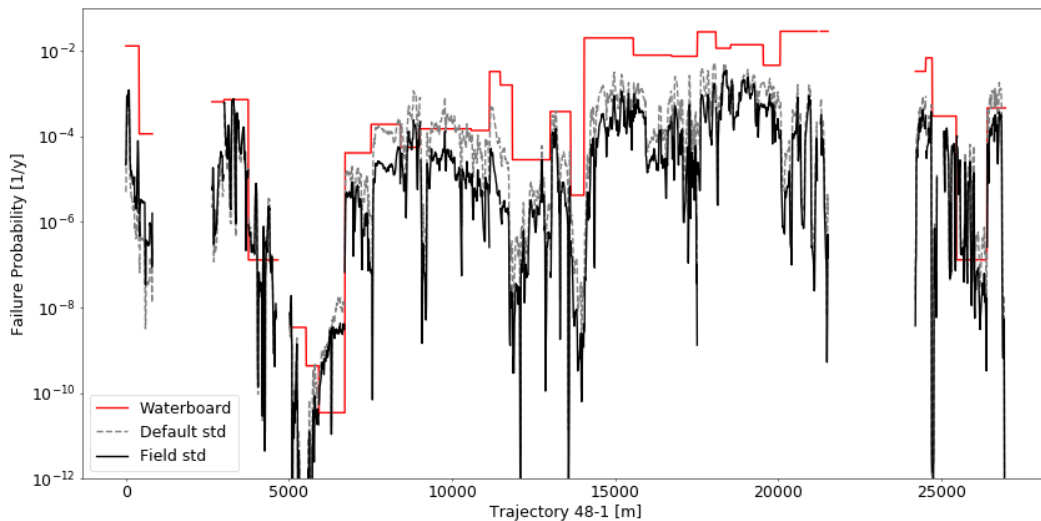


Figure 7.3: Semi-Probabilistic assessment trajectory 48-1 (spatial results versus sectional results)

Comparing the semi-probabilistic results with default uncertainties from the WBI and uncertainties from the data analysis, it is concluded that for most locations, especially the locations in the high failure domain, the failure probabilities reduces by taking field related uncertainties into account at small spatial intervals. Comparing the sectional failure probability from the waterboard in red with the computed spatial failure probability in black (default std) and grey (field std), it is concluded that at most sections certain conservatism is applied. At three of the 33 dike sections a certain underestimation of the failure probability is visible. In the next chapter these results will be discussed in detail.

7.2 Probabilistic Method

In a probabilistic approach, the distributions of the stochastic variables are used to evaluate the limit state functions. The derived spatial parameters along the trajectory serve as mean values in a predefined distribution with standard deviation (SD) or coefficient of variation (CV) conform Table 2.2 of the 'Schematiseringshandleiding Piping 2017' (RWS, 2017c). The propagation of stochastic variables to compute the failure probability can be done by a Monte Carlo approach (level III) or a First Order Reliability Method (level II). Note that in a semi-probabilistic approach the outside water level is considered as a deterministic value (water level at safety level) and in a probabilistic approach the outside water level needs to be included as a distribution (Gumbel or Student-t) or with fragility curves (combining conditional failure probabilities with water level probabilities).

Probabilistic calculations are performed at 272 Hydra-NL locations along trajectory 48-1. The water level statistics from Hydra-NL are used to fit distributions (Gumbel and Student-t) to the tail as shown in figure 7.4. In combination with strength parameters from field observations and interpolation techniques the probabilistic assessment is performed using the revised Sellmeijer model.

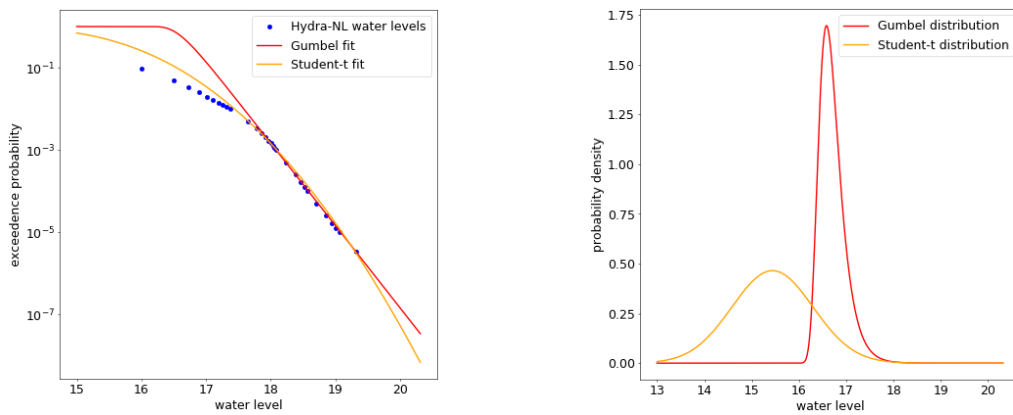


Figure 7.4: Water level distributions from Hydra-NL data-points

Furthermore, a probabilistic assessment is performed using fragility curves as shown in figure 7.5. From the water level statistics of Hydra-NL the probability of a water level is known. The conditional probability of failure is derived from a probabilistic calculation given a certain water level. Finally, the product gives the failure distribution which is integrated to obtain the failure probability.

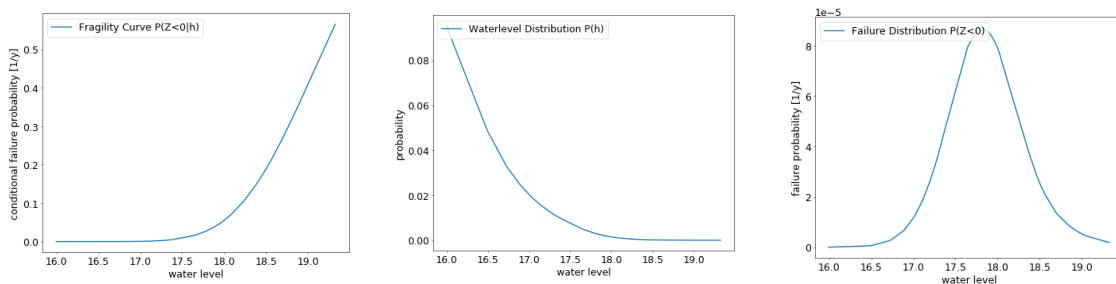


Figure 7.5: Fragility Curve approach using Hydra-NL data-points

The results from the FORM analysis are visualised for these three different approaches (Gumbel, Student-t, Fragility Curve) in figure 7.6. In order to make a reliable comparison with the sectional failure probabilities of the waterboard the same predefined distributions are applied for the (sub)surface stochastic variables. Besides the same values are used for the deterministic variables. Note that the entry line of seepage water is determined accurately by geophysical research and gives a realistic approximation. Based on this research the waterboard concluded that the predefined standard deviation on the seepage length can be reduced. *Since the software Riskeer, used by the waterboard, does not allow this computation the waterboard increased the sectional seepage length with 10 meters in order to increase the characteristic value following from the lower limit.*

In order to get realistic results from the probabilistic assessments, initial correlations between several stochastic variables are assumed. High permeabilities occur with large grain sizes ($\rho_{k,d70}$ of 0.7) (Aguilar Lopez et al., 2015) and high polder levels occur with high river levels (ρ_{h_w,h_p} of 0.5).

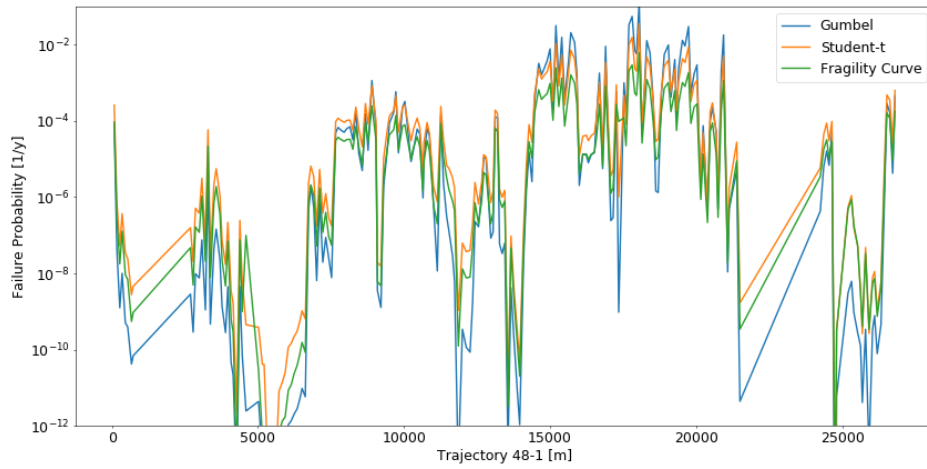


Figure 7.6: Probabilistic assessment trajectory 48-1 (distribution and fragility curve)

Comparing these probabilistic results with the semi-probabilistic results conform the WBI 2017, it is clear that the probabilistic approaches using water level distributions overestimate the probabilities at relative high failure probability locations compared to the approach using fragility curves. Furthermore, the semi-probabilistic approach results in higher failure probabilities than the probabilistic approach using fragility curves which is a result from applying the calibration formula.

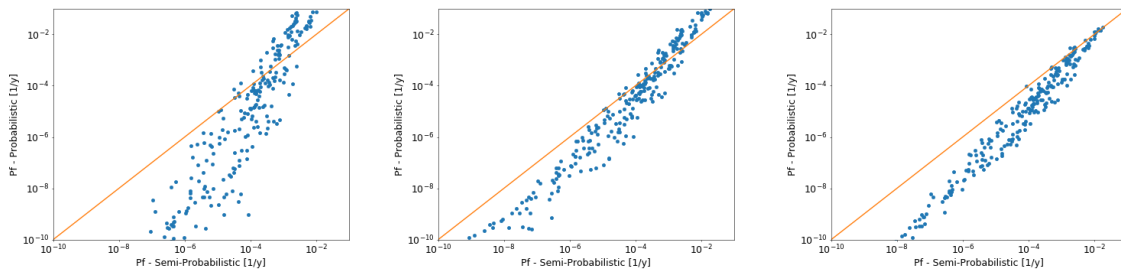


Figure 7.7: Semi-Probabilistic versus Probabilistic (Gumbel - Student-t - Fragility Curves)

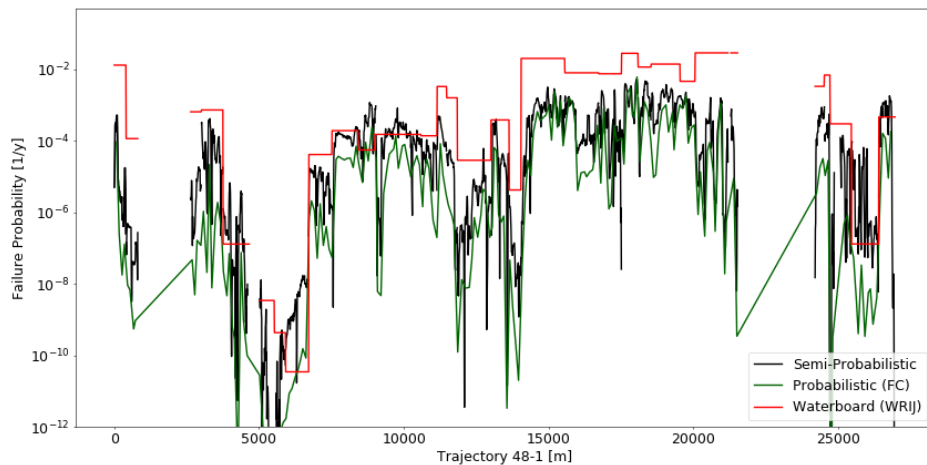


Figure 7.8: Comparison of probabilistic methods trajectory 48-1 (spatial versus sectional)

Next to the predefined standard deviations and coefficients of variations, uncertainty parameters are derived from the data analysis. The spatial uncertainties of the cover layer, grain size and permeability are already discussed and visualised in figures 6.12, 6.18 and 6.22. The coefficient of variation of the seepage length is already reduced based on geophysical research by the waterboard and will not be reduced further based on the spatial interval. The standard deviation of the polder level is not reduced based on the spatial interval. The aquifer thickness from REGISS II includes certain uncertainty because the bottom level of the aquifer is a quite uncertain level. Since an upper level is chosen in the interpolation the standard deviation is reduced to 0.3. No additional information is available of the volumetric weight and reduction factor, the standard deviations remain unchanged.

- Seepage length (CV) = 0.1 (*shift of 10*)
- Polder level (SD) = 0.1
- Grain size aquifer (CV) - figure 6.18
- Cover thickness (SD) - figure 6.12
- Aquifer thickness (SD) = 0.3
- Permeability aquifer (CV) - figure 6.22
- Volumetric weight cover (SD) = 0.9 (*shift of 10*)
- Reduction factor (SD) = 0.1

Finally, the obtained spatial probabilistic failure probability based on default and spatial standard deviations can be compared to the sectional failure probability reported by the waterboard Rijn & IJssel (WRIJ, 2018) in figures 7.9 and 7.10.

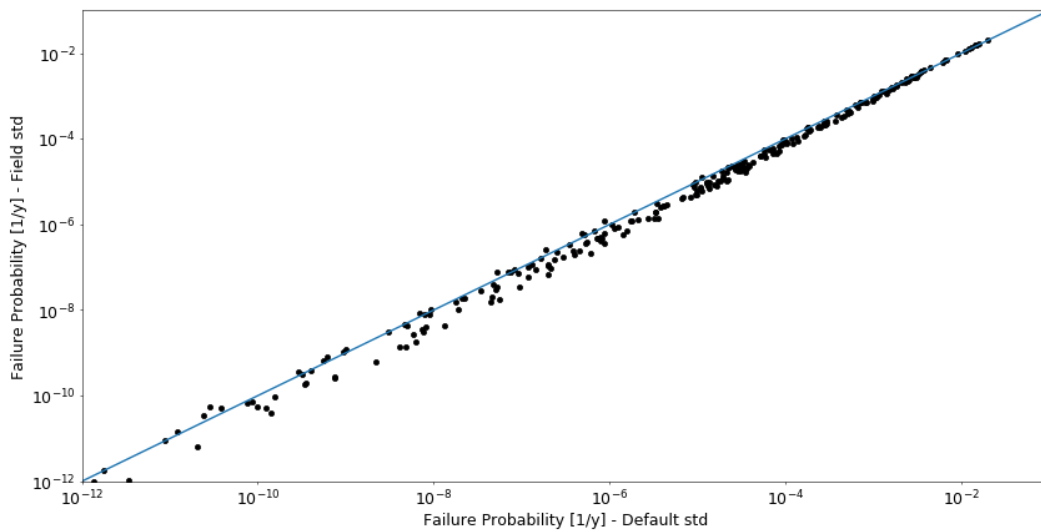


Figure 7.9: Probabilistic assessment trajectory 48-1 (σ_{field} versus $\sigma_{default}$)

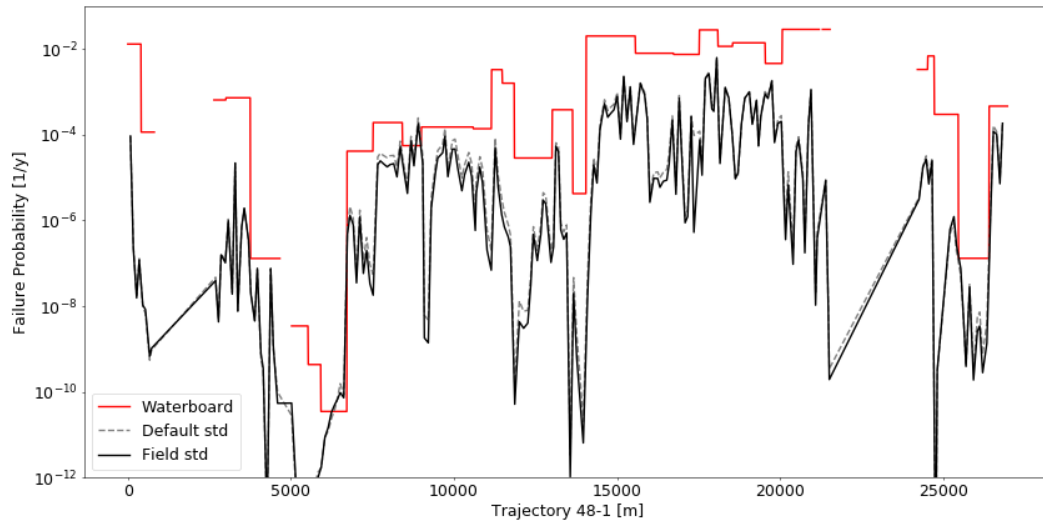


Figure 7.10: Probabilistic assessment trajectory 48-1 (spatial results versus sectional results)

Comparing the probabilistic results with default uncertainties from the WBI and uncertainties from the data analysis, it is concluded that for most locations, especially for locations in the high failure domain, the failure probabilities reduces by taking the field uncertainties into account at small intervals. Comparing the sectional failure probability from the waterboard in red with the computed spatial failure probability in black (default std) and grey (field std), it is concluded that at most sections certain conservatism is applied. Only at one of the 33 dike sections a certain underestimation of the failure probability is visible.

To check the accuracy and non-linearity of the results using FORM a Second Order Reliability Method (level II) is used. SORM approximates the limit state surface at the design point in the standard normal space by a quadratic surface. SORM is more accurate than FORM in case when the limit state function is quadratic in the design point. The result are given in figure 7.11 which indicates the accuracy and non-linearity of the probabilistic assessment. In the next chapter the results of the probabilistic assessment will be discussed in detail.

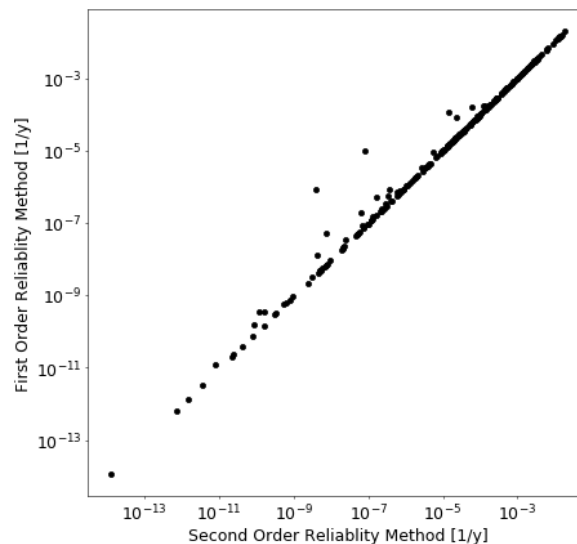


Figure 7.11: Comparison of first and second order reliability methods using fragility curves

7.2.1 Importance Factors

The importance factors from the FORM analysis at the design point are visualised for the fragility curve approach along the trajectory for both default and field related uncertainties. The theory behind the importance factors is given in appendix E. In contrast to the distribution approaches, conditional importance factors results from a fragility curve approach. Additional computations are necessary to determine the importance factor of the water level and to re-scale the other importance factors to the summation of one using equation 7.1 - 7.3. This is visualised in figures 7.12, 7.13, 7.14 and 7.15. It is clear that the relative importance of the outside water level (h) and the model factor piping (m_p) are dominant compared to the subsurface related parameters.

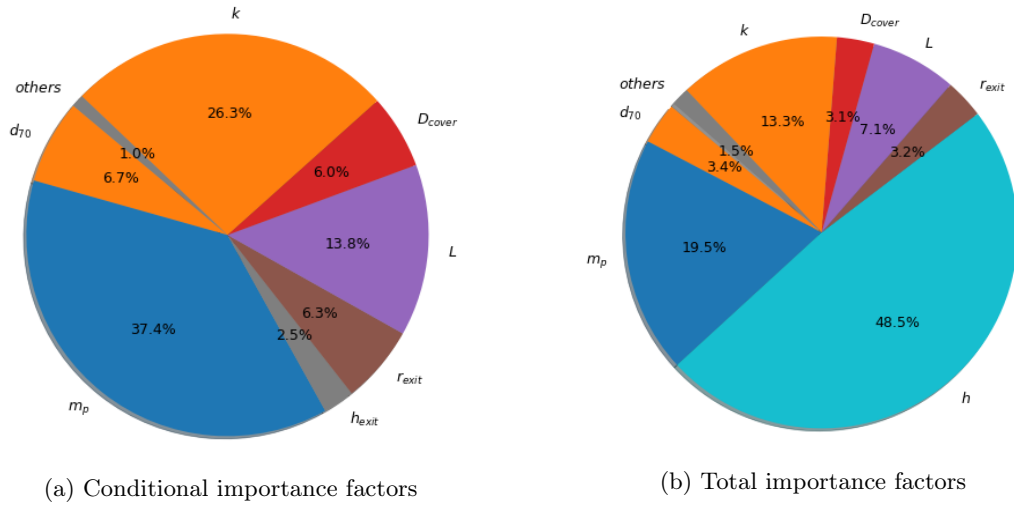


Figure 7.12: Average importance factors ($\sigma_{default}$)

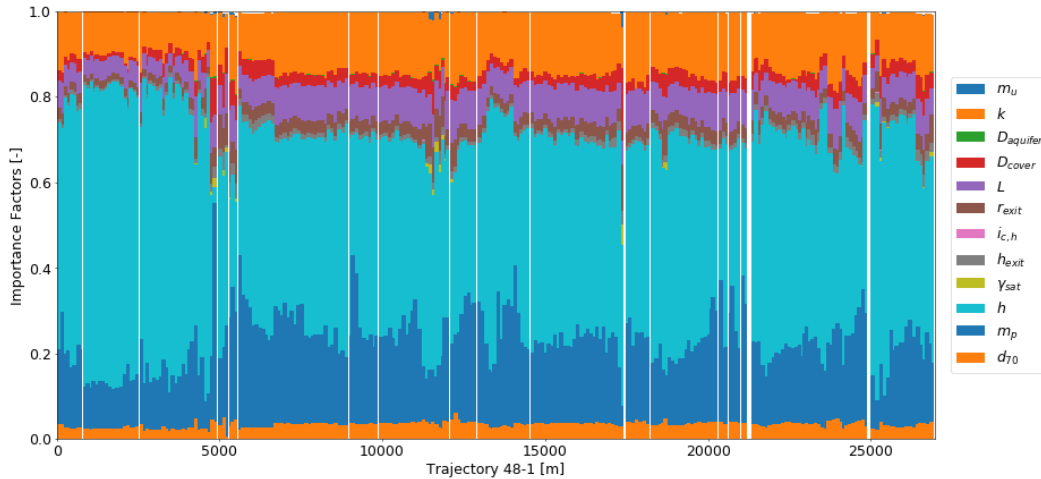
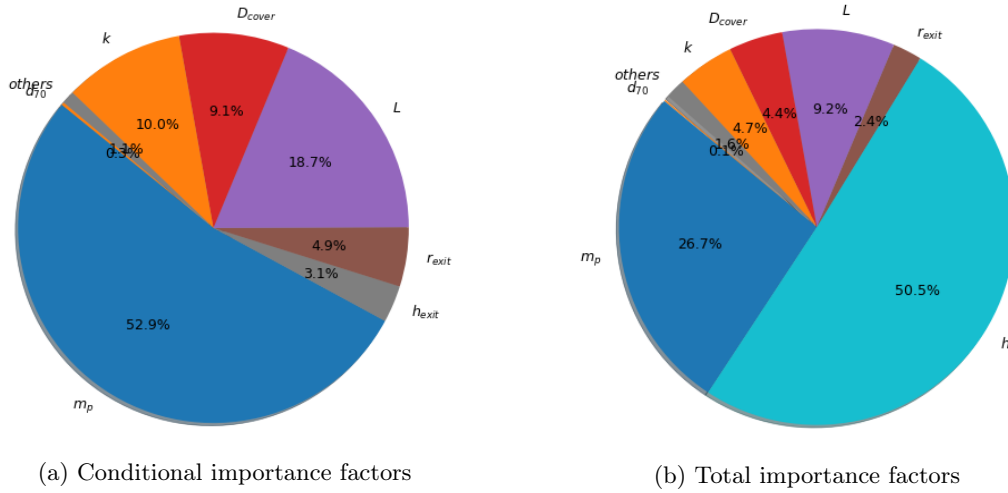
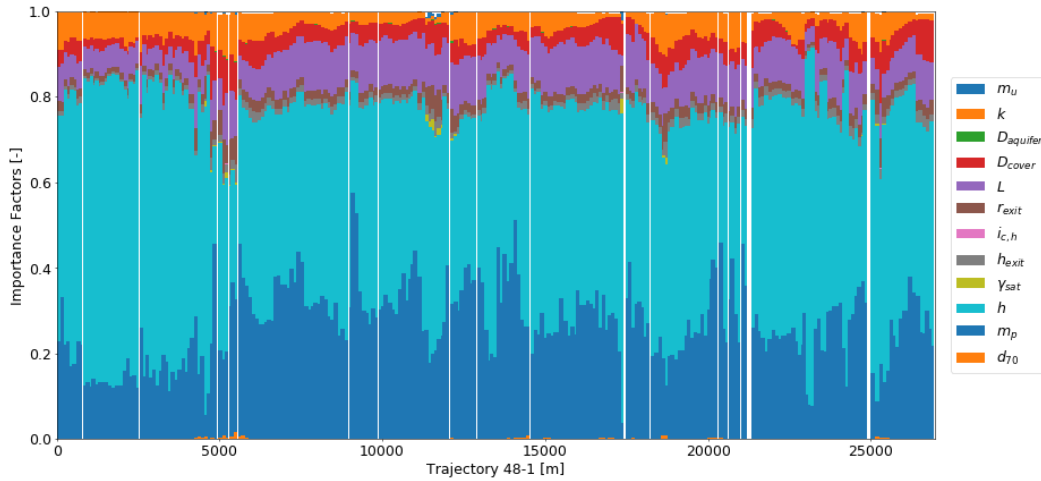


Figure 7.13: Importance factors ($\sigma_{default}$) trajectory 48-1

Figure 7.14: Average importance factors (σ_{field})Figure 7.15: Importance factors (σ_{field}) trajectory 48-1

Note that the importance factor of the water level (α_h) is excluded from the conditional FORM results since the water level is taken as a deterministic value. The 'total' importance factors can be derived from the 'conditional' importance factors by calculating and adjusting for the importance factor of the water level (α_h) (Schweckendiek et al., 2017)

$$\alpha_h = \frac{u^*}{-\beta} = \frac{\Phi^{-1}(F_h(h^*))}{\Phi^{-1}(P_f)} \quad (7.1)$$

where u^* indicates the design point as the inverse standard normal distribution of the cumulative water level distribution at the water level in the design point. β indicates the integrated failure probability following from the fragility curve approach.

From the 'conditional' importance factors the 'total' importance factors can be obtained by

$$\alpha_i^2 = (\alpha_i|h^*)^2 \cdot (1 - \alpha_h^2) \quad (7.2)$$

in order to fulfill the summation of the 'total' squared importance factors to be equal to one

$$\sum (\alpha_i|h^*)^2 + \alpha_h^2 = 1 \quad (7.3)$$

To validate the derivation of the importance factors based on the fragility curve approach the importance factors as a result of the distribution approach (Gumbel), fitted to the design point of the fragility curve approach, are used to compare. For most locations the Gumbel distribution is fitted to lower return periods compared to the initial fit to the tail of the return periods. Two examples are shown below in figure 7.16.

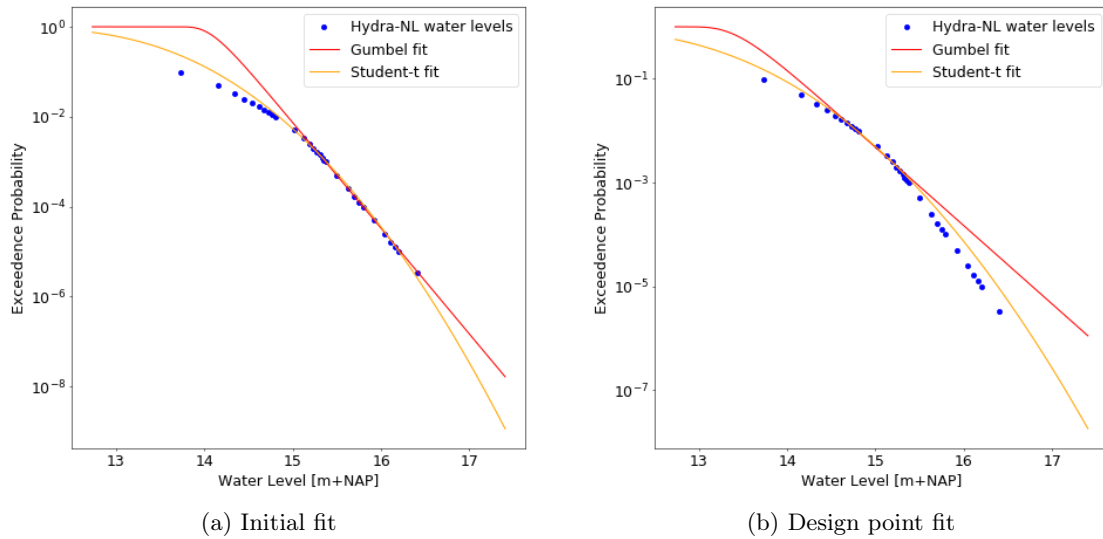


Figure 7.16: Gumbel distribution (initial and design point fit)

In an iterative way the design points of the distribution approach using a Gumbel distribution should match the design points of the fragility curve approach along the trajectory. This is visualised in figure 7.17 based on the default standard deviations from the WBI 2017.

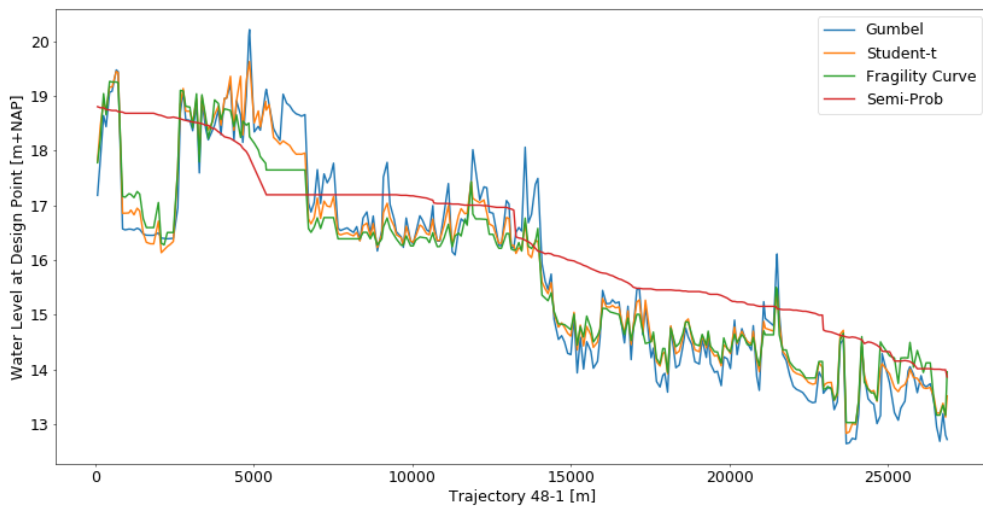


Figure 7.17: Water levels at the design point ($\sigma_{default}$) trajectory 48-1

As both design points are comparable the importance factors based on the two approaches can be compared. The importance factors computed from the fragility curve approach are already visualised in figure 7.13. The importance factors computed from the Gumbel distribution approach, fitted in the design point of the fragility curve approach, are visualised in figure 7.18.

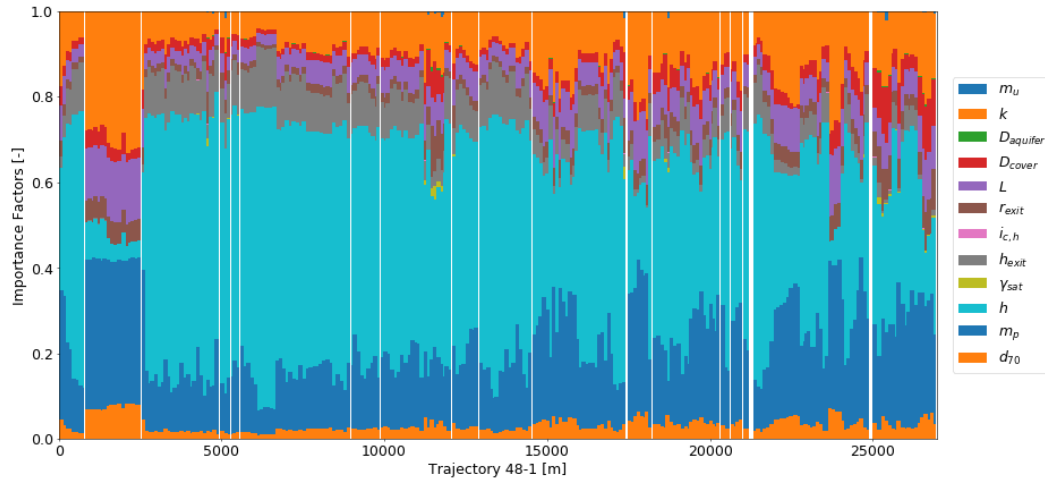
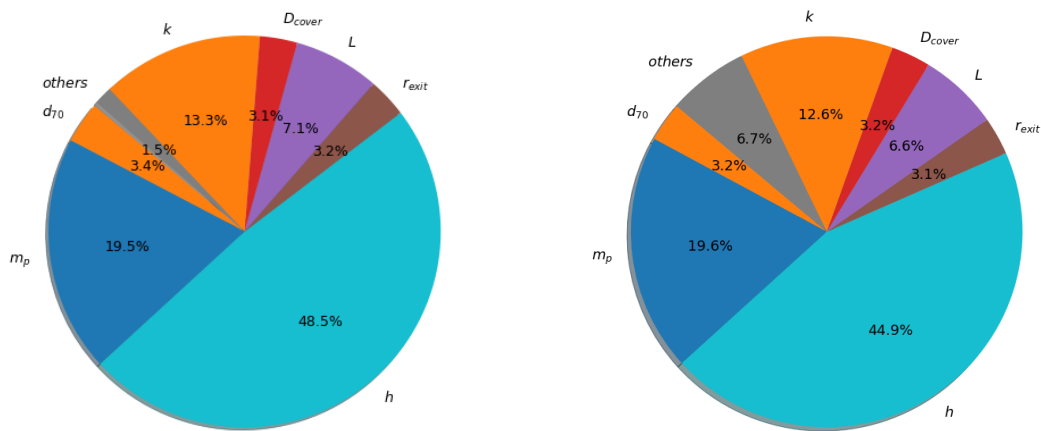


Figure 7.18: Importance factors ($\sigma_{default}$) trajectory 48-1 (design point fit)

Finally, a comparison between the importance factors can be made. It is clear that the derivation of the 'total' importance factors from the 'conditional' importance factors are quite similar to the importance factors resulting directly from the FORM analysis. The only difference between the two is the importance factor of the inner water level (or polder level) since the correlation between the inner and outer water level is taken into account. For the distribution approach this leads to a higher importance factor since the importance factor of the outer water level is high. For the fragility curve approach the importance factor of the inner water level is lower since the importance factor of the outer water level is low (zero) for the conditional situation.



(a) Importance factors (Fragility Curve)

(b) Importance factors (Gumbel distribution)

Figure 7.19: Average importance factor comparison ($\sigma_{default}$) (design point fit)

7.2.2 Parameter Sensitivities

The parameter sensitivities with respect to the reliability index β can be derived for the stochastic variables described by the distribution parameters ($\theta \in \theta_f$) and the constant variables known as limit state function parameters ($\theta \in \theta_g$). The parameter sensitivities of the reliability index with respect to the distribution parameters (θ_f) and limit state function parameters (θ_g) are given by the partial derivatives of β with respect to θ_f and θ_g for the FORM approximation of β (Der Kiureghian, 2019).

$$\nabla_{\theta_f} \beta = \alpha \cdot J_{u, \theta_f}(x^*, \theta_f) \quad (7.4)$$

$$\nabla_{\theta_g} \beta = \frac{1}{\|\nabla G(u^*, \theta_g)\|} \nabla_{\theta_g} g(x^*, \theta_g) \quad (7.5)$$

The derivation of these equations is discussed in appendix E. Here, the results for the normative cross-sections of the 33 dike sections within trajectory 48-1 will be discussed to derive which limit state function parameters (θ_g) or distribution parameters (μ_X or σ_X) of the stochastic variables have most influence on the uncertainty of the FORM approximated reliability index.

The gradient row vector ($\nabla_{\theta_f} \beta$) of equation 7.4 with respect to the the mean and standard deviation of the stochastic variables in the limit state function for the failure mechanism piping are summarized in tables 7.1 and 7.2 below. The results are given for the most critical cross-section of trajectory 48-1 (in dike section 28). In order to indicate the parameter sensitivities the results of equation 7.4 (1/unit) are multiplied by the standard deviation of the distribution parameter in question (unit). In other words, the standard deviation of the mean of the stochastic variables (σ_{μ_X}) and the standard deviation of the standard deviation of the stochastic variables (σ_{σ_X}). Since these uncertainties are not known, the following assumptions are made based on running a statistical hypothesis test on the data sets. This is discussed in appendix E by means of bootstrapping.

$$\sigma_{\mu_X} = \frac{1}{12} \sigma_X \quad \sigma_{\sigma_X} = \frac{1}{18} \sigma_X \quad (7.6)$$

Finally, the results of all normative cross-sections of the 33 dike sections are visualised in figures 7.20 and 7.21. The results are averaged in the last columns of tables 7.1 and 7.2 indicating the parameter sensitivities. Note that the orders of sensitivities of the most critical cross-section are representative for the trajectory. From these results it is clear that the reliability index is most sensitive to the mean value of the model parameter m_p and the variance of the water level h .

Variable (X)	$\nabla_{\mu_X} \beta$	σ_{μ_X}	$\nabla_{\mu_X} \beta \cdot \sigma_{\mu_X}$	$\overline{\nabla_{\mu_X} \beta \cdot \sigma_{\mu_X}}$
m_p	4.60E+00	1.00E-02	4.60E-02	4.13E-02
k	-1.97E+03	1.48E-05	-2.92E-02	-2.61E-02
d_{70}	3.33E+03	7.07E-06	2.35E-02	2.11E-02
$D_{aquifer}$	-2.06E-02	4.17E-02	-8.58E-04	-1.22E-03
h	-1.71E+00	1.47E-02	-2.53E-02	-2.42E-02
h_{exit}	1.71E+00	8.30E-03	1.43E-02	1.06E-02
D_{cover}	5.10E-01	4.86E-01	2.48E-02	1.94E-02
L	5.97E-02	4.33E-01	2.58E-02	2.46E-02

Table 7.1: Sensitivities parameters with respect to β ($\theta_f = \mu_X$)

Variable (X)	$\nabla_{\sigma_X} \beta$	σ_{σ_X}	$\nabla_{\sigma_X} \beta \cdot \sigma_{\sigma_X}$	$\overline{\nabla_{\sigma_X} \beta \cdot \sigma_{\sigma_X}}$
m_p	-1.10E+01	6.70E-03	-7.35E-02	-5.96E-02
k	-1.22E+03	9.90E-06	-1.21E-02	-9.33E-03
d_{70}	-3.17E+02	4.72E-06	-1.50E-03	-1.46E-03
$D_{aquifer}$	-5.32E-04	2.78E-02	-1.48E-05	-3.85E-05
h	-7.54E+00	9.80E-03	-7.41E-02	-9.24E-02
h_{exit}	1.61E+00	5.60E-03	8.90E-03	8.29E-03
D_{cover}	-5.59E-01	3.24E-02	-1.81E-02	-1.18E-02
L	-7.23E-02	2.89E-01	-2.09E-02	-1.86E-02

Table 7.2: Sensitivities parameters with respect to β ($\theta_f = \sigma_X$)

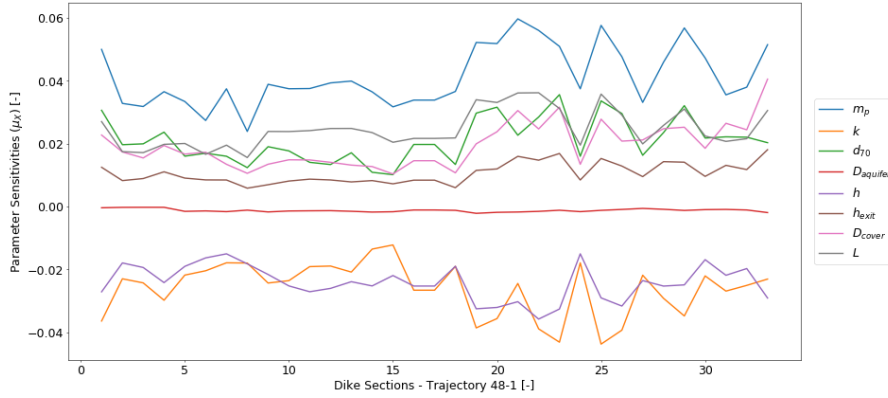


Figure 7.20: Sensitivities parameters with respect to β ($\theta_f = \mu_X$) trajectory 48-1

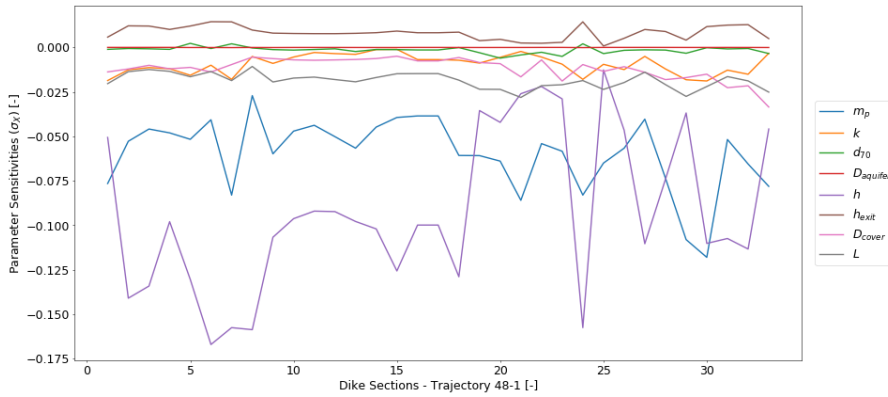


Figure 7.21: Sensitivities parameters with respect to β ($\theta_f = \sigma_X$) trajectory 48-1

The results of the gradient row vector ($\nabla_{\theta_g} \beta$) of equation 7.5 with respect to the the limit state function parameters (constants) for the failure mechanism piping is summarized in table 7.3 below. The results are given for the most critical cross-sections of trajectory 48-1 (in dike section 28). In order to indicate the parameter sensitivities the results of equation 7.5 (1/unit) are multiplied by the standard deviation of the limit state function parameter in question (unit). In other words, the standard deviation of the constants (σ_θ). Since these uncertainties are not known, the following assumptions are made in relation to current and previous flood risk analysis software (ENW, 2010).

$$\sigma_\eta = 0.1 \cdot \eta \quad \sigma_{\gamma_{sat,grains}} = 0.5 \quad \sigma_\theta = 2 \quad \sigma_{d_{70,m}} = 0.01 \cdot d_{70,m} \quad \sigma_\nu = 0.01 \cdot \nu \quad (7.7)$$

Finally, the results of all the normative cross-sections of the 33 dike sections taken into account for the assessment are visualised in figure 7.22. These results are averaged in the last columns of table 7.3 indicating the parameter sensitivities. Note that the orders of sensitivities of the most critical cross-section are representative for the trajectory. From these results it is clear that the reliability index is most sensitive to the variance of drag factor η and the internal friction angle of grains θ which uncertainties are currently covered by the model parameter m_p in the revised Sellmeijer method (under the assumption of constant η and θ).

Variable (θ)	$\nabla_{\theta} \beta$	σ_θ	$\nabla_{\theta} \beta \cdot \sigma_\theta$	$\overline{\nabla_{\theta} \beta \cdot \sigma_\theta}$
η	1.31E+01	2.50E-02	3.27E-01	3.05E-01
$\gamma_{sat,grains}$	1.98E-01	5.00E-01	9.92E-02	9.26E-02
θ	1.19E-01	2.00E+00	2.38E-01	2.22E-01
$d_{70,m}$	9.45E+03	2.08E-06	1.96E-02	1.83E-02
ν	-8.21E+05	1.33E-08	-1.09E-02	-1.02E-02

Table 7.3: Sensitivities parameters with respect to β ($\theta_g = \theta$)

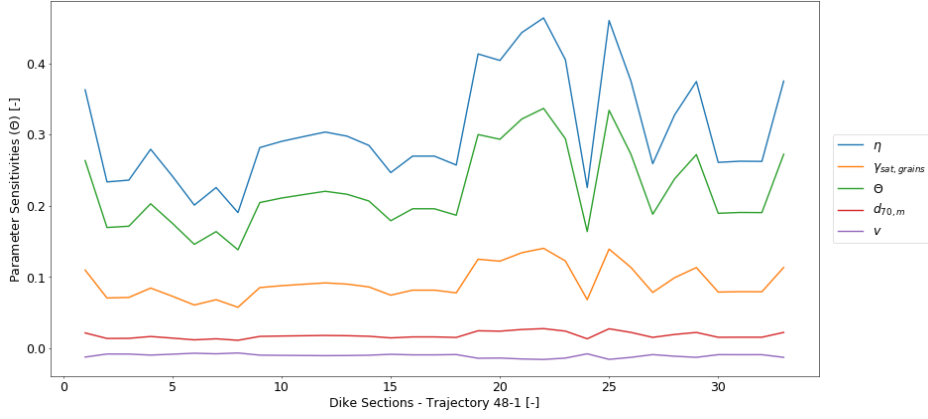


Figure 7.22: Sensitivities parameters with respect to β ($\theta_g = \theta$) trajectory 48-1

Furthermore, from the sensitivity vectors ($\nabla_{\theta_f} \beta$) the variance of the approximated reliability index using FORM can be approximated using equation 7.8 with respect to any of the distribution parameters ($\theta \in \theta_f$) (Lanzafame and Sitar, 2018).

$$\sigma_\beta \approx \nabla_{\theta_f} \beta' \cdot \sum_{\theta\theta} \cdot \nabla_{\theta_f} \beta \quad (7.8)$$

where $\sum_{\theta\theta}$ is the covariance matrix of the distribution parameter in question. In perspective to \sum_{XX} , the covariance matrix of the stochastic variables consisting of the variances and covariances, $\sum_{\theta\theta}$ consists of the variances and covariances of the distribution parameter based on the assumptions made in equation 7.6.

The results of the uncertainty of the reliability index with respect to the uncertainties of the mean σ_β (σ_{μ_X}) and standard deviation σ_β (σ_{σ_X}) of the stochastic variables are given in figure 7.23 below for each of the dike sections. The arithmetic mean of $\bar{\sigma}_\beta$ (σ_{μ_X}) equals 0.06 and $\bar{\sigma}_\beta$ (σ_{σ_X}) equals 0.12. Note that these uncertainties of the reliability index only include the effects of the distribution parameters that are included in the gradient row vector. In this case the distribution parameters μ or σ . Moreover, the uncertainties related tot the distribution parameters (σ_μ) or σ_σ) are based on bootstrapping. The bootstrapping method implicitly takes the variability inot account implied by the collected data but in reality it should also includes uncertainties related to measurement errors.

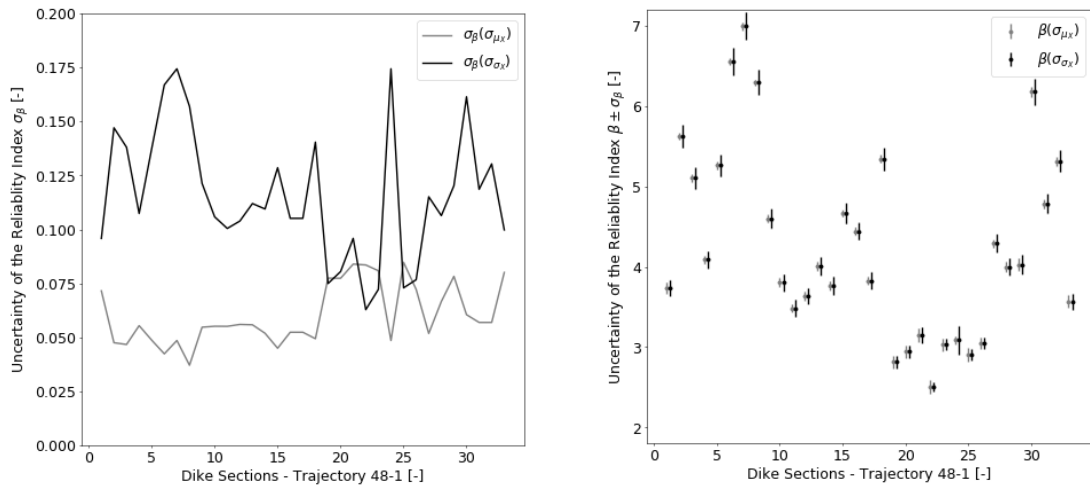


Figure 7.23: Uncertainty of the reliability index w.r.t. the distribution parameters (μ_X and σ_X)

Chapter 8

Conclusions of Sub Question 1

SQ1 *In what amount is the calculated cross-sectional failure probability representative for the statistically homogeneous section it represent?*

To answer the first research question, spatial data and uncertainties of the parameters required in the piping assessment are obtained to compute the failure probability along the trajectory over small intervals. Based on a semi-probabilistic approach with a spatial interval of 10 meters (sampling distance) and a probabilistic approach with a spatial interval of approximate 120 meters (Hydra-NL distance). These cross-sectional failure probabilities are obtained using default uncertainties from the WBI 2017 and field related uncertainties from the data analysis. All four methods are subsequently compared with the failure probabilities provided by the waterboard Rijn & IJssel for each of the dike sections (with according normative cross-section) along the trajectory. The normative cross-section within a section is first chosen at the location of the median seepage length and finally adjusted for a more critical combination of seepage length and ground level (at the exit point).

Figures 8.1 and 8.2 show the results of the reliability analysis in comparison to the initial sectional failure probabilities. Since the cross-sectional failure probabilities are smaller than the representative sectional failure probabilities from the waterboard it can be concluded that the sectional failure probabilities in red (without length-effects) are in general a conservative choice compared to the computed spatial failure probability in black based on a (semi) probabilistic approach using small spatial intervals and field related uncertainties. Furthermore, it can be concluded that the choice of dike sections is accurate and the overall trend of the spatial failure probability is followed. Only in sections dp118+061-129+077 and dp260+000-269+033 there is a jump in the trend of the spatial failure probability which could be discretized. Note that the choice of dike sections by the waterboard (WRIJ, 2018) is based on clear changes in dike geometries (ground level at exit points of seepage water), seepage lengths (entry and exit lines of seepage water), SOS segments (stochastic subsurface classification) and grain sizes segments (underneath the cover layer).

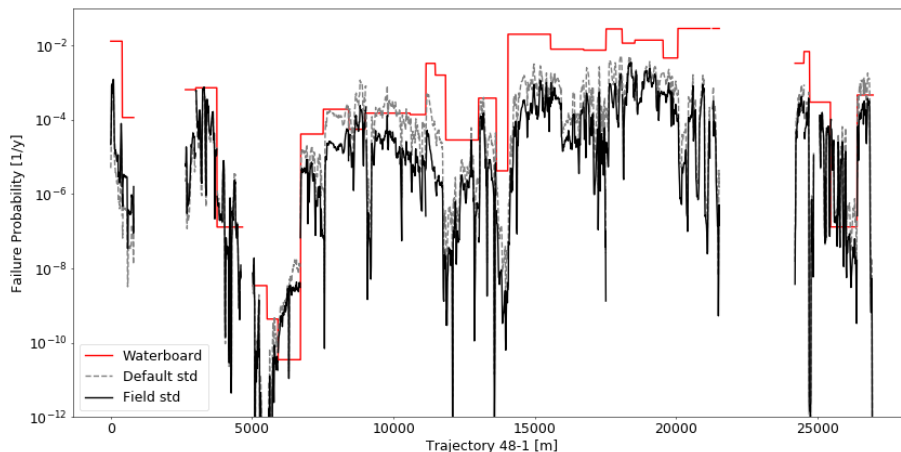


Figure 8.1: Semi-Probabilistic failure probability trajectory 48-1 ($Pf_{section}$)

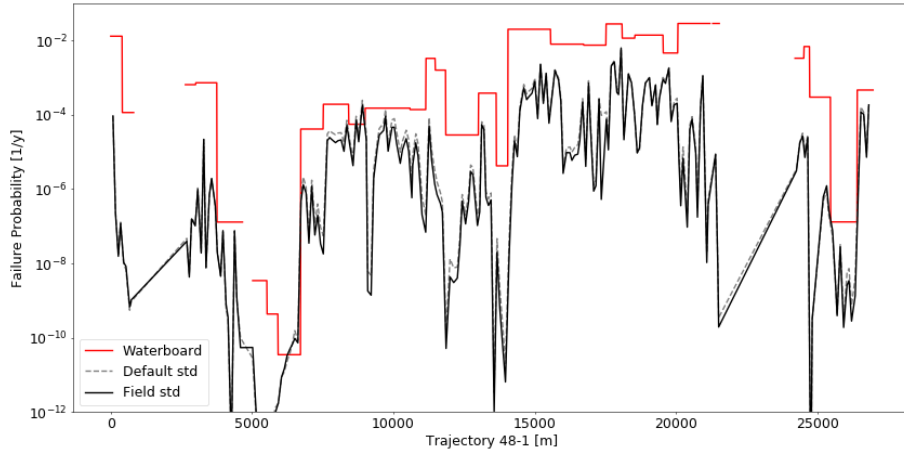


Figure 8.2: Probabilistic failure probability trajectory 48-1 ($Pf_{section}$)

Since the choice of dike sections is supported with the trend of the spatial failure probability, the maximum cross-sectional failure probability within dike sections are indicated as normative and listed in table 8.1. In general the current representative sectional failure probability of the dike sections (WRIJ) are conservative in comparison to the normative failure probabilities according to the reliability analysis. Summation of these maximum failure probabilities results in a trajectory failure probability of 1/60 [1/y] for the probabilistic approach based on fragility curves using field related uncertainties. In Chapter 14 the impact of these conclusions are discussed in comparison with the conclusions related to the other steps of the assembly procedure.

#Section	$Pf_{cross-sec}$ (WRIJ)	$Pf_{cross-sec}$ (SP) $\sigma_{default}$	$Pf_{cross-sec}$ (SP) σ_{field}	$Pf_{cross-sec}$ (P) $\sigma_{default}$	$Pf_{cross-sec}$ (P) σ_{field}
1	1.30E-02	5.19E-04	1.22E-03	9.33E-05	9.26E-05
2	1.15E-04	4.90E-07	3.40E-06	9.20E-09	1.06E-08
4	6.46E-04	1.87E-05	4.46E-05	1.66E-07	1.58E-07
5	7.26E-04	4.16E-04	7.58E-04	2.18E-05	2.18E-05
6	1.30E-07	6.72E-06	7.99E-06	7.56E-08	7.54E-08
12	3.46E-09	1.30E-08	1.91E-08	2.83E-11	5.50E-11
13	4.36E-10	5.15E-10	8.64E-11	1.34E-12	1.01E-12
14	3.51E-11	1.71E-08	4.31E-09	1.56E-10	9.65E-11
15	4.13E-05	2.00E-05	8.67E-06	2.10E-06	1.31E-06
16	1.92E-04	2.49E-04	5.76E-05	7.09E-05	5.20E-05
17	1.51E-04	1.17E-03	2.41E-04	2.45E-04	1.82E-04
18	1.51E-04	8.21E-04	1.31E-04	1.38E-04	9.15E-05
19	1.38E-04	1.13E-04	1.65E-05	3.07E-05	1.76E-05
20	3.29E-03	4.95E-04	5.24E-05	8.34E-05	5.04E-05
21	1.59E-03	5.58E-05	3.19E-06	1.56E-06	7.12E-07
22	2.86E-05	6.10E-05	2.89E-05	4.44E-06	2.97E-06
23	3.82E-04	3.96E-04	1.50E-04	6.45E-05	5.38E-05
24	4.23E-06	2.92E-06	3.56E-07	4.66E-08	2.00E-08
25	1.23E-03	3.16E-03	1.15E-03	2.43E-03	2.30E-03
26	7.94E-03	1.78E-03	9.92E-04	1.61E-03	1.57E-03
27	7.46E-03	2.67E-03	5.58E-04	8.21E-04	7.08E-04
28	2.78E-02	5.29E-03	1.74E-03	6.08E-03	6.27E-03
29	1.15E-02	4.67E-03	3.52E-03	1.22E-03	1.27E-03
30	1.39E-02	3.69E-03	2.42E-03	1.01E-03	9.86E-04
31	4.59E-03	2.27E-03	9.78E-04	1.84E-03	1.78E-03
32	2.86E-02	1.62E-03	8.88E-04	1.15E-03	1.09E-03
34	2.86E-02	7.75E-04	3.21E-04	8.92E-06	8.46E-06
37	2.29E-03	8.86E-04	4.18E-04	3.20E-05	2.69E-05
38	2.98E-04	5.52E-04	3.79E-04	2.83E-05	2.45E-05
39	2.98E-04	1.29E-05	1.14E-05	3.24E-10	3.21E-10
41	2.98E-04	1.42E-04	1.57E-04	8.61E-07	1.23E-06
42	1.31E-07	6.52E-05	5.60E-05	5.31E-08	7.54E-08
43	4.63E-04	1.80E-03	3.77E-04	1.79E-04	1.84E-04
SUM	1/6.30 ⁽¹⁾	1/29.65	1/59.91	1/58.25	1/59.57

Table 8.1: Overview of maximum cross-sectional failure probabilities (excluding the length-effects).
⁽¹⁾ The 1/6.3 [1/y] is not in line with the expectations of the waterboard Rijn & IJssel and is therefore reported as '>1/100' [1/y]. A reference is made to the disclaimer on page 7.

To get an idea of the amount of overestimation of the normative cross-sectional failure probability, the distance between the normative failure probability for dike sections as reported by the waterboard and the semi-probabilistic spatial cross-sectional failure probability at an interval of 10 meters along the trajectory is computed for the cases with default uncertainties and with field related uncertainties. The distances to the sectional failure probabilities (normative cross-sections) of waterboard Rijn & IJssel (WRIJ) are plotted in the histograms of figure 8.3 in the reliability domain where negative distances indicates underestimation and positive distances indicates overestimation. The standard deviation of the computed distances is 0.91 (default std) and 0.87 (field std).

$$\beta = -\Phi^{-1}(P_f) \quad (8.1)$$

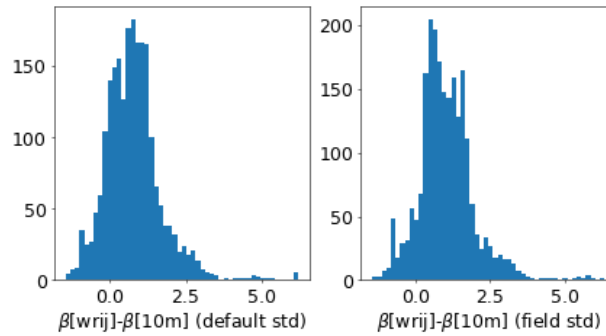


Figure 8.3: Differences in β -domain (semi-probabilistic)

Furthermore, the distance between the normative failure probability for dike sections as reported by the waterboard and the probabilistic spatial failure probability at an interval of 120 meters along the trajectory is computed for the cases with default uncertainties and with field related uncertainties. The distances to the sectional failure probabilities (normative cross-section) of waterboard Rijn & IJssel (WRIJ) are plotted in the histograms of figure 8.4 in the reliability domain. The standard deviation of the computed distances is 0.87 (default and field std).

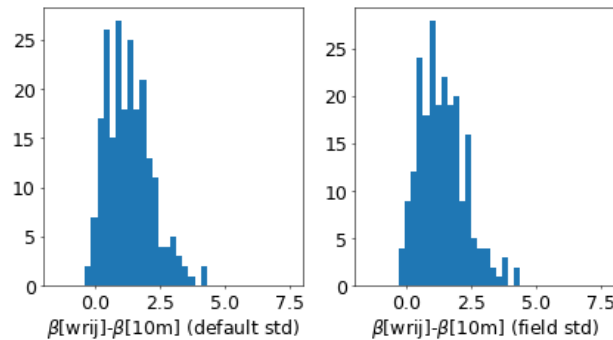


Figure 8.4: Differences in β -domain (probabilistic)

Concluding from figures 8.3 and 8.4, from the semi-probabilistic case using default uncertainties from the WBI 2017, which method is applied by the waterboard, to the probabilistic case using fragility curves and field uncertainties, which method is supposed to be most realistic, distances in the beta domain are overall above zero, indicating overestimation of the currently defined normative failure probabilities. For the probabilistic case this conservatism is larger than in the semi-probabilistic case. Note that including the length-effect within sections the histograms will show a clear shift in distance density to the right. So, the reported normative cross-sectional failure probabilities of the dike sections are not representative for the dike sections it represent since a lot of conservatism is applied to derive the cross-sectional failure probabilities, critical combinations of parameters from different locations within a dike section, neglecting the correlation between parameters and taking characteristic values for load and resistance, but also in the reliability method itself by translating safety factors into failure probabilities using the calibration formula.

Despite the overestimation, to compare the derivation of the reported normative cross-sections with the currently known spatial maximum failure probability within the dike sections, the parameters related to the chosen normative cross-section by the waterboard can be compared to the parameters related to the normative cross-sections of the semi-probabilistic result. Note that the choice of the normative cross-section to represent a section by the waterboard (WRIJ, 2018) is based on two steps. Initially the cross-section is chosen at the location of the median seepage length within a section and finally the location of the cross-section is adjusted for a more critical combination of seepage length and ground level (at the exit point).

In figure 8.5a a comparison is given between the chosen sectional seepage length by the waterboard (green points) and the seepage length at the location of the computed maximum failure probability within the sections based on small spatial intervals (red crosses). It can be concluded that at half of the number of sections the seepage length difference is more than five meters. In figure 8.5b a comparison is given between the chosen sectional ground level by the waterboard (green points) and the ground level at the location of the computed maximum failure probability within the sections based on small spatial intervals (red crosses). It can be concluded that for only 5 sections the difference is more than one meter which is quite large for the failure mechanism piping.

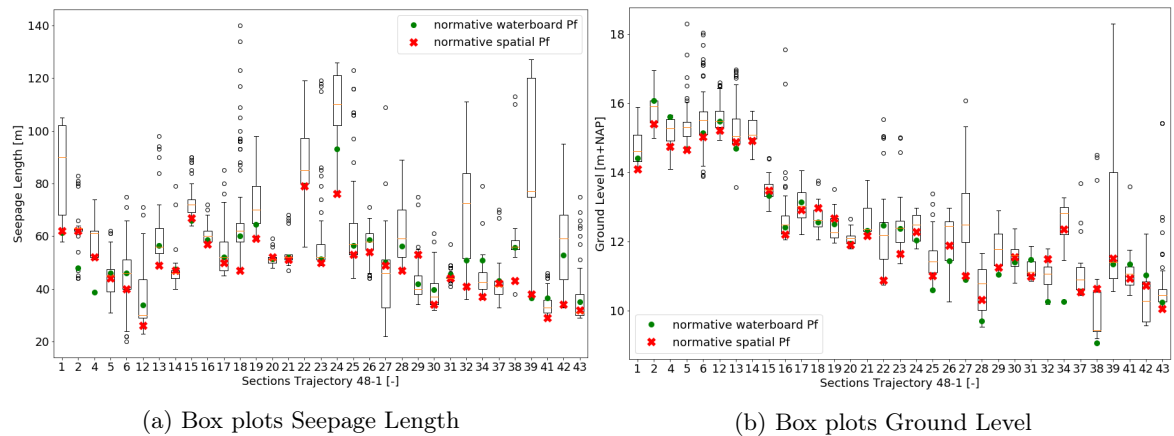


Figure 8.5: Choice of normative cross-sections in dike sections (WRIJ)

Concluding from figures 8.5a and 8.5b representative cross-sections are more difficult to choose than appears from the current 'box' approach where the subsurface classification are assumed homogeneous in combination with several scenarios. This difficulty originates from the influence of subsurface deviations within statistically homogeneous sections that have a major influence. The choice of normative cross-sections should not only be based on the seepage length and ground level but mainly on the subsurface parameter since spatial deviations at small intervals are controlled by subsurface parameters (grain size, permeability, seepage length). Including these deviation within the sections lead to different choices on normative cross-sections. So, it is recommended to use interpolation techniques instead of 'boxed' classifications and scenarios to include spatial deviations in statistically homogeneous sections. This will lead to more accurate choices of normative cross-sections and finally to a better assessment. To access a more accurate failure probability of the normative cross-sections the use of a probabilistic approach in combination with fragility curves will get a more location based results without the use of characteristic values and calibration formulas which leads to conservatism.

Part IV

Length-Effect within Sections

Chapter 9

Length-Effect within Sections

With increasing length of a dike section or dike trajectory the probability that a weak spot occurs will increase. So, with increasing length, the failure probability of a dike section or dike trajectory will increase. This is called the length-effect. The length-effect within sections is the result of combining spatial uncertainties in a section. The length-effect between sections is the result of combining sections with different correlations (Kanning, 2012). Here, the focus will be on the length-effect within sections.

'Helpdesk Water' defined the length-effect as the influence of the spatial variations of the dike and subsoil characteristics to the failure probability of a dike trajectory, mathematically equal to the relation between the sectional failure probability of a 'statistically uniform' dike section and a cross-sectional failure probability within the same dike section (RWS, 2017a).

The length-effect differs in magnitude for all failure mechanisms. This depends on the spatial distribution and fluctuations of the resistance of the dike against failure mechanisms. For failure mechanisms with a small length-effect the resistance has a small spatial distribution, like the height of the dike to resist overtopping. For failure mechanisms with a large length-effect the resistance has a large spatial distribution, like the cover layer thickness of the dike, to resist piping (VNK2, 2011).

So, the length-effect within sections of geotechnical failure mechanisms is a function of the length under consideration ($L_{section}$), the failure mechanism sensitive part (a) and a length measure for the intensity of the length-effect within this failure mechanism sensitive part (b). This is stated in equation 9.2 which formulation is currently used in the WBI for the assessment of geotechnical failure mechanisms with the software Riskeer (Deltares, 2017b).

$$Pf_{section} = N^* \cdot Pf_{cross-section} \quad (9.1)$$

$$N^* = 1 + \frac{a \cdot L_{section}}{b} \quad (9.2)$$

Previously, the length-effect within sections was covered by the Outcrossing Method in the VNK for the assessment of geotechnical failure mechanisms with the software PC-Ring (Vrouwenvelder, 2006). With this formulation the length-effect is a function of the length under consideration ($L_{section}$) and the equivalent independent length (l_{eq}). This is stated in equation 9.3 below.

$$N^* = 1 + \frac{L_{section}}{l_{eq}} \quad (9.3)$$

Piping

Factor a , the failure mechanism sensitive fraction, is dependent on the location of the trajectory. Based on studies of Lopez de la Cruz (Lopez de la Cruz et al., 2010) conservative values are proposed of 0.4 and 0.9, making a distinction between the lower river/lake/sea areas and upper river areas in the Netherlands (Rijkswaterstaat, 2016a). These values are roughly determined by comparing water level differences to the distance of the aquifer to the surface level in order to identify the piping sensitive locations. This broad study includes a lot of conservatism.

Factor b , the length measure for the intensity of the length-effect is in definition similar to the parameter l_{eq} , the independent length of equivalent elements, which is dependent on the location of the trajectory. Based on studies of Lopez de la Cruz (Lopez de la Cruz et al., 2010) approximations are in the order of 300-400m (Rijkswaterstaat, 2016a). These values are determined by the outcrossing approach where the importance factors and auto-correlation functions of each stochastic parameter are necessary. This study is based on four dike rings in the Netherlands.

In section 9.1 the outcrossing method is discussed which is used in the PC-Ring software of VNK. In section 9.2 the continuous model of the outcrossing method is discussed to calibrate the length-effect parameters which are currently used in the Riskeer software of the WBI. Both methods are applied to trajectory 48-1. Finally, in chapter 10 the methods are compared with a generic approach.

9.1 Outcrossing Method

In order to scale the cross-sectional failure probability to a sectional failure probability the spatial variability within a section should be quantified with the factor (N^*) given in equation 9.3. This factor results from the outcrossing approach using the probability of threshold exceedance which describes the probability of exceeding a predefined threshold as a function of length (Kanning, 2012). This is visualised in figure 9.1 below.

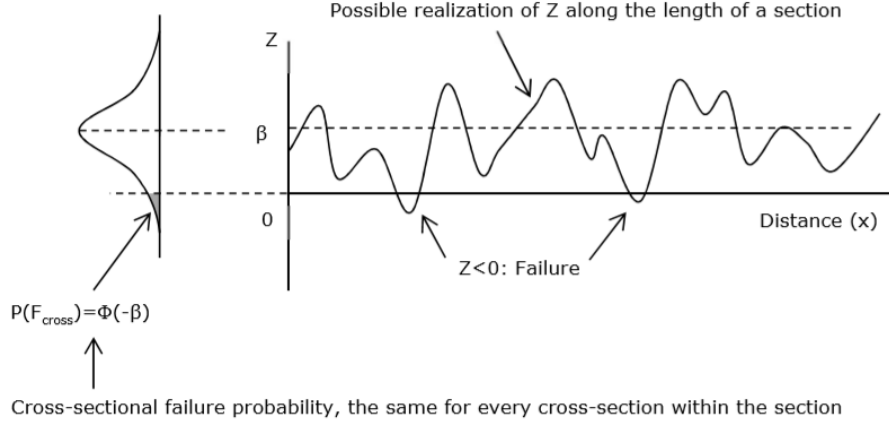


Figure 9.1: Outcrossing Method - Probability of threshold exceedance (Jongejan, 2017a)

Based on the outcrossing method, the probability that the limit state function (Z) becomes less than zero within a section of the domain $[0, L]$ is given by (Geodelft, 1994)

$$Pf(0, L) = P(Z(x) < 0 | 0 \leq x \leq L) \approx Pf(0) + (1 - Pf(0)) \cdot P(Z(x) < 0 | 0 \leq x \leq L) \quad (9.4)$$

where $Pf(0)$ is the cross-sectional failure probability at the origin and $P(Z(x) < 0 | 0 \leq x \leq L)$ is the probability that the limit state function (Z) becomes less than zero given it is higher than zero at the origin, as shown in figure 9.1.

An upper bound approximation of the sectional failure probability $Pf(0, L)$ is given by (Karadeniz and Vrouwenvelder, 2005)

$$Pf(0, L) \leq Pf(0) \cdot \int_0^L v(\xi) dv \quad (9.5)$$

where $v(\xi)$ is the outcrossing rate of the threshold ξ . For constant outcrossing rates the upper bound approximation reduces to (Karadeniz and Vrouwenvelder, 2005)

$$Pf(0, L) \approx Pf(0) + v \cdot L \quad (9.6)$$

The outcrossing of random fields based on a mean crossing rate v is given by Rice (1945)

$$v(\xi) = \int |\dot{x}| f_{x, \dot{x}}(\xi, \dot{x}) d\dot{x} \quad (9.7)$$

which is dependent on the derivative of the random process x (\dot{x}) and the joint density function of x and \dot{x} ($f_{x, \dot{x}}$). In the case of large thresholds (ξ) Rice (1945) derived an approximation of the mean crossing rate ($v(\xi)$) (Kanning, 2012)

$$v(\xi) \approx \exp\left(-\frac{1}{2} \frac{\xi^2}{\sigma_x^2}\right) \cdot \frac{1}{2} v_0 \quad (9.8)$$

Relating this outcrossing approach to the limit state function (Z), the threshold (ξ) can be expressed as the number of standard deviation (β) from the mean of the considered process (Kanning, 2012). The relation between ξ and β is given by the mean and standard deviation of the process

$$\xi = \mu + \beta \cdot \sigma \quad (9.9)$$

by substituting equations 9.8 and 9.9 the crossing rate (v) is given according to Dutch notation as (Vrouwenvelder, 2006) (Geodelft, 1994)

$$v = \frac{1}{2\pi} \exp\left(-\frac{1}{2}\beta^2\right) \cdot \sqrt{-\rho_Z''(0)} \quad (9.10)$$

where v is the number of crossings per unit length (L) above a threshold which depends on the cross-sectional reliability (β) and the second derivative of the autocorrelation function in the origin ($\rho_Z''(0)$). From the average crossing rate the average length of the crossing area can be derived which is given by (Geodelft, 1994)

$$l_d = 2\pi\Phi(-\beta)\exp\left(-\frac{1}{2}\beta^2\right) \frac{1}{\sqrt{-\rho_z''(0)}} \quad (9.11)$$

Finally, substituting equation 9.10 into equation 9.6 results in the upper bound approximation of the sectional failure probability $Pf(0, L)$

$$Pf(0, L) = Pf(0) + v \cdot L = Pf(0) + \frac{L}{2\pi} \exp\left(-\frac{1}{2}\beta^2\right) \cdot \sqrt{-\rho_Z''(0)} \quad (9.12)$$

This formulation to scale the cross-sectional failure probability to a sectional failure probability based on the outcrossing method for a continuous Gaussian field of length (L) is similar to the formulation of equations 9.1 and 9.3 which comply to the Dutch notation as derived below

$$\begin{aligned} Pf(0, L) &= Pf(0) + \frac{L}{2\pi} \exp\left(-\frac{1}{2}\beta^2\right) \cdot \sqrt{-\rho_Z''(0)} \\ &= Pf(0) + \frac{L}{2\pi} \frac{1}{Pf(0)} \exp\left(-\frac{1}{2}\beta^2\right) \cdot \sqrt{-\rho_Z''(0)} \cdot Pf(0) \\ &= \left(1 + \frac{L}{2\pi} \frac{1}{Pf(0)} \exp\left(-\frac{1}{2}\beta^2\right) \cdot \sqrt{-\rho_Z''(0)}\right) \cdot Pf(0) \\ &= \left(1 + \frac{L}{l_{eq}}\right) \cdot Pf(0) = N^* \cdot Pf(0) \end{aligned} \quad (9.13)$$

where the independent equivalent length (l_{eq}) is given by (Calle, 2010)

$$l_{eq} = 2\pi\Phi(-\beta)\exp\left(\frac{1}{2}\beta^2\right) \frac{1}{\sqrt{-\rho_z''(0)}} \quad (9.14)$$

where the second derivative of the autocorrelation function of the reliability function in the origin ($\rho_Z''(0)$) includes the spatial variability within a section. This parameter is an assembly of autocorrelation functions of the stochastic variables used in the reliability function (Z). The autocorrelation function for a single stochastic variable (ρ_i) is given by the lag parameter (τ), the correlation length (D) and the residual correlation (ρ_0). The assembly of autocorrelation functions is fulfilled using the importance factors (α) for each of the stochastic variables which result from a probabilistic assessment.

$$\rho_i(\tau) = (1 - \rho_{0,i}) \exp\left(-\left(\frac{\tau}{D_i}\right)^2\right) + \rho_{0,i} \quad (9.15)$$

$$\rho_z(\tau) = \sum_{i=1}^N \alpha_i^2 \rho_i(\tau) \quad (9.16)$$

The second derivative of the combined autocorrelation functions of the parameters used in the reliability function (Z) in the origin (or at a "lag" value of zero) is given by

$$\rho_z''(0) = - \sum_{i=1}^N \frac{2\alpha_i^2(1 - \rho_{0,i})}{D_i^2} \quad (9.17)$$

An approximation of the failure probability is given for sufficient large values of reliability indexes ($\beta \geq 2$) by (Vrouwenvelder, 2006)

$$\Phi(-\beta) \approx \frac{1}{\beta\sqrt{2\pi}} \exp\left(-\frac{1}{2}\beta^2\right) \quad (9.18)$$

In combination with equation 9.14, this yields in an approximation of the independent equivalent length (l_{eq}) for sufficient large values of threshold (β).

$$l_{eq} \approx \frac{\sqrt{2\pi}}{\beta} \frac{1}{\sqrt{-\rho_z''(0)}} \quad (9.19)$$

Furthermore, from a more generic perspective, the second derivative of the autocorrelation function ($\rho_z''(0)$) can be approached from a single dominant stochastic parameter which is described by a residual correlation (ρ_0), a correlation length (D) and a FORM importance factor (α). This approximation results in the most simplified form of the independent equivalent length (Calle, 2010)

$$l_{eq} \approx \frac{\sqrt{\pi} \cdot D}{\beta} \frac{1}{\alpha\sqrt{1-\rho_0}} \quad (9.20)$$

Substituting equation 9.20 into equations 9.1 and 9.3 results in a simplistic form of the length-effect within sections based on a single resistance parameter with zero residual correlation ($\rho_0 = 0$) and a fully correlated load.

$$P(0, L) = Pf(0) \cdot \left(1 + \alpha \frac{\beta L}{\sqrt{\pi} D}\right) \quad (9.21)$$

Note that it is of importance to avoid dike sections which are smaller than the equivalent independent length (or required length of failure) since the failure mechanisms models are based on (2D) analysis that require a certain interval to fail (Tigchelaar, 2017). Based on results from the PC-Ring software it is advised to distinguish dike sections larger than 300 meters. If dike sections are identified which are smaller than the equivalent independent length, the length-effect factor (N^*) of equation 9.3 can reduce to a value below one.

9.1.1 Field Application

In order to quantify the length-effect within sections based on the Outcrossing Method, the equivalent independent length (l_{eq}) needs to be determined based on the autocorrelation functions and FORM importance factors of the different stochastic variables used in the piping assessment of the case study.

The importance factors (α_i) of the limit state function parameters are given in figure 7.15 and for convenience visualised in figures 9.2 and 9.3 below. These importance factors are obtained from the probabilistic assessment based on field related means and standard deviations derived from the data analysis.

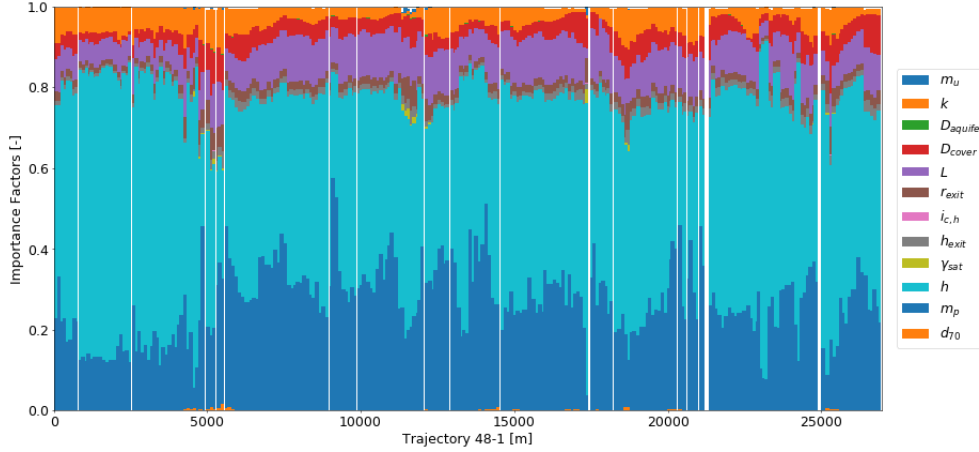


Figure 9.2: Importance factors (α_i^2) (σ_{field}) (48-1)

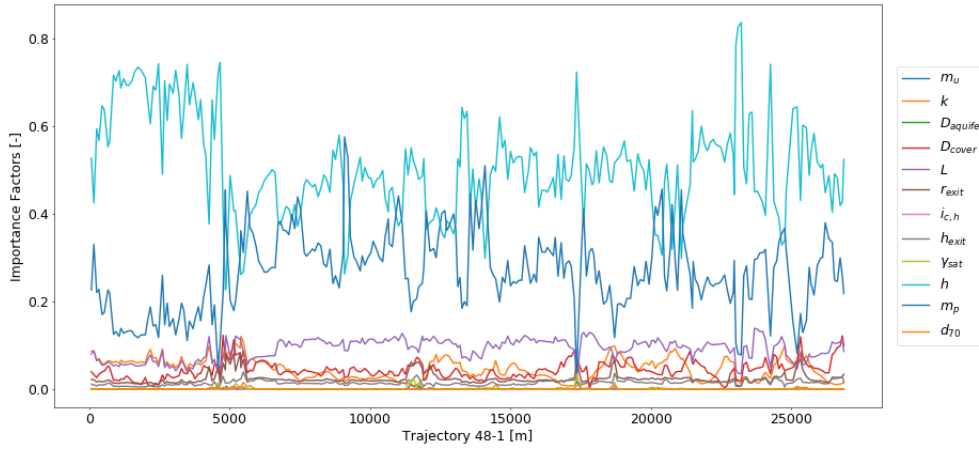


Figure 9.3: Importance factors (α_i) (σ_{field}) (48-1)

Next, the autocorrelation functions (ρ_i) of the parameters used in the limit state function are necessary. For parameters with a residual correlation ($\rho_{0,i}$) of one the autocorrelation drops out the second derivative of the combined autocorrelation functions at the origin, as stated by equation 9.17. For the model factor uplift and piping (m_u and m_p), damping factor (r_{exit}), inner and outer water level (h_{exit} and h) a residual correlation of one is assumed conform the WBI 2017 (Deltares, 2019). For parameters with a residual correlation ($\rho_{0,i}$) below one the correlation distance (D_i) and the residual correlation ($\rho_{0,i}$) are of importance. For the cover layer thickness (D_{cover}), grain size (d_{70}), permeability (k) and seepage length (L) the autocorrelation function given in equation 9.15 is fitted to the spatial correlations at different spatial distances (lags) to obtain the correlation distance and residual correlation. This procedure is discussed in appendix F. For the remaining parameters the correlation distance and the residual correlation is derived from the list of parameters relevant to the WBI (Deltares, 2019). These field related values are given in table 9.1 next to the values stated by the WBI 2017. All autocorrelation functions necessary are visualised in figures 9.4 and 9.5 below.

Parameter X	Spatial Variability (48-1)		Spatial Variability (WBI)	
	D_X	$\rho_{0,X}$	D_X	$\rho_{0,X}$
Model factor m_u	10000	1	10000	1
Permeability k	250	0	–	–
Aquifer layer $D_{aquifer}$	4000	0	4000	0
Cover layer d_{cover}	650	0.2	200	0
Seepage length L	350	0.1	3000	0
Damping factor r_{exit}	2000	1	10000	1
Water level h	10000	1	10000	1
Polder level h_{exit}	1000	1	1000	1
Saturated weight γ_{sat}	300	0	300	0
Heave gradient $i_{c,h}$	300	0	300	0
Model factor m_p	10000	1	10000	1
Grain size d_{70}	300	0	–	–

Table 9.1: Autocorrelation parameters 48-1 versus WBI

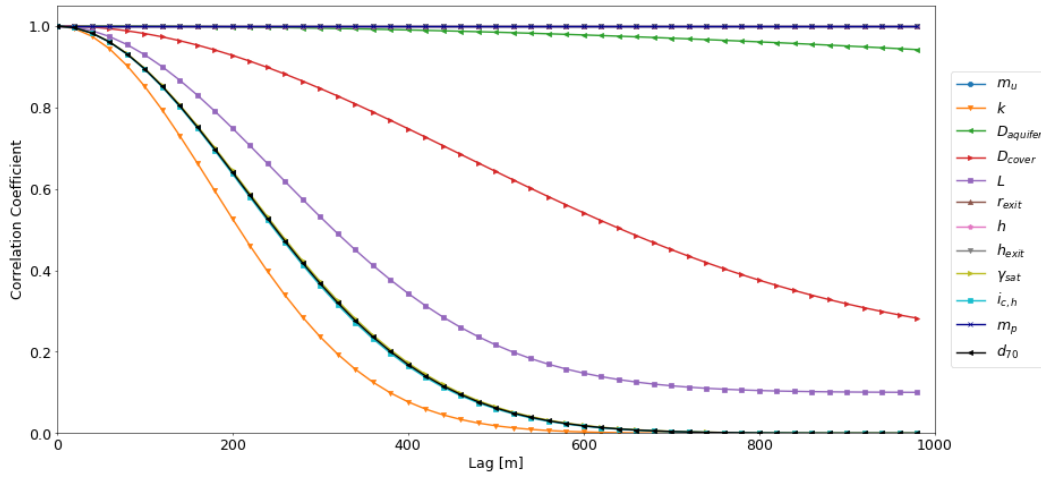


Figure 9.4: Autocorrelation functions (48-1)

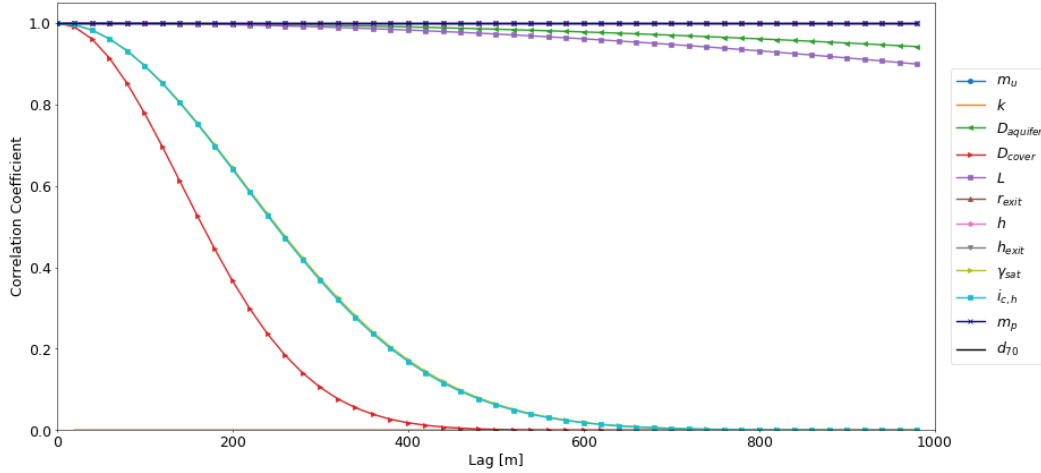


Figure 9.5: Autocorrelation functions (WBI)

To research the influence of the field related and default autocorrelation functions, upper (UL) and lower (LL) limits of the correlation length and residual correlation are assumed to define the upper and lower bounds of the Outcrossing Method. These values are given in table 9.2. All autocorrelation functions necessary are combined in figures 9.6 and 9.7 below.

Parameter X	Spatial Variability (48-1)		Spatial Variability (UL)		Spatial Variability (LL)	
	D_X	$\rho_{0,X}$	D_X	$\rho_{0,X}$	D_X	$\rho_{0,X}$
Model factor m_u	10000	1	10000	1	1000	1
Permeability k	250	0	500	0.4	125	0
Aquifer layer $D_{aquifer}$	4000	0	8000	0.6	1000	0
Cover layer d_{cover}	650	0.2	1300	0.6	325	0
Seepage length L	350	0.1	700	0.4	175	0
Damping factor r_{exit}	2000	1	2000	1	500	0
Water level h	10000	1	10000	1	1000	1
Polder level h_{exit}	1000	1	2000	1	1000	1
Saturated weight γ_{sat}	300	0	600	0.4	150	0
Heave gradient $i_{c,h}$	300	0	600	0.4	150	0
Model factor m_p	10000	1	10000	1	1000	1
Grain size d_{70}	300	0	600	0.4	150	0

Table 9.2: Autocorrelation parameters 48-1 versus UL and LL

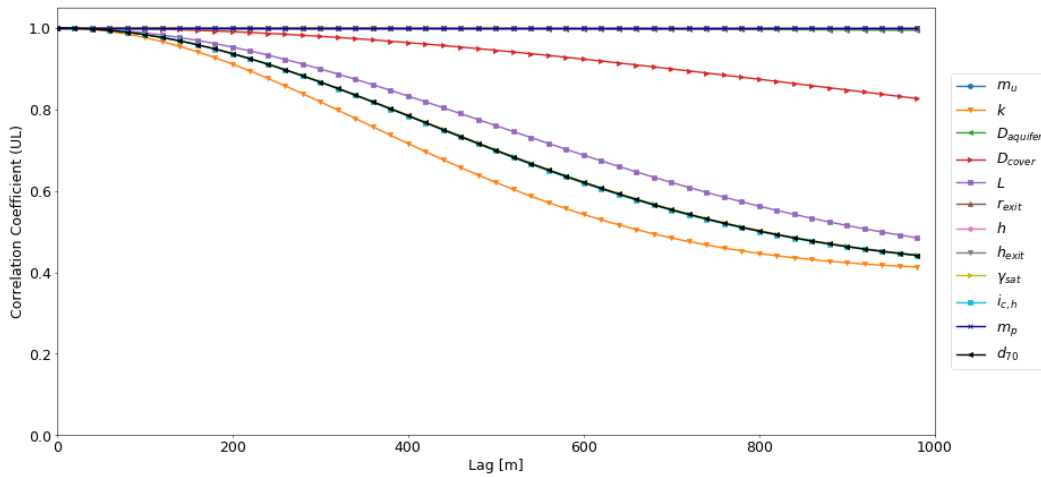


Figure 9.6: Autocorrelation functions (UL)

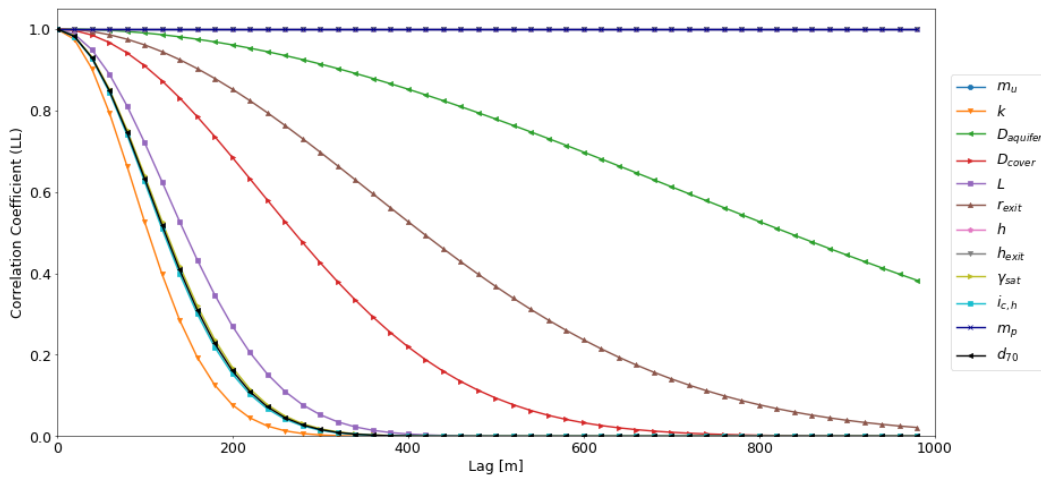


Figure 9.7: Autocorrelation functions (LL)

Combining the importance factors and autocorrelation functions of the stochastic variables in the second derivative of the combined autocorrelation function of the reliability function (Z) results in a spatial autocorrelation function using equation 9.22. This is visualised in figure 9.8 for trajectory 48-1 specific.

$$\rho_z''(0) = - \sum_{i=1}^N \frac{2\alpha_i^2(1 - \rho_{0,i})}{D_i^2} \quad (9.22)$$

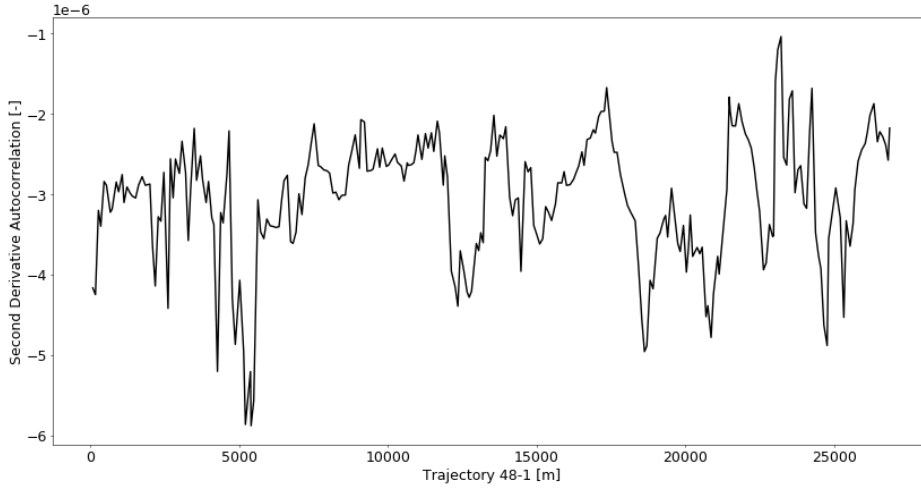


Figure 9.8: Second derivative of the combined autocorrelation function ($\rho_z''(0)$) (48-1)

Finally, the spatial expected length of failure for the failure mechanisms piping (l_{eq}) can be derived from the cross-sectional reliability index (β) and the spatial variability in terms of the second derivative of the autocorrelation function of the reliability function at the origin ($\rho_z''(0)$). This autocorrelation function is based on the residual correlations and correlation distances according to table 9.1. This is visualised in figure 9.9 including upper (UL) and lower (LL) bounds based on high and low residual correlations and correlation distances according to table 9.2.

$$l_{eq} = 2\pi\Phi(-\beta)\exp\left(\frac{1}{2}\beta^2\right)\frac{1}{\sqrt{-\rho_z''(0)}} \quad (9.23)$$

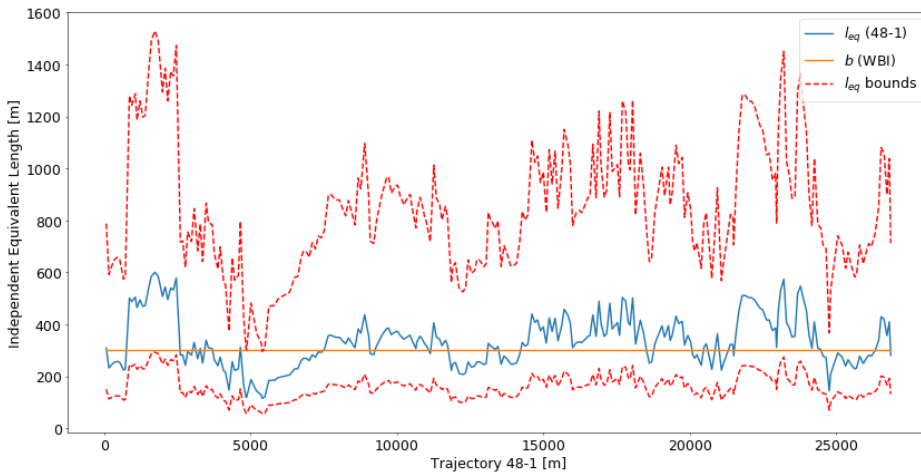


Figure 9.9: Equivalent independent length (l_{eq}) (48-1)

The impact on the sectional length-effect parameter (N^*) is visualised in figure 9.10 below where the N^* factor of the Outcrossing Method in VNK (PC-Ring software) is compared to the current definition of the sectional length-effect parameter based on the WBI calibration (Riskier Software) for 33 dike sections of trajectory 48-1. These definitions are given in equations 9.13 and 9.2. The WBI calibration procedure will be discussed in the next section. Note that the equivalent independent length (l_{eq}) is chosen according to the most critical cross-sections within the dike sections according to a 'weakest link' approach. Finally, the sectional failure probability based on the maximum cross-sectional failure probability is obtained by multiplication with the length-effect parameter as stated in equation 9.1. An overview is given in figure 9.11 in relation to the cross-sectional failure probability.

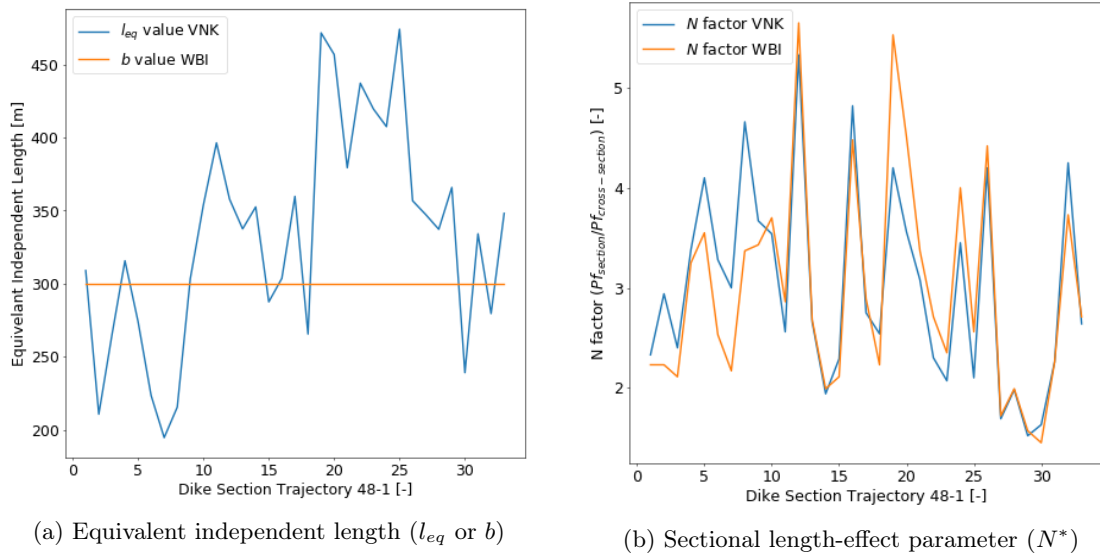


Figure 9.10: Comparison of the sectional length-effect (VNK vs WBI) of trajectory 48-1

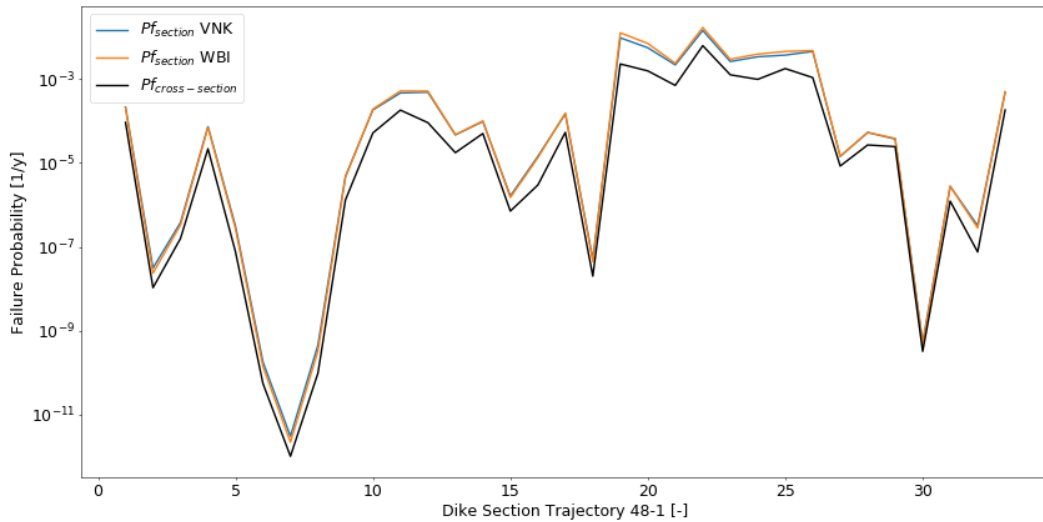


Figure 9.11: Comparison of the length-effect within sections (VNK vs WBI) of trajectory 48-1

9.2 Continuous Model of the Outcrossing Method

Starting point of the calibration of the length-effect parameters ('a' and 'b') in the WBI 2017 is the reliability index of the cross-sections for a failure mechanism specific. This reliability can be derived from semi-probabilistic or probabilistic methods. However, since importance factors are necessary for the calibration of the length-effect parameters, a probabilistic methods is required.

With the total length of the trajectory (L) a relation, identical to equation 9.1, can be found between the trajectory and cross-sectional failure probability of a failure mechanism specific using a continuous model of the outcrossing method. This relation is given in equation 9.24. Within a continuous model no discretization of dike sections is necessary. This approach is based on the papers of Lopez de la Cruz et al. (2010) and Calle (2010) for the calibration of the WTI2011.

$$Pf_{trajectory,mech} = \left(1 + \frac{L}{l_{eq}}\right) \cdot Pf_{cross-section,mech} \quad (9.24)$$

where the expected length of failure for a failure mechanisms (l_{eq}) depends on the cross-sectional reliability index (β) and spatial correlation in terms of the second derivative of the autocorrelation function of the reliability function (Z) at the origin ($\rho_z''(0)$).

$$l_{eq} = 2\pi\Phi(-\beta)\exp\left(\frac{1}{2}\beta^2\right)\frac{1}{\sqrt{-\rho_z''(0)}} \quad (9.25)$$

$$\beta = -\Phi^{-1}(Pf) \quad (9.26)$$

Note that the autocorrelation function of the reliability function of a failure mechanism (ρ_z) is an assembly of autocorrelation functions of the parameters used in the reliability function (Z). The autocorrelation function of a single parameter (ρ_i) is given by the lag parameter (τ), the correlation length (D) and the residual correlation (ρ_0). The assembly of autocorrelation functions is fulfilled using the importance factors (α) for each of the parameters specific as a result from a probabilistic assessment.

$$\rho_i(\tau) = (1 - \rho_{0,i})\exp\left(-\left(\frac{\tau}{D_i}\right)^2\right) + \rho_{0,i} \quad (9.27)$$

$$\rho_z(\tau) = \sum_{i=1}^N \alpha_i^2 \rho_i(\tau) \quad (9.28)$$

The second derivative of the combined autocorrelation functions of the parameters used in the reliability function (Z) at a "lag" value of zero is given by

$$\rho_z''(0) = -\sum_{i=1}^N \frac{2\alpha_i^2(1 - \rho_{0,i})}{D_i^2} \quad (9.29)$$

In order to make the relation given in equation 9.24 continuous over the length of the trajectory it is integrated over the probability distribution for the reliability index ($\beta = \xi$) using the following integral (Calle, 2010)

$$Pf_{trajectory,mech} = \int_{+\infty}^{-\infty} \Phi(-\xi) \cdot \left(1 + \frac{L}{l(\xi)}\right) \frac{\exp\left(-\frac{1}{2}\left(\frac{\xi - \mu_\beta}{\sigma_\beta}\right)^2\right)}{\sqrt{2\pi}\sigma_\beta} d\xi \quad (9.30)$$

This equation can be written as the sum of two integrals.

$$Pf_{trajectory,mech} = \int_{+\infty}^{-\infty} \Phi(-\xi) \frac{\exp\left(-\frac{1}{2}\left(\frac{\xi - \mu_\beta}{\sigma_\beta}\right)^2\right)}{\sqrt{2\pi}\sigma_\beta} d\xi + \int_{+\infty}^{-\infty} \Phi(-\xi) \frac{L}{l(\xi)} \frac{\exp\left(-\frac{1}{2}\left(\frac{\xi - \mu_\beta}{\sigma_\beta}\right)^2\right)}{\sqrt{2\pi}\sigma_\beta} d\xi \quad (9.31)$$

In the first part of this summation a transformation ($t = \frac{\xi - \mu_\beta}{\sigma_\beta}$) is substituted for the integral variable (ξ) which can be used to approximate the first part using a Taylor function. This results in the following approximation of the first integral (Calle, 2010)

$$\int_{+\infty}^{-\infty} \Phi(-\xi) \frac{\exp(-\frac{1}{2}(\frac{\xi - \mu_\beta}{\sigma_\beta})^2)}{\sqrt{2\pi}\sigma_\beta} d\xi = \quad (9.32)$$

$$\int_{+\infty}^{-\infty} \Phi(-(\mu_\beta + t \cdot \sigma_\beta)) \frac{\exp(-\frac{1}{2}t^2)}{\sqrt{2\pi}} dt = \quad (9.33)$$

$$\Phi(-\mu_\beta) + \frac{\exp(-\frac{1}{2}\mu_\beta^2)}{\sqrt{2\pi}} \left(\frac{1}{2}\mu_\beta\sigma_\beta^2 + \frac{1}{4}(\mu_\beta^3 - 3\mu_\beta)\sigma_\beta^4 \right) \quad (9.34)$$

In the second part of this summation a relation, given in equation 9.25, for the expected length of failure for a failure mechanisms ($l(\xi)$) is substituted. This results in the following approximation of the second integral (Calle, 2010)

$$\int_{+\infty}^{-\infty} \Phi(-\xi) \frac{L}{l(\xi)} \frac{\exp(-\frac{1}{2}(\frac{\xi - \mu_\beta}{\sigma_\beta})^2)}{\sqrt{2\pi}\sigma_\beta} d\xi = \quad (9.35)$$

$$\int_{+\infty}^{-\infty} \Phi(-\xi) \frac{L\sqrt{-\rho_z''(0)}}{2\pi\Phi(-\xi)\exp(\frac{1}{2}\xi^2)} \frac{\exp(-\frac{1}{2}(\frac{\xi - \mu_\beta}{\sigma_\beta})^2)}{\sqrt{2\pi}\sigma_\beta} d\xi = \quad (9.36)$$

$$\frac{L\sqrt{-\rho_z''(0)}}{2\pi\sqrt{1 + \sigma_\beta^2}} \exp\left(-\frac{1}{2}\left(\frac{\mu_\beta^2}{1 + \sigma_\beta^2}\right)\right) \quad (9.37)$$

Combining the two parts results in the following relation where the trajectory failure probability of a failure mechanism specific is a function of the mean and standard deviation of the cross-sectional reliability index (β), the total length of the trajectory (L) and the second derivative of the autocorrelation function of the reliability function at a "lag" value of zero ($\rho_z''(0)$).

$$Pf_{trajectory,mech} = F(\mu_\beta, \sigma_\beta, \rho_z''(0), L) = \quad (9.38)$$

$$\frac{L\sqrt{-\rho_z''(0)}}{2\pi\sqrt{1 + \sigma_\beta^2}} \exp\left(-\frac{1}{2}\frac{\mu_\beta^2}{1 + \sigma_\beta^2}\right) + \Phi(-\mu_\beta) + \frac{\exp(-\frac{1}{2}\mu_\beta^2)}{\sqrt{2\pi}} \left(\frac{1}{2}\mu_\beta\sigma_\beta^2 + \frac{1}{4}(\mu_\beta^3 - 3\mu_\beta)\sigma_\beta^4 \right) \quad (9.39)$$

Vice versa, when a required trajectory failure probability is known, a relation can be obtained for the required cross-sectional reliability based on the required trajectory failure probability of a failure mechanism specific, the length of the trajectory and the second derivative of the autocorrelation function.

$$\mu_\beta = F(Pf_{trajectory,mech}, \sigma_\beta, \rho_z''(0), L) \quad (9.40)$$

Note that the required trajectory failure probability of a failure mechanism specific can be obtained using the failure allocation or 'faalkansbegroting' (ω) and the safety requirements of dike trajectories.

$$Pf_{trajectory,mech} = Pf_{trajectory} \cdot \omega \quad (9.41)$$

Finally, the required reliability index on cross-sectional scale will be given by the 95% confidence level as a calibration criterion based on the 5% lower limit.

$$\beta_{cross-section,mech} = \mu_\beta - 1.65\sigma_\beta \quad (9.42)$$

Piping

To calibrate the length-effect for Dutch trajectories of the failure mechanism piping the following data is used based on the VNK2 trajectory studies (DR 5, 10, 14, 17). The data is used to find a relation between the required cross-section and trajectory reliability (Lopez de la Cruz et al., 2010).

- Required reliability index $\beta_{trajectory}$ of 3.78, 3.89, 4.06 and 4.26
- Allocation of failure mechanisms ω of 0.1 (piping)
- Standard deviation $\sigma_{\beta_{cross-section}}$ of 0.2 (upper limit)
- Length of the trajectory L ranging from 0 to 100 km
- Autocorrelation function $\rho_z''(0)$ of $-1.8e-05$ (average value)

The calibration of equation 9.40 - 9.42 to four Dutch trajectories using the data from the VNK2 trajectory studies is given in figure 9.12a. By fitting equation 9.24 to the results as shown in figure 9.12b a relation results from which the length-effect parameters (a and b) can be derived. This relation is given in equation 9.43.

$$Pf_{cross-section, mech} = \frac{Pf_{trajectory, mech}}{1 + \frac{\alpha \cdot L}{l}} = \frac{Pf_{trajectory, mech}}{1 + 0.0028 \cdot L} \quad (9.43)$$

The calibration results in a α/l ratio of 0.0028 (or 1/350). Values of a and b used in the WBI for equations 9.1 and 9.3 are 0.4-0.9 and 300m respectively, making a distinction between upper river and lower river areas. Note that the value of a can be adjusted for the length of the sensitive part of the trajectory for the failure mechanism specific based on local information (Lopez de la Cruz et al., 2010). These values are used in the WTI2017 (RWS, 2017c). An overview is given in figure 9.12b.

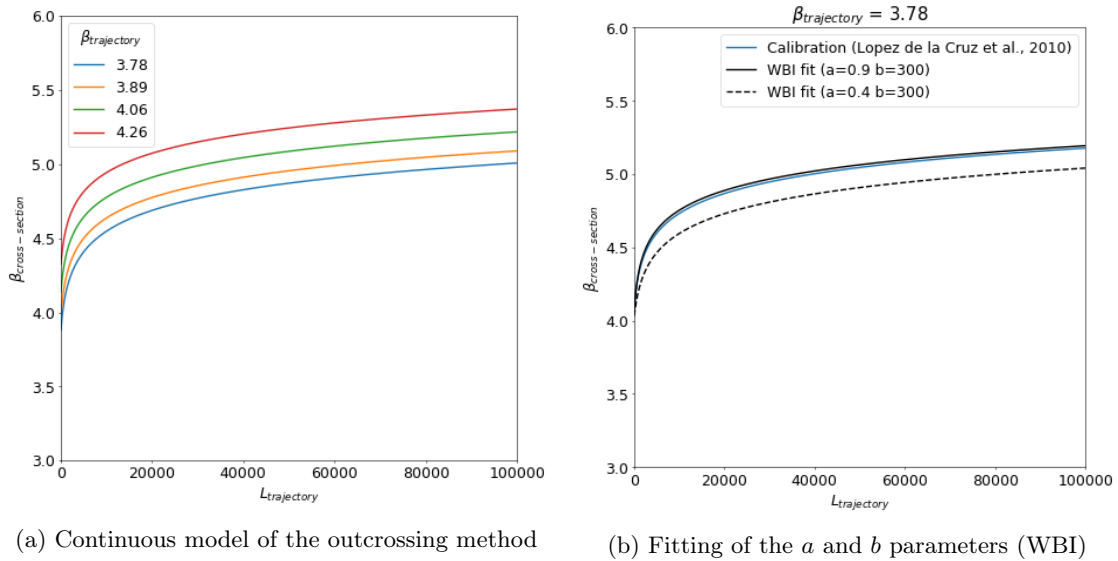


Figure 9.12: Calibration of the length-effect for the WBI 2017 (Continuous Model)

9.2.1 Field Calibration

In order to calibrate the length-effect parameters ('a' and 'b') for a specific trajectory, the required reliability index of the trajectory, the length of the trajectory, the autocorrelation functions and importance factors of the stochastic parameters used in the piping assessment are necessary to find a location specific relation between the required cross-section and trajectory reliability index (Lopez de la Cruz et al., 2010). For trajectory 48-1 the following parameters are used.

- Required reliability index $\beta_{trajectory}$ of 4.0 (1/30000)
- Allocation of failure mechanisms ω of 0.24 (piping)
- Standard deviation $\sigma_{\beta_{cross-section}}$ of 0.2 (upper limit)
- Length of the trajectory L ranging from 0 to 27 km
- Autocorrelation function $\rho_z''(0)$ of $-\sum_{i=1}^N \frac{2\alpha_i^2(1-\rho_{0,i})}{D_i^2}$ (spatial value)

The importance factors (α_i) of the limit state function parameters are given in figure 7.15 and for convenience visualised in figures 9.13 and 9.14. These importance factors are obtained from the probabilistic assessment based on field related mean values derived from the data analysis with the default WBI standard deviations since the calibration procedure of the length-effect is based on these uncertainties.

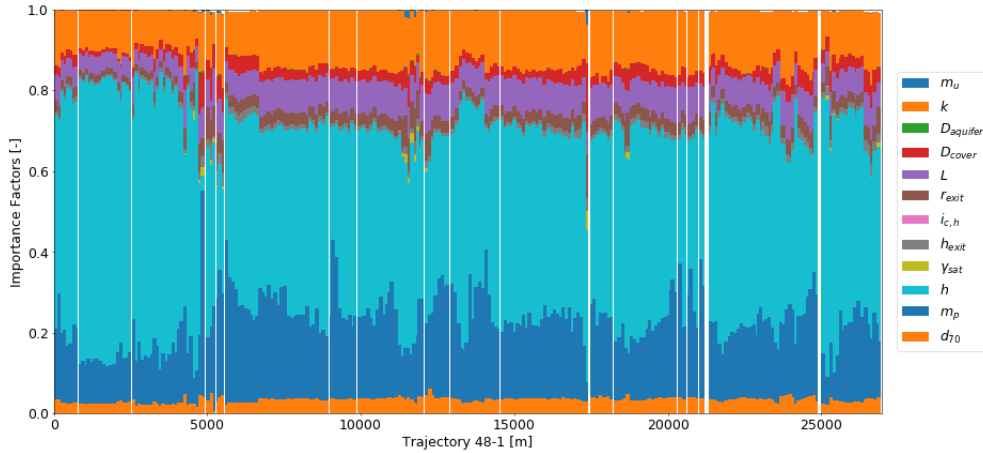


Figure 9.13: Importance factors (α_i^2) (σ_{wbi}) (48-1)

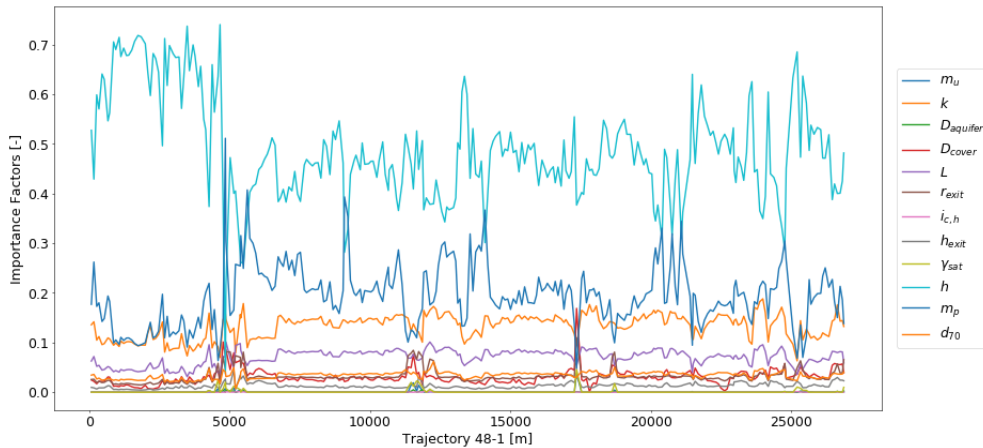


Figure 9.14: Importance factors (α_i) (σ_{wbi}) (48-1)

Next, the autocorrelation functions (ρ_i) of the parameters used in the limit state function are necessary. For parameters with a residual correlation ($\rho_{0,i}$) equal to one the autocorrelation drops out the second derivative of the combined autocorrelation functions at the origin, as stated by equation 9.17. For the model factor uplift and piping (m_u and m_p), damping factor (r_{exit}), inner and outer water level (h_{exit} and h) a residual correlation of one is assumed conform the WBI 2017 (Deltares, 2019). For the remainder parameters with a residual correlation ($\rho_{0,i}$) below one the correlation distance (D_i) and the residual correlation ($\rho_{0,i}$) are of importance. These field related values are given in table 9.1 next to the values conform the WBI 2017. The application of field specific autocorrelation functions is the key difference between the field calibration and the WBI calibration. All autocorrelation functions necessary are visualised in figure 9.4 and for convenience shown in figure 9.15 below.

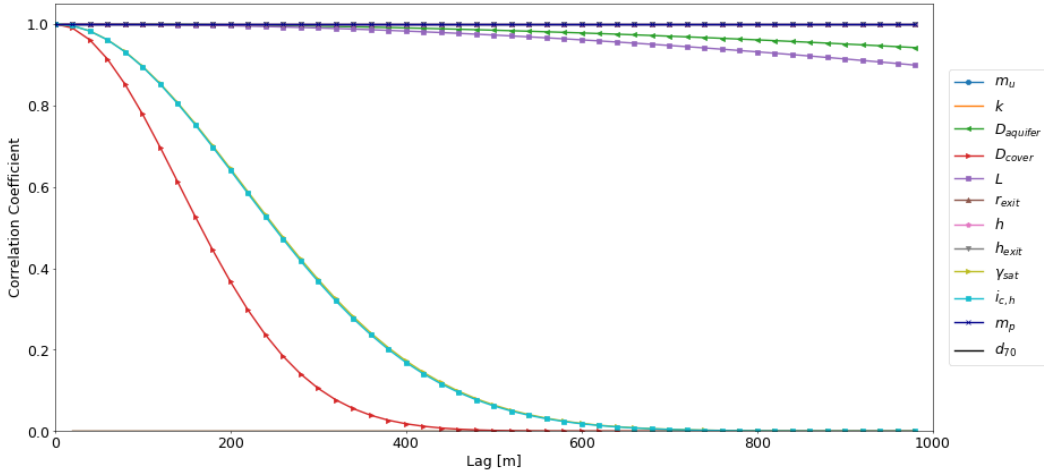


Figure 9.15: Autocorrelation functions (WBI)

Combining the importance factors and autocorrelation functions of the stochastic variables used into the second derivative of the combined autocorrelation function of the reliability function (Z) results into a spatial autocorrelation function using equation 9.22. This is visualised in figure 9.16 for trajectory 48-1.

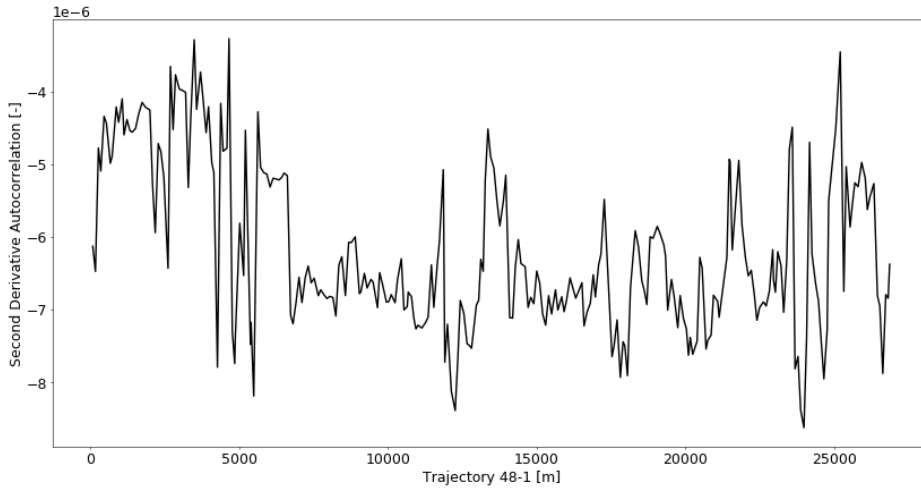


Figure 9.16: Second derivative of the combined autocorrelation function ($\rho_z''(0)$) (48-1)

Finally, the spatial expected length of failure for the failure mechanisms piping (l_{eq}) can be derived from the cross-sectional reliability index (β) and the spatial variability in terms of the second derivative of the autocorrelation function of the reliability function at the origin ($\rho_z''(0)$). This is visualised in figure 9.17 including an upper and lower bound based on high and low residual correlations and correlation distances.

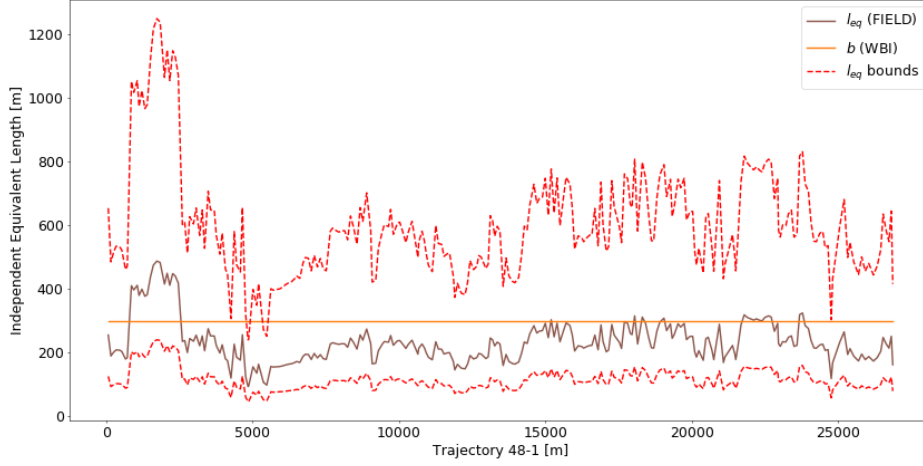
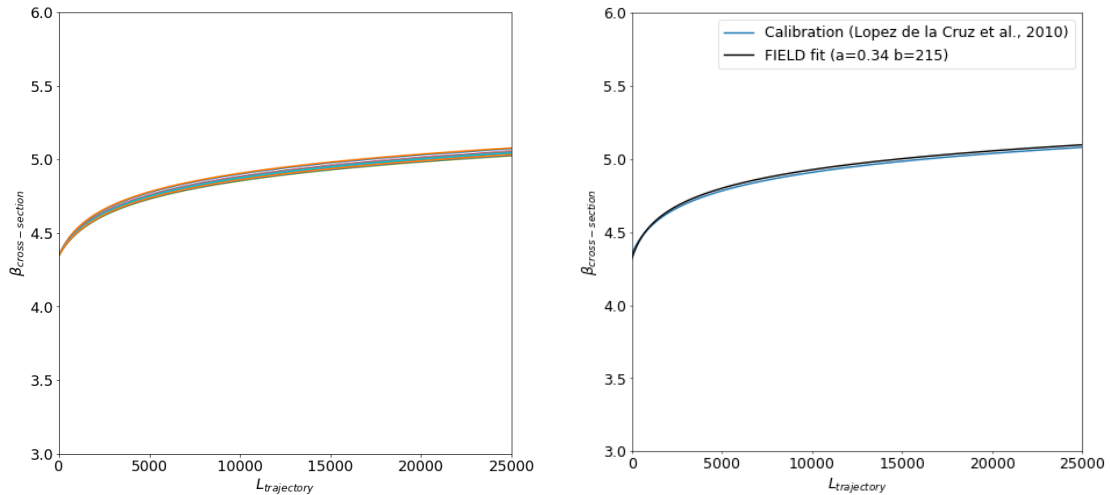


Figure 9.17: Equivalent independent length (l_{eq}) (48-1)

The calibration of equation 9.40 - 9.42 to trajectory 48-1 using the data from the field calibration as discussed is given in figure 9.18a. By fitting equation 9.24 to the results as shown in figure 9.18b a relation results from which length-effect parameters (a and b) can be derived. This procedure is repeated for multiple locations.

$$Pf_{cross-section, mech} = \frac{Pf_{trajectory, mech}}{1 + \frac{\alpha \cdot L}{l}} = \frac{Pf_{trajectory, mech}}{1 + 0.0016 \cdot L} \quad (9.44)$$

The calibration results in a α/l ratio of 0.0016 (or 1/633). Values of a and b used in the field for equations 9.1 and 9.3 are 0.36 and 215m respectively, based on an average equivalent independent length (l_{eq}) or "b" of 215m. Note that the value of "a" fits all locations since the equivalent independent length and the second derivative of the autocorrelation function ($\rho_z''(0)$) change spatially in the same order, making the fit of "a" spatially constant. A single example of fitting a to a specific location is given in figure 9.18



(a) Cross-sectional reliability versus Length for $\sigma_{beta}=0.2$ and $\rho_z''(0)$ according to figure 9.16

(b) Fitting of equation 9.24 to the spatial data of trajectory 48-1 (single example)

Figure 9.18: Field calibration of trajectory 48-1 (Continuous Model)

The impact on the sectional length-effect parameter (N^*) is visualised in figure 9.19 below where the N^* factor as a result of the field calibration (48-1) using the Continuous Model of the Outcrossing Method is compared to the current definition of the sectional length-effect parameter based on the WBI calibration (Riskeer Software) for 33 dike sections of trajectory 48-1. These definitions are given in equations 9.44 and 9.2. Note that the equivalent independent length (l_{eq}) is chosen according to the most critical cross-sections within the dike sections according to a 'weakest link' approach. Finally, the sectional failure probability based on the maximum cross-sectional failure probability is obtained by multiplication with the length-effect parameter as stated in equation 9.1. An overview is given in figure 9.20 in relation to the cross-sectional failure probability.

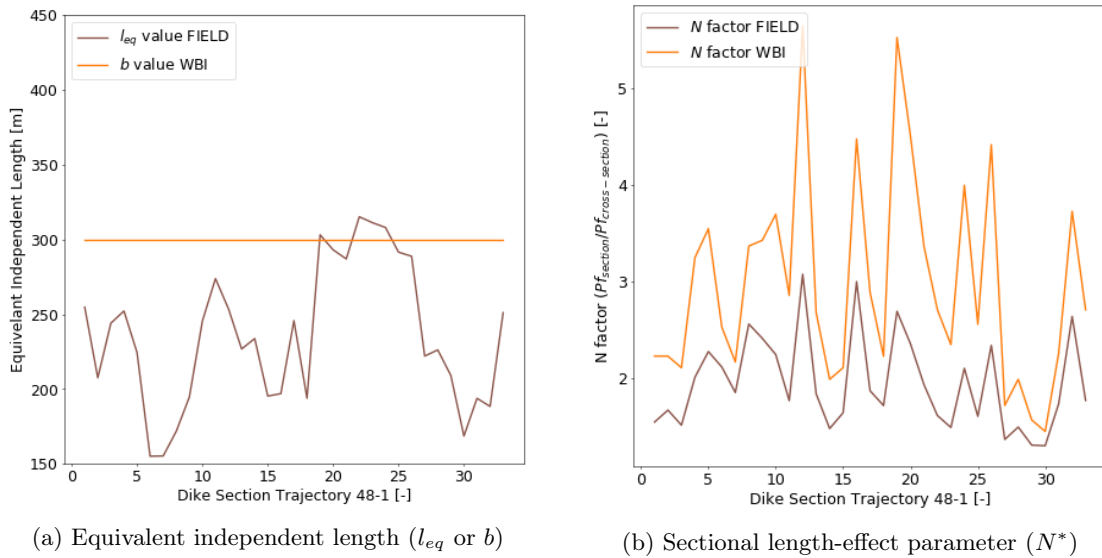


Figure 9.19: Comparison of the sectional length-effect (WBI(field) vs WBI) of trajectory 48-1

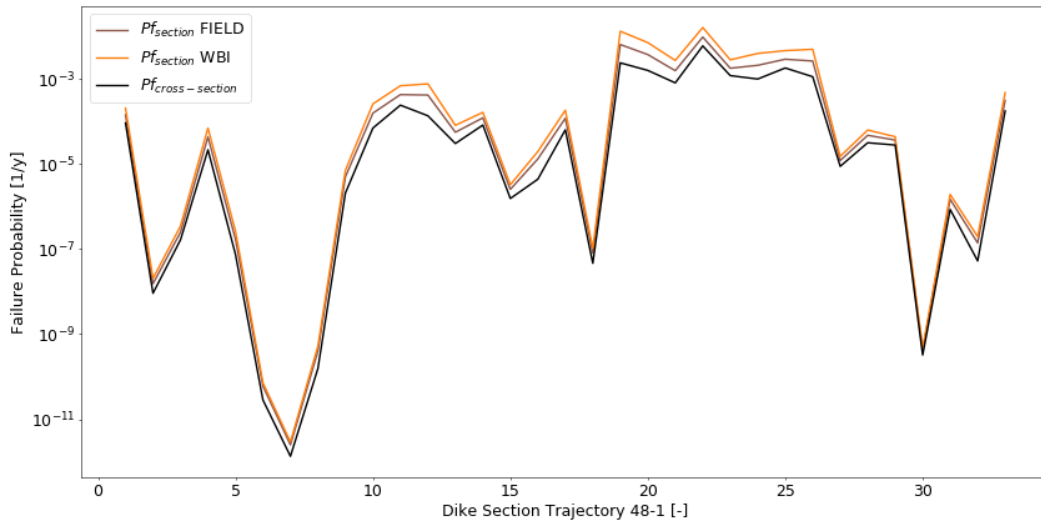


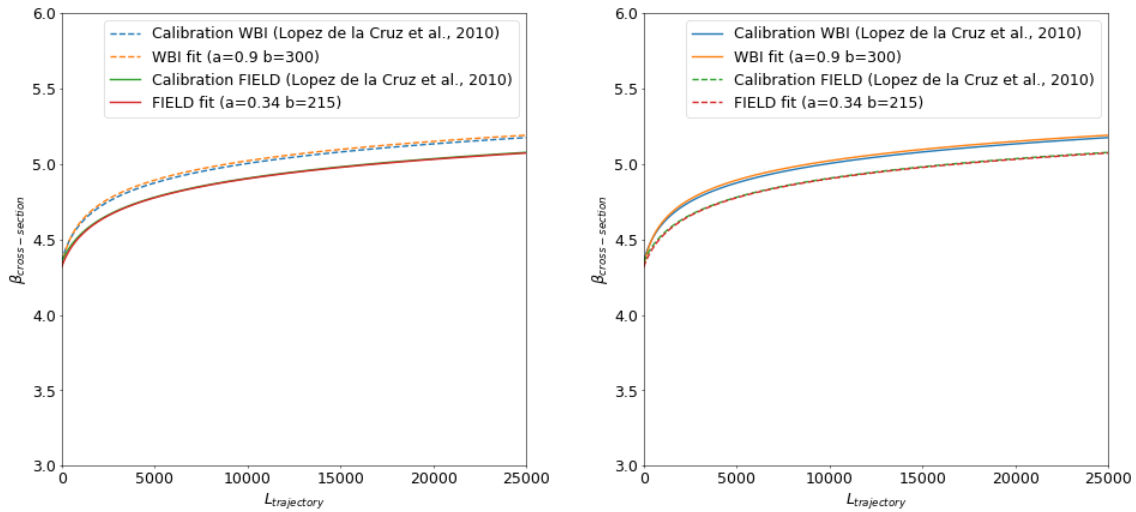
Figure 9.20: Comparison of the length-effect within sections (WBI(field) vs WBI) of trajectory 48-1

Chapter 10

Conclusions of Sub Question 2

SQ2 *How to use the length-effect on sectional scale correctly to scale the failure probability from cross-sectional level to sectional level?*

To answer the second research question, spatial importance factors and fitted autocorrelation functions of the parameters required for the piping assessment are obtained from the data and reliability analysis. The sectional length-effect in the current Dutch flood risk analysis software (Riskeer) is derived from the WBI calibration study based on four dike trajectories in the Netherlands. This WBI calibration study is based on a Continuous Model of the Outcrossing Method which is discussed in section 9.2. This model is used to fit the independent equivalent length (b) and the failure mechanism sensitive fraction (a) to the results of the calibration study which in the end are applied to all dike trajectories in the Netherlands, making a distinction between the lower and upper river areas. Next, the Continuous Model of the Outcrossing Method is applied to the case study using the mean values and standard deviations from the field. Finally, this Field calibration of the case study is compared to the current definition of the length-effect within sections based on the WBI calibration study. Figure 10.1a highlights the result of the calibration of the length-effect for trajectory 48-1 specific and figure 10.1b highlights the result of the calibration of the length-effect for the WBI 2017.



(a) Cross-sectional reliability versus Length for $\sigma_{beta}=0.2$ and $\rho_z''(0)$ of $-3.1e-06$ (average value)

(b) Cross-sectional reliability versus Length for $\sigma_{beta}=0.2$ and $\rho_z''(0)$ of $-1.8e-05$ (average value)

Figure 10.1: Field calibration (FIELD) versus WBI calibration (WBI) of trajectory 48-1

From the calibration of the length-effect it can be concluded that the sectional length-effect is currently overestimated for trajectory 48-1 which originates mainly from the conservative choice of the failure mechanism sensitive fraction (a). In comparison to the derived results, a reference is made to the thesis of Kanning (2012). In this thesis the length-effect parameters based on four dike systems are derived resulting in an a -value of 0.36 and a b -value of 262m for the failure mechanism piping. Note that in the calibration report of the WBI a and b -values are derived for the same dike systems resulting in an a -value of 0.90 and b -value of 300m (Lopez de la Cruz et al., 2010).

In figure 10.2b the sectional length-effect factors are visualised using the ' a ' and ' b ' parameters derived from the field calibration according to equation 9.44. These results are compared to the current sectional length-effect factors using the ' a ' and ' b ' parameters from the WBI calibration study according to equation 9.43. Both using the Continuous Model of the Outcrossing Method.

The Outcrossing Method of section 9.1, which is used in previous Dutch flood risk analysis (VNK), is applied to the case study using the mean and standard deviation values as derived from the data analysis. Based on the Outcrossing Method the length-effect within sections can be defined by the sectional length-effect parameter according to equation 9.13. The results of the Outcrossing Method are compared to the current definition of the length-effect within sections which is used in the Legal Assessment Instrument (WBI). This definition is given in equation 9.2. In figure 10.2a this comparison is visualised. It can be concluded that the previous definition of the length-effect (VNK) is similar to the current definition of the length-effect (WBI) based on the calibration study.

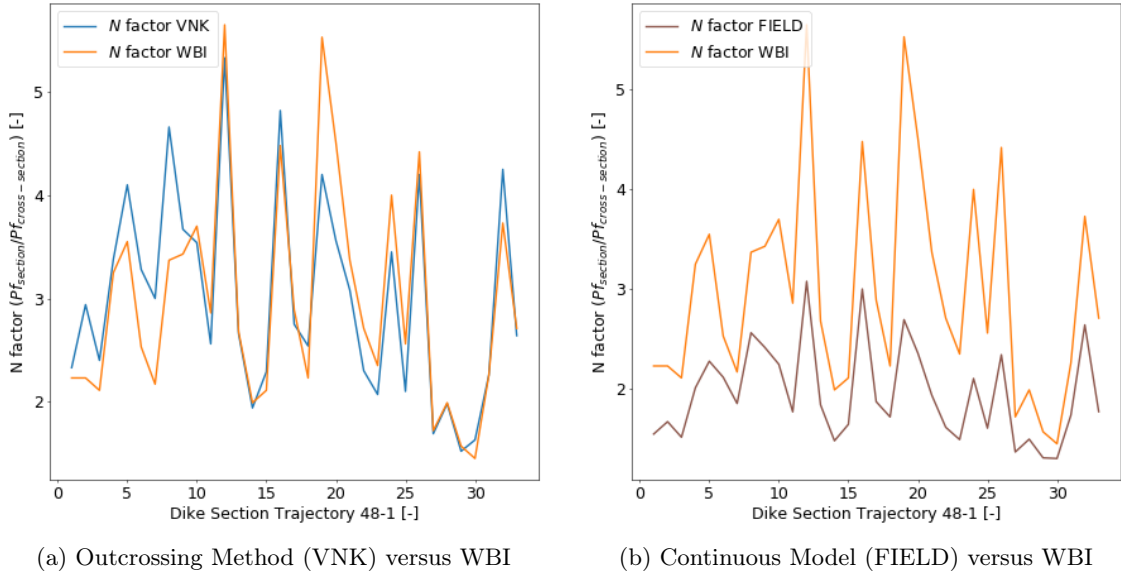


Figure 10.2: Sectional length-effect parameter (N^*) of trajectory 48-1

So, in figure 10.2 both the Outcrossing Method (VNK) as the Continuous Model of the Outcrossing Method (FIELD) are applied to the case study, and compared to the Calibration Study of the WBI which is currently used in practice. In the case study the two different methods are based on a probabilistic approach with a spatial interval of approximate 120 meters. Since this interval is smaller than the equivalent independent length and therefore also smaller than the defined dike sections, the ratio of the independent summation of the cross-sectional failure probabilities ($\sum P f_i$) to the maximum cross-sectional failure probability ($\max P f_i$) within a section gives a good indication of an upper limit of the sectional length-effect. This is given in equation 10.1 and visualised in figure 10.3.

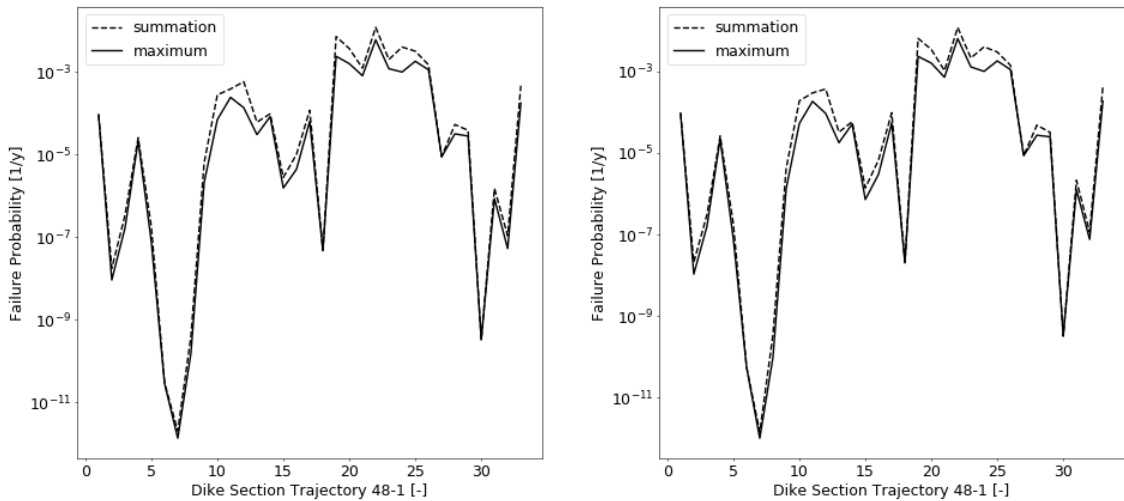


Figure 10.3: Summation versus maximum within sections based on (σ_{WBI}) left and (σ_{field}) right

$$N^* = \frac{\sum(Pf_i)}{\max(Pf_i)} \quad i \in L_{section} \quad (10.1)$$

In short, if the length of a section increases the summation of the failure probabilities increases and so N^* , if the number of contributing (normative) cross-sections increases the summation of failure probabilities increases and so N^* and if only one cross-section contributes to the summation of failure probabilities the ratio will approach one. Increase of the length of sections can be interpreted as an increase in the ratio L/b and the increase of the number of contributing cross-sections can be interpreted as an increase in the factor a as in equation 10.2.

$$N^* = 1 + \frac{a \cdot L_{section}}{b} \quad (WBI) \quad (10.2)$$

In figure 10.4a the ratio of independent summation to the maximum failure probabilities is based on a probabilistic approach using field related uncertainties and compared to the length-effect factor as defined in the dike safety analysis of the WBI and VNK according to equations 9.2 and 9.13 respectively. In figure 10.4b the ratio of independent summation to the maximum failure probabilities is based on a probabilistic approach using default uncertainties from the WBI and compared to the length-effect factor as a result of the calibration study for the WBI 2017 and from applying the calibration study to a field specific location (48-1) according to equations 9.2 and 9.44 respectively. From these figures it is clear that the length-effect within sections is overestimated for both the outcrossing approach as the current definition of the length-effect within the WBI 2017. The field calibrated length-effect parameter shows less conservatism in relation to the ratio of equation 10.1.

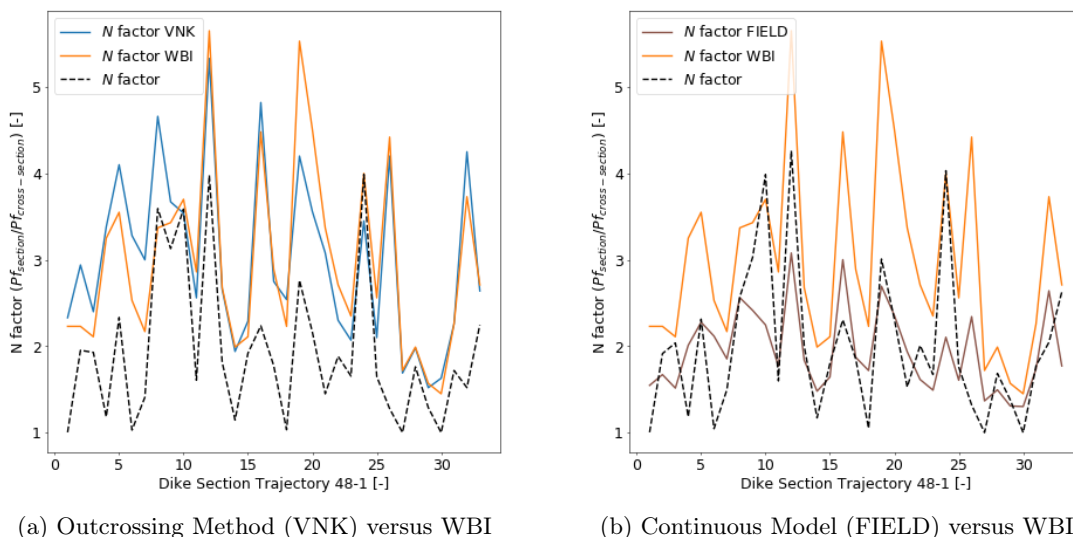


Figure 10.4: Sectional length-effect parameter (N^*) of trajectory 48-1

Other causes of the overestimation of the current length-effect within sections originates from the fundamentals of the Outcrossing Method and the Continuous Model. (1) These approaches are based on a Gaussian field of lengths much longer than the correlation distance of the limit state function. However, in reality much smaller dike sections are identified close to the equivalent independent length where the model shows rapid increase of the length-effect factor as shown in figure 10.1. Furthermore, (2) these approaches are based on an statistically constant reliability within dike sections, known as the theoretical 'homogeneous sections'. However, in practice section are not statistically homogeneous and with the assessment of dikes for specific failure mechanisms one searches for a conservative cross-section or 'weakest link' to represent the dike section instead of a statistically constant value. As shown in figure 10.5, the overestimation of the length-effect occurs mainly at sections with relative high failure probabilities which originates from the fundamentals of the methods. (3) Since the outcrossing method (made continuously with the Continuous Model) is an upper bound of the failure probability, this approximation is only justified if the outcrossing rate and initial failure probability are small. However, for critical dike sections this is not the case and consequently this upper bound 'double counts' the probability of events within a Gaussian field (Rijkswaterstaat, 2016b).

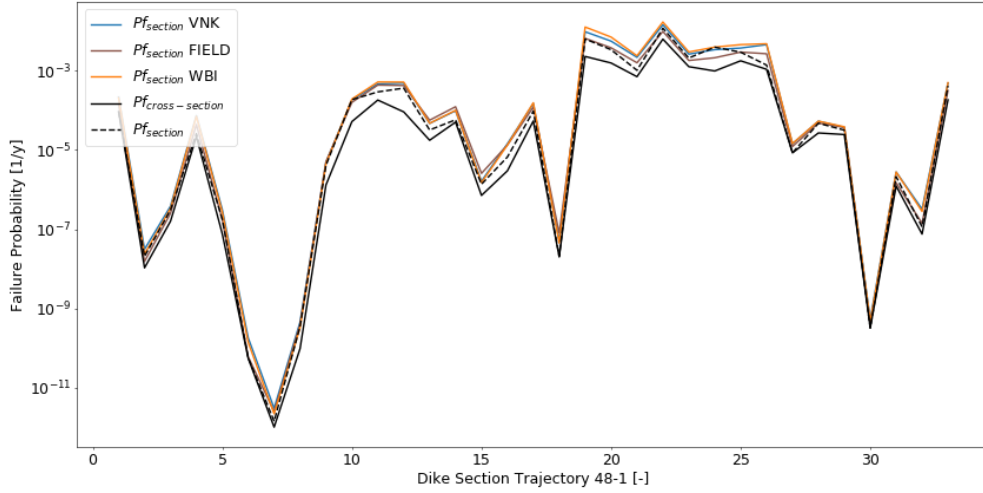
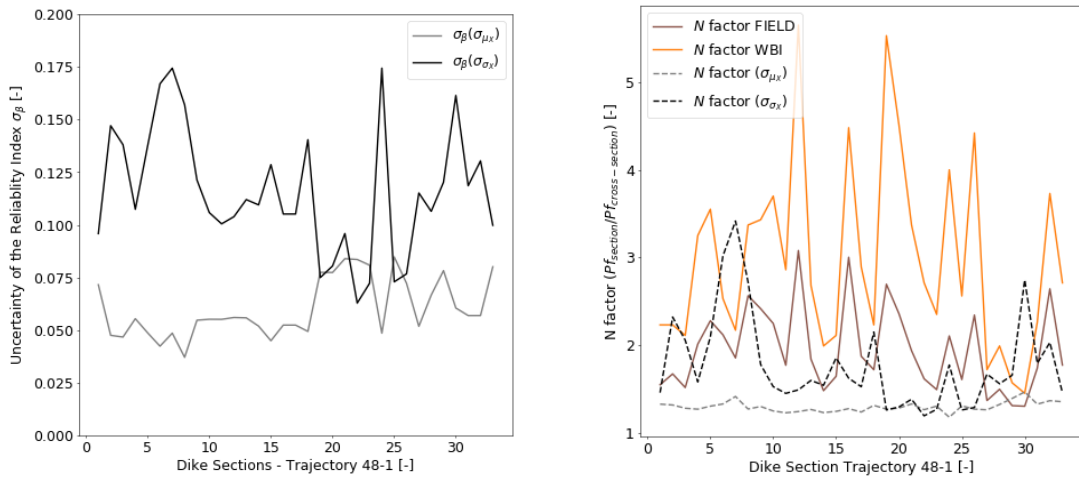


Figure 10.5: Comparison of the length-effect within sections of trajectory 48-1. The numerical results of these different approaches to account for the length-effect are listed in table 10.1 below.

In addition to the discussed comparisons of the length-effect within sections, the results of the sensitivity analysis of section 7.2 can be included in a comparison. With the use of the uncertainties related to the reliability index with respect to the distribution parameters (μ and σ) a sectional length-effect factor can be derived which is given in equation 10.3.

$$N^* = \frac{\Phi(-\beta_{cross-section} - \sigma_\beta)}{\Phi(-\beta_{cross-section})} \quad (10.3)$$

This definition of the sectional length-effect only includes the uncertainties related to the distribution parameters of the limit state function in a FORM analysis. These uncertainties are unknown and assumptions are made based on bootstrapping. In figure 10.6a the uncertainties of the reliability index of all normative cross-sections of the 33 dike sections are repeated. With the use of equation 10.3 a comparison with the length-effect within sections is given in figure 10.6b. In most cases the magnitude of increase due to the uncertainty related to the reliability of the normative cross-section σ_β (with respect to μ_X and σ_X) is smaller than the increase due to the current length-effect factors. For the two locations where it is the other way around the failure probability is really low, such that an increase in beta results in a high factor of increase. This indicates the difficulty of the comparison due to the sensitivity to the magnitude of the reliability.



(a) Uncertainty of the reliability index w.r.t. the distribution parameters (μ_X and σ_X)

(b) Comparison of the uncertainty of the reliability index with the sectional length-effect (WBI)

Figure 10.6: Comparison of the uncertainty of the reliability index with the sectional length-effect

So, it can be concluded that the length-effect within sections based on a continuous model of outcrossing method is currently overestimated. This conservatism originates from the calibrated length-effect parameters ('a' and 'b'). More accurate length-effect parameters results from this calibration procedure based on field related importance factors and autocorrelations. These field related length-effect factors coincide more with the physical upper limit of the ratio between the summation of failure probabilities to the maximum failure probability within a dike section compared to the current length-effect factors. Moreover, these field related length-effect parameters coincide more with the uncertainties related to the reliability of the normative cross-sections within sections.

Furthermore, the methods used in the Dutch flood risk analysis to quantify the sectional length-effect are based on theoretical assumptions that mismatch the practical applicability because the method is in most cases not applied to intervals much larger than the independent equivalent length, the method is in most cases not applied to intervals with statistically constant reliability and the method is based on the upper bound of the outcrossing method which is only a good approximation for small failure probabilities and outcrossing rates.

Since the field calibrated 'a' and 'b' parameters reduce the length-effect significantly, but still include conservatism resulting from the mismatch between the theoretical assumptions and practical applicability, the length-effect within sections approaches one indicating no length-effect if the assessment is based on the 'weakest link' within a section with variable or small reliability and sectional lengths not much larger than the equivalent independent length. The 'weakest' cross-sections are selected over intervals ($\pm 120\text{m}$) by assessing the cross-sectional reliability using spatially interpolated limit state function parameters and modeled hydraulic loads. In Chapter 14 the impact of these conclusions are discussed in comparison to the conclusions related to other assembly procedure steps.

#Section	$Pf_{cross-sec}(\mathbf{P})$	σ_{field}	$Pf_{cross-sec} \times N_{WBI}^*$	$Pf_{cross-sec} \times N_{V NK}^*$	$Pf_{cross-sec} \times N_{FIELD}^*$	$\sum Pf_{cross-sec,i} \quad i \in sec$
1	9.26E-05		2.08E-04	2.15E-04	1.54E-04	9.37E-05
2	1.06E-08		2.05E-08	3.12E-08	1.52E-08	1.76E-08
4	1.58E-07		3.50E-07	3.79E-07	2.63E-07	3.38E-07
5	2.18E-05		7.09E-05	7.36E-05	4.77E-05	2.58E-05
6	7.54E-08		2.68E-07	3.13E-07	1.77E-07	1.75E-07
12	5.50E-11		7.16E-11	1.80E-10	5.11E-11	2.96E-11
13	1.01E-12		2.91E-12	3.03E-12	2.17E-12	2.01E-12
14	9.65E-11		5.26E-10	4.50E-10	3.51E-10	4.01E-10
15	1.31E-06		7.20E-06	4.81E-06	4.79E-06	6.36E-06
16	5.20E-05		2.62E-04	1.84E-04	1.72E-04	2.83E-04
17	1.82E-04		7.02E-04	4.67E-04	4.86E-04	3.93E-04
18	9.15E-05		7.79E-04	4.88E-04	4.76E-04	5.88E-04
19	1.76E-05		8.23E-05	4.68E-05	5.79E-05	6.16E-05
20	5.04E-05		1.66E-04	9.76E-05	1.27E-04	9.77E-05
21	7.12E-07		3.29E-06	1.63E-06	2.47E-06	2.81E-06
22	2.97E-06		1.99E-05	1.43E-05	1.26E-05	1.02E-05
23	5.38E-05		1.86E-04	1.48E-04	1.29E-04	1.20E-04
24	2.00E-08		1.04E-07	5.09E-08	7.68E-08	4.89E-08
25	2.30E-03		1.35E-02	9.65E-03	8.24E-03	7.32E-03
26	1.57E-03		7.27E-03	5.59E-03	4.60E-03	3.73E-03
27	7.08E-04		2.77E-03	2.18E-03	1.85E-03	1.25E-03
28	6.27E-03		1.65E-02	1.45E-02	1.16E-02	1.22E-02
29	1.27E-03		2.86E-03	2.63E-03	2.08E-03	2.03E-03
30	9.86E-04		4.04E-03	3.41E-03	2.61E-03	4.08E-03
31	1.78E-03		4.71E-03	3.74E-03	3.35E-03	3.23E-03
32	1.09E-03		5.06E-03	4.56E-03	3.21E-03	1.51E-03
34	8.46E-06		1.53E-05	1.43E-05	1.23E-05	8.93E-06
37	2.69E-05		6.37E-05	5.32E-05	4.87E-05	5.39E-05
38	2.45E-05		4.44E-05	3.72E-05	3.68E-05	3.90E-05
39	3.21E-10		4.70E-10	5.22E-10	4.01E-10	3.24E-10
41	1.23E-06		1.95E-06	2.78E-06	1.43E-06	1.53E-06
42	7.54E-08		1.98E-07	3.21E-07	1.30E-07	1.09E-07
43	1.84E-04		4.85E-04	4.86E-04	3.40E-04	4.70E-04
SUM	1/59.57		1/16.74	1/20.59	1/25.25	1/26.57

Table 10.1: Overview of maximum sectional failure probabilities (including the length-effects)

Finally, the understanding of the length-effect is currently lacking since the length-effect is calculated from a probabilistic assessment and applied to a semi-probabilistic assessment in order to incorporate the combination of spatial uncertainties. In relation to complex approaches a simplified approach based on the definitions of the length-effect parameters is discussed in appendix I.

Part V

Length-Effect between Sections

Chapter 11

Length-Effect between Sections

With increasing length of a dike section (or dike trajectory) the probability that a weak spot occurs will increase. So, with increasing length, the failure probability of a dike section (or dike trajectory) will increase. This is called the length-effect. The length-effect within sections is the result of combining spatial uncertainties within a section. The length-effect between sections is the result of combining sections with different correlations (Kanning, 2012). In this chapter, the focus will be on the length-effect between sections.

'Helpdesk Water' defined the length-effect as the result of combining dike sections with correlated hydraulic loads and fluctuating resistances. Due to the fluctuating resistances, dike sections are considered as independent sections. The loads are fully correlated. The interaction of load and resistance can be interpreted as a serial system where the load within each section is equal but the strength differs. Therefore, combining failure probabilities of dike sections results in a higher failure probability on trajectory scale for failure mechanisms (RWS, 2017a).

The length-effect differs in magnitude for all failure mechanisms. This depends on the spatial distribution and fluctuations of the resistance of the dike against the failure mechanisms. For failure mechanisms with a small length-effect the resistance has a small spatial variation (overflow/overtopping). The trajectory failure probability is approximated with mutual dependence using the length-effect on trajectory scale (N). For failure mechanisms with a larger length-effect the resistance has a large spatial variation (internal erosion/macro-stability). The trajectory failure probability is approximated with mutual independence (VНК2, 2011).

So, the length-effect between sections of geotechnical failure mechanisms is a function of the sectional failure probabilities ($Pf_{section}$). This is stated in equation 11.1 which formulation is currently used in the assessment of geotechnical failure mechanisms with the software Riskeer (Deltares, 2017b).

$$Pf_{trajectory} = \min\left(1 - \prod_{i=1}^n (1 - Pf_{section,i}); N \cdot \max(Pf_{section,i})\right) \quad (11.1)$$

$$N = 1 + \frac{a \cdot L_{trajectory}}{b} \quad (11.2)$$

Piping

As discussed for geotechnical failure mechanism, the length-effect on trajectory scale (N) is a large factor such the minimum of equation 11.1 is given by independent summation. In the WBI consecutive dike sections are added independently since no specific information about the mutual dependence of consecutive dike section is available due to the semi-probabilistic assessments. Within the serial system approach a conservative choice is made to assume the upper bound of mutual independence.

Performing a probabilistic assessment gives an indication about the mutual dependence of dike sections within a dike trajectory. Based on this information consecutive dike sections can be added together to an equivalent dike section until one equivalent dike section remains representing the trajectory. This approach is based on the Equivalent Planes Method based on the theory of Hohenbichler and Rackwitz which is applied in the previous Dutch flood risk analysis in VНК using the software PC-Ring (Vrouwenvelder and Steenhergen, 2003).

In section 11.1 the fundamental boundaries discussed which is used in the WBI software. In section 11.2 the Ditlevsen boundaries of series systems are discussed to make more narrow boundaries. In section 11.3 the Equivalent Planes method is discussed which is used in the PC-Ring software. In each section the methods are applied to trajectory 48-1. Finally, in chapter 12 the methods are compared with a generic approach to include lithology.

11.1 Fundamental Boundaries

Within discrete series system, failure of a single section will always lead to the failure of the entire series system. The failure space of discrete series system with multiple sections is bounded by the fundamental boundaries. The lower bound is valid for fully dependent sections ($\rho = 1$) and the upper bound is valid for mutually exclusive sections ($\rho = -1$) (Jonkman et al., 2017).

$$\max(Pf_i) \leq Pf \leq \sum_{i=1}^n (Pf_i) \quad (11.3)$$

Note that for a discrete series system with independent sections ($\rho = 0$) the system failure probability is given by the complements of the reliability (probability of non-failure).

$$Pf = 1 - \prod_{i=1}^n (1 - Pf_i) \quad (11.4)$$

The independent and dependent boundaries gives the currently considered failure space within the WBI 2017.

$$\max(Pf_i) \leq Pf \leq 1 - \prod_{i=1}^n (1 - Pf_i) \quad (11.5)$$

In the mutually exclusive, independent and dependent cases an analytical expression is available to determine the system failure probability Pf . For other cases the system failure probability will be a function of the correlation coefficient such in the Ditlevsen method.

11.2 Ditlevsen Boundaries

Ditlevsen developed a method to calculate a smaller failure space of discrete series systems. Note that the more narrow boundaries in comparison to the fundamental boundaries are approximated based on an assumed (or known) correlation between consecutive sections. The Ditlevsen boundaries of the system failure probability are given in equations 11.6 to 11.10 where the lower and upper bound are valid for an according calculated correlation between normally distributed reliability functions (Jonkman et al., 2017).

$$\sum_{i=1}^n Pf_i - \sum_{i=2}^n \min\left(\sum_{j=1}^{i-1} Pf_{i,j-UP}, Pf_i\right) \leq Pf \leq \sum_{i=1}^n Pf_i - \sum_{i=2}^n \max_{j < i} Pf_{i,j-LOW} \quad (11.6)$$

$$Pf_{i,j-UP} = \text{sum}(\Phi(-\beta_i) * \Phi(-\beta_j^*); \Phi(-\beta_j) * \Phi(-\beta_i^*)) \quad (11.7)$$

$$Pf_{i,j-LOW} = \text{max}(\Phi(-\beta_i) * \Phi(-\beta_j^*); \Phi(-\beta_j) * \Phi(-\beta_i^*)) \quad (11.8)$$

$$\beta_i = -\Phi^{-1}(Pf_i), \quad \beta_j = -\Phi^{-1}(Pf_j) \quad (11.9)$$

$$\beta_i^* = \frac{\beta_i - \rho \cdot \beta_j}{\sqrt{1 - \rho^2}}, \quad \beta_j^* = \frac{\beta_j - \rho \cdot \beta_i}{\sqrt{1 - \rho^2}} \quad (11.10)$$

A more accurate estimate of the failure probability of discrete series systems is obtained using the Equivalent Planes Method based on the theory of Hohenbichler and Rackwitz. This method is more complex and requires larger calculation capacity than the Ditlevsen method.

11.3 Equivalent Planes Method

In Dutch flood risk assessments, an efficient method for computing the failure probability of discrete series systems with correlated sections is the Equivalent Planes method. The Equivalent Planes method computes the failure probability of a system of two correlated component, and by applying it iterative the failure probability of a system of any number of components (Roscoe et al., 2003).

Starting point of the Equivalent Planes method are the failure probabilities of each section and correlations between consecutive sections. The failure probabilities and importance factors of each individual dike section results from a probabilistic (FORM) assessment. In order to compute the correlation between sections additional information is needed about the autocorrelation functions of the random variables in the limit state function. Once the autocorrelations and importance factors for each of the dike sections are known the correlation between two (consecutive) sections can be calculated using equation 11.11.

$$\rho(Z_1, Z_2) = \sum_n^k \alpha_{ik} \cdot \alpha_{jk} \cdot \rho_{ijk} \quad (11.11)$$

From this starting point the Equivalent Planes method computes an equivalent failure probability and equivalent importance factors to represent two sections connected in series. The strategy is to replace the conditional probability with an equivalent marginal distribution. Note that this procedure is iterative, once two sections have been combined to a single equivalent section, it can be combined with a third section to a new equivalent section. This will be repeated until a single equivalent section results representing the trajectory with an according failure probability.

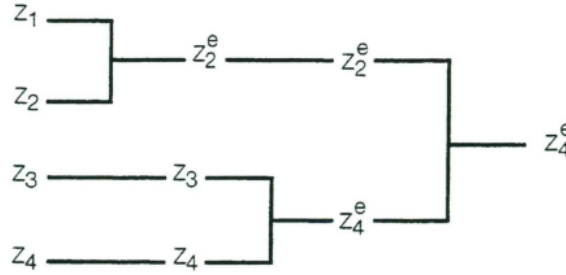


Figure 11.1: Hohenbichler and Rackwitz method (Vrouwenvelder and Steenhergen, 2003)

In order to combine an equivalent section, representing two sections in series, the equivalent failure probability and importance factors are required. In the software PC-Ring of VNK the theory of Hohenbicher and Rackwitz is used to determine the equivalent failure probability. The complexity of the problem lies in determining the conditional probability as shown in equation 11.15.

$$P(Z^e < 0) = P(Z_1 < 0 \cup Z_2 < 0) \quad (\text{equivalent}) \quad (11.12)$$

$$P(Z_1 < 0 \cup Z_2 < 0) = P(Z_1 < 0) + P(Z_2 < 0) - P(Z_1 < 0 \cap Z_2 < 0) \quad (\text{series}) \quad (11.13)$$

$$P(Z_1 < 0 \cap Z_2 < 0) = P(Z_1 < 0) * P(Z_2 < 0 | Z_1 < 0) \quad (\text{parallel}) \quad (11.14)$$

$$P(Z_2 < 0 | Z_1 < 0) = P(\beta_2 - (\rho \cdot w'_1 + \sqrt{1 - \rho^2} \cdot w_2^*) < 0) \quad (\text{conditional}) \quad (11.15)$$

Since the correlation between two sections is known, using equation 11.11, the limit state function of each section can be written in terms of a single standard normally distributed variable (w_i). This is shown in equation 11.17 below. Note that this formulation is equivalent to equation 11.16 which is a result of a level II reliability method (or FORM method) where the limit state function is linearized in the design point (Roscoe et al., 2003).

$$Z_i = \beta_i - \alpha_{i,1} \cdot u_{i,1} - \alpha_{i,2} \cdot u_{i,2} - \dots - \alpha_{i,n} \cdot u_{i,n} \quad (11.16)$$

$$Z_i = \beta_i - w_i \quad (11.17)$$

Since the reliability index (β_i) is a constant the correlation between Z_1 and Z_2 is equal to w_1 and w_2 . So, the variable w_2 can be written a function of w_1 and an independent standard normally distributed variable w_2^* to ensure that the correlation between the two sections is preserved and ensured that w_2 is standard normally distributed (Roscoe et al., 2003).

$$Z_1 = \beta_1 - w_1 \quad (11.18)$$

$$Z_2 = \beta_2 - w_2 = \beta_2 - (\rho \cdot w_1 + \sqrt{1 - \rho^2} \cdot w_2^*) \quad (11.19)$$

$$P(Z_2 < 0 | Z_1 < 0) = P(\beta_2 - (\rho \cdot w_1 + \sqrt{1 - \rho^2} \cdot w_2^*) < 0 | \beta_1 - w_1 < 0) \quad (11.20)$$

The condition $Z_1 < 0$ is equivalent to the condition $w_1 > \beta_1$. So, to consider the domain of $Z_1 < 0$ the distribution w_1 is replaced by w_1' to capture the tail of w_1 where $w_1 > \beta_1$. This simplifies the conditional failure probability of equation 11.20 to equation 11.22 (Roscoe et al., 2003).

$$Z_2' = \beta_2 - w_2 = \beta_2 - (\rho \cdot w_1' + \sqrt{1 - \rho^2} \cdot w_2^*) \quad (11.21)$$

$$P(Z_2 < 0 | Z_1 < 0) = P(Z_2' < 0) = P(\beta_2 - (\rho \cdot w_1' + \sqrt{1 - \rho^2} \cdot w_2^*) < 0) \quad (11.22)$$

Note that the problem of equation 11.16 is now reduced to a two-dimensional problem in equation 11.21 instead of a n-dimensional problem (n number of variables in the limit state function). Computing the marginal distribution $P(Z_2' < 0)$ can be done with numerical integration since it is only a two dimensional problem (Vrouwenvelder and Steenhergen, 2003). Finally, using equation 11.12 to 11.15 the equivalent failure probability representing two dike sections can be obtained.

In order to continue the iterative process of combining a third section with the 'equivalent two section system', equivalent importance factors are needed to compute the correlation between the third section and the equivalent result following equation 11.11. For each variable (u_k) of the two limit states (i and j) a correlated situation ($u_{k,c}$) and an uncorrelated situation ($u_{k,uc}$) is considered.

$$u_{jk} = u_{ik} \cdot \rho_{ijk} + u_{jk}'' \sqrt{1 - \rho_{ijk}^2} \quad (11.23)$$

where the variable u_{jk}'' is independent of u_{ik} . Taking the partial derivative of the 'equivalent two section system' reliability relative to the correlated (equation 11.24) and uncorrelated part (equation 11.26) of each variable the importance factor of each variable is obtained by equation 11.28. These partial derivatives can be obtained by calculating the gradient using a very small step (ϵ_k) indicating the effect on the equivalent reliability (Vrouwenvelder and Steenhergen, 2003).

$$\frac{\partial \beta_e}{\partial u_{k,c}} = \frac{\beta^e(\epsilon_k) - \beta^e(0)}{\epsilon_k} \quad (11.24)$$

$$\beta_e(\epsilon_k) = \phi^{-1}[P(Z_i < -\alpha_{ik} \cdot \epsilon_k \cup Z_j < -\alpha_{jk} \cdot \epsilon_k \rho_{ijk})] \quad (11.25)$$

$$\frac{\partial \beta_e}{\partial u_{k,uc}} = \frac{\beta^e(\epsilon_k'') - \beta^e(0)}{\epsilon_k''} \quad (11.26)$$

$$\beta_e(\epsilon_k'') = \phi^{-1}[P(Z_i < -\alpha_{ik} \cdot \epsilon_k'' \cup Z_j < -\alpha_{jk} \cdot \epsilon_k'' \sqrt{1 - \rho_{ijk}^2})] \quad (11.27)$$

$$\alpha_k^e = \sqrt{\left(\frac{\partial \beta_e}{\partial u_{k,c}}\right)^2 + \left(\frac{\partial \beta_e}{\partial u_{k,uc}}\right)^2} \quad (11.28)$$

Now the equivalent failure probability and importance factors of the 'two sections system' are known together with the failure probability of and the correlation with the third section the procedure discussed can be repeated iterative until a single equivalent 'section' results that represents the trajectory.

$$Z^e = \beta^e - \alpha_1^e \cdot u_1 - \alpha_2^e \cdot u_2 - \dots - \alpha_n^e \cdot u_n \quad (11.29)$$

11.3.1 Field Application

Applying the length-effect between sections to the sectional failure probabilities of trajectory 48-1 will increase the failure probability of the trajectory due to combining sections with different correlations. The starting point are the fundamental boundaries of fully independent and dependent sections. Combining the 33 dike sections of trajectory 48-1 in an upstream to downstream direction results in a dependent boundary of 1/160 [1/y] and an independent boundary of 1/60 [1/y]. Note that the conservative independent boundary is currently applied in the Dutch flood risk analysis (WBI 2017).

Next, a more narrow failure space can be obtained by the Ditlevsen boundaries. Combining the 33 dike sections of trajectory 48-1 by taking the dependence between consecutive dike sections into account results in a lower boundary of 1/101 [1/y] and an upper boundary of 1/67 [1/y]. Note that an average value of dependence of 0.81 is obtained by computing the dependencies of consecutive dike sections using equation 11.11. In this equation the product of the importance factors of each section (α_{ik} and α_{jk}) and spatial correlation between consecutive sections (ρ_{ijk}) of each stochastic variable are summed. Based on the autocorrelation functions of figure 9.4 at a lag value of 500 meters, the following spatial correlations are assumed: $\rho_{ij,m_u}=1$, $\rho_{ij,k}=0$, $\rho_{ij,D_{aquifer}}=0.9$, $\rho_{ij,D_{cover}}=0.5$, $\rho_{ij,L}=0.2$, $\rho_{ij,r_{exit}}=1$, $\rho_{ij,h}=1$, $\rho_{ij,h_{exit}}=1$, $\rho_{ij,\gamma_{sat}}=0$, $\rho_{ij,i_{c,h}}=0$, $\rho_{ij,m_p}=1$ and $\rho_{ij,d_{70}}=0$.

Finally, the Equivalent Planes Method takes the length-effect between sections in greater detail into account by computing iterative the spatial correlation of combined dike sections (equivalent hyperplane) with the next to be combined dike section. This procedure is efficient since the equivalent failure probability is computed with the theory of Hohbichler and Rackwitz which calculate the failure probability of a discrete series system by subtracting the overlapping (parallel) failure domain which is approximated by a conditional probability. This approximation reduces the problem to a two-dimensional problem which makes the method so efficient. This iterative process of combining the 33 dike sections results in a trajectory failure probability of 1/93 [1/y].

All approaches discussed to take the length-effect between sections into account are visualised in figure 11.2 below where the 33 dike sections of trajectory 48-1 are combined in an upstream to downstream direction.

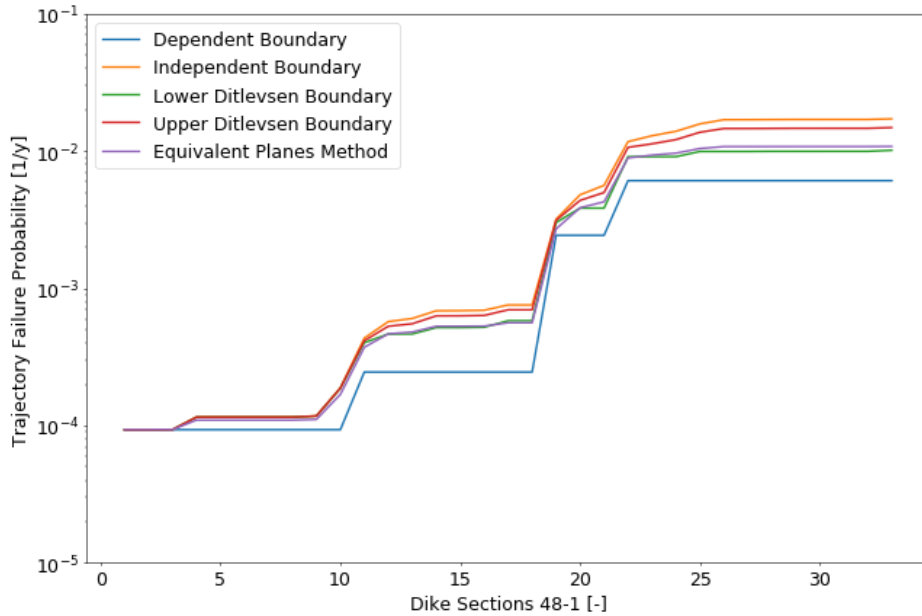


Figure 11.2: Equivalent Planes Method applied to trajectory 48-1

Lithology

The spatial correlation between consecutive dike sections are mainly the result of the high importance factors and fully correlated hydraulic loads. In contrast, the spatial correlation of subsoil parameters are almost uncorrelated based on the derived autocorrelation functions. From a geological perspective more spatial correlation can be introduced based on the the idea of spatial correlated geological deposits. Starting point are the six SOS-segments, stochastic subsurface classification segments, defined along trajectory 48-1. These segments are indicated in figure 11.3. According to 'Helpdesk Water' the stochastic subsurface classifications (SOS) are schematizations of the subsurface structure based on the expected patterns by the deposition environment (Helpdesk, 2017). Within each SOS-segment the following spatial correlations are assumed: $\rho_{ij,m_u}=1$, $\rho_{ij,k}=1$, $\rho_{ij,D_{aquifer}}=1$, $\rho_{ij,D_{cover}}=0.8$, $\rho_{ij,L}=0.6$, $\rho_{ij,r_{exit}}=1$, $\rho_{ij,h}=1$, $\rho_{ij,h_{exit}}=1$, $\rho_{ij,\gamma_{sat}}=0.4$, $\rho_{ij,i_{c,h}}=0.4$, $\rho_{ij,m_p}=1$ and $\rho_{ij,d_{70}}=1$. Note that between the different SOS-segments the assumed spatial correlations between dike sections are assumed. This results in a trajectory failure probability of 1/143 [1/y] which is visualised in figure 11.5.

- SOS-segment 48012: DP0+00 - DP37+49
- SOS-segment 48011: DP37+49 - DP106+01
- SOS-segment 48010: DP106+01 - DP139+90
- SOS-segment 48009: DP139+90 - DP166+66
- SOS-segment 48008: DP166+66 - DP236+39
- SOS-segment 48007: DP236+39 - DP274+95

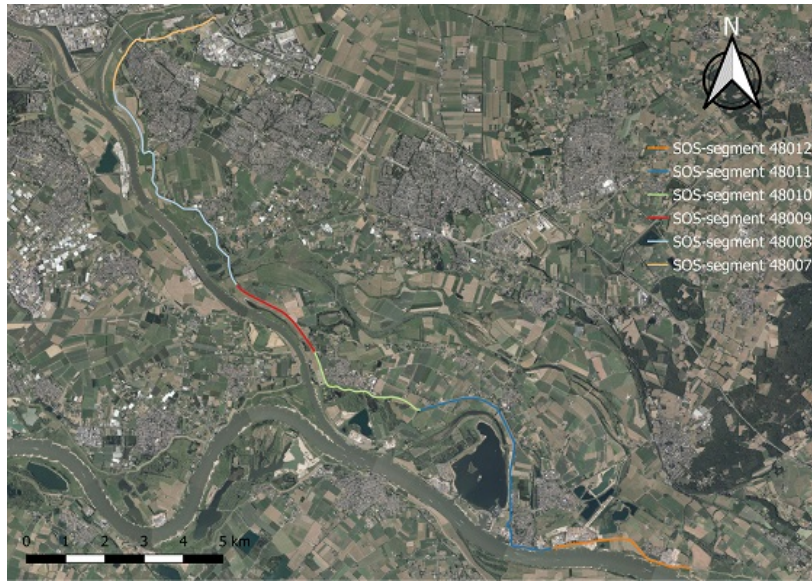


Figure 11.3: SOS-segments of trajectory 48-1

Next to these SOS-segments defined by the WBI a map of historical (fluvial) sand deposits, known as the 'Zandbanenkaart', from the University Utrecht can be used to define segments based on different geological deposits. The map of delta geomorphology showing the 'sand depth' of various sand deposits to the ground level is available at the province Gelderland (Cohen et al., 2017). Along trajectory 48-1 eight different subsurface structures are classified based on the build up of deltaic deposits which are given in figure 11.4. Within each Sand Deposit-segment the following spatial correlations are assumed: $\rho_{ij,m_u}=1$, $\rho_{ij,k}=1$, $\rho_{ij,D_{aquifer}}=1$, $\rho_{ij,D_{cover}}=0.8$, $\rho_{ij,L}=0.6$, $\rho_{ij,r_{exit}}=1$, $\rho_{ij,h}=1$, $\rho_{ij,h_{exit}}=1$, $\rho_{ij,\gamma_{sat}}=0.4$, $\rho_{ij,i_{c,h}}=0.4$, $\rho_{ij,m_p}=1$ and $\rho_{ij,d_{70}}=1$. Note that between the Sand Deposit-segments the assumed spatial correlations between dike sections are assumed. These assumptions results in a trajectory failure probability of 1/122 [1/y]. This is visualised in figure 11.5.

- Fluvial Sand of unembankend rivers (<1m- GL): DP0+00 - DP26+27
- Sand Deposit of embanked rives (<1 or 2m- GL): DP26+27 - DP74+97
- Fluvial Sand of unembankend rivers (<1m- GL): DP74+97 - DP84+19
- Pleistocene Sand (<1 or 2m- GL): DP84+19 - DP135+89
- Sand Deposit of embanked rives (<1 or 2m- GL): DP135+89 - DP174+52
- Fluvial Sand of unembankend rivers (<2m- GL): DP174+52 - DP212+45
- Sand Deposit of embanked rives (<1 or 2m- GL): DP212+45 - DP252+46
- Disturbed (Sand Extraction) : DP252+46 - DP274+95

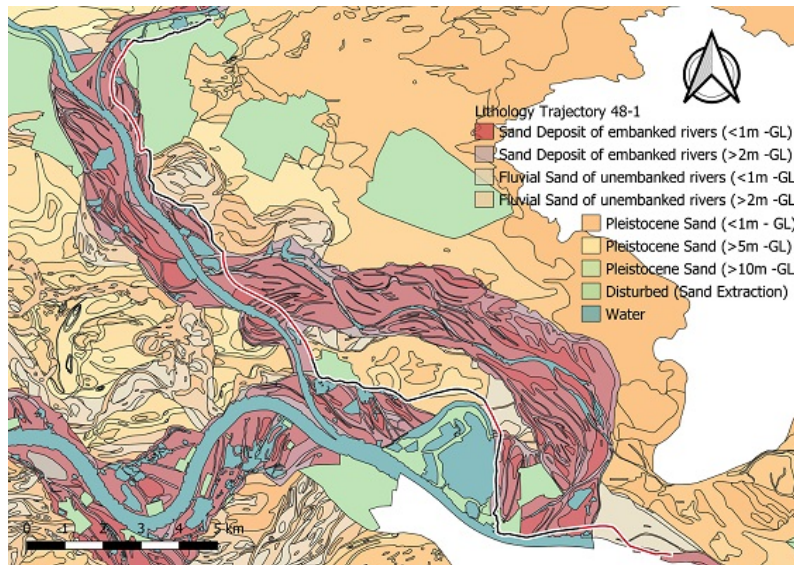


Figure 11.4: Fluvial deposits of trajectory 48-1

These approaches based on the subsurface schematizations (SOS) and sand deposits (SD) segments give a lower boundary for the length-effect between sections by introduction less conservative values for spatial correlations of the subsoil parameters. These two approaches are compared to the assumed spatial correlations between the identified dike sections (DS) in figure 11.5 below.

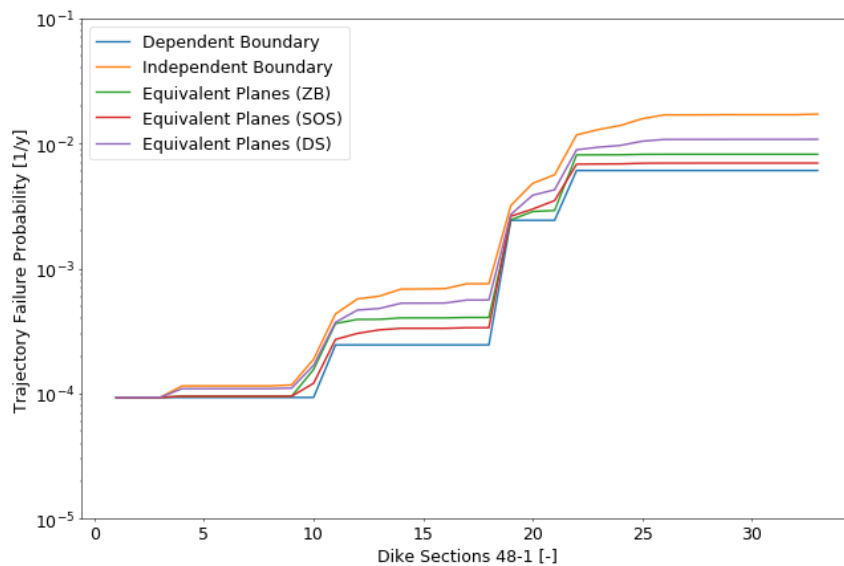


Figure 11.5: Equivalent Planes Method including lithology of trajectory 48-1

V

Chapter 12

Conclusions of Sub Question 3

SQ3 *How to use the length-effect between sections correctly by taking dependency into account for combining sectional failure probabilities to a trajectory failure probability?*

To answer the third research question, the importance factors and autocorrelation functions of the parameters required for the piping assessment are necessary to compute the dependence between consecutive dike sections ($\rho(Z_1, Z_2)$) of trajectory 48-1. Using this dependence more narrow boundaries than the fundamental boundaries can be derived using the Ditlevsen method. To approximate the failure probability of discrete series systems with correlated sections, the Equivalent Planes method is used and considered as an efficient method. This method takes the length-effect between sections into account by combining dike sections with the highest mutual dependency to an equivalent section. Iterative, the trajectory failure probability is derived.

Note that for the Ditlevsen bounds and the Equivalent Planes method a Level II reliability method is necessary. Since the current approach of the WBI is based on a Level I method the Fundamental bounds are considered of which the independent upper bound is applied to the geotechnical failure mechanisms. Here, the conservatism of the length-effect between sections originates.

The methods discussed are visualised in figure 11.2 of the previous Chapter, each taking the length-effect between sections differently into account. The Fundamental upper bound is equal to $1/60$ [1/y], the Ditlevsen upper bound equal to $1/67$ [1/y] and the Equivalent Planes method equal to $1/93$ [1/y]. Concluding, the fundamental independent boundary is a conservative assumption compared to methods including the mutual dependence between sections. In Chapter 14 the impact of these conclusions are discussed in comparison to the conclusions of the other assembly steps.

These methods are initially applied to the length-effect between dike sections. As discussed in the lithology section of the previous Chapter, additional spatial correlation can be introduced within the same SOS-segments or Sand Deposit-segments. Since in the assessment of the spatial failure probabilities interpolation techniques are used instead of the SOS-segments, the identified correlations by experts can be introduced. These approaches based on the subsurface schematizations (SOS) and sand deposits (SD) give an lower boundary for the length-effect between sections by assuming less conservative values for spatial correlations of the subsoil parameters.

Note that the SOS-segments from figure 11.3 are not identical to the different Sand Deposits from figure 11.4 underneath the dike trajectory 48-1, this is shown in figure 12.1. Therefore, both approaches have different results in relation to the initial approach based on dike sections.

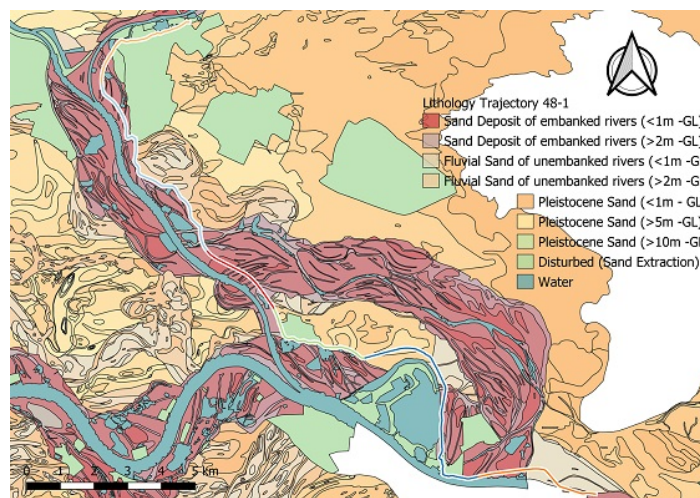


Figure 12.1: SOS-segments versus Sand Deposit segments

These two approaches are compared to the original spatial correlations of the identified dike sections (DS). This comparison is for convenience repeated in figure 12.2 below. It is clear that if more spatial correlation is introduced the length-effect between sections will shift from the independent to the dependent boundary. The fundamental upper boundary is equal to $1/60$ [1/y], the Equivalent Planes method (DS) equal to $1/93$ [1/y] and the Equivalent Planes method based on the sand deposits (ZB) equal to $1/121$ [1/y] and based on the stochastic subsurface segments (SOS) equal to $1/143$ [1/y].

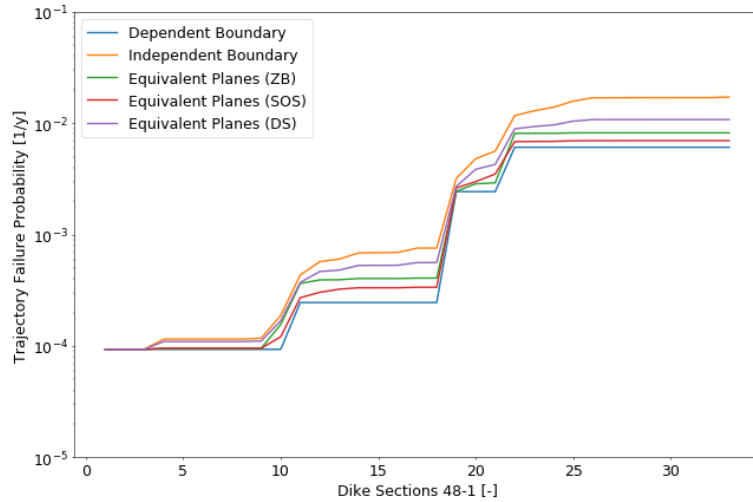


Figure 12.2: Equivalent Planes Method applied to trajectory 48-1

Note that these approaches use the sectional failure probabilities determined by a Level II reliability method (FORM). So, a certain uncertainty of the computed failure probabilities is present, as discussed in Chapter 7.2. The approximated confidence bounds ($\pm\sigma_\beta$) as a result of the uncertainties related to the mean values of the stochastic parameters in the limit state function is given in figure 12.3. These bounds are really rough approximations since the uncertainties of the mean values are not known but approximated based on bootstrapping. However, in comparison to the different approaches based on the Equivalent Planes method it can be concluded that the uncertainties related to the FORM approximation cannot be ignored. These bounds should be made more accurate in order to be compared to the length-effect between sections. Moreover, the model factors in the limit state function account for certain uncertainties related to the approximations made by the revised Sellmeijer model. It is not known if these parameters account for the discussed uncertainties related to the reliability approximation.

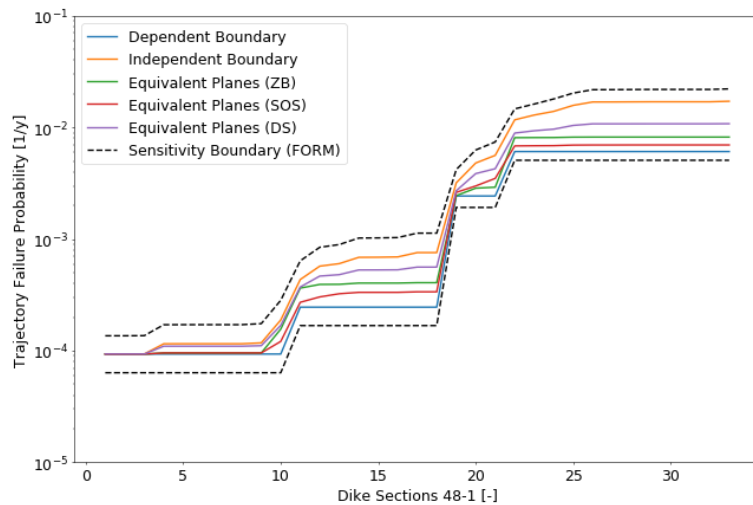


Figure 12.3: Sensitivity boundaries with respect to the computed reliabilities (FORM)

Chapter 13

Discussion

The main objective of this study is to investigate the assembly procedure of failure probabilities using the length effect within and between dike sections. This is done by performing a data and reliability analysis for the assessment of the failure mechanisms piping. The data analysis results in autocorrelation functions describing the spatial correlation of parameters. The reliability analysis results in importance factors describing the influence of the parameters on the reliability. From the autocorrelations and importance factors the length-effect within and between sections is made explicit. This results in a more realistic assembly procedure for geotechnical failure mechanisms.

Data Analysis

The seepage length along the trajectory is derived from the entry and exit lines provided by the waterboard. The mean values are based on the distance between these two lines perpendicular to the crest of the dike and a standard deviation are based on expert judgement according to the WBI 2017. But the uncertainty related to the mean values as a result of uncertain entry and exit lines is not taken into account. After performing the reliability analysis it is clear that the mean value of the seepage length has significant influence on the reliability and therefore the uncertainty related to the mean values should be included.

The polder level along the trajectory is determined based on a saturated polder due to rainfall and seepage during high water events. In practice the outside and inside water levels are related parameters. In order to take this into account a correlation (0.5) is assumed between the river and polder level. However, the behaviour of the system, runoff or storage of rainfall and seepage water is not researched in detail. Runoff would cause a lower polder level and storage would cause a higher polder level. Based on a comparison between the ground level of the inner toe of the dike and the hinterland, a first approximation is made of possible runoff or storage. Additional storage due to emergency measures are not taken into account.

The variation of the grain sizes along the trajectory are based on the sample data of grain sizes of the aquifer layer just underneath the cover layer. The related uncertainties are larger than uncertainties based on expert judgement according to the WBI 2017. But the sample data is not filtered based on the known geological deposits which could reduce this variation related to the grain sizes based on the filtered data of the sieve analysis.

The derivation of the permeability from grain sizes using the Den Rooijen (1992) equation is one of the most practical approximations. This equation indicates significant correlation (0.7) between grain size and permeability which is taken into account. However, in-situ pumping tests would be more accurate, including effects of anisotropy and heterogeneity. The bulk permeability of the aquifer is of importance and not spatial specific values of the subsurface. After performing the reliability analysis it is clear that the mean value of the permeability has significant impact on the reliability.

The reduction factor is assumed as a stochastic parameter with constant mean and standard deviation along the trajectory. In practice the reduction factor is dependent on resistance related parameters of the subsoil. In order to take this into account correlations (± 0.2) are assumed between the reduction factor and permeability, grain size, seepage length, polder level, saturated weight and thickness of the cover layer and thickness of the aquifer layer. If this is sufficient to account for the spatial variability of the reduction factor is not known.

Reliability Analysis

The reliability analysis is based on a Gumbel distribution, Student-t distribution and conditional probabilities in combination with Fragility Curves. From a comparison of these methods to a semi-probabilistic method it results that the approach using Fragility Curves is most accurate. The failure probabilities from the Fragility Curve approach at the Hydra-NL locations along the trajectory are

based on the revised Sellmeijer model. Reliability updating to account for time dependency, anisotropy, emergency measures, residual strength and survival cases will lead to more realistic findings.

The importance vectors resulting from a FORM analysis indicate that, next to the outside water level, the model factor piping has a high impact on the reliability. The model factor is related to the uncertainties of modeling the erosion resistance of earthen dikes. The importance of the model factor originates from the assumed constant parameters within the theoretical Sellmeijer equation which are in reality uncertain. After performing the reliability analysis it is clear that uncertainty of the constant drag factor and internal friction angle has significant influence on the reliability. However, if the model factor piping accounts for these and/or more uncertainties related to the revised Sellmeijer model is not described in the literature of the WBI 2017.

The sensitivity vectors resulting from a FORM analysis indicate the sensitivities of the stochastic and constant parameters in relation to the reliability index. The importance of the outside water level, model factor piping, permeability, seepage length and grain size are in accordance with current knowledge about the failure mechanism piping. From these sensitivity vectors uncertainties of the reliability index can be derived. But these uncertainties depend on the uncertainties of the distribution parameters which are difficult to approximate and should be researched in more extent in order to compare the confidence bounds of the reliability index to the bounds resulting from the length-effect.

Length-Effect within Sections

The length-effect within sections is based on a continuous model of the outcrossing method. In other words, the outcrossing method integrated over the probability distribution of the reliability index. In theory this method is valid for intervals much larger than the independent equivalent length and with statistically constant reliability. Furthermore, the method is based on the upper bound of the outcrossing method which is only a good approximation for large reliabilities (small failure probabilities) and small outcrossing rates. In practice most assessments are based on the 'weakest link' of dike sections with variable or small reliability and sectional lengths not much larger than the equivalent independent length. This leads to an overestimation of the length-effect within sections.

The field calibrated length-effect parameters ('a' and 'b') equal to 0.34 and 215m reduce the length-effect significantly in comparison to the WBI calibrated length-effect parameters equal to 0.9 and 300m. A reference is made to the thesis of Kanning (2012) where the length-effect parameters based on four dike systems are derived resulting in an 'a' value of 0.36 and a 'b' value of 262m.

Since the reduced length-effect parameters still include conservatism resulting from the mismatch between theoretical assumptions and practical applicability of the continuous model of the outcrossing method, the length-effect within sections approaches one. This indicates no length-effect within sections if the assessment is based on the normative cross-section of a dike section ('weakest link'). However, the uncertainty of the reliability approximation using FORM remains. This uncertainty originates from choosing distribution parameters of stochastic variables in the limit state function. Note that the uncertainty related to these distribution parameters are difficult to determine and it is possible that the model factors accounts for these uncertainties.

Length-Effect between Sections

The length-effect between sections is based on the fundamental independent boundary of serial systems. In other words, all dike sections are considered to be independent. In practice, dike sections are correlated in a certain amount. This correlation is mainly the result of the fully correlated load but also certain resistance parameters with large residual correlation or correlation lengths contribute to the correlation of dike sections.

Furthermore, the model factors piping and uplift are assumed to be fully correlated along the trajectory according to the WBI 2017. However, if the importance or residual correlation of the model factors is overestimated the mutual dependence of dike sections is overestimated as well.

Using the Equivalent Planes method mutual dependence between dike sections can be accounted for. This method indicates to combine dike sections with the highest correlation iteratively. But from a practical point of view it is chosen to combine the dike sections located next to each other iteratively. Introducing more correlation between resistance parameters of dike sections within the same fluvial deposits or SOS segments defined by the WBI 2017 indicates an upper bounds of the equivalent planes method. However, applying additional correlation to the autocorrelations is not supported by the Equivalent Planes method itself.

Improved Assembly Procedure

The result of the improved assembly procedure is a trajectory failure probability of $1/96$ [1/y] for the failure mechanism piping with according lower limit or independent boundary of $1/60$ [1/y] and upper limit or dependent boundary of $1/160$ [1/y]. Note that the most critical cross-section for the failure mechanism piping according to the revised Sellmeijer model is located at the Loodijk in front of a small lake named 'de waai'. This is a Dutch term for a small lake which originates from a dike breach. This indicates the capability of the application of the revised Sellmeijer method.

If a trajectory failure probability of $1/96$ [1/y] is a realistic annual probability of flooding for the failure mechanisms piping is by all means hard to tell. However, since sand boils are encountered along the dike trajectory during high water events over the past thirty years and no reliability updating is performed to account for time dependency, anisotropy, emergency measures, residual strength and survival cases, it is considered to be representative for the assumptions made. Including the indicated possibilities for reliability updating will lead to an even more realistic result.

Chapter 14

Conclusion

The purpose of this master thesis is to investigate if the current Dutch method of combining failure probabilities of geotechnical failure mechanisms can be improved. This research is elaborated in a case study for the failure mechanism piping of trajectory 48-1. The reliability method, length-effect within and between sections is investigated including the effects on the trajectory failure probability of the failure mechanism. This Chapter provides an answer to the following main research question:

RQ *Can the current Dutch assembly procedure of combining failure probabilities of geotechnical failure mechanisms be improved, and if so, how?*

The current assembly procedure of combining failure probabilities is based on the assessment of cross-sectional failure probabilities with a semi-probabilistic method, scaling to sectional failure probabilities using a length-effect equation based on nationwide calibrated parameters and combining sections independently to a trajectory failure probability. This results in a conservative assembly procedure. This master thesis shows that this conservatism is avoided using the following aspects.

Normative cross-sections

Starting point are the representative failure probabilities of the dike sections as a result of a semi-probabilistic assessment according to the WBI 2017. These are conservative failure probabilities in relation to the normative cross-sections of the dike sections resulting from a (semi) probabilistic assessment over small spatial intervals. This conservatism originates from a 'box' approach where conservative choices within a dike section result in high failure probabilities. In other words, creating critical combinations of parameters, neglecting correlation between parameters and taking characteristic values for load and resistance within dike sections. The conservatism is also a result of the Level I reliability method by translating safety factors to failure probabilities using the calibration formula. More realistic failure probabilities of the normative cross-sections of dike sections are obtained by combining parameters based on spatial interpolation techniques, making use of field related uncertainties and taking correlation between parameters into account with the use of a Level II method.

Length-effect within sections

The length-effect within sections based on a continuous model of the outcrossing method is currently overestimated. This conservatism originates from the calibrated length-effect parameters ('a' and 'b') which are derived in a calibration study for the WBI 2017. Applying this calibration procedure to the case study with field related importance factors and autocorrelations a lower combination of the length-effect parameters (especially 'a') are derived. This reduces the length-effect within sections significantly. Compared to the WBI calibrated length-effect parameters, the field related length-effect parameters show more correspondence with the defined physical upper limit of the length-effect within sections. This physical upper limit is defined as the ratio between the summation of failure probabilities and the maximum failure probability within a dike section.

In theory the continuous model of the outcrossing method is only valid for intervals much larger than the independent equivalent length and with statistically constant reliability. Furthermore, the method is based on the upper bound of the outcrossing method which is only a good approximation for small failure probabilities and outcrossing rates. In practice most assessments are based on the critical cross-section of a dike section which consists of variable or small reliability and lengths not much larger than the equivalent independent length. This leads to an overestimation of the length-effect within sections. Since the field calibrated length-effect parameters reduce the length-effect significantly but still include conservatism as a result from the mismatch between the theory and practice, the length-effect within sections approaches one. This indicates no length-effect within dike sections if the assessment is based on the 'weakest link' of a dike section with variable or small reliability and sectional lengths not much larger than the equivalent independent length.

Length-effect between sections

The length-effect between sections based on the fundamental independent boundary of series systems is currently overestimated. This conservatism originates from neglecting the mutual dependence between consecutive sections in the WBI 2017. Using the Equivalent Planes Method mutual dependence between dike sections can be accounted for. Applying the Equivalent Planes Method to the case study with field related importance factors and autocorrelations results in a lower combination of sectional failure probabilities compared to the original independent summation.

The mutual dependence of dike sections originates mainly from the fully correlated load (outside water level). Introducing more correlation between resistance (subsurface) parameters from a geological perspective of fluvial deposits reduces the trajectory failure probability even more. Indicating upper bounds of the equivalent planes method. Note that in order to include the correlation between dike sections a probabilistic assessment is required.

Impact on the assembly procedure

Applying the improved assembly procedure to the case study of trajectory 48-1 leads to a lower trajectory failure probability of the failure mechanism piping compared to the current assembly procedure of the WBI 2017. The more realistic result is based on a probabilistic assessment, without the length-effect within sections (but the selection of the critical cross-section as representative) and with the length-effect between sections using the equivalent planes method. The impact of each of the assembly steps separately is discussed below. Starting point is the reported trajectory failure probabilities of $1/6.3$ [1/y] as a result of a semi-probabilistic assessment according to the WBI 2017. Note that this result is not in line with the expectations of the waterboard Rijn & IJssel and is therefore reported as '>1/100' [1/y]. A reference is made to the disclaimer on page 7.

1. The impact of performing the assessment over small spatial intervals using interpolation techniques compared to the assessment of dike sections using a 'box approach' is a factor 5 ($1/30$ versus $1/6.3$). This result is obtained with the independent summation of the normative cross-sectional failure probabilities of dike sections.
2. The impact of a probabilistic method based on field related uncertainties compared to a semi-probabilistic method based on uncertainties from expert judgements in the WBI 2017 is a factor 2 ($1/60$ versus $1/30$). This result is obtained with the independent summation of the normative cross-sectional failure probabilities of dike sections.
3. The impact of reducing the length-effect within sections to one compared to the length-effect according to the WBI 2017 is a factor 3 ($1/60^1$ versus $1/17^2$). This result is obtained with independent summation of the normative cross-sectional failure probabilities multiplied by the length-effect within sections.
4. The impact of reducing the length-effect between sections with the equivalent planes method compared to the length-effect according to the WBI 2017 is a factor 1.5 ($1/93$ versus $1/60$). This result is obtained by including the dependence in the summation of the normative cross-sectional failure probabilities of dike sections

Finally, in comparison to the dike safety assessment of trajectory 48-1 by the waterboard Rijn & IJssel, the trajectory failure probability of $1/6.3$ [1/y] is reduced over a factor 10 to $1/93$ [1/y]. This indicates the conservatism of the original assessment according to the WBI but is in line with the reported trajectory failure probability by the waterboard of '>1/100' [1/y]. The waterboard made a conscious decision not to report such high failure probability since it is not in line with the expectations. A reference is made to the disclaimer on page 7.

¹ $1/60$ is obtained by reducing the length-effect within sections according to this research

² $1/17$ is obtained by applying the length-effect within sections according to the WBI 2017

Chapter 15

Recommendation

This Chapter provides recommendations based on the findings in this master thesis. The recommendations are given for both implementations of the findings as further research. Both related to the geotechnical failure mechanisms.

1. The current use of the failure mechanism sensitive interval (a) results in overestimation of the length-effect within sections. It is recommended to calibrate an a -value for each dike section in a dike trajectory.
2. The current assumption of independent dike sections results in an overestimation of the length-effect between sections. It is recommended to include the mutual dependence between dike sections in a dike trajectory.
3. The results in this thesis are based on a study of the length-effects. Including width-effects (anisotropy and residual strength) and time-effects (time dependency) will improve the accuracy of the results.
4. It is recommended to describe the model factors of the revised Sellmeijer model with more accuracy in order to determine the inclusion of uncertainties related to constant parameters and/or distribution parameters in the reliability approximations.
5. It is recommended to research the uncertainty of the FORM approximated reliability index with more accuracy in order to indicate the ratio of the confidence bounds to the length-effects.
6. Further research of the applicability of the outcrossing method to the length-effect within sections in comparison to other methods is recommended.
7. It is recommended to be aware of the theoretical assumptions of the length-effect within sections before applying it in practice for the assessment of dike trajectories.
 - (a) In assessments based on a 'statistically homogeneous' cross-section representing a dike section with lengths much larger than the independent equivalent length it is recommended to reduce the length-effect within sections according to a field calibration study.
 - (b) In assessments based on a 'critical' cross-section representing a dike section with lengths not much larger than the independent equivalent length it is recommended to reduce the length-effect within sections to one.
8. Improving the correlation lengths and residual correlations of the limit state parameters, including the model factors, will lead to a more realistic length-effect between sections.

References

- J.P. Aguilar Lopez, Warmink J.J., Schielen R.M.J., and S.J.M.H. Hulscher. *Correlation Effect in Probabilistic Design against Piping in Multi-Functional Flood Defences*. 2015.
- Gregory B. Baecher and John T. Christian. *Reliability and Statistics in Geotechnical Engineering*. Springer, 2019.
- Z.P. Bazant. Handbook of materials behavior models, 2001. URL <https://www.sciencedirect.com/topics/engineering/leonardo-da-vinci.html>.
- Ed Calle. *Lengte-effect en kalibratie van een toetsregel*. Deltares, 2010.
- K.M. Cohen, E. Stouthamer, W.Z. Hoek, H.J.A. Berendsen, and H.F.J. Kempen. *Zand in Banen*. Rijksoverheid, 2017.
- Deltares. *Voorstel tot aanpassing rekenmethode assemblage*. Deltares, 2017a.
- Deltares. *Gebruikershandleiding Ringtoets*. Deltares, 2017b.
- Deltares. *Complete WTI parameterlijst Aquo - Bijlage 1 Procedure*. Deltares, 2019.
- A. Der Kiureghian. *First and Second Order Reliability Methods*. University of California - Berkeley, 2005.
- A. Der Kiureghian. *Importance and Sensitivity Vectors*. University of California - Berkeley, 2019.
- Ferdinand Diermanse, Kin Sun Lam, and Han Knoeff. *Assemblageprotocol WBI2017*. Deltares, 2017.
- ENW. *Piping, realiteit of rekenfout?* Expertise Netwerk Waterveiligheid, 2010.
- Ulrich Forster, Geeralt van den Ham, Ed Calle, and Gerard Kruse. *Onderzoeksrapport Zandmeevoerende Wellen*. Deltares, 2012.
- Geodelft. *MPOSTAB - user's manual PC-MODEL - Probabilistic analysis of stability of earth slopes*. Geodelft, 1994.
- Helpdesk. *Is het SOS conservatief?* Rijksoverheid, 2017.
- ILT. *Analyse hoge overstromingskansen WBI-2017*. Inspectie Leefomgeving en Transport, 2019.
- R. Jongejan. *WBI2017 Code Calibration - Reliability-based code calibration and semi-probabilistic assessment rules for the WBI2017*. Ministerie van Infrastructuur en Milieu, 2017a.
- Ruben Jongejan. *Vaststellen uitgangspunten definitieve kalibratie*. Deltares, 2013.
- Ruben Jongejan. *Kennisplatform Risicobenadering*. KPR, 2017b.
- S.N Jonkman, R.D.J.M. Steenbergen, O. Morales-Napoles, A.C.W.M Vrouwenfelder, and J.K. Vrijling. *Probabilistic Design: Risk and Reliability Analysis in Civil Engineering*. TU Delft, 2017.
- S.N Jonkman, R.E. Jorissen, T. Schweckendiek, and J.P. van den Bos. *Flood Defences*. TU Delft, 2018.
- W. Kanning. *The Weakest Link - Spatial Variability in the Piping Failure Mechanism of Dikes*. 2012.
- H. Karadeniz and A.C.W.M. Vrouwenfelder. *Overview Reliability Methods*. SAFERELNET, 2005.
- O. Kroezen. *De splitsing van de rijen en ijssel bij arnhem - 7-1-2018*, 2018. URL <https://www.dronewatch.nl/2018/01/10/kijken-hoogwater-in-beeld-gebracht-door-drones/>.
- R. Lanzafame and N. Sitar. *Reliability Analysis of the Influence of Woody Vegetation on Levee Performance*. University of California - Berkeley, 2018.

- Juliana Lopez de la Cruz, Timo Schweckendiek, Cong Mai Van, and Wim Kanning. *SBW Hervalidatie piping HP8b Kalibratie van de veiligheidsfactoren*. Deltares, 2010.
- K.A. Ogori. *Spatial interpolation (2/2): Kriging*. TU Delft, 2018.
- G. Pleijter and D. Knops. Excel-tool piping assessment. In *HKV Lijn in Water*, 2019.
- Rijkswaterstaat. *Achtergrondrapport Ontwerpinstrumentarium 2014*. Ministerie van Infrastructuur en Milieu, 2016a.
- Rijkswaterstaat. *Hydra-Ring 2.0*. Rijkswaterstaat, 2016b.
- Rijkswaterstaat and ENW. *Addendum bij het technisch rapport waterkerende grondconstructies*. Drukkerij Ando, 2007.
- K. Roscoe, A.C.W.M. Vrouwenvelder, and F. Diermanse. *System reliability with correlated components: Accuracy of the Equivalent Planes method*. TNO, 2003.
- RWS. *Schematiseringshandleiding Macrostablieit*. Ministerie van Infrastructuur en Milieu, 2016.
- RWS. *Regeling veiligheid primaire waterkeringen 2017 - Bijlage 1 Procedure*. Ministerie van Infrastructuur en Milieu, 2017a.
- RWS. *Regeling veiligheid primaire waterkeringen 2017 - Bijlage 3 Sterkte en Veiligheid*. Ministerie van Infrastructuur en Milieu, 2017b.
- RWS. *Schematiseringshandleiding Piping*. Ministerie van Infrastructuur en Milieu, 2017c.
- T. Schweckendiek, M. van der Krogt, B. Rijnveld, and A.M. Teixeira. *Handreiking Faalkansanalyse Macrostablieit - Groene Versie*. Deltares, 2017.
- Aerd Statistics. Spearman's rank-order correlation, 2018. URL <https://statistics.laerd.com/statistical-guides/spearmans-rank-order-correlation-statistical-guide.php>.
- TAW. *Leidraad voor het ontwerpen van rivierdijken deel 2 - Appendices*. Uitgeverij Waltman, 1989.
- TAW. *Druk op de Dijken 1995*. Technische Adviescommissie voor de Waterkeringen, 1995.
- TAW. *Technisch rapport waterkerende grondconstructies*. Ministerie van Verkeer en Waterstaat, 2001.
- J. Tigchelaar. *Factsheet KPR vakgrootte*. Kennisplatform Risicobenadering, 2017.
- VNK2. *De methode van VNK2 nader verklaard*. Projectgroep VNK, 2011.
- A.C.W.M. Vrouwenvelder and I.M.G.M. Steenhergen. *Theoriehandleiding PC-Ring - Deel C: Reken-technieken*. TNO, 2003.
- T. Vrouwenvelder. *Spatial effects in reliability analysis of flood protection systems*. International Forum on Engineering Decision Making, 2006.
- Hans Wackernagel. *Multivariate Geostatistics: An Introduction with Applications*. Springer, 2003.
- WRIJ. *Achtergrondrapport Piping (STPH) (48-1)*. Waterschap Rijn & IJssel, 2018.
- WRIJ. *Eerste beoordeling primaire waterkeringen (48-1)*. Waterschap Rijn & IJssel, 2019.
- C. Zwanenburg, A. van Duinen, and A. Rozing. *Technisch Rapport Macrostablieit*. Deltares, 2013.

List of Figures

1.1	Fault tree of a dike trajectory (Jonkman et al., 2018)	1
1.2	Schematic representation of the spatial scales	1
1.3	Internal erosion (TAW, 1995)	2
2.1	Disassembly and Assembly procedure of the WBI 2017	6
3.1	Disassembly and Assembly procedure of the WBI 2017	9
3.2	Research Objective - an improved assembly approach	10
4.1	Schematic representation of the assembly procedure	11
4.2	Level I and Level II (FORM) reliability methods	12
4.3	Overestimation within the assessment of dike sections	12
4.4	Length-effect within sections (1)	13
4.5	Length-effect within sections (2)	13
4.6	Length-effect between sections (1)	14
4.7	Length-effect between sections (2)	14
4.8	Overview of the assembly procedure - Calculate Scale Combine	15
4.9	Sensitive parameters of the revised Sellmeijer Model	15
5.1	Dike trajectory 48-1 (WRIJ, 2019)	17
5.2	Assessment of the failure mechanism piping (STPH) of trajectory 48-1 (WRIJ, 2019) .	18
5.3	Fault tree of the failure mechanism internal erosion (Jonkman et al., 2018)	18
6.1	Water level trajectory 48-1 (<i>WBI2017-Bovenrijn- 48-1-v03</i>)	23
6.2	Water level detail section 139+090 - 155+000	23
6.3	Seepage length trajectory 48-1	24
6.4	Seepage length detail section 139+090 - 155+000	24
6.5	Ground level trajectory 48-1	25
6.6	Ground level detail section 139+090 - 155+000	25
6.7	Polder level trajectory 48-1	26
6.8	Polder level detail section 139+090 - 155+000	26
6.9	Bottom level clay layer trajectory 48-1	27
6.10	Bottom level clay layer detail section 139+090 - 155+000	27
6.11	Kriging interpolation of the bottom clay level trajectory 48-1	28
6.12	Standard deviation of the bottom clay level trajectory 48-1	28
6.13	Bottom level aquifer layer trajectory 48-1	29
6.14	Bottom level aquifer layer detail section 139+090 - 155+000	29
6.15	Grain size trajectory 48-1	30
6.16	Grain size detail section 139+090 - 155+000	30
6.17	Kriging interpolation of the grain size trajectory 48-1	31
6.18	Coefficient of variation of the grain size trajectory 48-1	31
6.19	Permeability trajectory 48-1	32
6.20	Permeability detail section 139+090 - 155+000	32
6.21	Kriging interpolation of the permeability trajectory 48-1	33
6.22	Coefficient of variation of the permeability trajectory 48-1	33
6.23	Volumetric weight trajectory 48-1	34
7.1	Level I and Level II (FORM) reliability methods	37
7.2	Semi-Probabilistic assessment trajectory 48-1 (σ_{field} versus $\sigma_{default}$)	39
7.3	Semi-Probabilistic assessment trajectory 48-1 (spatial results versus sectional results) .	39
7.4	Water level distributions from Hydra-NL data-points	40
7.5	Fragility Curve approach using Hydra-NL data-points	40

7.6	Probabilistic assessment trajectory 48-1 (distribution and fragility curve)	41
7.7	Semi-Probabilistic versus Probabilistic (Gumbel - Student-t - Fragility Curves)	41
7.8	Comparison of probabilistic methods trajectory 48-1 (spatial versus sectional)	41
7.9	Probabilistic assessment trajectory 48-1 (σ_{field} versus $\sigma_{default}$)	42
7.10	Probabilistic assessment trajectory 48-1 (spatial results versus sectional results)	43
7.11	Comparison of first and second order reliability methods using fragility curves	43
7.12	Average importance factors ($\sigma_{default}$)	44
7.13	Importance factors ($\sigma_{default}$) trajectory 48-1	44
7.14	Average importance factors (σ_{field})	45
7.15	Importance factors (σ_{field}) trajectory 48-1	45
7.16	Gumbel distribution (initial and design point fit)	46
7.17	Water levels at the design point ($\sigma_{default}$) trajectory 48-1	46
7.18	Importance factors ($\sigma_{default}$) trajectory 48-1 (design point fit)	47
7.19	Average importance factor comparison ($\sigma_{default}$) (design point fit)	47
7.20	Sensitivities parameters with respect to β ($\theta_f = \mu_X$) trajectory 48-1	49
7.21	Sensitivities parameters with respect to β ($\theta_f = \sigma_X$) trajectory 48-1	49
7.22	Sensitivities parameters with respect to β ($\theta_g = \theta$) trajectory 48-1	50
7.23	Uncertainty of the reliability index w.r.t. the distribution parameters (μ_X and σ_X)	50
8.1	Semi-Probabilistic failure probability trajectory 48-1 ($Pf_{section}$)	51
8.2	Probabilistic failure probability trajectory 48-1 ($Pf_{section}$)	52
8.3	Differences in β -domain (semi-probabilistic)	53
8.4	Differences in β -domain (probabilistic)	53
8.5	Choice of normative cross-sections in dike sections (WRIJ)	54
9.1	Outcrossing Method - Probability of threshold exceedance (Jongejan, 2017a)	58
9.2	Importance factors (α_i^2) (σ_{field}) (48-1)	61
9.3	Importance factors (α_i) (σ_{field}) (48-1)	61
9.4	Autocorrelation functions (48-1)	62
9.5	Autocorrelation functions (WBI)	62
9.6	Autocorrelation functions (UL)	63
9.7	Autocorrelation functions (LL)	63
9.8	Second derivative of the combined autocorrelation function ($\rho_z''(0)$) (48-1)	64
9.9	Equivalent independent length (l_{eq}) (48-1)	64
9.10	Comparison of the sectional length-effect (VNK vs WBI) of trajectory 48-1	65
9.11	Comparison of the length-effect within sections (VNK vs WBI) of trajectory 48-1	65
9.12	Calibration of the length-effect for the WBI 2017 (Continuous Model)	68
9.13	Importance factors (α_i^2) (σ_{wbi}) (48-1)	69
9.14	Importance factors (α_i) (σ_{wbi}) (48-1)	69
9.15	Autocorrelation functions (WBI)	70
9.16	Second derivative of the combined autocorrelation function ($\rho_z''(0)$) (48-1)	70
9.17	Equivalent independent length (l_{eq}) (48-1)	71
9.18	Field calibration of trajectory 48-1 (Continuous Model)	71
9.19	Comparison of the sectional length-effect (WBI(field) vs WBI) of trajectory 48-1	72
9.20	Comparison of the length-effect within sections (WBI(field) vs WBI) of trajectory 48-1	72
10.1	Field calibration (FIELD) versus WBI calibration (WBI) of trajectory 48-1	73
10.2	Sectional length-effect parameter (N^*) of trajectory 48-1	74
10.3	Summation versus maximum within sections based on (σ_{WBI}) left and (σ_{field}) right	74
10.4	Sectional length-effect parameter (N^*) of trajectory 48-1	75
10.5	Comparison of the length-effect within sections of trajectory 48-1. The numerical results of these different approaches to account for the length-effect are listed in table 10.1 below.	76
10.6	Comparison of the uncertainty of the reliability index with the sectional length-effect	76
11.1	Hohenbichler and Rackwitz method (Vrouwenvelder and Steenhergen, 2003)	83
11.2	Equivalent Planes Method applied to trajectory 48-1	85
11.3	SOS-segments of trajectory 48-1	86

11.4	Fluvial deposits of trajectory 48-1	87
11.5	Equivalent Planes Method including lithology of trajectory 48-1	87
12.1	SOS-segments versus Sand Deposit segments	89
12.2	Equivalent Planes Method applied to trajectory 48-1	90
12.3	Sensitivity boundaries with respect to the computed reliabilities (FORM)	90
A.1	Disassembly and Assembly procedure WBI 2017	110
B.1	Failure mechanism internal erosion (or piping) (Jonkman et al., 2018)	111
B.2	Failure mechanism macro-stability (RWS, 2016)	113
B.3	Lay-out of the LiftVan method for macro-stability (Zwanenburg et al., 2013)	114
C.1	Bottom level aquifer layer trajectory 48-1 (REGISS II)	115
C.2	Comparison of high water events and rainfall events (RWS and KNMI)	115
D.1	Semivariogram Cloud (no bins) and Semivariogram (bins)	119
D.2	Ordinary Kriging (estimation point and variance)	119
D.3	Semivariogram Cloud (no bins) and Semivariogram (bins)	120
D.4	Ordinary Kriging (estimation point and variance)	120
D.5	Semivariogram Cloud (no bins) and Semivariogram (bins)	121
D.6	Ordinary Kriging (estimation point and variance)	121
E.1	FORM and SORM approximations (Der Kiureghian, 2005)	123
E.2	Series (a) and Parallel (b) FORM approximations (Der Kiureghian, 2005)	124
F.1	Spatial correlation (lag=500m) - Autocorrelation function (cover layer)	127
F.2	Spatial correlation (lag=500m) - Autocorrelation function (grain size)	128
F.3	Spatial correlation (lag=500m) - Autocorrelation function (permeability)	128
F.4	Spatial correlation (lag=500m) - Autocorrelation function (seepage length)	128
G.1	Trajectory versus cross-section reliability for $\sigma_{beta}=0.1$ and $\rho_z''(0)$ of $-6.4e-06$	131
G.2	Cross-section versus trajectory reliability for $\sigma_{beta}=0.1$ and $\rho_z''(0)$ of $-1.8e-06$	132
G.3	Fitting of equation G.5 to the data from the VNK2 studies	133
H.1	Failure probability of $1e-03$ Mutual dependence of 0.8 Length-effect factor of 3	136
H.2	Failure probability of $1e-03$ Mutual dependence of 0.2 Length-effect factor of 80	136
H.3	Failure probability of $1e-03$ Mutual dependence of 0.2 Length-effect factor of 80	137
H.4	Failure probability of $1e-02$ Mutual dependence of 0.2 Length-effect factor of 80	137
H.5	Dependency of random variables (Jonkman et al., 2017)	138
H.6	Monotonic and Linear Monotonic Non-Monotonic (Statistics, 2018)	138
I.1	Autocorrelation function of the spatial failure probabilities of trajectory 48-1	139
I.2	Piping sensitive interval of trajectory 48-1	139
I.3	Piping sensitive interval of trajectory 48-1	140

List of Tables

5.1	Data analysis of the failure mechanism internal erosion (or piping)	20
7.1	Sensitivities parameters with respect to β ($\theta_f = \mu_X$)	48
7.2	Sensitivities parameters with respect to β ($\theta_f = \sigma_X$)	48
7.3	Sensitivities parameters with respect to β ($\theta_g = \theta$)	49
8.1	Overview of maximum cross-sectional failure probabilities (excluding the length-effects). (¹) The 1/6.3 [1/y] is not in line with the expectations of the waterboard Rijn & IJssel and is therefore reported as '>1/100' [1/y]. A reference is made to the disclaimer on page 7.	52
9.1	Autocorrelation parameters 48-1 versus WBI	62
9.2	Autocorrelation parameters 48-1 versus UL and LL	63
10.1	Overview of maximum sectional failure probabilities (including the length-effects) . . .	77
E.1	Uncertainties of the distribution parameters (θ_f)	126
G.1	Length-effect parameters according to the WBI 2017 (Deltares, 2017b)	129

Appendices

Appendix A

Assembly Procedure WBI 2017

With the use of the 'Wettelijk Beoordelings Instrumentarium 2017' or WBI 2017, waterboards will assess the hydraulic structures, mostly dikes, to the water safety requirements from the 'Waterwet'. Assessments for the dike failure mechanisms are included in the WBI 2017 to determine the failure probability of a dike cross-section, representing a dike section in which strength, load and geometry can be supposed to be relatively homogeneous within the dike trajectory. Each of these assessments results in the failure probability of a dike cross-section and failure mechanism specific.

These results will be compared to the safety requirements on dike section and failure mechanism level by disassembling the safety requirement on trajectory level for all failure mechanisms combined. This will be discussed in the Disassembly Procedure of Riskeer. Furthermore, these assessment results will be combined to dike trajectory level for all failure mechanisms combined and compared the safety requirement. This will be discussed in the Assembly Procedure of Riskeer.

Assembly Procedure

In order to combine the assessment results in terms of the failure probabilities of dike cross-sections for a single failure mechanism ($Pf_{cross-section}$) to the failure probability of the dike trajectory for all failure mechanism combined ($Pf_{trajectory}$), the following procedure is applied by Riskeer (Diermanse et al., 2017). Starting point is the failure probability of the dike cross-sections ($Pf_{cross-section}$). First step of assembling is to estimate the failure probability of a dike section (i) for a single failure mechanism (j) ($Pf_{i,j}$) represented by the failure probability result of the assessment for a single dike cross-section ($Pf_{cross-section}$) using the length-effect factor (N^*) based on the length of the section (Deltares, 2017a).

$$Pf_{i,j} = N^* \cdot Pf_{cross-section} \quad (A.1)$$

From $Pf_{i,j}$ a section assessment for a single failure mechanism can be derived (I_v-VI_v). Second step of assembling is to estimate the failure probability of the trajectory for a single failure mechanism (Pf_j) based on mutual independence of the sections which suits sections with a low degree of dependence.

$$Pf_j = 1 - \prod_{i=1}^n (1 - Pf_{i,j}) \quad (A.2)$$

Third step of assembling is to estimate the failure probability of the trajectory for a single failure mechanism (Pf_j) based on the largest failure probability of the sections multiplied by the length-effect factor (N), based on the length of the trajectory, which suits sections with a high degree of dependence

$$Pf_j = N \cdot \max(Pf_{i,j}) \quad (A.3)$$

Finally, choose the minimum of the approximated trajectory failure probabilities which lead to the failure probability of the dike trajectory for a single failure mechanism specific

$$Pf_j = \min(Pf_j) \quad (A.4)$$

From Pf_j a trajectory assessment for a single failure mechanism can be derived (I_t-VI_t). In order to get a safety assessment for a dike trajectory, one should combine the failure probabilities of the dike trajectory for the single failure mechanisms Pf_j into the trajectory failure probability $Pf_{trajectory}$ for all failure mechanisms combined, the following procedure is applied by Riskeer (Diermanse et al., 2017).

Estimate the failure probability of the trajectory based on mutual independence of the failure mechanisms which results in an upper bound since failure mechanisms will have some degree of dependence.

$$P_{f_{trajectory}} = 1 - \prod_{i=1}^n (1 - P_{f_j}) \quad (\text{A.5})$$

From $P_{f_{trajectory}}$ a safety assessment for a dike trajectory including all failure mechanism can be derived (A^+-D).

Disassembly Procedure

The derivation of individual dike section and failure mechanism safety requirements ($P_{i,j}$) from the dike trajectory safety requirement (P) are of importance. Theory of the length-effect (N) on trajectory scale is used to divide the system failure probability to the failure probabilities of the sections. Expert judgements of the failure probability contributions of failure mechanisms or 'faalkansbegroting' (ω) to divide the trajectory failure probability to the failure probabilities of the failure mechanisms is stated in the WBI 2017 (RWS, 2017b). The following procedure is applied by Riskeer (Diermanse et al., 2017).

$$P_{i,j} = \frac{\omega \cdot P}{N} \quad (\text{A.6})$$

From the failure probability demand for each section and failure mechanism specific a section assessment for a single failure mechanism can be derived (I_v-VI_v).

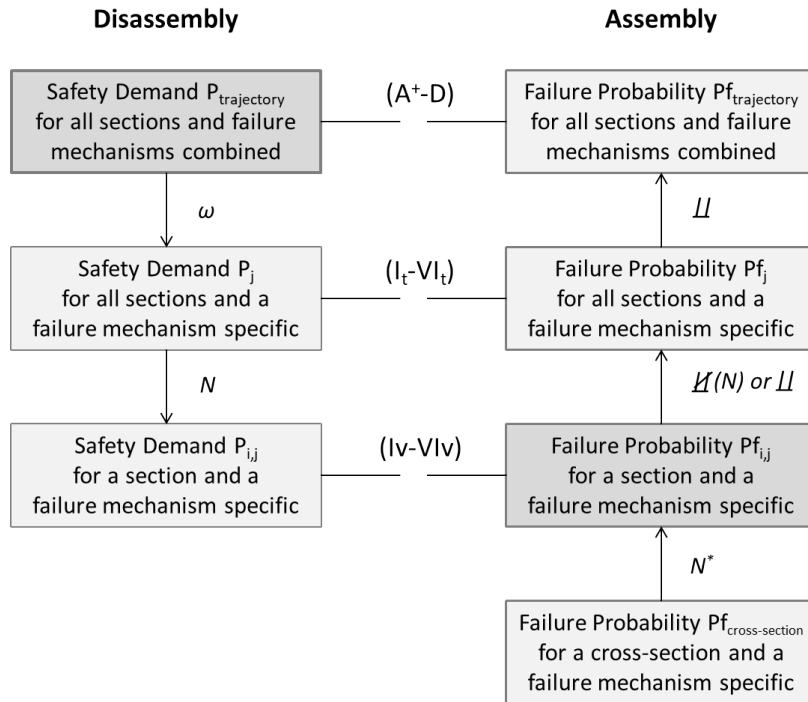


Figure A.1: Disassembly and Assembly procedure WBI 2017

Appendix B

Geotechnical Failure Mechanisms

The starting point of the assembly procedure of Riskeer in the WBI 2017 are the assessment results in terms of the failure probabilities of dike cross-sections for a single failure mechanism ($P_{f_{cross-section}}$). The assessment of the geotechnical failure mechanisms, internal erosion (or piping) and macro-stability, will be discussed below using the 'Schematiseringshandleidingen' from the WBI 2017.

Piping

During high waters, the increasing water pressure of the river against the dike induces the flow of groundwater through sand layers underneath the dike. This flow of groundwater will seepage into the polder at places with small resistance, like thin clay layers, causing the entrainment of sand. The continuous entrainment of sand results in a sand boil and could lead to subsidence and failure of the dike (TAW, 1995). This failure mechanism is called internal erosion (or piping).

Failure of a dike due to piping can only occur if multiple sub-failure mechanisms occur. These sub-failure mechanisms Uplift, Heave and Piping should all occur in order to make the dike unstable such it loses the water retaining function. This can be schematized as a parallel system where a water pressure difference between the outer- and inner dike water level makes the cohesive cover layer lift and eventually heave such that the resulting water flow underneath the dike driven by the same water pressure difference transports sand grains to the surface. This 'pipe' will continue to grow until the dike settles and a breach can occur due to overflow. This is visualised in figure B.1 below.

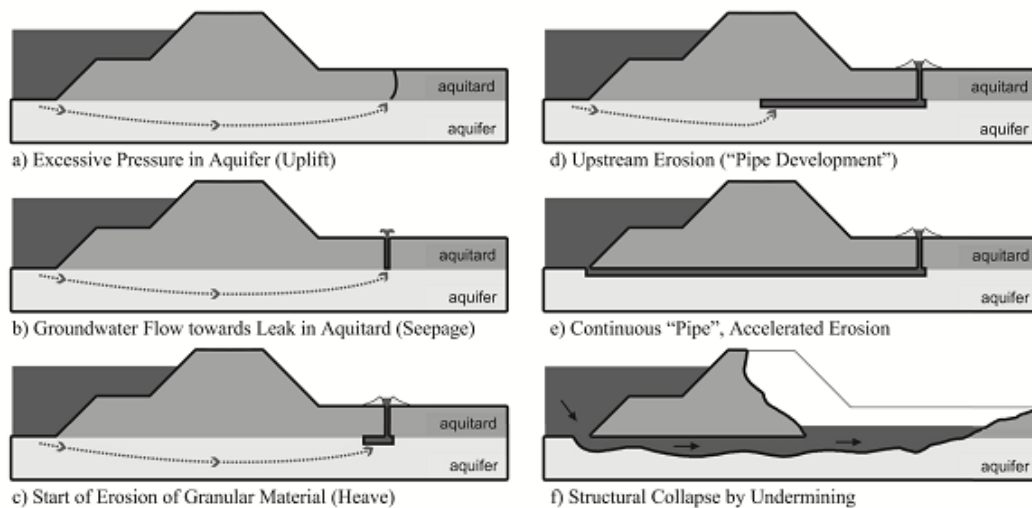


Figure B.1: Failure mechanism internal erosion (or piping) (Jonkman et al., 2018)

Piping is calculated following the 'Schematiseringshandleiding Piping 2017' (RWS, 2017c) using the revised Sellmeijer model. The limit state functions of Uplift, Heave and Piping will be discussed below. Note that the limit state functions are applied to cross-sections which are representative for the chosen dike sections. The choice of section division conform the 'Schematiseringshandleiding Piping 2017' (RWS, 2017c) will be explained.

- Uplift - The limit state function of uplift is based on a comparison between the downward soil pressure from the weight of the cover layer (resistance) and the upward water pressure in the aquifer underneath the cover layer (load).

$$Z_u = \Delta\phi_{c,u} - (\phi_{exit} - h_{exit}) \quad (B.1)$$

$$\Delta\phi_{c,u} = \frac{D_{cover}(\gamma_{sat,cover} - \gamma_{water})}{\gamma_{water}} \quad (B.2)$$

$$\phi_{exit} = \phi_{polder} + r_{exit}(h - \phi_{polder}) \quad (B.3)$$

where;

D_{cover} Thickness cover layer

ϕ_{exit} water pressure aquifer at exit point

h_{exit} Polder level

D_{cover} Thickness cover layer

$\gamma_{sat,grains}$ Volumetric weight grains

γ_{water} Volumetric weight water

h Water level

r_{exit} Damping factor

ϕ_{polder} water pressure aquifer at polder level

- Heave - The limit state function of heave is based on a comparison between the critical heave gradient at the exit point (resistance) and the actual heave gradient at the exit point (load).

$$Z_h = i_{c,h} - i \quad (B.4)$$

$$i = \frac{(\phi_{exit} - h_{exit})}{D_{cover}} \quad (B.5)$$

where;

$i_{c,h}$ Critical heave gradient

ϕ_{exit} water pressure aquifer at exit point

h_{exit} Polder level

D_{cover} Thickness cover layer

- Piping - The limit state function of piping is based on a comparison between the critical water pressure difference (resistance) and the actual water pressure difference between entry and exit point (load).

$$Z_p = m_p \Delta H_c - (h - h_{exit} - r_c D_{cover}) \quad (B.6)$$

$$\Delta H_c = F_{resistance} F_{scale} F_{geometry} L_{seepage} \quad (B.7)$$

$$F_{resistance} = \eta \frac{\gamma_{sat,grains}}{\gamma_{water}} \tan(\theta) \quad (B.8)$$

$$F_{scale} = \frac{d_{70,m}}{\sqrt[3]{\kappa L_{seepage}}} \left(\frac{d_{70}}{d_{70,m}} \right)^{0.4} \quad (B.9)$$

$$F_{geometry} = 0.91 \left(\frac{D_{aquifer}}{L_{seepage}} \right)^{\frac{0.28}{(D_{aquifer}/L_{seepage})^{2.8-1}} + 0.04} \quad (B.10)$$

$$L_{seepage} = x_{exit} - x_{entry} \quad (B.11)$$

where;

m_p Model factor

h Water level

h_{exit} Polder level

r_c	Reduction factor
D_{cover}	Thickness cover layer
η	Coefficient of White
$\gamma_{sat,grains}$	Volumetric weight grains
γ_{water}	Volumetric weight water
θ	Internal friction angle
κ	Intrinsic permeability of aquifer
d_{70}	Grain size top of aquifer
$d_{70,m}$	Grain size reference value
$D_{aquifer}$	Thickness aquifer
$L_{seepage}$	Seepage length
x_{exit}	Exit point of the seepage path
x_{entry}	Entry point of the seepage path

To determine the lay-out of the sections (or section division) the 'Schematiseringshandleiding Piping 2017' (RWS, 2017c) states that the essence of the section division is to choose a dike section in such a way that it is sufficient homogeneous for the failure mechanism specific such a representative cross-section can be assigned. No general rules are given for practical lengths/borders of dike sections but the following steps are advised.

- administrative boundaries (management, flood defence type, safety requirement, etc.)
- load and resistance boundaries (geometry, water level, subsoil, ditches, etc.)

Macro-Stability

During high waters, the increasing water pressure of the river against the dike induces the increase of water pressures in the subsoil and the earthen dike. This increase of groundwater pressure will reduce the resistance of the dike against shearing, causing the instability of the earthen dike body. The continuous increase of water pressures results in shearing of the inner slopes and could lead to failure of the dike (RWS, 2016). This failure mechanisms is called macro-stability (or instability) and is visualised in figure B.2 below.

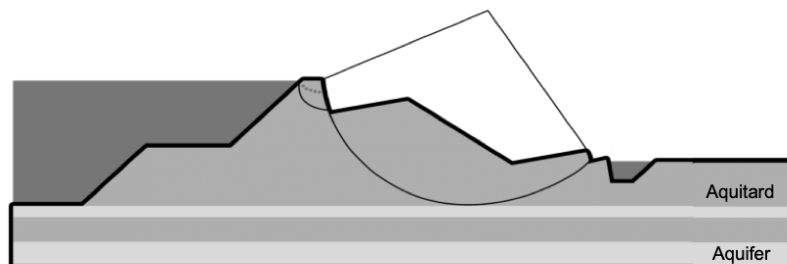


Figure B.2: Failure mechanism macro-stability (RWS, 2016)

Macro-Stability is calculated following the 'Schematiseringshandleiding Macrostabilliteit 2017' (RWS, 2016) using the LiftVan model. Failure of a dike due to macro-instability can only occur if large soil bodies of a dike shear along shear planes. The shear planes should reach the full width of the crest of the dike in order to make the dike unstable such it loses the water retaining function.

The stability factor for Macro-Stability can be determined by calculating which ratio between the shear strength along the shear plane and stability factor leads to an equilibrium. The model is executed within D-Geo-Stability to determine the stability factors for several LiftVan slip-surfaces. Note that the model is applied to cross-sections which are representative for the chosen dike sections.

The choice of section division conform the 'Schematiseringshandleiding Macrostabiliteit 2017' (RWS, 2016) will be explained.

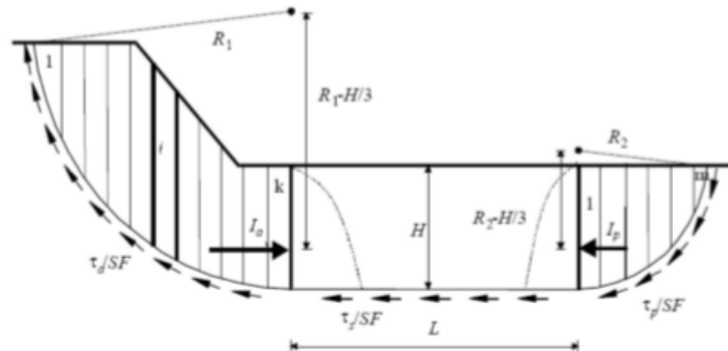


Figure B.3: Lay-out of the LiftVan method for macro-stability (Zwanenburg et al., 2013)

To determine the lay-out of the sections (or section division) the 'Schematiseringshandleiding Macrostabiliteit 2017' (RWS, 2016) states that the essence of the section division is to choose a dike section in such a way that it is sufficient homogeneous for the failure mechanism specific such a representative cross-section can be assigned. No general rules are given for practical lengths/borders of dike sections but the following steps are advised.

- administrative boundaries (management, flood defence type, safety requirement, etc.)
- load and resistance boundaries (geometry, water level, subsoil, revetment, etc.)

Appendix C

Data Analysis Details

REGISS II model

The bottom level of the aquifer layer is determined from the REGIS II model of the DinoLoket provided by TNO. In the REGIS II interpolation dark red (KRTWk1) and green (HLc and OOz2) indicates clay layers. The upper sand layer is identified as light red (KRz4 and KRz3). The bottom of the aquifer layer is at the boundary of these two geological layers. In figure C.1 the horizontal axis shows the length of the trajectory (m) and the vertical axis shows the elevation w.r.t. NAP (m).

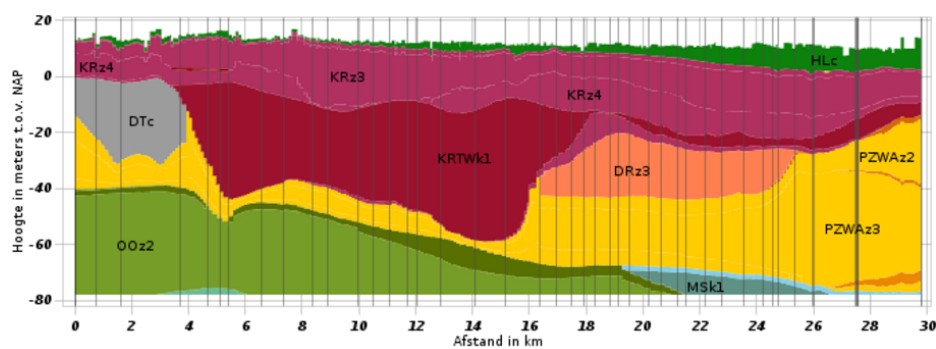


Figure C.1: Bottom level aquifer layer trajectory 48-1 (REGISS II)

Polder level

The water levels during high water events at the Rhine are compared to the rainfall events in the same time interval. The water level data is obtained from Rijkswaterstaat Waterinfo at location Lobith. The rainfall data is obtained from the KNMI at location Deelen (275). Comparing the water level and rainfall of four high water events at the Rhine shows that there is sufficient rainfall present to cause a saturated polder together with the seepage of groundwater through the earthen dikes. In figure C.2 the vertical axis on the left shows the water level (cm+NAP) and the vertical axis on the right shows the rainfall (mm/d) and the horizontal axis shows the high water events.

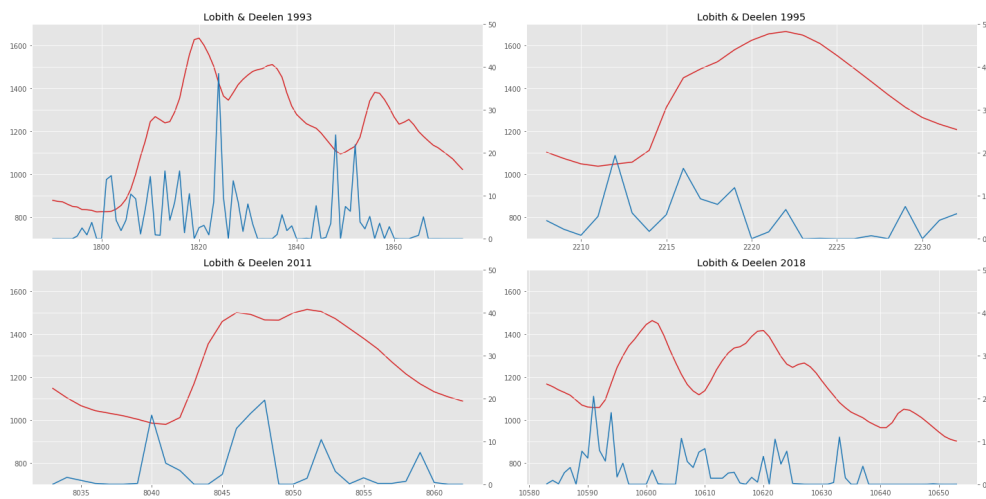


Figure C.2: Comparison of high water events and rainfall events (RWS and KNMI)

Appendix D

Kriging Interpolation

Kriging is a widely used interpolation method, developed by Georges Matheron based on the earlier work of Danie Krige. Initially the method was used to estimate the gold yields of mines in South Africa. Currently the method serves to estimate a value at a specific location using the surrounding data in the neighborhood. This estimation method uses a statistical model to take the varying uncertainty and spatial correlation of a dataset into account. Here, Ordinary Kriging, which is the most used Kriging method, will be discussed and applied in order to find the most likely values for the variables of interest along the dike trajectory (Baecher and Christian, 2019).

Starting point of the ordinary Kriging method is the realization of the (semi) variogram. A variogram ($2\gamma(h)$) is a function that describes the degree of spatial dependence of a spatial random field or stochastic process (Z). In other words, the variance of the difference between sample points at different distances (h) (Wackernagel, 2003).

$$2\gamma(h) = Var(Z(x+h) - Z(x)) = (Z(x+h) - Z(x))^2 \quad (D.1)$$

A semivariogram ($\gamma(h)$) is half the variogram. In other words, half the average squared difference between sample points separated at a distance (h).

$$\gamma(h) = \frac{1}{2}(Z(x+h) - Z(x))^2 \quad (D.2)$$

where x is a sample point, h is the distance from x to another sample point and $Z(x)$ is the value of a random variable at x (stochastic process). Note that the (semi) variogram takes the uncertainty and the spatial correlation of the sample points into account, in contrast to the theoretical variance.

A semivariogram cloud is computed by calculating the semivariogram for every possible pair of data points separated with distances h . A scatter plot of the semi-variances ($\gamma(h)$) versus the distances (h) shows how the dissimilarity of a sample of a random variable changing with the distance between the sample points. Like nearby sample points tend to more similar values and sample points over larger distances tend to more dissimilarities (Ohuri, 2018).

In practice, a semivariogram cloud shows wide variations due to the large amount of possible pairs of data points. By averaging the dissimilarities for every possible pair of data points separated with the distance (h) in a certain interval h^* (bin), an experimental semivariogram results by plotting the average semi-variance ($\gamma^*(h^*)$) versus the distance interval bins (h^*) (Ohuri, 2018).

$$\gamma^*(h^*) = \frac{1}{2 \cdot n} \sum (Z(x+h) - Z(x))^2 \quad \text{for all } h \text{ in } h^* \quad (D.3)$$

where n is the number of data point pairs in the distance interval bin. Note that an experimental semivariogram shows a much clearer variations due to the averaging of the possible pairs of data points in bins. In order to avoid unreliable dissimilarities it is practice to compute the experimental variogram for distances intervals up to half of the size of the region covered by the dataset. From these experimental semivariograms a few parameters results which describes the stochastic process.

- the sill: the upper bound of $\gamma^*(h)$
- the range: the value of $|h|$ when it converges
- the nugget: the value of $\gamma^*(h)$ when $|h|=0$

Depending on the shape of the theoretical semivariogram multiple theoretical semivariogram functions, like the Exponential, Gaussian and Spherical functions, can be used to represent the dataset using the sill, range, and nugget parameters (Ohuri, 2018).

Next, after selecting the right theoretical semivariogram, the Ordinary Kriging interpolation can be defined similar to other interpolation methods using a weighted average. The most likely value of a random variable (Z) at a specific location (x_0) is given by the weighted average of its value at the various locations (x_i) of the n sample points within the dataset of the random variable (Wackernagel, 2003).

$$Z_{OK}(x_0) = \sum_{i=1}^n w_i \cdot Z(x_i) \quad (D.4)$$

Note that the Ordinary Kriging has the characteristics to be unbiased, weights (w_i) to sum up to one, and to minimise the variance of the estimation.

$$\sum_{i=1}^n w_i = 1 \quad (D.5)$$

$$Var(Z_{OK}(x_0)) = -\gamma(x_0 - x_0) - \sum_{i=1}^n \sum_{j=1}^n w_i \cdot w_j \cdot \gamma(x_i - x_j) + 2 \sum_{i=1}^n w_i \cdot \gamma(x_i - x_0) \quad (D.6)$$

where x_i and x_j iterate over all the possible pairs of sample points within the dataset. Now, by minimizing the estimation variance under the constraint of the weights to sum up to one using the minimisation method known as Lagrange multipliers, the Ordinary Kriging interpolation method results (Wackernagel, 2003):

$$\begin{bmatrix} \gamma(x_1 - x_1) & \dots & \gamma(x_1 - x_n) & 1 \\ \dots & \dots & \dots & \dots \\ \dots & \dots & \dots & \dots \\ \gamma(x_n - x_1) & \dots & \gamma(x_n - x_n) & 1 \\ 1 & \dots & 1 & 0 \end{bmatrix} \begin{bmatrix} w_1 \\ \dots \\ \dots \\ w_n \\ \mu(x_0) \end{bmatrix} = \begin{bmatrix} \gamma(x_1 - x_0) \\ \dots \\ \dots \\ \gamma(x_n - x_0) \\ 1 \end{bmatrix} \quad (D.7)$$

where the first matrix (A) describes the dissimilarities between all the possible data sample pairs of the dataset using the theoretical semivariogram, the second matrix (w) describes the weights to be assigned to the data values and the Lagrange parameter and the third matrix (b) describes the dissimilarities between each data point with the estimation point using the theoretical semivariogram.

Finally, when the first matrix (A) of equation D.7 is inverted and multiplied with the last matrix (b) of equation D.7, the weights (w_i) to be assigned to the data values and the Lagrange parameter ($\mu(x_0)$) are obtained for the estimation point (x_0) (Ohoiri, 2018):

$$w = A^{-1} \cdot b \quad (D.8)$$

Now, the Ordinary Kriging estimation of the estimation point is given by (Wackernagel, 2003):

$$Z_{OK}(x_0) = \sum_{i=1}^n w_i \cdot Z(x_i) \quad (D.9)$$

And the Ordinary Kriging estimation variance of the estimation point is given by (Wackernagel, 2003):

$$Var(Z_{OK}(x_0)) = \mu(x_0) - \gamma(x_0 - x_0) + \sum_{i=1}^n w_i \cdot \gamma(x_i - x_0) \quad (D.10)$$

Practice

Using the data of the case study for the failure mechanism piping of trajectory 48-1, the Ordinary Kriging interpolation method can be applied to the bottom level of the cover (clay) layer, the grain size (70th percentile) and the (bulk) permeability of the aquifer (sand) layer. The data is available through Cone Penetration Tests and Sieve Analysis.

Ordinary Kriging Cover Layer

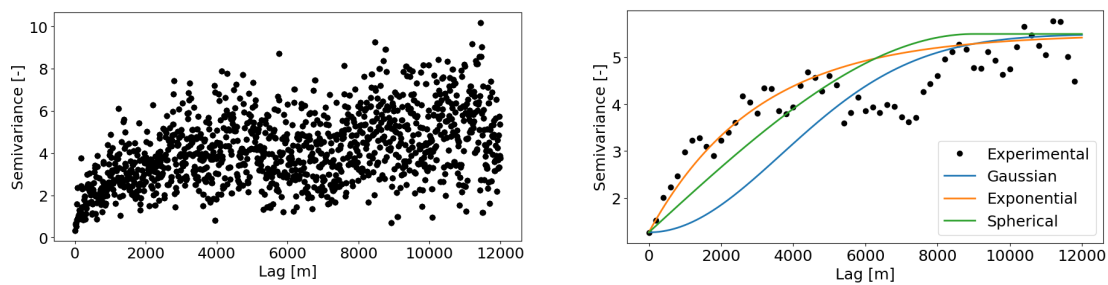


Figure D.1: Semivariogram Cloud (no bins) and Semivariogram (bins)

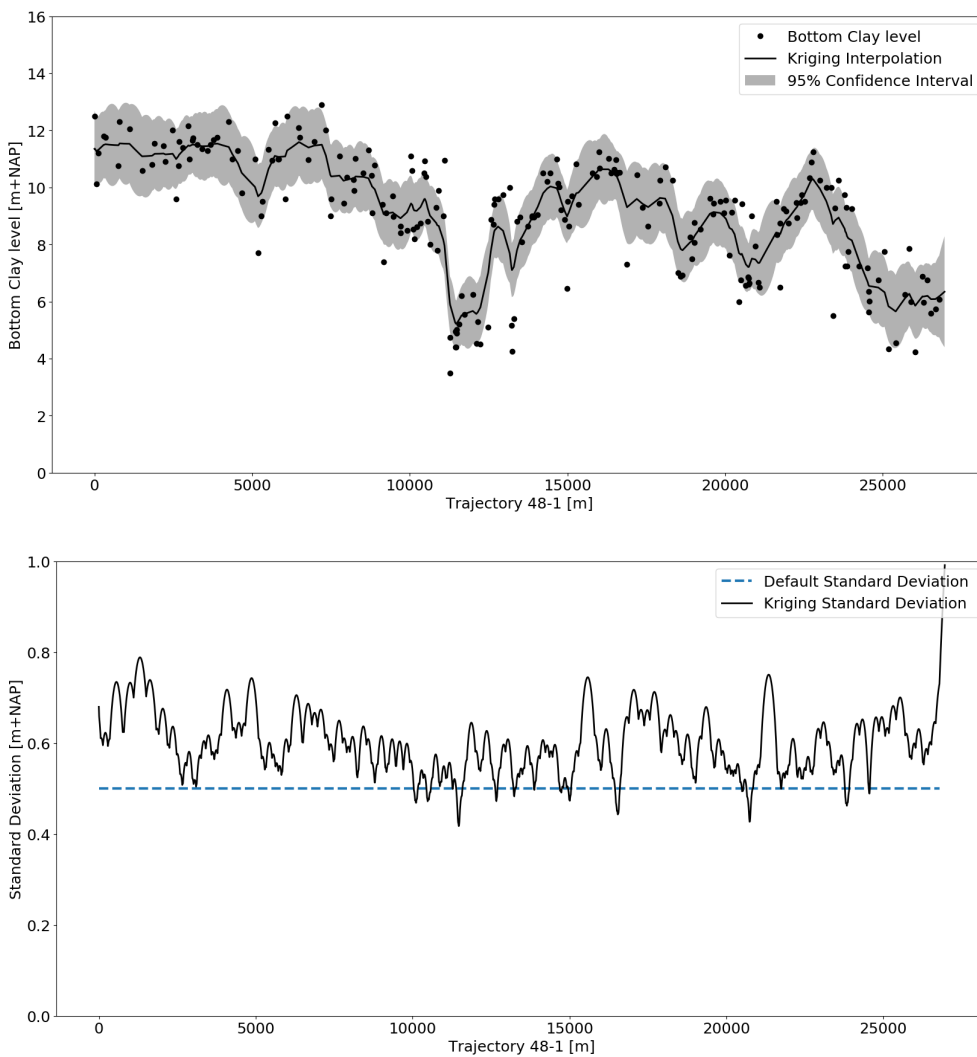


Figure D.2: Ordinary Kriging (estimation point and variance)

Ordinary Kriging Grain Size

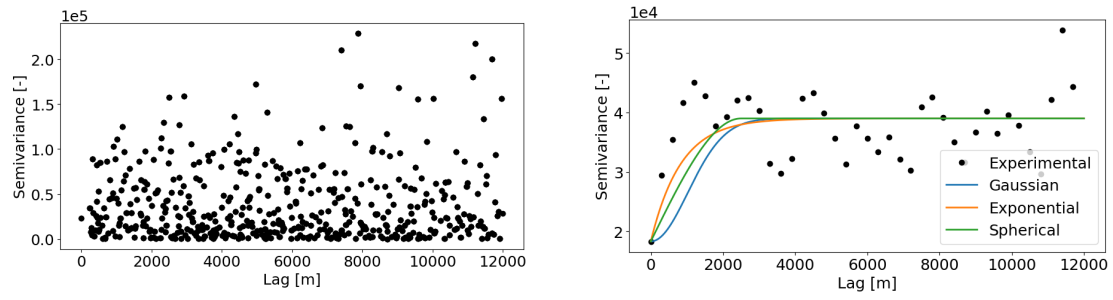


Figure D.3: Semivariogram Cloud (no bins) and Semivariogram (bins)

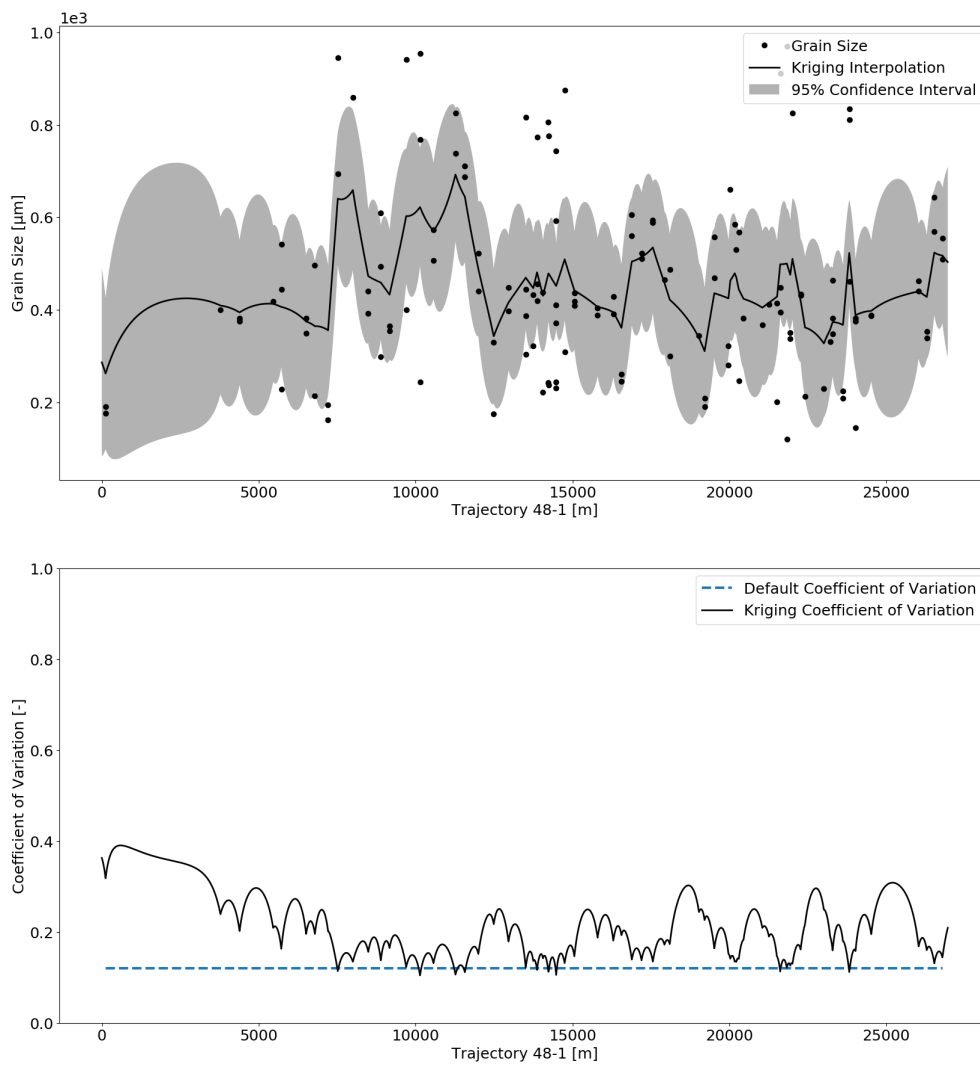


Figure D.4: Ordinary Kriging (estimation point and variance)

Ordinary Kriging Permeability

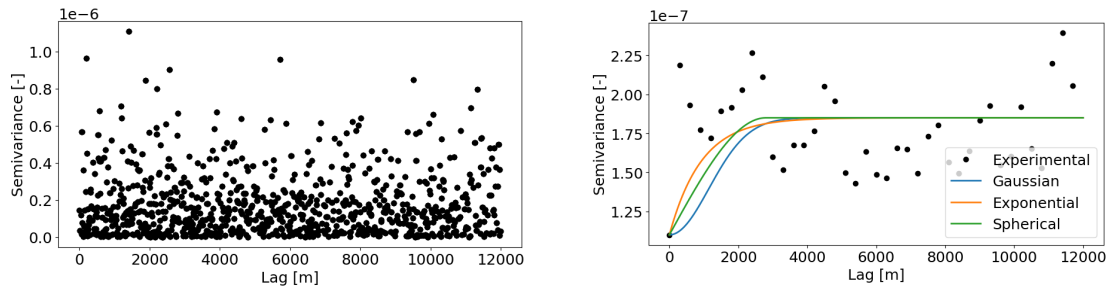


Figure D.5: Semivariogram Cloud (no bins) and Semivariogram (bins)

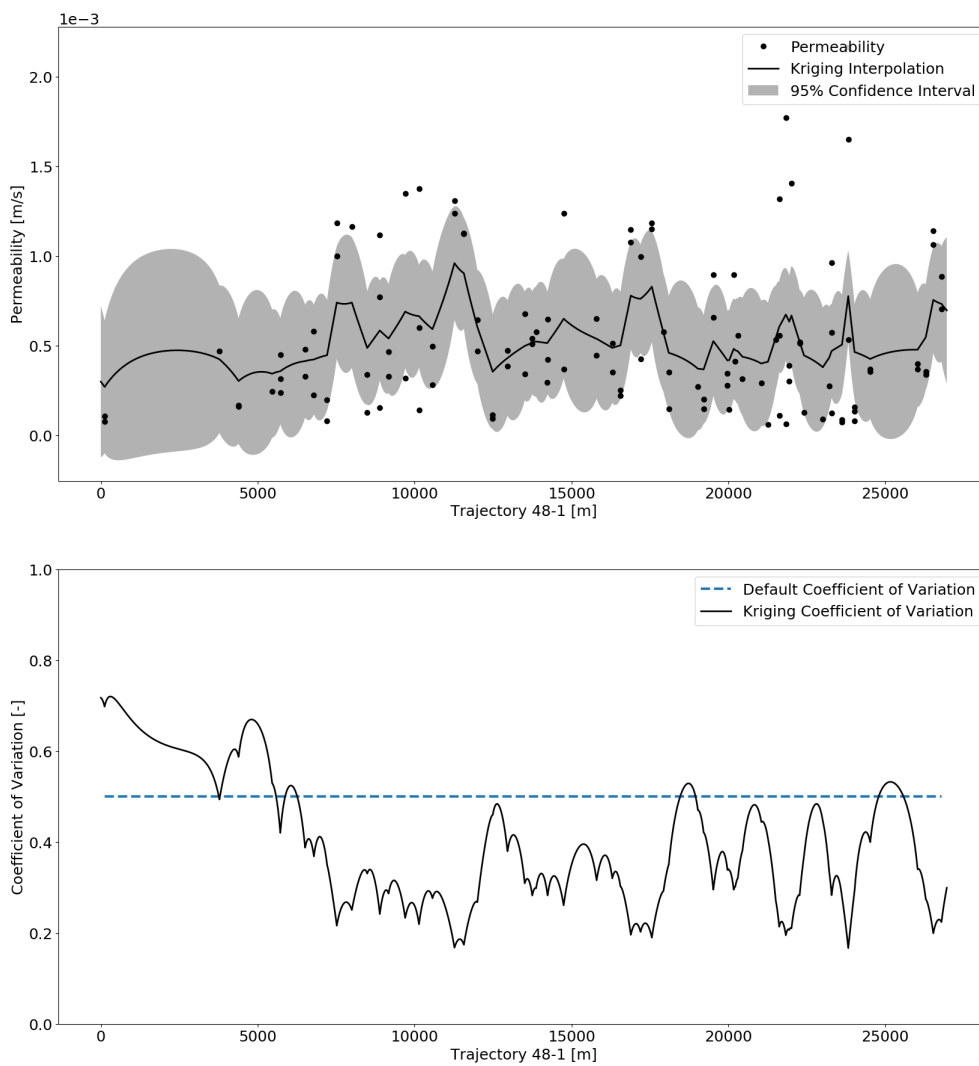


Figure D.6: Ordinary Kriging (estimation point and variance)

Appendix E

Reliability Modelling

Component Reliability

Within the broader field of reliability theory, reliability problems can be characterized by: X the input vector of random variables, $f(X)$ its joint density probability function, Ω the outcome space which defines the failure domain and $g(X)$ the limit state function describing this failure domain. The objective of component reliability modelling is to evaluate the probability content of a failure event ($\Omega \equiv g(X) \leq 0$) which is given by (Der Kiureghian, 2005)

$$P_f = P(g(X) \leq 0) = \int_{\Omega} f(X) dX \quad (\text{E.1})$$

which represent the probability of events, represented by random variables, to occur in the failure space $P_f = P(X \in \Omega)$. This problem is challenging since no closed form of the integral exist. Furthermore, numerical integration is impractical for more than two random variables. Currently, a number of methods are developed to approximate this probability integral. Here the First Order Reliability Method (FORM) or the Hasofer–Lind Approach is discussed.

The First Order Reliability Method is based on the fundamental assumption of a linearized limit state function in the standard normal space at the design point which is continuous and differential. Transforming the random variables into the standard normal space, the probability content of the failure event is given by (Der Kiureghian, 2005)

$$P_f = \int_{g(X) \leq 0} f(X) dX = \int_{G(u) \leq 0} \phi_n(u) du \quad (\text{E.2})$$

which represent the probability of events, represented by random variables, to occur in the failure space using the limit state function in the standard normal space $G(u)$. The FORM approximation is based on linearizing the limit state function at the design point (u^*) which is defined by (Der Kiureghian, 2005)

$$u^* = \operatorname{argmin}(\|u\| | G(u) = 0) \quad (\text{E.3})$$

where 'arg min' indicate the argument of the minimum of a function. So, the design point (u^*) is located on the limit state function at a minimum distance to the origin in the standard normal space ($G(u^*) = 0$). Since around the origin concentric contours of equal probability density occur in the standard normal space, the design point represent the highest probability density among all events in the failure domain (Der Kiureghian, 2005). In other words, the area close to the design point has the largest contribution to the integral which represents the failure event.

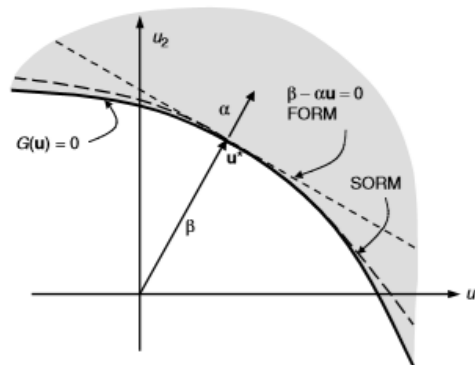


Figure E.1: FORM and SORM approximations (Der Kiureghian, 2005)

Now, the linearized limit-state function ($G_1(u)$) can be defined, where the subscript 1 is used to indicate a first-order approximation (FORM) (Der Kiureghian, 2005)

$$G(u) \approx G_1(u) = \nabla G(u^*)(u - u^*) = \|\nabla G(u^*)\|(\beta - \alpha u) \quad (\text{E.4})$$

where $\nabla G(u^*)$ is the gradient vector in the design point representing the derivative of the limit state function to the random variables ($|\partial G/\partial u_1^*|; \dots; \partial G/\partial u_n^*|$) and α is the normalized negative gradient vector at the design point ($-\nabla G(u^*)/\|\nabla G(u^*)\|$). The product of the importance vector α and the design point values of the random variables u^* denotes the reliability index β ($\alpha \cdot u^*$) which is equivalent to the distance to the tangent plane (Der Kiureghian, 2005). Note that the importance factors in the unit vector α indicate the nature, load or resistance, and importance of the random variables in the standard normal space (Der Kiureghian, 2019).

The reliability index of the linearized problem must be the ratio of the mean (μ_{G_1}) to the standard deviation (σ_{G_1}) of ($G_1(u)$) since the linearization in the design point replaces the failure space ($G_1(u) \leq 0$) by the half space ($\beta - \alpha u \leq 0$) (Der Kiureghian, 2019).

$$\mu_{G_1} = \beta \quad (\text{E.5})$$

$$\sigma_{G_1}^2 = \alpha \sum_{uu} \alpha^T = \alpha \alpha^T = \|\alpha\|^2 = \alpha_1^2 + \alpha_2^2 + \dots + \alpha_n^2 = 1 \quad (\text{E.6})$$

So, α_i^2 is the contribution of the random variable in the standard normal space to the total variance of the limit stat function which is equal to one. Because of this unity, the failure probability based on the first order approximation is completely defined by the reliability index (β).

$$Pf \approx Pf_1 = \theta\left(\frac{\mu_{G_1}}{\sigma_{G_1}}\right) = \theta(-\beta) \quad (\text{E.7})$$

Note that this First Order Reliability Method does not function properly if the surface of the limit state function is strongly nonlinear or the optimization results in multiple minimum distances to the origin along the limit state function. To deal with the nonlinearity of the limit state function, a higher order reliability method, such as Second Order Reliability Method (SORM), can be used. Multiple design points are quite rare but if these occur multiple linearizations in the design points are necessary which can be linked in a series system in a First Order Reliability Method (Der Kiureghian, 2005).

System Reliability

Reliability problems can be characterized by: X the input vector of random variables, $f(X)$ its joint density probability function, Ω the outcome space which defines the failure domain and $g(X)$ the limit state function describing this failure domain. The objective of system reliability modelling is to evaluate the probability content of the union ($\Omega \equiv \cup [g_k(X) \leq 0]$) or intersection ($\cap [g_k(X) \leq 0]$) of multiple failure events which is given by (Der Kiureghian, 2005)

$$P_f = P(\cup [g_k(X) \leq 0]) \quad (\text{union}) \quad (\text{E.8})$$

$$P_f = P(\cap [g_k(X) \leq 0]) \quad (\text{intersection}) \quad (\text{E.9})$$

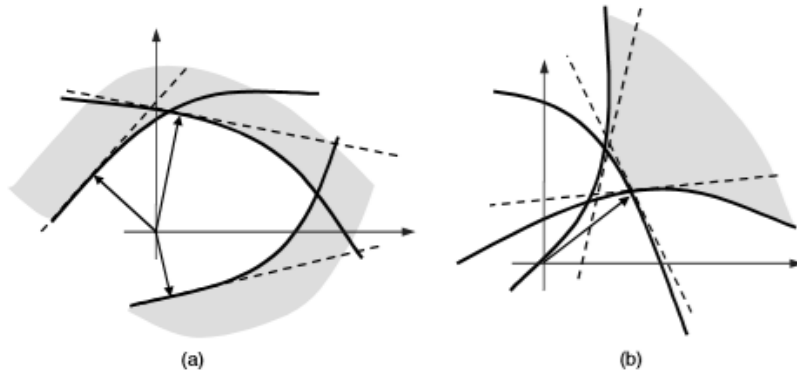


Figure E.2: Series (a) and Parallel (b) FORM approximations (Der Kiureghian, 2005)

Software

With the OpenTurns toolbox in Python and FERUM module in Matlab a First (and Second) Order Reliability Method can be performed to approximate the probability content of the failure event. Starting point is a stochastic model describing an event, the random variables are transformed into the standard normal space (u), the design point is located which represent the failure event with maximum likelihood (u^*) and the limit state function is linearized in the standard space at the design point ($G(u)$).

The following steps can be distinguished in the FORM procedure of OpenTurns and FERUM

- Create the marginal distributions of the random variables used in the stochastic model
- Create the joint probability distribution of the marginal distributions using the normal copula
- Create the limit state function of the stochastic model using the joint probability distribution
- Run the First Order Reliability Method to obtain the design point (physical and standard space), importance factors (normalized) and reliability index (vice versa failure probability)

Note that with the FERUM module in Matlab the parameter sensitivities can be derived much easier compared to the OpenTurns toolbox in Python. The parameter sensitivities are of importance to get insight in the influence of the constant variables and the distribution parameters of the stochastic variables of the limit state function on the reliability index. This will be discussed below.

Parameter Sensitivities

The parameter sensitivities of the reliability index β can be derived for the stochastic variables described by the distribution parameters ($\theta \in \theta_f$) and the constant variables known as limit state function parameters ($\theta \in \theta_g$). The parameter sensitivities of the reliability index with respect to the distribution parameters (θ_f) and limit state function parameters (θ_g) are given by the partial derivatives of β with respect to θ_f and θ_g for the FORM approximation of the reliability index (Der Kiureghian, 2019)

$$\nabla_{\theta_f} \beta = \alpha \cdot J_{u, \theta_f}(x^*, \theta_f) \quad (\text{E.10})$$

$$\nabla_{\theta_g} \beta = \frac{1}{\|\nabla G(u^*, \theta_g)\|} \nabla_{\theta_g} g(x^*, \theta_g) \quad (\text{E.11})$$

For the case of $\theta \in \theta_f$, the sensitivity vector with respect to the distribution parameters are computed with equation E.10. This gradient vector can be computed by solving the FORM problem to determine the importance vector α and the design point in the original space x^* . Next, the Jacobian of the probability transformation to the normal space ($u = u(x, \theta_f)$) with respect to the distribution parameters and the random variables fixed at the design point $J_{u, \theta_f}(x^*, \theta_f)$ is derived (Der Kiureghian, 2019).

$$J_{u, \theta_f}(x^*, \theta_f) = \frac{\partial u(x^*, \theta)}{\partial \theta} \quad \theta \in \theta_f \quad (\text{E.12})$$

the required Jacobian matrix can be obtained by taking the partial derivative of each stochastic variable (X) with respect to each of the distribution parameters (θ) at the design point (x^*) in the standard normal space. This Jacobian matrix is a (N*N) matrix for N stochastic parameters which is multiplied by the importance vector α (1*N) to obtain the gradient vector of equation E.10 (1*N). This can be derived for each of the six distribution parameters (μ_X , σ_X , p_1 , p_2 , p_3 and p_4).

For the case of $\theta \in \theta_g$, the sensitivity vector with respect to the limit state function parameters are computed with equation E.11. This gradient vector can be computed by solving the FORM problem to determine the norm ($\|\nabla G(u^*, \theta_g)\|$) of the gradient vector and the design point in the original space x^* . Next, the gradient of the limit state function with respect to the limit state function parameters and the random variables fixed at the design point $\nabla_{\theta_g} g(x^*, \theta_g)$ is derived (Der Kiureghian, 2019).

$$\nabla_{\theta_g} g(x^*, \theta_g) = \frac{\partial g(x^*, \theta)}{\partial \theta} \quad \theta \in \theta_g \quad (\text{E.13})$$

the required gradient of the limit state function can be obtained by taking the partial derivative of each constant (X) with respect to the limit state function parameters (θ) at the design point

(x^*) in the original space. This gradient vector is a (1^*N) vector for N constant parameters which is normalized by the inverse of $(\|\nabla G(u^*, \theta_g)\|)$ (1^*1) to obtain the gradient vector of equation E.11 (1^*N) .

$$\|\nabla G(u^*, \theta_g)\| = -\frac{\partial g(x^*, \theta)}{\partial \theta} / \frac{du^*}{d\theta} \quad \theta \in \theta_g \quad (\text{E.14})$$

where the derivative of u at the design point with respect to θ can be obtained by taking the partial derivative of each stochastic variable (X) with respect to each of the distribution parameters (θ) at the design point (x^*) in the standard normal space.

$$\frac{du^*}{d\theta} = \frac{\partial u(x^*, \theta)}{\partial \theta} \quad \theta \in \theta_g \quad (\text{E.15})$$

Furthermore, from the sensitivity vectors $(\nabla_{\theta_f} \beta)$ the variance of the approximated reliability index using FORM can be approximated using equation E.16 with respect to any of the distribution parameters ($\theta \in \theta_f$) (Lanzafame and Sitar, 2018).

$$\sigma_\beta \approx \nabla_{\theta_f} \beta' \cdot \sum_{\theta\theta} \cdot \nabla_{\theta_f} \beta \quad (\text{E.16})$$

where $\sum_{\theta\theta}$ is the covariance matrix of the distribution parameter in question. In perspective to \sum_{XX} , the covariance matrix of the stochastic variables consisting of the variances and covariances, $\sum_{\theta\theta}$ consists of the variances and covariances of the distribution parameter based on the assumptions made with bootstrapping. A summary of the bootstrapping results for the case study is given in table E.1 below.

Bootstrapping Method

The bootstrapping method uses the dataset of a limit state function parameter. By sampling with replacement a new sample of the same size (bootstrap sample) is obtained. This is repeated a large number of times (10.000) and for each of these bootstrap samples the mean and standard deviation (bootstrap estimates) is computed. Taking the standard deviation of the bootstrap mean and standard deviation results in the uncertainties of the distribution parameters. The result for three limit stat function parameters (k , d_{70} and D_{cover}) are summarised below.

Variable (X)	σ_{μ_X}	σ_{σ_X}
k	1/10.8 σ_k	1/15.3 σ_k
d_{70}	1/12.5 $\sigma_{d_{70}}$	1/17.3 $\sigma_{d_{70}}$
D_{cover}	1/14.1 $\sigma_{D_{cover}}$	1/22.3 $\sigma_{D_{cover}}$
MEAN	1/12 σ_X	1/18 σ_X

Table E.1: Uncertainties of the distribution parameters (θ_f)

Appendix F

Autocorrelation Function

The autocorrelation function describes the spatial structure of variation in the residuals by the spatial correlation. This correlation is computed for parameters with itself over space. If a parameter is correlated with itself, the value at a location provides information on the probable value at another location. The strength of this association is defined with the correlation coefficient (ρ). For two variables (z_1 and z_2) the correlation coefficient is described by the covariance of the two variables and the variances of the variables (Baecher and Christian, 2019).

$$\rho(z_1, z_2) = \frac{\text{cov}(z_1, z_2)}{\sqrt{\text{var}(z_1) \cdot \text{var}(z_2)}} \quad (\text{F.1})$$

Plotting the residuals of all the data pairs separated by equal distances or lags (δ) the correlation coefficient can be calculated using equation F.1 for the separation distance specific. Data pairs with close separation have a higher correlation than data pairs with large separation distances.

The observed correlations at different lags can be described by an autocorrelation function ($\rho(\delta)$) where the correlation of a variable with itself is a function of the separation distance (δ). Therefore, at a lag value of zero the correlation equals one. An example of an autocorrelation function is given in equation F.2 below which describes the spatial correlation as a function of the separation distance (δ), residual correlation (ρ_0) and the correlation length (D). Note that the constants are derived from fitting the autocorrelation function to the spatial correlations at different lags.

$$\rho(\delta) = (1 - \rho_0) \exp\left(-\left(\frac{\delta}{D}\right)^2\right) + \rho_0 \quad (\text{F.2})$$

Practice

Using the data of the case study for the failure mechanism piping of trajectory 48-1, the autocorrelation function can be derived for the bottom level of the cover (clay) layer, the grain size (70th percentile), the (bulk) permeability of the aquifer (sand) layer and the seepage length of ground water. The data is available through Cone Penetration Tests, Sieve Analysis and Geophysical Research.

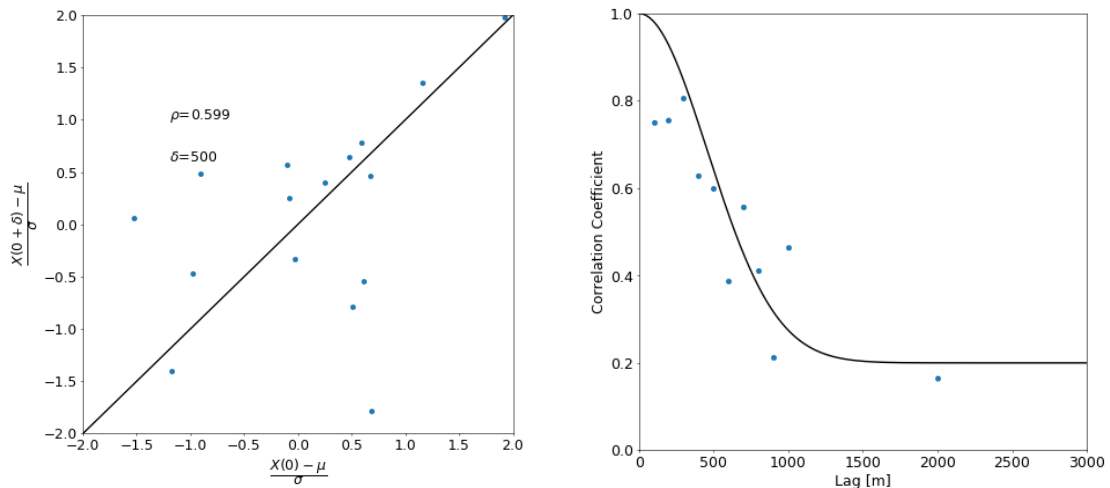


Figure F.1: Spatial correlation (lag=500m) - Autocorrelation function (cover layer)

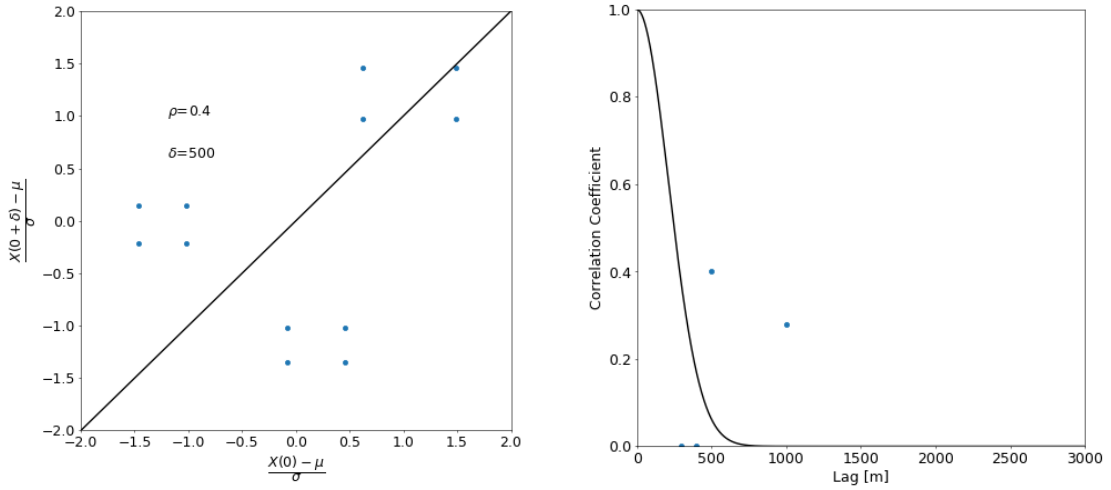


Figure F.2: Spatial correlation (lag=500m) - Autocorrelation function (grain size)

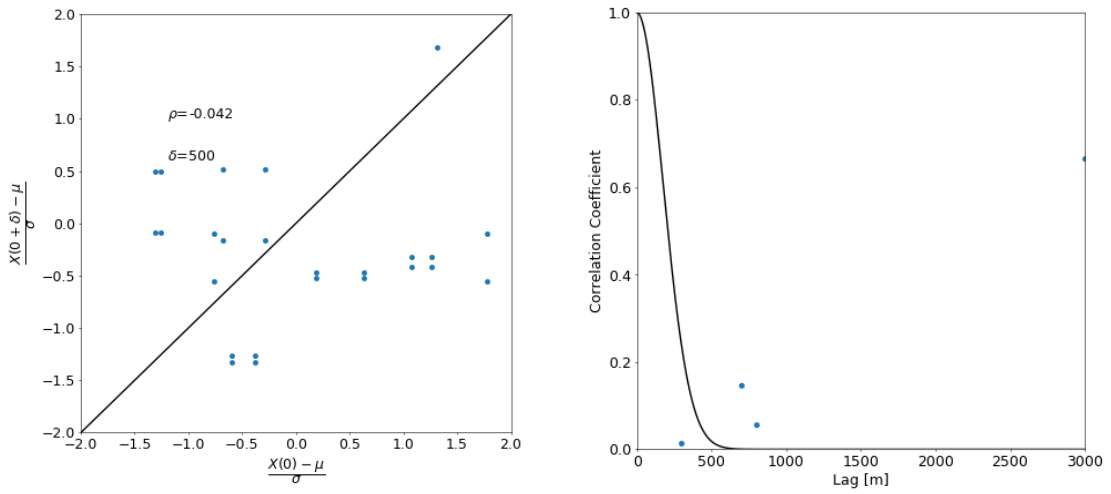


Figure F.3: Spatial correlation (lag=500m) - Autocorrelation function (permeability)

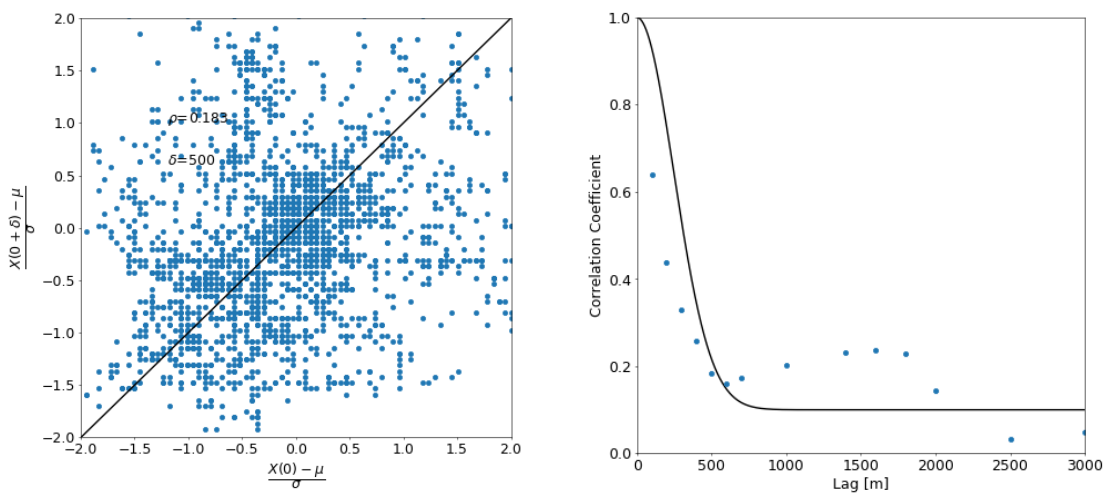


Figure F.4: Spatial correlation (lag=500m) - Autocorrelation function (seepage length)

Appendix G

Derivation of Length-Effects

With increasing length of a dike trajectory (or dike section) the probability that a weak spot occurs will increase. So, with increasing length, the failure probability of a dike trajectory (or dike section) will increase. This is called the length-effect. The length-effect differs in magnitude for all failure mechanisms. This depends on the spatial distribution and fluctuations of the resistance of the dike against the failure mechanisms. For failure mechanisms with a small length-effect the resistance has a small spatial distribution, like the height of the dike to resist overtopping. For failure mechanisms with a large length-effect the resistance has a large spatial distribution like the thickness of the cover layer to resist piping (VNK2, 2011).

The length-effect of geotechnical failure mechanisms is a function of the length under consideration ($L_{trajectory}$ or $L_{section}$), the failure mechanism sensitive part (a) and a length measure for the intensity of the length-effect within this failure mechanism sensitive part (b). This is stated in equation G.1 and G.2 (Deltares, 2017b).

$$N^* = 1 + \frac{a \cdot L_{section}}{b} \quad (G.1)$$

$$N = 1 + \frac{a \cdot L_{trajectory}}{b} \quad (G.2)$$

Piping

Factor a , the failure mechanism sensitive fraction, is dependent on the location of the trajectory. Based on studies of Lopez de la Cruz (Lopez de la Cruz et al., 2010) conservative values are proposed of 0.4 and 0.9, making a distinction between the lower river/lake/sea areas and upper river areas in the Netherlands (Rijkswaterstaat, 2016a).

Factor b , the independent length of equivalent elements, is dependent on the location of the trajectory. Based on studies of Lopez de la Cruz (Lopez de la Cruz et al., 2010) approximations are in the order of 300-400m (Rijkswaterstaat, 2016a).

Macro-Stability

Factor a , the failure mechanism sensitive fraction, is dependent on the location of the trajectory. Based on studies of RWS and ENW (Rijkswaterstaat and ENW, 2007) a conservative value is proposed of 0.033 (Rijkswaterstaat, 2016a). Factor b , the independent length of equivalent elements, is dependent on the location of the trajectory. Based on studies of RWS and ENW (Rijkswaterstaat and ENW, 2007) approximations are in the order of 40-50m (Rijkswaterstaat, 2016a).

Failure Mechanisms	Parameter a [-]	Parameter b [m]
Piping (STPH)	0.4 - 0.9	300
Macro-Stability (STBI/STBU)	0.033	50

Table G.1: Length-effect parameters according to the WBI 2017 (Deltares, 2017b)

Equations G.1 and G.2 for the length-effect of geotechnical failure mechanisms are derived from the Technisch Rapport Waterkerende Grondconstructies (TAW, 2001) which again are based on the formulations for macro-stability and piping in the Leidraad Ontwerpen Rivierdijken (LOR2) (TAW, 1989) given in equation G.3 and G.4 below.

$$N = 1 + \alpha \cdot \frac{L}{l} \quad \text{Macro-Stability} \quad (G.3)$$

Here, the length-effect is a function of the of the length of the trajectory (L), the representative element length for a cross-section (l) and the factor for the correlated amount of contribution of the elements within the trajectory (α) (TAW, 1989).

$$N = r \cdot \frac{L}{c} \quad \text{Piping} \quad (\text{G.4})$$

Here, the length-effect is a function of the of the length of the trajectory (L), the correlation distance of the thickness variations of the clay cover layer (c) and the reduction factor for the correlated amount of contribution of the elements within the trajectory (r) (TAW, 1989).

Derivation of the Length-Effect for Piping

Starting point are the reliability indexes of the cross-section assessments of the failure mechanism piping. These reliability indexes differ between the various sections of a dike trajectory and can be specified by an expected value and a standard deviation (μ_β , σ_β). With the total length of the trajectory (L) and the expected length of failure for the failure mechanisms specific (l) a relation can be found between the trajectory reliability and the cross-section reliability demand for the failure mechanism piping specific using the length-effect. This derivation is based on the papers of Lopez de la Cruz (Lopez de la Cruz et al., 2010) and Calle (Calle, 2010) for the calibration of the WTI2011.

$$Pf_{cross-section} = \frac{Pf_{trajectory}}{1 + \frac{L(i)}{l(i)}} \quad (\text{G.5})$$

Where the expected length of failure for a failure mechanisms (l) depends on the local reliability index (β) and spatial correlation in terms of the second derivative of the autocorrelation function of the reliability function (Z) at a "lag" value of zero ($\rho'_z(0)$).

$$l(i) = 2\pi\Phi(-\beta)\exp\left(\frac{1}{2}\beta^2\right)\frac{1}{\sqrt{-\rho'_z(0)}} \quad (\text{G.6})$$

Note that the autocorrelation function of the reliability function of a failure mechanism specific is an assembly of autocorrelation functions of the parameters used in the reliability function (Z). This autocorrelation function for a parameter specific is given by the lag parameter (τ), the correlation length (D) and the restcorrelation (ρ_0). The assembly of autocorrelation functions is fulfilled using importance factors (α) for each of the parameters specific.

$$\rho_i(\tau) = (1 - \rho_{0,i})\exp\left(-\left(\frac{\tau}{D_i}\right)^2\right) + \rho_{0,i} \quad (\text{G.7})$$

$$\rho_z(\tau) = \sum_{i=1}^N \alpha_i^2 \rho_i(\tau) \quad (\text{G.8})$$

The second derivative of the combined autocorrelation functions of the parameters used in the reliability function (Z) at a "lag" value of zero is given by

$$\rho''_z(0) = -\sum_{i=1}^N \frac{2\alpha_i^2(1 - \rho_{0,i})}{D_i^2} \quad (\text{G.9})$$

In order to make the relation given in equation G.5 continuous over the trajectory it is integrated over the probability distribution for the reliability index ($\beta = \xi$) using the following integral.

$$Pf_{trajectory} = \int_{+\infty}^{-\infty} \Phi(-\xi) \cdot \left(1 + \frac{L}{l(\xi)}\right) \frac{\exp\left(-\frac{1}{2}\left(\frac{\xi - \mu_\beta}{\sigma_\beta}\right)^2\right)}{\sqrt{2\pi}\sigma_\beta} d\xi \quad (\text{G.10})$$

This equation can be written as the sum of two integrals.

$$Pf_{trajectory} = \int_{+\infty}^{-\infty} \Phi(-\xi) \frac{\exp\left(-\frac{1}{2}\left(\frac{\xi - \mu_\beta}{\sigma_\beta}\right)^2\right)}{\sqrt{2\pi}\sigma_\beta} d\xi + \int_{+\infty}^{-\infty} \Phi(-\xi) \frac{L}{l(\xi)} \frac{\exp\left(-\frac{1}{2}\left(\frac{\xi - \mu_\beta}{\sigma_\beta}\right)^2\right)}{\sqrt{2\pi}\sigma_\beta} d\xi \quad (\text{G.11})$$

In the first part of this summation a transformation ($t = \frac{\xi - \mu_\beta}{\sigma_\beta}$) is substituted for the integral variable (ξ) which can be used to approximate the first part using a Taylor function. This results in the following approximation for the first integral.

$$\int_{+\infty}^{-\infty} \Phi(-\xi) \frac{\exp(-\frac{1}{2}(\frac{\xi - \mu_\beta}{\sigma_\beta})^2)}{\sqrt{2\pi}\sigma_\beta} d\xi = \quad (G.12)$$

$$\int_{+\infty}^{-\infty} \Phi(-(\mu_\beta + t \cdot \sigma_\beta)) \frac{\exp(-\frac{1}{2}t^2)}{\sqrt{2\pi}} dt = \quad (G.13)$$

$$\Phi(-\mu_\beta) + \frac{\exp(-\frac{1}{2}\mu_\beta^2)}{\sqrt{2\pi}} \left(\frac{1}{2}\mu_\beta\sigma_\beta^2 + \frac{1}{4}(\mu_\beta^3 - 3\mu_\beta)\sigma_\beta^4 \right) \quad (G.14)$$

In the second part of this summation a relation, given in equation G.6, for the expected length of failure for a failure mechanisms ($l(\xi)$) is substituted. This results in the following approximation for the second integral.

$$\int_{+\infty}^{-\infty} \Phi(-\xi) \frac{L}{l(\xi)} \frac{\exp(-\frac{1}{2}(\frac{\xi - \mu_\beta}{\sigma_\beta})^2)}{\sqrt{2\pi}\sigma_\beta} d\xi = \quad (G.15)$$

$$\int_{+\infty}^{-\infty} \Phi(-\xi) \frac{L\sqrt{-\rho_z''(0)}}{2\pi\Phi(-\xi)\exp(\frac{1}{2}\xi^2)} \frac{\exp(-\frac{1}{2}(\frac{\xi - \mu_\beta}{\sigma_\beta})^2)}{\sqrt{2\pi}\sigma_\beta} d\xi = \quad (G.16)$$

$$\frac{L\sqrt{-\rho_z''(0)}}{2\pi\sqrt{1 + \sigma_\beta^2}} \exp\left(-\frac{1}{2}\left(\frac{\mu_\beta^2}{1 + \sigma_\beta^2}\right)\right) \quad (G.17)$$

Combining the two parts results in the following relation where the trajectory failure probability is a function of the cross-section reliability index (β), the total length of the trajectory (L) and the second derivative of the autocorrelation function of the reliability function at the origin ($\rho_z''(0)$).

$$Pf_{trajectory} = F(\mu_\beta, \sigma_\beta, \rho_z''(0), L) = \quad (G.18)$$

$$\frac{L\sqrt{-\rho_z''(0)}}{2\pi\sqrt{1 + \sigma_\beta^2}} \exp\left(-\frac{1}{2}\frac{\mu_\beta^2}{(1 + \sigma_\beta^2)}\right) + \Phi(-\mu_\beta) + \frac{\exp(-\frac{1}{2}\mu_\beta^2)}{\sqrt{2\pi}} \left(\frac{1}{2}\mu_\beta\sigma_\beta^2 + \frac{1}{4}(\mu_\beta^3 - 3\mu_\beta)\sigma_\beta^4 \right) \quad (G.19)$$

$$\beta_{trajectory} = -\Phi^{-1}(Pf_{trajectory}) \quad (G.20)$$

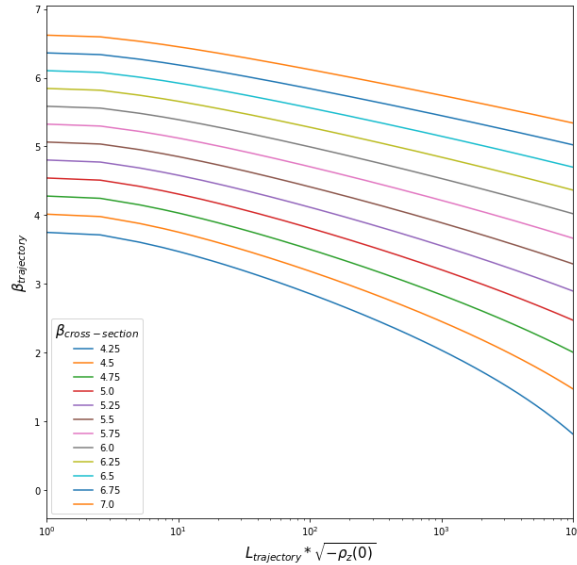


Figure G.1: Trajectory versus cross-section reliability for $\sigma_{beta}=0.1$ and $\rho_z''(0)$ of $-6.4e-06$

Vice versa when now an allowable trajectory failure probability is known a relation can be found for the cross-section reliability based on the trajectory failure probability, the length of the trajectory and given autocorrelation value using equation G.21.

$$\mu_\beta = F(Pf_{trajectory}, \sigma_\beta, \rho_z''(0), L) \quad (G.21)$$

The required reliability index on cross-section level will then be given by the 95% confidence level.

$$\beta_{cross-section} = \mu_\beta - 1.65\sigma_\beta \quad (G.22)$$

For the calibration of Dutch trajectories to find a relation between the cross-section and trajectory reliability index the following data is used based the VNK2 trajectory studies (DR 5, 10, 14, 17) (Lopez de la Cruz et al., 2010).

- $\beta_{trajectory}$ of 3.5-4.5
- σ_{beta} of 0.1
- L between 0-100 km
- $\rho_z''(0)$ of -1.8e-06

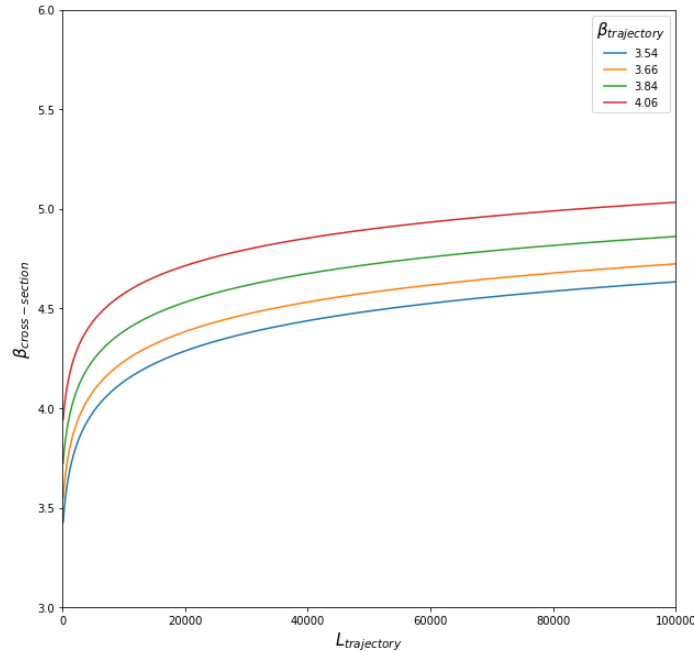


Figure G.2: Cross-section versus trajectory reliability for $\sigma_{beta}=0.1$ and $\rho_z''(0)$ of -1.8e-06

Based on the calibration of equation G.19 and G.21 to Dutch trajectories using the data from the VNK2 trajectory studies (DR 5, 10, 14, 17) the following relation results from fitting equation G.5 to the data.

$$Pf_{cross-section} = \frac{Pf_{trajectory}}{1 + \frac{L(i)}{l(i)}} = \frac{Pf_{trajectory}}{1 + 0.0028 \cdot L} \quad (G.23)$$

This results in conservative values for a and b for equation G.2 of 0.4-0.9 and 300m respectively, making a distinction between upper river and lower river areas. Note that the value of a can be adjusted for the total length of the the sensitive part of the trajectory to the failure mechanism specific based on local information (Lopez de la Cruz et al., 2010). These values are used in the WTI2017 (RWS, 2017c). An overview is given in figure G.3

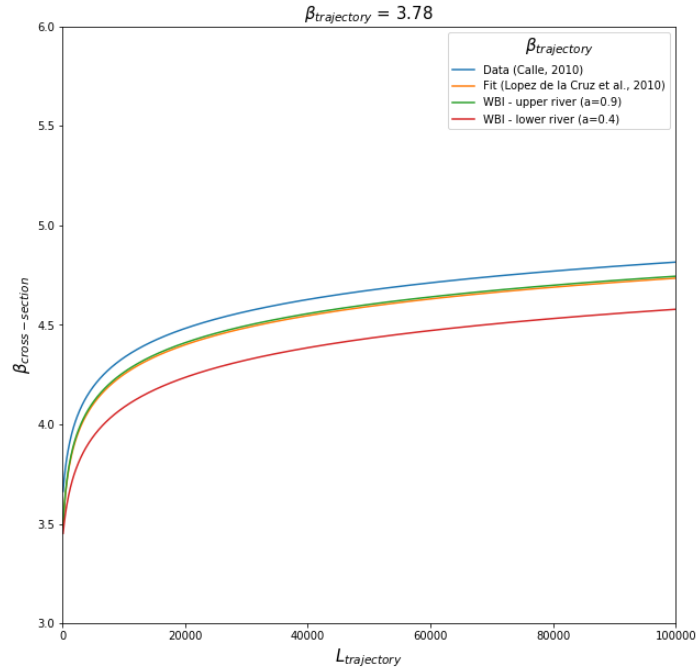


Figure G.3: Fitting of equation G.5 to the data from the VNK2 studies

Derivation of the Length-Effect for Macro-Stability

In this derivation it will be explained how the cross-section reliability demand for the failure mechanism macro-stability specific can be determined from the reliability demand on trajectory level for the failure mechanism specific using the length-effect. This length-effect is a function of the length of the dike trajectory (L), the representative element length for a cross-section (l) and the factor for the correlated amount of contribution of the elements within the trajectory (α). This derivation is based on the papers of ENW (Rijkswaterstaat and ENW, 2007) and Leidraad Ontwerpen Rivierdijken (LOR2) (TAW, 1989) for the calibration of the WTI2011.

$$Pf_{cross-section} = \frac{Pf_{trajectory}}{1 + \alpha \cdot \frac{L(i)}{l(i)}} = \frac{Pf_{trajectory}}{1 + 0.00066 \cdot L} \quad (G.24)$$

Based on studies within the Leidraad Ontwerpen Rivierdijken (LOR2) (TAW, 1989) on the Al-blasserwaard, the length-effect factor is approximated to be 50 based on $\alpha = 1/30$, $l = 50m$ and $L_{traject} = 70km$. This results in values for a and b for equation G.2 of 0.033 and 50m respectively (TAW, 1989). These values are used in the WTI2017 (RWS, 2016).

Appendix H

Length-Effect of Serial Systems

A dike trajectory can be considered as a series system of dike sections in which strength, load and geometry can be supposed to be homogeneous. Failure of a single section will always lead to the failure of the entire system within a series system. Theories to combine the failure probabilities of these sections to one trajectory failure probability for a failure mechanism specific will be discussed in order to compare it to the current assembly method applied within Riskeer (WBI 2017).

Discrete Series Systems

Here the general case is considered of a series system consisting of multiple sections n with known failure probabilities Pf_i . The upper and lower boundaries of the trajectory failure probability Pf can be determined by taking possible cases of dependence into account (Jonkman et al., 2017).

Fundamental boundaries of the system failure probability are given by equation H.1 where the lower bound is valid for dependent sections and the upper bound for mutually exclusive sections.

$$\max(Pf_i) \leq Pf \leq \sum_{i=1}^n (Pf_i) \quad (\text{H.1})$$

Note that for a series system with independent sections the system failure probability is given by

$$Pf = 1 - \prod_{i=1}^n (1 - Pf_i) \quad (\text{H.2})$$

In the cases of mutually exclusive, independent and dependent an analytical expression is available to determine the system failure probability Pf . For other cases the system failure probability will be a function of the correlation coefficient.

Ditlevsen boundaries of the system failure probability are given by equation H.3 where the lower and upper bound are valid for an according calculated correlation between normally distributed reliability functions.

$$\sum_{i=1}^n Pf_i - \sum_{i=2}^n \min\left(\sum_{j=1}^{i-1} Pf_{i,j}, Pf_i\right) \leq Pf \leq \sum_{i=1}^n Pf_i - \sum_{i=2}^n \max_{j < i} Pf_{i,j} \quad (\text{H.3})$$

Hohenbichler and Rackwitz method uses a transformation of non-normally distributed dependent variables to standard normally distributed independent variables. This approximation method is less simple and requires a greater calculation capacity than the Ditlevsen method. The approximation is given by equation H.4 which is valid for combining two elements (Z_1 and Z_2) into an equivalent single element (Z^e). To solve H.6 a FORM-Design Point Method is used. Note that this procedure will be repeated until a single equivalent element results representing the system with an according failure probability.

$$P(Z^e < 0) = P(Z_1 < 0 \cup Z_2 < 0) = P(Z_1 < 0) + P(Z_2 < 0) - P(Z_1 < 0 \cap Z_2 < 0) \quad (\text{H.4})$$

$$P(Z_1 < 0 \cap Z_2 < 0) = P(Z_1 < 0) * P(Z_2 < 0 | Z_1 < 0) \quad (\text{H.5})$$

$$P(Z_2 < 0 | Z_1 < 0) = P(Z_2' < 0) = P(\beta_2 - \rho u' - w\sqrt{1 - \rho^2} < 0) \quad (\text{H.6})$$

Comparison of Methods

For comparing the assembly methods for serial systems as discussed in the previous section, imagine a dike trajectory consisting of identical dike sections which all have an equal failure probability of $1e-03$. Two cases are considered, one with dike sections having a mutual dependence of 0.8 (assumed to be representative for a small length-effect i.e. geometrical failure mechanisms) and one with dike sections having a mutual dependence of 0.2 (assumed to be representative for a large length-effect i.e. geotechnical failure mechanisms).

For both cases a reference is made to the assembly procedure of the WBI 2017 as discussed in appendix A. In the case of a high mutual dependence a representative length-effect factor of 3 is chosen, in the case of a low mutual dependence a representative length-effect factor of 80 is chosen which leads to an upper and lower boundary of which the minimum is chosen conform equation A.4.

Both cases are visualised in figure H.1 and H.2 below.

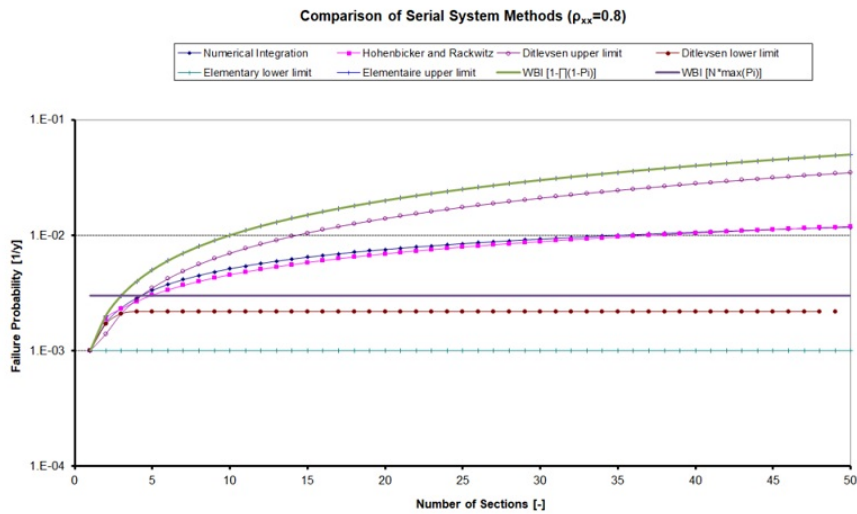


Figure H.1: Failure probability of $1e-03$ | Mutual dependence of 0.8 | Length-effect factor of 3

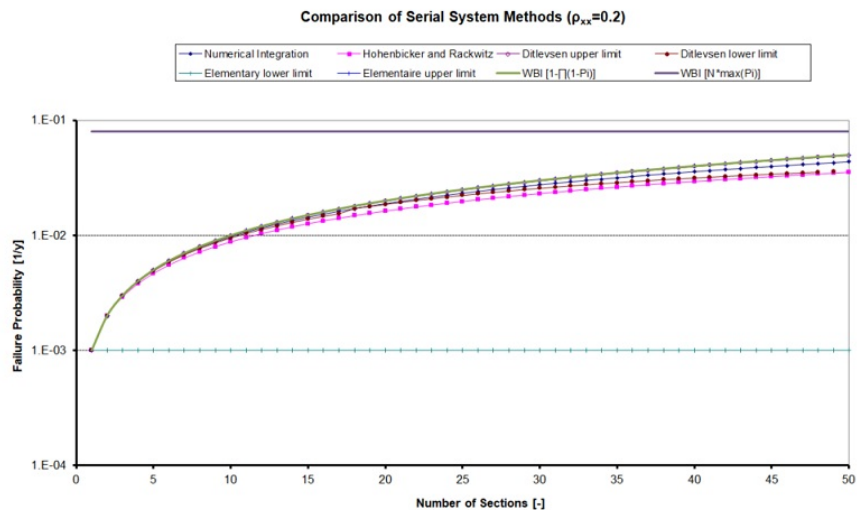


Figure H.2: Failure probability of $1e-03$ | Mutual dependence of 0.2 | Length-effect factor of 80

It can be concluded that for low mutual dependence the assembly methods are close to each other compared to the case with high mutual dependence. This indicates that the assumption of mutual independence is actually a good approximation. In order to visualise the impact of a different sectional failure probability another two cases are considered, one with dike sections having identical failure probabilities of 1e-03 and one with dike sections having identical failure probabilities of 1e-02.

Both cases are visualised in figure H.3 and H.4 below.

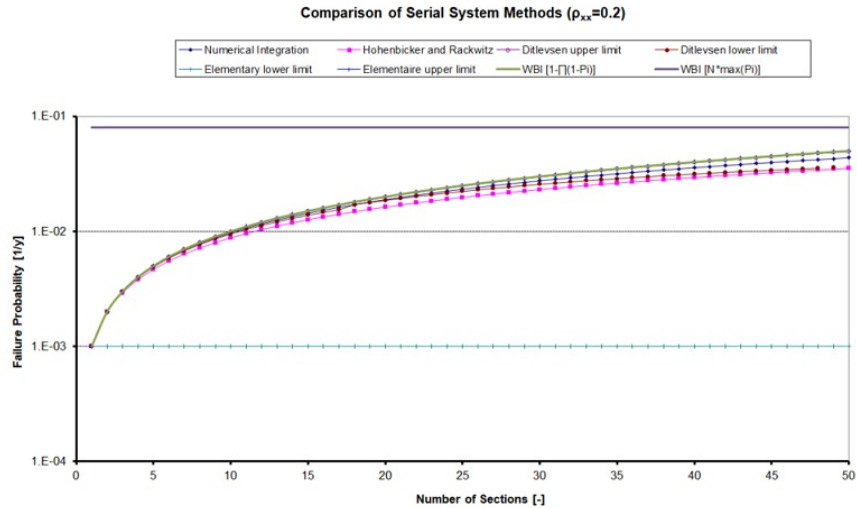


Figure H.3: Failure probability of 1e-03 |Mutual dependence of 0.2 |Length-effect factor of 80

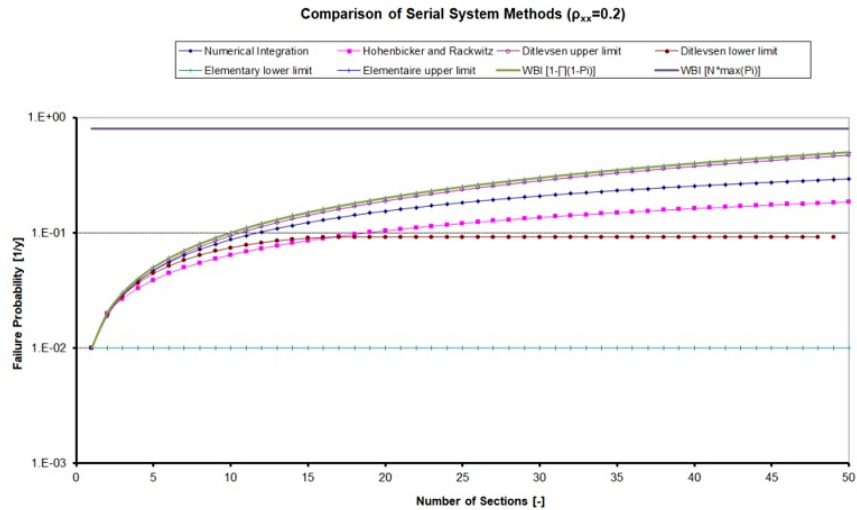


Figure H.4: Failure probability of 1e-02 |Mutual dependence of 0.2 |Length-effect factor of 80

It can be concluded that for low mutual dependence the assembly methods are close to each other in the case of small failure probabilities compared to the case with large failure probabilities. This indicates that the assumption of mutual independence is not a good approximation for dike sections with large failure probabilities.

Mutual Dependency of Sections

The mutual dependence between sections can be related to the dependence between stochastic variables representative for the division of sections. Each stochastic variable is subjected to variation and can be described by a probability density function. Important measures for random variables are mean values, or the expected value, and variances, or the dispersion around the mean value (Jonkman et al., 2017).

Next to the mean and variance of random variables, the covariance is a third important statistical measure. The covariance is a measure of linear dependence between two random variables. Random variables (X,Y) have a positive dependency if an arbitrary value of X larger than zero corresponds to values of Y larger than zero. Vice versa have random variables a negative dependency if an arbitrary value of X smaller than zero corresponds to values of Y smaller than zero. This is visualised in figure H.5 (Jonkman et al., 2017).

$$cov(X, Y) = E[(X - E(X))(Y - E(Y))] \quad (H.7)$$

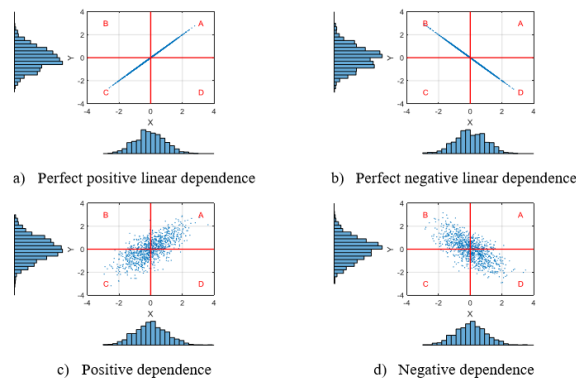


Figure H.5: Dependency of random variables (Jonkman et al., 2017)

Another statistical measure of statistical dependence, related to the covariance, is the Pearson's product moment correlation coefficient. If two random variables (X,Y) are independent the correlation coefficient is zero, if X and Y are positive dependent the correlation coefficient is between zero and one and vice versa if X and Y are negative dependent the correlation coefficient is between zero and minus one (Jonkman et al., 2017).

$$\rho(X, Y) = \frac{cov(X, Y)}{\sigma(X)\sigma(Y)} \quad (H.8)$$

A third concept for statistical dependence is the Spearman's Rank correlation coefficient. This concept is a way to extend linear dependency to monotonic dependency by using Pearson's product moment correlation with the ranks of random variables $(F(X),F(Y))$ instead of the random variables (X,Y) (Jonkman et al., 2017).

$$r(X, Y) = \rho(F(X), F(Y)) \quad (H.9)$$

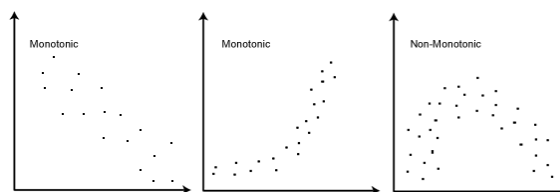


Figure H.6: Monotonic and Linear | Monotonic | Non-Monotonic (Statistics, 2018)

Appendix I

Generic Approach of Length-Effects

First, the length-effect within sections is based on the parameter b which indicates the intensity of the length-effect and is assumed to be representative for the failure mechanism specific. In other words, over every equivalent independent length b within a homogeneous section the sectional failure probability will increase with the cross-sectional failure probability. By creating the autocorrelation function of the spatial failure probabilities and comparing the correlation distance to the equivalent independent length a simple approximation of the b value is derived. According to the autocorrelation function for a single parameter, given in equation 9.22, the correlation distance of the spatial failure probability is equal to approximate 350 meters.

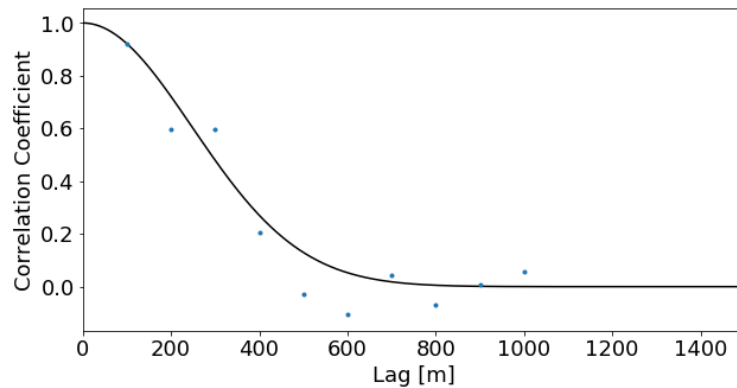


Figure I.1: Autocorrelation function of the spatial failure probabilities of trajectory 48-1

Second, the length-effect within sections is based on the parameter a which indicates the failure mechanism sensitive part of the trajectory. By assessing the historical wells along the trajectory and creating rough intervals along the trajectory that are suspected to be piping sensitive a simple approximation for the a value is derived. According to historical data approximate 8.2km of the 26.9km is piping sensitive (30%).

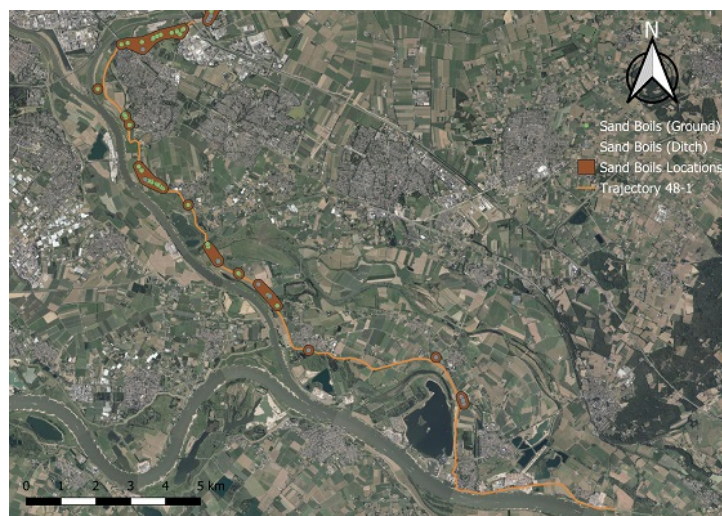


Figure I.2: Piping sensitive interval of trajectory 48-1

Assigning a threshold of 34% for the probabilistic assessment using field uncertainties results in a threshold for failure probabilities that are taken into account based on the calibration procedure. In other words, from all the probabilistic calculations taken into account for the assessment the upper 34% are appointed to be piping sensitive. This results in a threshold failure probability of $1.88e-05$ (or a reliability index of 4.1). The trajectory interval above the threshold is equal to approximate 8.5km of the 26.9km (31.5%). A threshold failure probability of $1.88e-05$ is in the same order of the accepted individual risk for a flooding which is equal to $1.0e-05$ (Jonkman et al., 2017). Note that the individual risk of driving a car, equal to $1.0e-04$, is higher since the risks accepted by individuals is dependent on the extent of voluntary participation. In other words, smaller individual risk values are accepted of involuntary activities for which the risks are imposed by others, like floodings (Jonkman et al., 2017).

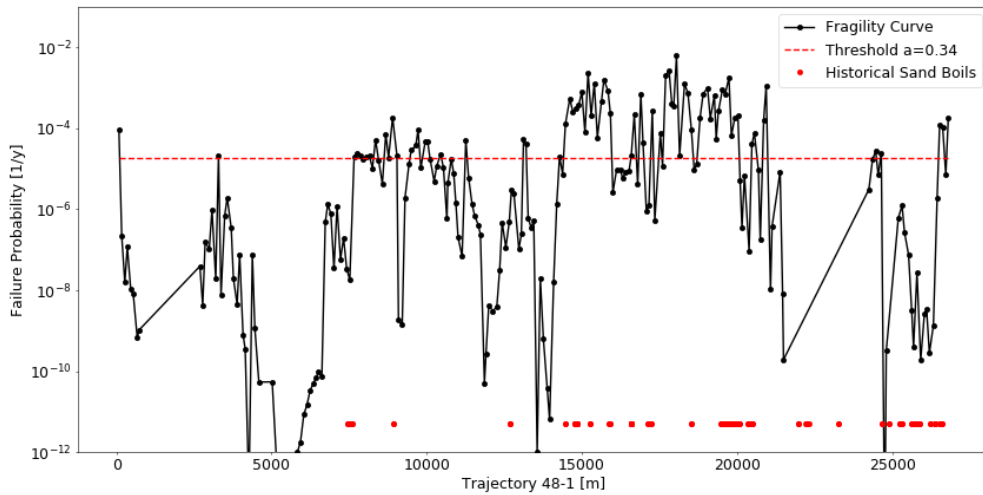


Figure I.3: Piping sensitive interval of trajectory 48-1

Note that most of the historical sand boils are located along the piping sensitive trajectory according to a threshold value of $1.88e-05$. A clear difference is identified for the final part of the trajectory between 25.2km and 26.0km (dp252 to dp260). This difference can be a result of taking the retaining of seepage water by 'seepage dikes' behind the primary dike into account. The 'seepage dikes' reduce the water level difference over the primary dike. However, it should be considered as a piping sensitive interval, indicating the importance of taking local experience into account.